L.F. TORRES DUEÑAS

FLOOD RISK ASSESSMENT OF THE CLEAR CREEK WATERSHED

CONSIDERING COMPOUND EVENTS

TU Delft

Deltares
Enabling Delta Life

Department of Hydraulic Engineering
Section Hydraulic Structures and Flood Risk

Flood risk assessment of the Clear Creek watershed considering compound events

M.Sc. Thesis

By

Luisa Fernanda Torres Dueñas

In partial fulfilment of the requirements for the degree of

Master of Science
In Civil Engineering

At the Delft University of Technology,
To be defended publicly on Wednesday August 29th, 2018 at 3:30 PM.

Chair Committee:	Prof. dr. ir Jonkman, S.N.	TU Delft
Committee members:	Dr. Bricker. J.D	TU Delft
	Dr. Sebastian, A.G.	Rice University
	Dr. de Bruijn, K.	Deltares
	Dr. Hrachowitz, M	TU Delft

An electronic version of this thesis is available at **http://repository.tudelft.nl/**

Cover:	Hurricane Harvey making landfall in Texas	NASA
	Aftermath of Harvey	Reuters
	Lessons hurricane Ike taught Houstonians	Houston Chronicle

Preface

This master thesis represents the culmination of a two-year learning cycle in the field of Hydraulic Engineering at the Delft University of Technology. This research was carried out in cooperation with Deltares in the city of Delft, within the departments of Flood Risk Management and Applied Morphodynamics and therefore my sincere gratefulness with everyone involved.

I would like to thank all members of my committee for their constant interest and continuous feedback during my research process. Thanks Bas for your orientation and your broader perspective on flood risk assessment. Thanks Toni for enlightening me with this new world of compound flooding and for all your shared insight and knowledge about the interesting Galveston area. Karin, thanks for your careful reviews about my reporting and for your invaluable help during the transition from hazard to risk delineation. Many thanks to Jeremy and his experience with FEMA and flood modelling which always gave me new ideas and thanks to Markus for showing interest in my work. Additionally, I would like to acknowledge the support I received both from Maarten and Tim regarding the SFINCS model, your help was really valuable and I appreciate being part of the team who works in this inspiring model. It was both an honor and a pleasure to work with everyone.

Furthermore, I want to thank Dennis, Ferdinand and Kymo at Deltares for all time and discussion regarding detailed probability definitions, flood mapping and for guiding me through the flood impact modelling using Delft-FIAT. You all are excellent mentors and also very nice colleagues to work with. In General I would like to thank Deltares for an amazing year at their headquarters in Delft, the working environment and thirst of knowledge of all the organization is truly inspiring. For all my colleagues at FRM it was great to learn from all of you, thanks for all lunches together and for your constant curiosity regarding my project. Likewise, many thanks to the Deltares volleyball team, especially, thanks to Maria Luisa, Alessio and Cristina for making me feel at home.

Lastly, but no less importantly, I would like to thank Stephen, Luis and Juan for being such a support through some challenging phases of the Master. Finding your friendship was one of the biggest presents I obtained after these two years. And of course, my endless gratitude to my partner, Yuri, for being so loving and patient during this period of my life, you are extraordinary and you bring joy and happiness to my days in unimaginable ways: I love you. Finally, there are not enough words to describe how grateful I am for having my parents backing me up in every life decision I make, I love you immensely and this and all my achievements are always going to be dedicated to you.

L.F Torres Dueñas
Delft, August 2018

Abstract

Tropical cyclones generate risk of compound flooding in coastal watersheds due to both precipitation and storm surge. For regions prone to this phenomenon, it is clear that in order to properly quantify flood hazard and flood risk to latter use these estimates in the implementation of mitigation, adaptation and prevention measures that are effective on decreasing the flood risk, it is necessary that compound flooding is taken into account since not contemplating the simultaneous occurrence of different flood drivers and their joint dynamic interaction, will immediately leave out the worst case scenario.

Nonetheless, this is not the regular practice carried out by risk agencies as is the case of the Federal Emergency Management Agency (FEMA) of the United States, which delineates floodplains considering only one flood driver at the time and has ignored the co-occurrence of both mechanisms. Recent studies have shown that in the United States, the current estimated flood hazard generally underestimates the actual flood losses in coastal areas (Blessing et. al. 2017). This is highly problematic since the delineation of the flood hazardous zones drives policy decisions such as urban planning, flood mitigation measures, and most relevant for the U.S case, the decision whether or not to take flood insurance policies which are all important strategies to effectively reduce and distribute flood risk.

This thesis aims to delineate flood hazard and flood risk in a coastal watershed including the effect of compound flooding using the SFINCS model; a semi-advanced 2D model which was developed to solve all relevant processes in coastal catchments with computational efficiency (Leijnse, 2018). The research is divided into four phases: **(1)** an overview of the Clear Creek coastal watershed and validation of the SFINCS model for two major hurricane events triggering compound flooding in the area, **(2)** delineation of boundary conditions for a compound flood analysis based on synthetic data, **(3)** new estimation of flood hazard and flood risk for the Clear Creek watershed, and **(4)** discussion on how relevant it is to include compound flooding in a flood risk assessment and how the results can be used to improve actual floodplain delineation and insurance rate estimates in the area.

In the first phase, an introduction to FEMA's floodplain delineation methodology is given in addition to its relationship with the area of study (the Clear Creek watershed) with the intention of illustrating the actual setbacks of the current methodology in the region which are mainly related to the use of a single flood driver in the area (Brody et al., 2013). Afterwards, the two latest major storms making landfall in the region (Ike and Harvey) are described and used for **validation of the SFINCS model** since these hurricanes triggered high precipitation rates and considerable storm surge, and therefore, were adequate examples to determine if SFINCS can capture compound flooding in the area. Results show that the model behaves adequately and that it can capture both inland and coastal flooding processes in a computational efficient manner, making it an appropriate choice to simulate compound flooding conditions, hence improving flood hazard and flood risk estimations in coastal watersheds.

The second phase focuses on the **determination of the boundary conditions** needed for the SFINCS model in order to do a compound flood analysis of the area. This was done by post processing an already existing synthetic dataset of storms in the Gulf of Mexico (generated by Sebastian et. al. (2017)) via the use of copulas, determination of multivariate return periods and a numerical integration grid. In addition, in this phase the SFINCS model is compared with the results obtained by the FEMA delineation methodology, in order to identify main differences between the two approaches and possible drawbacks of each method. Results show that both methodologies have essential differences, but in general SFINCS captures more flooding outside of the main waterways due to the inclusion of 2-D flow and also it generates similar flooding extents nearby the main channels due to riverine flooding when the resolution of the model is kept high enough and hypothetically, when similar discharge values as the ones used by FEMA are used within the model. In addition, if joint storm surge plus rainfall is being considered, SFINCS captures flood

16% additional hazard zones (total capture of 67% of claims) that are ignored by the current FEMA approach (which only captures 51% of the claims) making it a useful tool to improve flood hazard estimation in these areas.

In the third phase the ensemble of selected boundary conditions for compound flooding in the Clear Creek watershed are run in SFINCS in order to obtain an **updated flood hazard of the region**. Two different flood hazard maps are obtained in this phase: the first one delineating **the maximum flood extent if design 100-year compound events are considered** (useful for predicting flooded areas if a 100-year compound event materializes), and the second one, a map depicting the **100-year flood depth** in the watershed if a complete set of probabilistic compound events are analyzed. The results show that with the both approaches, regions nearby the outlet of the watershed experience more flooding than what is estimated by FEMA. Subsequently, an indicative risk map is generated for the catchment taking into account compound flooding hazards in the area and the vulnerability information of the region based on exposure data involving the type of land use. This step of going from a hazard to risk approach gives additional information to the communities affected by flooding, since there are estimated annual losses per year per land parcel for all the regions within the catchment.

Finally, phase four summarizes the conclusions and discussion derived from the new flood hazard and flood risk maps determined for the area, focusing mainly on the relevancy of including compound flooding in a flood risk assessment of a coastal watershed and how the results can be used to improve actual floodplain delineation and insurance rate estimates in the Clear Creek watershed.

Contents

List of Figures

CHAPTER 1

CHAPTER 2

CHAPTER 3

CHAPTER 4

CHAPTER 5

CHAPTER 6

CHAPTER 7

APPENDIX A

APPENDIX B

APPENDIX C

List of Tables

CHAPTER 2

CHAPTER 3

CHAPTER 4

CHAPTER 5

CHAPTER 6

APPENDIX A

APPENDIX B

List of Acronyms and Symbols

Below the used acronyms, Greek and Roman symbols are summed up

Acronyms	Description
ADCIRC	Advanced CIRculation model
AIC	Akaike Information Criterion
ANN	Artificial Neural Networks
BFE	Base Flood Elevation
BLTE	Bivariate Logistic Threshold-Excess
BN	Bayesian Network
CaMa Flood	Catchment-bases Macro scale Floodplain model
CBA	Cost-Benefit-Analysis
CDF	Cumulative Distribution Function
CE	Compound Event
CI	Critical Infrastructure
D-Flow -FM	Software Engine for hydrodynamical simulations on unstructured grid in 1-2-3D
Delft 3D	3D modeling suite for fluvial, estuarine and coastal environments
DEM	Digital Elevation Model
DTM	Digital Terrain Model
EAD	Expected Annual Damage
EWS	Early Warning System
FEMA	Federal Emergency Management Agency of the U.S
FEMs	Finite Element Models
FD	Flood – Damage curve
FHBM	Flood Hazard Boundary Map
FIAT	Flood Impact Assessment Tool
FIRM	Flood Insurance Rate Map
FIS	Flood Insurance Study
FRM	Flood Risk Management
GEV	Generalized Extreme Value
GPD	Generalized Pareto Distribution
GTSR	Global Tide and Surge Reanalysis
H-GAC	Houston-Galveston Area Council
HAZUS-MH	Hazards U.S Multi-Hazard
HCFCD	Harris County Flood Control District
HEC-HMS	Hydrologic Engineering Center – Hydrologic Modeling System

HEC-RAS	Hydrologic Engineering Center – River Analysis System
HGBR	Houston Galveston Bay Region
HSC	Houston Ship Channel
HSs	Hazard Scenarios
IBTrACS	International Best Track Archive for Climate Stewardship
ICDF	Inverse cumulative distribution function
IPCC	Intergovernmental Panel on Climate Change
JRC	Joint Research Centre
LULC	Land Use / Land Cover
MIKE 21/3	Model based Incremental Knowledge engineering (Hydrodynamic 2&3D Model)
NED	National elevation dataset
NFIP	National Flood Insurance Program
NOAA	National Oceanic and Atmospheric Administration
NPBN	Non-Parametric Bayesian Network
NRSC	National Resources Conservation Service
NTDE	National Tidal Datum Epoch
PCCs	Pair Copula Constrictions
PDF	Probability distribution Function
SCS	Soil Conservation Service
SFHA	Special Flood Hazard Area
SFINCS	Super Fast Inundation of CoastS Model
SLR	Sea Level Rise
SOBEK	Integrated software package for river, urban or rural management
SREX	Special Report on managing the risks of Extreme events
SRLP	Severe Repetitive Loss Properties
SSPEED Center	Severe Storm Prediction, Education and Evacuation from Disasters Center
SWAN	Simulating Waves Nearshore
SWASH	Simulating Waves till Shore
SWE	Shallow Water Equations
TC	Tropical Cyclone
TSARP	Tropical Storm Allison Recovery Project
U.S	United States
USACE	US Army Corps of Engineers
USDA	United States Department of Agriculture
USGS	US Geological service
Vflo	Vieux Flow (Physically-based hydrologic model)
WL	Water Level

Greek Symbols	**Description**	**Unit**
α	Heuristic time step reduction factor	[-]
Δt	Adaptive time step	[s]
Δx	SFINCS grid resolution in x direction	[m]

Δy	SFINCS grid resolution in y direction	[m]
θ	Copula Parameter	
θ	Numerical weighting factor	[-]
θ	Threshold parameter GPD	[-]
ζ	Free-Surface elevation	[m]
ρ_a	Air Density	[kg/m^3]
σ	Scale Parameter GPD	[-]
μ_T	Inter arrival Time between storms	[years]

Roman Symbols	**Description**	**Unit**
C	Copula	[-]
C_n	Empirical Copula	[-]
C_θ	Theoretical Copula	[-]
C_d	Drag Coefficient	[-]
d	Water Depth	[m]
d_i	Damage scenario *i*	[€]
$E(d)$	Risk	[€/year]
$F_{D,i}$	Mortality at Scenario *i*	[Casualties]
$F_{E,i}$	Evacuation Factor	[-]
$F_X(x)$	Marginal Distribution of variable x	[-]
$F_{XY}(x,y)$	Joint Distribution of variables x and y	[-]
$F_Y(y)$	Marginal Distribution of variable x	[-]
g	Gravitational acceleration	[m/s^2]
H	Wave Height or Water Level	[m or m + MSL]
h_t	Maximum value of water depth at computation domain in SFINCS	[m]
$h_{u,tresh}$	Flow Depth Limiter in SFINCS	[m]
K	Shape Parameter GPD	
n	Manning roughness coefficient	[s/m$^{1/3}$]
P_i	Probability Scenario *i*	[1/year]
$q_{\inf}$	Infiltration discharge	[m^3/s]
q_{src}	Point discharge	[m^3/s]
q_x	Momentum Flux in x–direction	[m^2/s]

q_y	Momentum Flux in y–direction	[m^2/s]
T	Wave Period	[s]
t	time	[s]
$\overline{u}$	Flow velocity due to residual current	[m]
u^+	Velocity of incoming wave component w.r.t mean current	[m/s]
u_b	Velocity at boundary of SFINCS grid	[m/s]
w_{prec}	Precipitation flux	[mm/h]

1 Introduction

1.1. Background and Motivation

Floods are the most common and frequent natural disaster worldwide as well as one of the leading causes of natural disaster fatalities and higher associated economic damages. Just in the 20th century, floods were responsible for 6.8 million deaths and the damages are escalating each year at some locations due to the continuous development in coastal areas and floodplains, in addition to the accelerated population growth and changes in land use patterns (Doocy et. al., 2013). The causes and factors that may trigger flooding in an area are very diverse, main factors can include *hydrological processes* and *weather phenomena* (such as heavy precipitation, storm surge due to storms and cyclones, snow melting processes, tsunamis caused by earthquakes, etc.), *human induced causes* (such as failure of dike sections or dams, changes in land cover that increase the amount of impervious areas, inappropriate design of drainage systems, etc.) or even *geophysical characteristics* that may make a location more susceptible to inundations (low lying areas with soils with low infiltration capacity, or basins with scarce vegetation, etc.). Hence, it is crucial to understand what the main flood drivers are in an area in order to do a correct analysis of the flood hazard and also to evaluate what is the exposure of assets in the region, since only the analysis of both parts will allow the implementation of measures that can cope with or even reduce flood risk.

Flood risk can be defined as *"the combination of the probability of a flood event and of the potential adverse consequences for human health, the environment, cultural heritage and economic activity associated with a flood event"* (European Parliament & Council of the European Union, 2007). Estimating the consequences of a flood for the environment or the cultural heritage is most of the times a difficult task since those are intangible assets. As a consequence, the potential damage is usually related to economic losses and hence flood risk is normally given as expected losses per year (in Euros or Dollars) as it can be seen in Figure 1. Taking into account the previous definition and considering the latest climate change scenarios, land subsidence due to groundwater extraction and the estimated population growth pattern, it doesn't come as a surprise that flood risk will continue to increase if no counter measures are taken, especially in coastal areas since at these locations most of the previously described phenomena are exacerbated.

A study performed by Kulp & Strauss (2017) looked into the top 25 U.S cities most vulnerable to coastal flooding and the results showed that within the 100-year coastal floodplains, approximately 1.8 million people are exposed in this areas and the number will increase to 2.4 million by 2050. In addition to this, the U.S has two of three top at-risk coastal cities regarding exposed assets to flooding and 17 port cities with populations larger than 1 million (Moftakhari et. al., 2017), which all sums up to a present and future increase of flood risk in the country.

Zooming into the Atlantic and Gulf Coast of the U.S, long-term sea-level rise has been the main driver for accelerating flooding along these coasts (Wahl et. al., 2015). In addition, population and assets in these coastal watersheds are highly prone to experience tropical cyclones, which can trigger both oceanic and fluvial flooding, amplifying the impacts in the region.

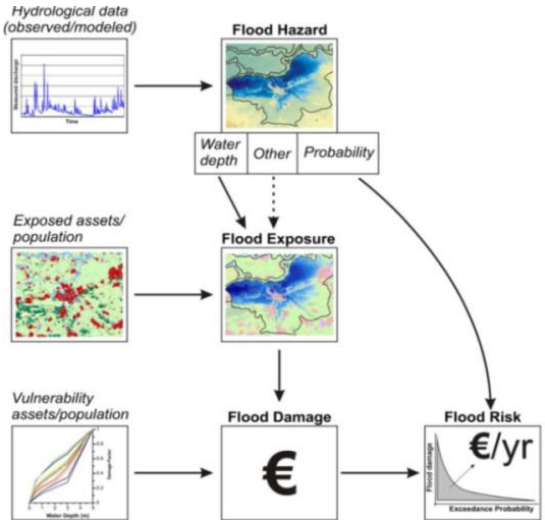

Figure 1. Conceptual overview of general flood assessment. Source: (de Moel et al., 2015)

As Figure 2 shows, in the US floods are contributing significantly to the total number of disasters. In 2013, NOAA published the National Coastal Population Report which stated that in 2010, 52% of the entire U.S population lived in Coastal watershed Counties and 39% lived in Coastal Shoreline Counties (NOAA, 2013). According to NOAA, for 2020 the population is expected to increase in 9% which is the equivalent to 15 million more people living in these areas, thus significant efforts have to be done in understanding this type of hazard since this is a serious threat that will continue to affect the population in these coastal regions.

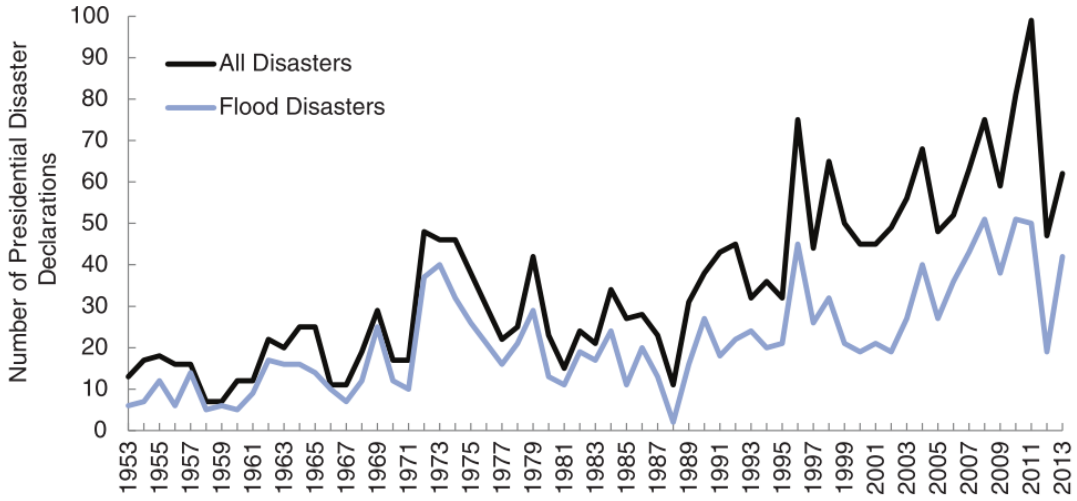

Figure 2. Number of presidential disaster declarations (U.S) from 1993 to 2013. Source: (National Research Council, 2015)

To cope with the flood threat, the competent authority in the U.S (FEMA) has made available insurance and has taken measures focusing on the delineation of floodplains along rivers, main streams and coasts based on the concept of the *"100-year flood"* which takes into consideration a flood that has an annual chance of occurrence of 1% percent in order to identify the land susceptible to inundation. Based on the identification of the aforementioned floodplains, the federal government defines which places of the U.S are part of the flood control regulations and which ones are not. Meaning that if a land parcel is within the boundaries defined by the 100-year flood, all constructions within the parcel must be adapted to withstand at least the 100-year flood and also must be insured in order to claim federal aid in case a flood hazard materializes. The insurance rates are partially assigned based on the flood risk of the area (See Figure 1) but many policies around the U.S are still subsidized by the government. A similar process is repeated for coastal shoreline counties, with the exception that the annual 1% percent probability is related to a still-water level coming from the sea which is afterwards modified to include wave effects.

From the above-mentioned information it is important to realize that in deltaic regions both coastal and riverine flooding can occur. Nevertheless, FEMA delineates floodplains considering only one flood driver at the time and has ignore the occurrence of both mechanisms at the same time (or in close succession) which automatically leaves out the worst case scenario for coastal catchments. Studies have proven that when heavy precipitation and storm surge co-occur, the potential for flooding in low-lying coastal areas is much greater than from either in isolation (Wahl et al., 2015), reason why just overlaying the coastal and riverine floodplains in an area is not enough since the dynamic between the two mechanisms is being overlooked. This highlights the importance of why estimating the probability of compound events is essential for identifying the adequate flood plains (in coastal watershed prone to this joint phenomena) and hence carrying out mitigation and prevention plans to decrease the associated risk.

Taking into account the aforementioned facts, the present M.Sc. research analyze flood hazard and flood risk considering compound events on the Clear Creek watershed, which is located in the state of Texas, near the Galveston Bay. This particular region has been historically marked by severe hurricanes and associated flooding, having on average a hurricane every 9 years making landfall in the area and having as the most recent example the landfall of hurricane Harvey in 2017; which according to the National Hurricane Center, has been the second costliest storm in the U.S history with estimated damages of $125 billion (NOAA & NHC, 2018) and which broke the national rainfall record for a single tropical storm with approximately 1.3m in 5 days in the Cedar Bayou (Amadeo, 2018) in addition to high water levels at the bay who persisted for several days according to tide gauge measurements in the area.

1.2. Problem Definition

The development of strategies for flood risk management that are more effective, cost-efficient and socially acceptable depend significantly on the in-depth understanding of the flood behavior and its drivers, as well as a proper identification of the risks associated with the hazard itself. The current methodology used by the U.S governmental entity (FEMA) to identify flood hazards, assess flood risk and provide data to guide communities through mitigation actions is falling short in coastal zones due to two main reasons: The first one is that the complexity of the flooding phenomena is being overlooked and simplified to a single cause event (either precipitation inducing riverine flooding, or storm surge causing coastal flooding). In low-lying coastal watersheds with a quick response and especially those located in hurricane-prone areas, flooding is often the result of the co-occurrence of storm surge or high tide and rainfall (Sebastian, 2016). Hence, there is a need to update the current method to include the probability of these compound events, in order to adequately estimate the hazards and afterwards, (in combination with exposure and damages) estimate the risks to properly evaluate the feasibility and effectiveness of measures to reduce flood risk.

Secondly, FEMA publishes mainly the floodplains and depending of the area and availability of detailed river cross sections, some additional information on flood depth and velocities related to the 100- and 500-year flood. This means that the analysis remains mainly on estimating flood hazard (see Figure 1) but information on risk (e.g. flood risk maps) is not available to the public and therefore risk in not fully understood across the U.S. Indeed, FEMA uses a risk based approach for assigning some insurance rates but this information is processed internally and the final policy holder only knows the rate he or she has to pay. In addition, there are some drawbacks on how damage itself is being estimated in order to assess flood risk and hence assign insurance rates. FEMA bases its calculation on previous damage claims which have an upper limit of $250,000 (maximum value for which a claim can be filed) and they are averaged amongst different building classes, which means that real damage estimation (based on household) is not being done and therefore, the associated risks are not a reflection of reality. This all sums up to the previous discussion that the current National Flood Insurance Program (NFIP) methods should be modified since the models used to determine the probability of flooding do not capture the complexity of the hazard in coastal zones, in addition to the fact that there are not flood risk maps available for communities to improve decision making and neither the estimation of damage is done properly, making questionable the internal flood risk estimates produced by the NFIP.

The Houston Galveston Bay Region (HGBR) has a long experience with coastal flooding that started at the early 1900's when the Galveston hurricane landed on the area. This triggered the construction of the Galveston Sea wall at the shoreline (5.2m of height and 16km of length), which also caused that the surviving infrastructure was lifted to the levee level and initiated a large back-filling processes towards the bay which modified completely the west end of the Galveston region. In 1915 another category 4 hurricane which impacted the region, prompted the decision to build a deep-water channel (HSC) to move the economic center towards inland Houston. After this, on 1965 the Texas City Levee and Dike was constructed due to a hurricane study developed by the USACE and NOOA who stated that Texas City was the most vulnerable location within the Galveston Bay (Brand et. al., 2015). After the conclusion of this project, not any other structural project has been approved for flood mitigation purposes, even though the region has changed drastically and the flood risk has increased considerably over time (population increases since 1965 to 2013 in 4 million people, urban and paved areas have increased towards the coast, as well as the economic assets and value of the area due to port activity). With hurricane Ike in 2008 and recently hurricane Harvey 2017, the HGBR has been exposed once again, showing a catastrophic scenario which not only created a storm surge in the bay, but also induced a high amount of precipitation in the area resulting in which looks to be one of the most damaging natural disasters in U.S history. These hurricane events in combination with the drawbacks of the current FEMA methodology triggered the research on compound events on the area, which have focused mainly on the characterization of the joint probability of storm surge and precipitation (see e.g. (Torres et. al., 2015), (Couasnon, 2017),(Sebastian et. al., 2017)). Nevertheless, little work has been done to implement the compound events on a 2-D model that could resolve the flooding extent due to both storm surge and precipitation in an efficient and effective way and also give an estimation of the associated flood risk due to a compound event in order to be used as a tool for improvement of the actual premium insurance rates or implementation of both prevention and mitigation strategies for the area.

1.3. Research Questions and Objectives

Based on the problem described in the previous section, the primary research objective of this M.Sc. Thesis is to ***develop a method to delineate compound flood hazard and risk analysis, applied to the Clear Creek watershed as a case study.***

This watershed was specifically selected since research by Sebastian (2016) on compound flooding has been already done in the area (giving estimates of the joint probability) and also due to the fact that there is availability of hydro-meteorological data for the latest events hitting the HGBR (Ike and Harvey), which allows an appropriate data-collection for the validation of a semi-advanced 2-D model of the region. In addition, this area has a long history shaped by chronic flooding dating back to the late 1800's (Sebastian, 2016), which makes it a relevant case study for understanding how important compound flooding is for the loss estimation in the area and therefore for the assignment of premium insurance rates and flood risk reduction strategies.

In order to answer the main research objective, this study seeks to quantify flood hazard and flood risk associated with compound flooding induced mainly by tropical cyclones, through the use of a semi-advanced 2D-model and the use of appropriate damage curves with the aim of comparing the results to the current existing practices. The following research questions and sub objectives are delineated to achieve the final result of this research:

Research questions:

1. **How can flood hazard estimates be improved in coastal watersheds by the inclusion of compound events in the analysis via the use a of a semi- advanced 2D model (SFINCS)?**

2. **What may be the implications of delineating new flood hazard maps considering compound flooding for flood risk assessment, implementation of flood risk management strategies and insurance rates in the Clear Creek watershed?**

Sub Objectives:

I. Collect storm surge levels, precipitation and flooding water levels for two main events happening in the Clear Creek watershed on the last decade (Ike and Harvey)

II. Construct and validate the SFINCS model using the two main events and its respective boundary conditions

III. Choose the boundary conditions for the joint probability events (storm surge and precipitation) from synthetic data from the BN constructed by Sebastian et al. (2017) in order to delineate flood hazard and flood risk in the region

IV. Model on SFINCS only riverine flooding based on design values of precipitation (without considering storm surge at the bay) and compare flooding extent of the SFINCS model with the flooding maps published by FEMA for the Clear Creek watershed

V. Model on SFINCS the selected scenarios (Objective III) and delineate the 100-year compound flood extent and the 100-year compound flood depth hazard map of the Clear Creek watershed

VI. Estimate flood damages for ensemble of compound scenarios and associated flood risk based on exposure data build on land use type and global depth-damage functions extracted from the Joint Research Centre (JRC) (Huizinga et. al., 2017)

VII. Look at the implications and uses of the new flood hazard and flood risk maps generated for the Clear Creek watershed.

1.4. Methodology

In order to achieve the objectives and answer the main questions of this research, multiple steps have been implemented as it can be seen in Figure 3. First an overview of the area of study is given focusing on the two latest major storm events hitting the area (Ike and Harvey), for which a hydro-meteorological data collection of is performed in order to validate the SFINCS model. This data collection included sea water levels, storm surge and precipitation values in the Clear Creek watershed. Afterwards, a data gathering of the main geomorphological data such as the digital elevation model of the watershed (DEM), land use, soil type, etc. was carried out and based on all the above data, the SFINCS model was validated based for the most recent mayor storms hitting Texas.

Secondly, based on previous studies performed for the area (Sebastian et al., 2017), the boundary conditions for compound flooding in the Clear Creek watershed were determined using the synthetic data generated by Sebastian et al. (2017), which included 100,000 possible values of storm surge and precipitation that could co-occur in the Clear Creek area given that a hurricane makes landfall nearby the Galveston Bay.

Thirdly, the SFINCS model was used to run multiple scenarios along the 100 year return period curve (coming from the synthetic data) in addition to running an ensemble of probabilistic scenarios covering all possible combinations of events in the area (disregarding the return period) in order to be able to delineate the 100-year compound flooding hazard of the area considering both extent and flood depth. In parallel, the model was run using as the upstream condition the 100- year design precipitation value and setting as the downstream boundary condition the mean sea level. This process was tested for the actual design precipitation value of the Clear Creek watershed, in order to compare how the SFINCS model relates to the actual FEMA practice of delineating floodplains. The results of both approaches (including compound effects and neglecting them) were compared with the existing flood hazard maps of the watershed and some initial conclusions were drawn regarding the importance of including compound events in the Clear Creek watershed.

Finally as a step forward to the current methodology of FEMA's NFIP, a flood risk map was delineated by using a proper damage estimation method using global depth-damage functions based on exposed land use and using the Delft-FIAT Model. The flood risk map had the objective to allow property owners to better visualize their possible losses and make a more conscious decision on the acquisition of flood insurance policies. The flood risk map obtained for the design compound event was the core for the discussion on how this information could be used to improve the estimation of actuarial rates for people inside or outside the floodplains, and how it could be also used as a prioritization tool to implement flood mitigation or prevention measures that reduce the flood risk to an accepted level.

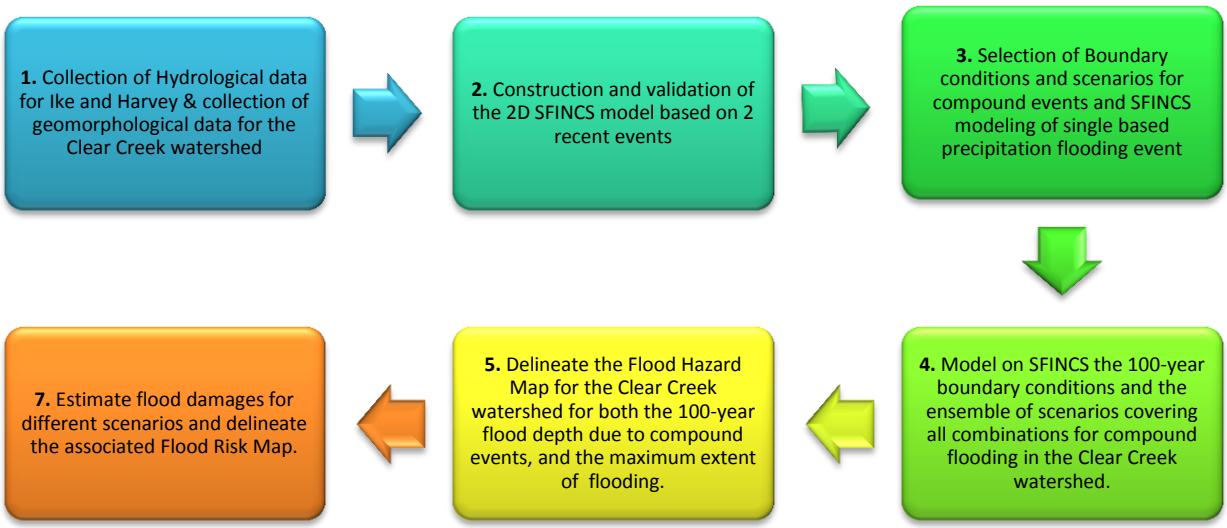

Figure 3. Flow Chart M.Sc. Research

1.5. Reader's guide

This report is divided in 8 parts as can be seen in Figure 4. Chapter 2 gives background information about the methodology carried in the US to estimate flood hazards and flood risk and also it exposes a literature review of the methodologies carried until now to account for compound flooding in coastal areas. Chapter 3 presents a description of the study area and the data collection for the Clear Creek watershed including information about previous storms (Ike and Harvey) in order to implement and validate the SFINCS model regarding compound events. Chapter 4 deals with the determination of the joint probability between storm surge and precipitation based on a synthetic dataset (Sebastian et al., 2017) and the selection of the boundary conditions for compound flooding relative to a specific return period. This chapter deals as well with a comparison between the SFINCs model flooding extent output and the flood maps generated by FEMA when only a single based flood driver is being analysed (design precipitation event). Chapter 5 focuses on the general food risk assessment of the area considering the boundary conditions established on chapter 4. Chapter 5 will deal with both the flood hazard mapping and the estimation of damage in the area to delineate the flood risk map of the catchment. Finally, chapter 6 includes the general conclusion about the relevance of compound flooding for the area and also a discussion about the utility of flood risk maps for both the assignment of insurance premiums in the area and for general acknowledgement of citizens to improve decision making and planning for mitigating and preventing flood risk, while the last chapter states the future recommendations and improvement to continue the research.

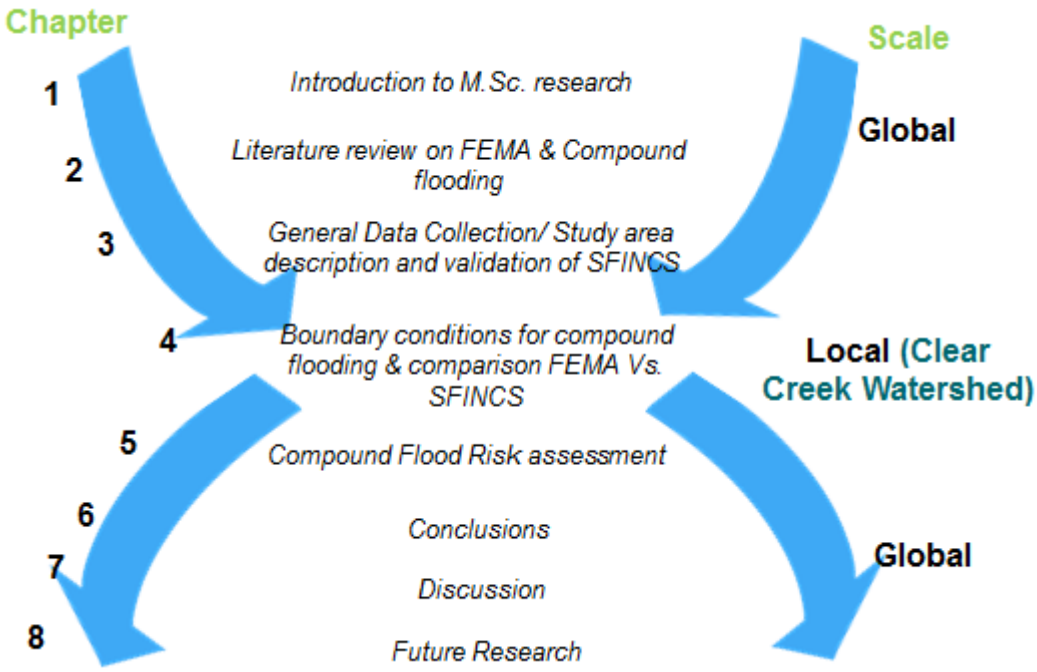

Figure 4. General structure of the M.Sc. research

2

Literature Review

2.1. Introduction

In this literature review some background information is going to be given on flood risk analysis in order to contextualize the reader and agree on some Flood Risk Management (FRM) terminology. Secondly, an overview of the methodology used by the Federal Emergency Management Agency of the United States Department of Homeland Security (FEMA) for assessing flood hazard is going to be explained, as well as its relationship with the National Flood Insurance Program (NFIP) and a general description on FEMAs flood loss estimation methodology in order to understand what is the procedure followed in the U.S to assess flood hazard and flood risk and also understand the drawbacks of the method. Afterwards, a section on compound flooding and its relevance regarding the Galveston bay is going to be included as well as some methodologies that have been used to express the joint probability of these events. Finally, given the gaps found in the research and the identified weaknesses of the FEMA approach, the focus of this M.Sc. research is going to be further justified.

2.2. Flood Risk Analysis Overview

2.2.1 Flood risk quantification

Under the context of FRM, **flood risk** is considered to be the Expected Annual Damage (EAD) or the Annual Average Loss. This metric represents a summary statistic that combines all possible flood events, their probabilities and their corresponding damages into one figure.

As explain briefly on chapter 1 in the background and motivation section, the unit of risk ($E(d)$) is often given in Euro (€) or Dollar ($) per year (€/year). In the case of a single event, with probability P_i (1/year) and associated damage d_i (€), the risk will be represented by equation 2.2.1.

$$E(d) = P_i \cdot d_i \qquad \textbf{(2.2.1)}$$

Nevertheless, in real life situations many possible events might occur in a given location and calculating the probability and damage of one event alone is therefore not enough to get a full picture of the situation and hence any rational decision making regarding flood mitigation, prevention or adaptation measures will be compromised if only one scenario is considered. For this reason, in flood risk assessment studies equation 2.2.2 is often used in order to take into account multiple discrete scenarios (Kaplan & Garrick, 1981).

$$EAD = E(d) = \sum_{Sc=1}^{n} P_i \cdot d_i \qquad \textbf{(2.2.2)}$$

In the estimation of the EAD some information is lost when the figure is reported as a single value since there is not an indication about the contribution of individual scenarios to the total risk. For this reason, risk is also represented by the risk curve (FD) which shows the probability of exceedance (given in a logarithmic scale) of a certain damage (D) value (S. N. Jonkman et al., 2017). In the case of an FD curve, the

EAD can be also computed by integrating the FD curve by using equation 2.2.3, since damage is being represented as a function of the exceedance probability (p).

$$EAD = Risk = \int damage(\mathrm{p})\,\mathrm{dp} \qquad \textbf{(2.2.3)}$$

The consequences or damages can be also represented by the number of casualties or fatalities in which case the risk curve is known as a FN curve as depicted in Figure 5. For the purpose of this M.Sc. research, the consequences are going to be always represented by direct tangible losses[1] due to a flood event.

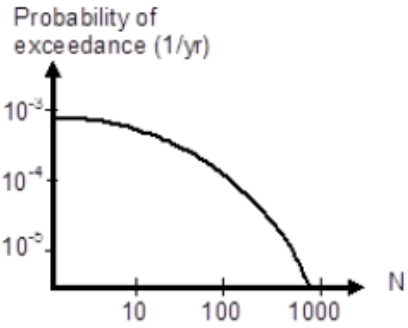

Figure 5. FN Curve representation. N represents fatalities
Source:(Jonkman et al., 2017)

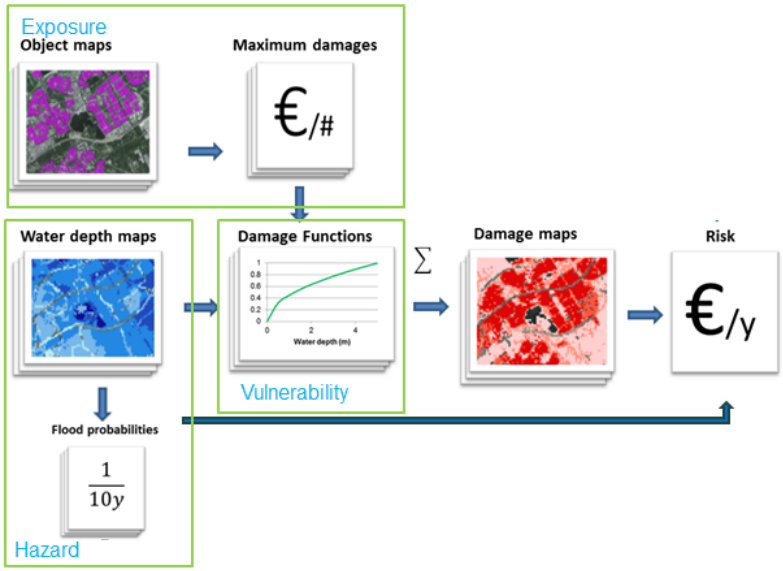

Figure 6. General Scheme for Flood Risk estimation. Source:(Wagenaar, 2018)

In FRM, there are additional terms such as exposure, hazard and vulnerability that are also going to be used across this research and therefore they are illustrated in Figure 6 and explained below.

- **Exposure:** refers to the people and assets (object maps Figure 6) located within the hazard zones (e.g. floodplains) that are subject to potential losses (S. N. Jonkman et al., 2017)
- **Hazard:** refers to the source of danger and its associated characteristics and probability of occurrence (e.g. flood water depth, flood water velocity). The hazard is estimated by means of hydrological and hydraulic data; either by observed events or by the use a model (see Figure 1)
- **Vulnerability:** refers to the potential consequences than may occur given that the hazard materializes (damage functions Figure 6). Normally, the damage is given as a curve (function) that shows the losses given certain flood depth, flow velocity or sometimes flood duration

All the information presented before builds up towards the definition of risk in terms of economic damages. This is highly important since it allows to use this metric (EAD) in decision making processes, in which is more useful to express the impact of flooding in money terms in order to compare between the costs and benefits of implementing certain measure to reduce flooding in an area. Additionally, this metric could be also used in the response phase of the disasters since it allows via Flood risk maps to assess where to send aid first or it could also serve in the mitigation phase in which estimation of flood risk in an area can be used to set insurance premiums.

It is important to acknowledge that flood risk is not only related to economic damages but also to loss of life. When relating impacts of flooding to casualties, two different metrics are generally used: the **Individual** and the **Societal** risk.

1 In FRM there are multiple categories for classifying flood damage. Direct tangible losses include damages associated to capital loss (Houses, crops, cars, factory buildings, etc.) production and income losses. Direct intangible losses refer to casualties, social disruption and damage to the ecosystem amongst others. On the other hand, indirect tangible assets refer to migration, loss of utility services outside the flooded area and unemployment while indirect intangible assets may cover things such as reputation damage or loss of potential for attracting investors (Wagenaar, 2018)

- Individual Risk (IR) is related to the probability of a person dying in a certain location (x, y) (see equation 2.2.3) due to a flood event. In this metric the effect of evacuation due to implementation of flood warning systems is also considered, since evacuation reduces the mortality rate
- Societal Risk is related to expected number of fatalities and is often associated to the FN-curve (see Figure 5)

2.2.2 Flood risk visualization

Once flood risk is understood and computed according to the definition presented in the previous section (see equation 2.2.3 and Figure 7), is clear that this value will only be a constant given that the hazard, exposure and vulnerability remain the same at a specific location. As soon as there is a zoom out to a broader area, the flood risk will vary spatially since exposure can differ greatly from location to location (e.g. from an urban to a rural land use) as well as flood characteristics (e.g. changes in topography, roughness, soil type, etc.) along an area. As a result, flood risk maps are a powerful tool to visualize the variability of risk along an area since not only they give additional information than the one given by the total EAD metric, but also they allow identifying the most critical locations allowing the prioritization of measures and interventions to reduce the impacts of flooding.

Figure 7. Risk definition as an overlay of the Hazard, Vulnerability and Exposure in an area. Source: (Wagenaar, 2018)

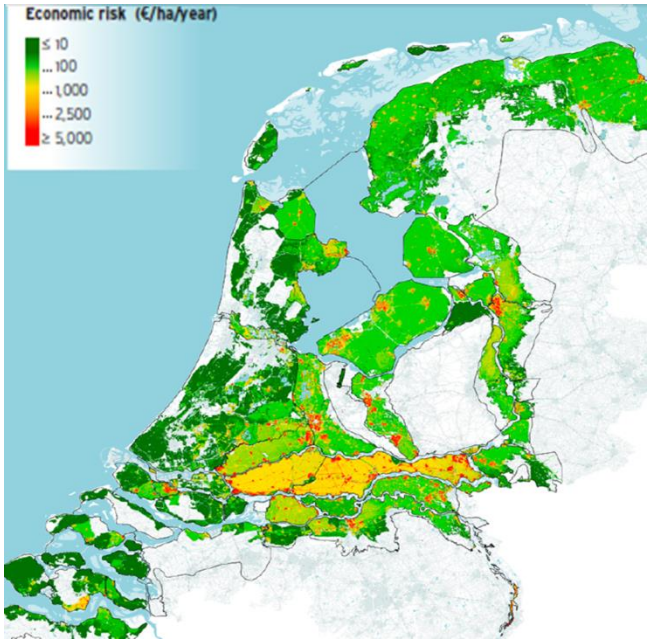

Figure 8. Flood Risk Map of the Netherlands. (considering only economical losses and floods from the main rivers, large lakes and sea) Source: (Rijkswaterstaat VNK Project, 2014)

The approach of using Flood Risk maps for decision-making strategies has been implemented actively in the Netherlands by means of the VNK project, in which a National Flood Risk Analysis has been performed for the entire country (Rijkswaterstaat VNK Project, 2014).

In the case of the Netherlands, the probability of flooding is associated with the likelihood that a flood defense structure (levee, storm surge barrier, etc.) will fail or breach at some point, in opposition to the traditional approach of considering the probability of exceedance of a certain water level. This approach allows increasing the understanding about the relevant failure mechanism that will determine whether or not a flood defense fails triggering flooding in an area.

Once the probability of flooding is computed, the hazard with its associated probability of occurrence can be overlaid with the exposure maps of the area and by mean of the FD curves a risk estimation can be performed for each location along the area as depicted in Figure 8, in which a flood risk map of the Netherlands can be observed showing the annual expected value for economic losses per hectare

2.2.3 Flood risk evaluation

In order to evaluate flood risk is important to define what are the maximum losses that a community is willing to accept or in other words, what is the acceptable risk for a given location? Answering this question is not a simple task as it depends of many factors including not only technical and economical remarks but also societal and political reasons. In general terms it can be said as found in Jonkman et al. (2017), that risks can be evaluated following the next criteria:

1. "Limit Individual risk (IR) to prevent that certain people are exposed to disproportionally large risks"

$$IR(x,y) = \sum_{i}^{n} Pi \cdot F_{D,i}(\mathrm{x},\mathrm{y}) \cdot (1 - F_{E,i}) \qquad \textbf{(2.2.3)}$$

$$IR(x,y) \leq IR_{acc} \qquad \textbf{(2.2.4)}$$

In which IR_{acc} is the accepted individual risk which is often associated with a minimum safety standard (e.g. in the Netherlands this value is set to 10^{-6} for most applications) while IR is the individual risk given the probability of certain scenario $Pi \cdot$(1/year), the mortality of that scenario at certain location ($F_{D,i}$) and the evacuation fraction for the scenario ($F_{E,i}$).

2. "Limit societal risk to prevent the risk of large scale accidents with many fatalities"

3. "Economic optimization to balance investments in risk reduction from an economic point of view"

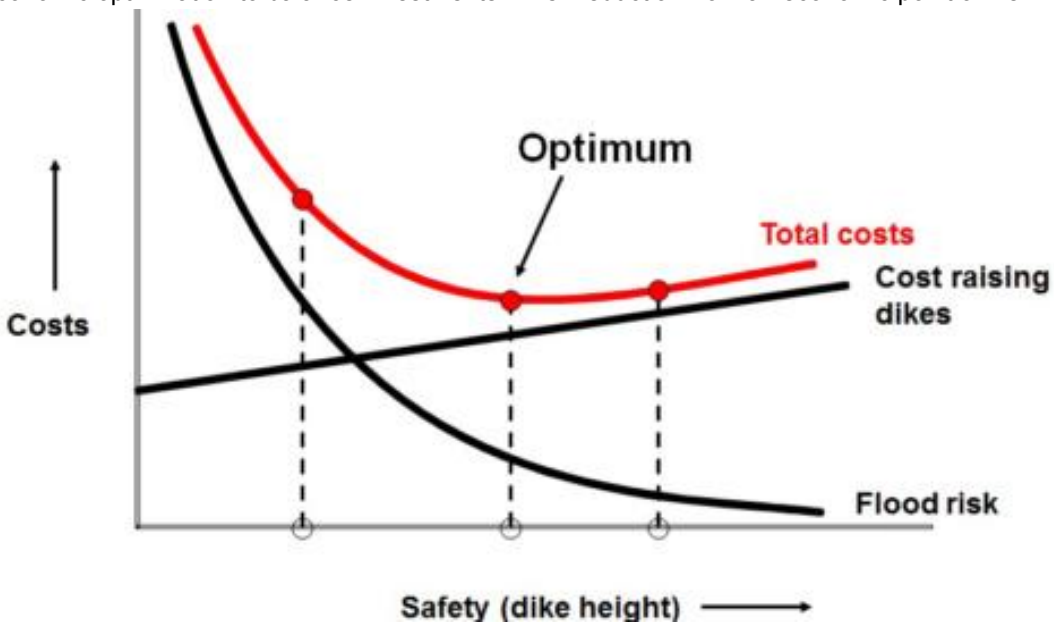

Figure 9. Economic optimization as a function of flood risk. Costs related to improve flood risk (heightening dikes). Source: (Jonkman et al., 2017)

In which an optimum is seek-out regarding the costs necessary to reduce the flood risk as illustrated in Figure 9. In the previous figure the measure that is being evaluated to reduce flood risk is to raise dike heights. It can be seen that as the height is increase the associated cost of the measure increase but the flood risk decreases. The optimum then will be the minimum point found along the curve obtained from the subtraction between the flood risk curve and the costs of raising the dikes (see red line Figure 9).

2.3. FEMAs NFIP background

2.3.1 History of the NFIP program

The federal government of the United States has been involved in floodplain management even as early as the 1800's when the main interest was to assure the navigability of the main rivers across the country. Nevertheless, it was only till 1927 after a major flooding occurred along the Mississippi River that the government created the Flood Control Acts (1928 -1936) in order to build flood defenses that protected vulnerable areas against riverine, coastal and flash flooding. The projects included the construction of dams, levees and floodwalls whose main objective was to reduce flood losses. This objective was not achieved, since in the 1960's a study concluded that the damages caused by floods were increasing, despite of the flood structures implemented in the country. One of the main drivers for this failure was the increasing establishment of people and infrastructure within and around the floodplains; therefore, the response of the government changed towards including policies that were not merely structural measures, but also measures that included regulations on development of certain areas, warning systems and evacuation plans and most importantly, the creation of an insurance program as an alternative to disaster relief (FEMA, 1998).

The NFIP was created in 1968 and it encompassed not only the insurance policy, but it also accounted for the distribution of responsibility for floodplain management to all levels of government and the private sector as well as a comprehensive floodplain mapping program across the U.S. This program also focused more in the protection and restoration on the environment; consequently, watershed management was also included in order to achieve multi-purpose solutions for flood risk management. This Unified National Program delineates the framework for "Floodplain Management" in the country and it was defined by the federal agency as "a decision-making process that aims to achieve the wise use of the nation's floodplains", understanding by "wise use" the reduction of flood losses and protection of the functions of floodplains and the natural resources. The main strategies of the program can be summarized in the following bullets:

1. **Modify human susceptibility to flood damage** (reduce disruption by avoiding hazardous, uneconomic or unwise use of floodplains, e.g. Relocation of buildings, implementation of emergency plans, etc.)
2. **Modify the impact of flooding** (Assist individual and communities to prepare for, respond to and recover from a flood)
3. **Modify flooding itself** (Develop project that control floodwater, e.g. dikes, reservoirs, diverting high flows around developed areas, etc.)
4. **Preserve and restore natural resources** (Renew vitality and purpose of floodplains by re-establishing and maintaining floodplain environments in their natural state)

The National Flood Insurance Act of 1968 (which created the NFIP), had the objective of transferring the costs of private property flood losses from the taxpayers, to floodplain property owners through flood insurance premiums in addition to provide financial aid to both the property owners and floodplain residents after the hazard had materialized. In the early beginnings of the NFIP, the participation grew very slowly until 1973, when hurricane Agnes triggered the enactment of the Flood Disaster Protection Act, who required that properties located in identified flood hazard areas have mandatory flood insurance as a condition for receiving federal aid. In 1979 the NFIP was transferred to a newly created agency (FEMA) that achieved in 1986 with the help of the previous administration, a self-supported program that is funded primarily though premium income, which pays all administrative and mapping costs as well as claims. This is no longer the present case of the program, which since 2005 (after hurricane Katrina made landfall in New Orleans) is in red numbers and up till late 2017 (when hurricane Harvey flooded Texas) it still had more than a thousand claims left over from hurricane Sandy in addition to having exhausted their $30 billion borrowing capacity according to the New York Times (Williams, 2017). A study carried in 2017 by the Congressional Budget Office (CBO) stated that under the current NFIP structure, inland policyholders are subsidizing policy holders in coastal counties. The study showed that there were approximately 5 million active policies (up to 2016) and it estimated that the NFIP faces $5.7 billion in costs, while only producing $4.3 billion in revenues, leaving a yearly shortfall of $1.4 billion (Congressional Budget Office, 2017).

2.3.2 Floodplain delineation in the NFIP- Flood Hazard approach

As a whole, the NFIP consists of three parts: **Mapping** (which includes two kinds of maps: the Flood Hazard Boundary Map (FHBM) and the Flood Insurance Rate Map (FIRM)), **Insurance** (based on Insurance premiums for Post-FIRM buildings and subsidized insurance for pre-FIRM buildings) and **Regulations** (designed to ensure that new infrastructure and development will not worsen the flood hazard). From the three parts described above, mapping is the main core since based on this information, insurance is assigned and regulations are established.

The national standard used by FEMAs NFIP for mapping the so called Special Flood Hazard Areas (SFHA), is the "Base flood" which consists in the one-percent annual chance flood or in layman terms, the flood that has one-percent (1%) probability to occur in any given year. This standard is normally known in the U.S as the 100-year flood and it represents an annual exceedance probability. Based on this standard, the land that is covered by floodwaters is delineated (SFHA) and is within this area that the NFIP enforces the floodplain management regulations and corresponding insurance rates. Another term used by the NFIP is the base flood elevation (BFE) which is the water level corresponding to the 100-year flood.

Table 1. Probability of being flooded. Source:(FEMA, 1998)

Chance of Flooding over a Period of Years

Time Period	Flood Size 10-year	25-year	50-year	100-year
1 year	10%	4%	2%	1%
10 years	65%	34%	18%	10%
20 years	88%	56%	33%	18%
30 years	96%	71%	45%	26%
50 years	99%	87%	64%	39%

Is important to realize that according to Table 1, a property during 30 years of lifetime has a 26% chance to flood due to a 100-year flood in the SFHA, and that even when a bigger flood (but less frequent) as the 500-year flood is considered, the probability of flooding during a 30-year mortgage is still considerable (6% chance, see Figure 10) when compared to other world standards (The Netherlands has safety standards in some locations even of 0.00001% (value related to failure probability of the flood defenses, rather than a return period of design loads). When the opposite situation is analyzed (a smaller but more frequent flood) e.g. the 10-year flood, the probability increases dramatically to 96%, which means that is certain that at some point the property will flood, especially if it is located in very low lying areas. In addition, the metric of the 100-year flood also carries in its construction a series of inaccuracies such as the limited observations, changes in climate and various assumptions made in the statistical modelling techniques (Brody et. al., 2013).

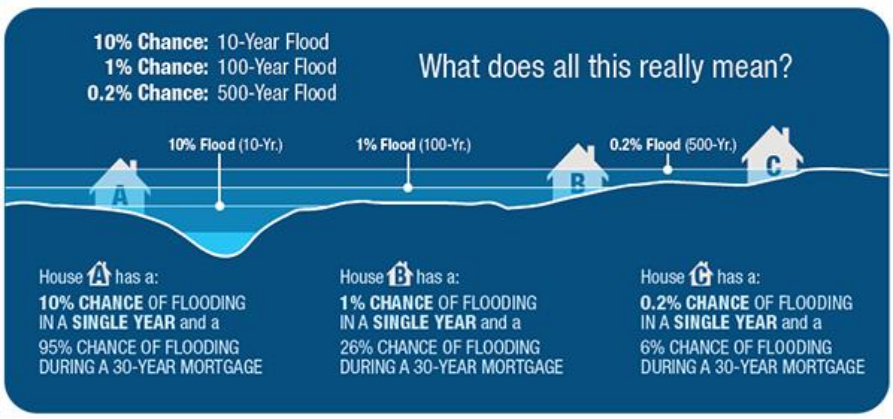

Figure 10. Floodplain delineation according to annual flood probability occurrence. Source: (Project Brays, 2018)

The maps generated by NFIP include the flood elevations, velocities, floodway dimensions and insurance rating zones. All this is compiled in each community Flood Insurance Study (FIS) and it serves as the basis for implementing measures or regulating development in the area. The studies are conducted differently for each type of flooding in which the main ones are riverine and coastal flooding. In the case of riverine flooding, the study consists on gathering hydrological information of the watershed (precipitation, runoff) as well as the detailed topography of the area including cross sectional areas of the main streams and estimations for the roughness coefficients along the floodplain. After this information is collected, the data is processed through a hydraulic model (HEC-RAS model developed by the U.S Army corps of Engineers) in order to study how water will move in the stream and most importantly in the floodplain. The final result of the model will be the flood elevation, flow velocities and floodplain widths at each cross section for the selected flood return period. The complete study will show elevations for the 10-, 50-, 100- and 500-year floods for management purposes, but property insurance will be only related to the 100-year flood. The concluding process is to transfer the flood elevations to a topographic map of the area, therefore the accuracy will depend as well on the resolution of the digital elevation maps. The main information will be summarized in FIRMs (see example of Figure 11) which will be used to assign insurance rates.

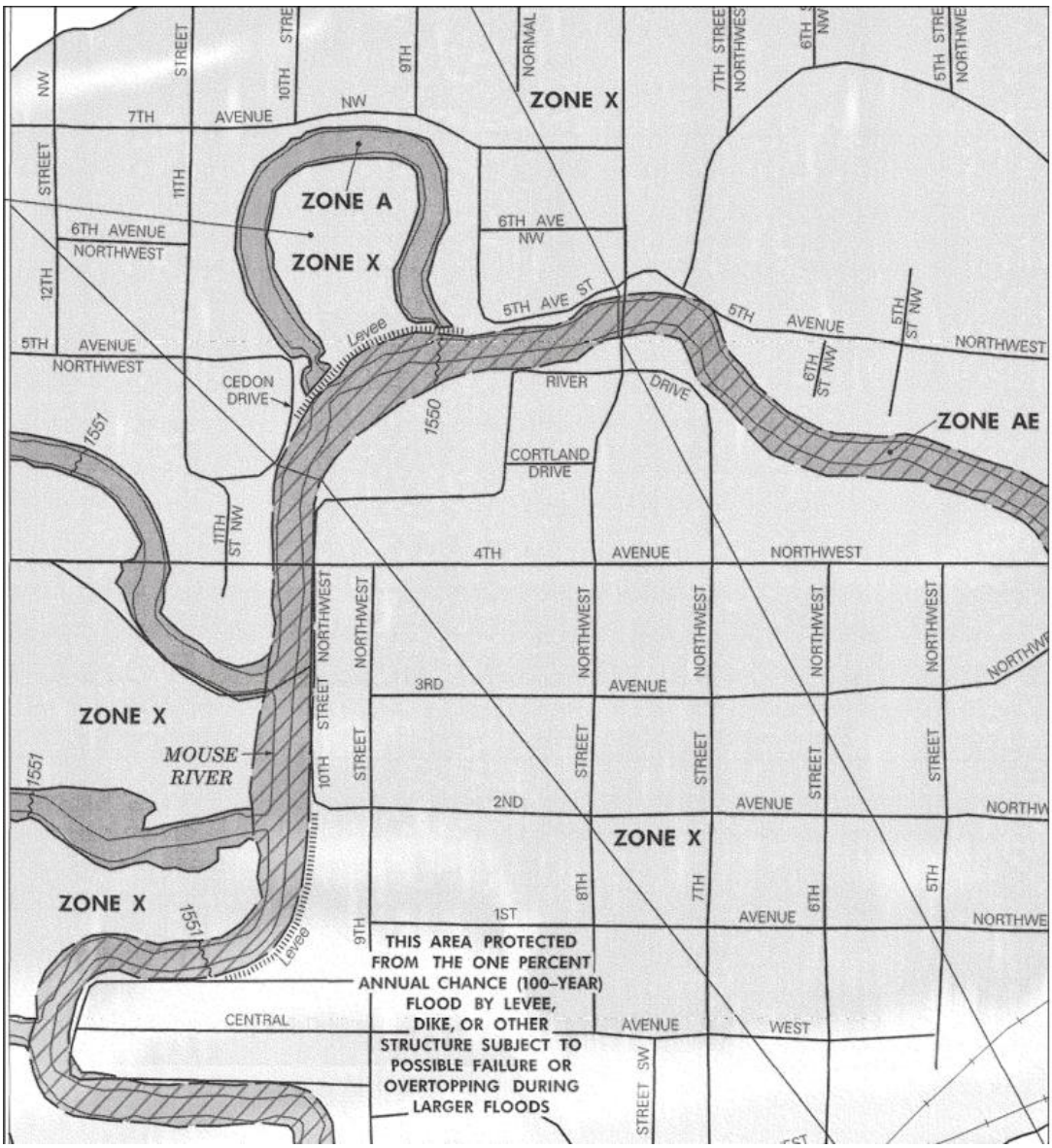

Figure 11. Portion of a FIRM of Ward County, North Dakota.
Dark Grey areas are the (SFHA) and light gray areas represent moderate risk to flooding. The diagonal lines are the cross sections taken for the study (see Table 2 for explanation of the zones)
Source:(National Research Council, 2015)

2.3.2. NFIP Floodplain delineation

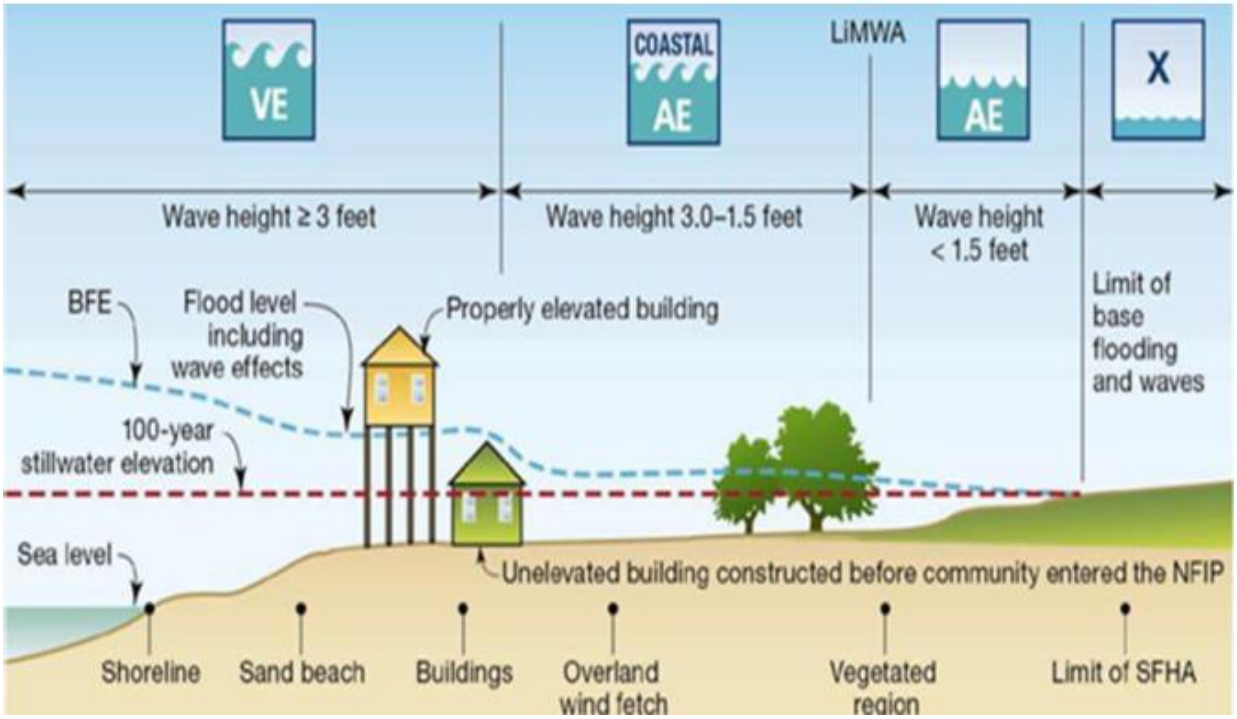

Figure 12. Coastal Special Flood Hazard Areas (SFHA) divided in VE (>0.9m) and AE zones (<0.9m). In coastal areas the BFE includes the wave height. Source:(Sebastian, 2016)

In the case of coastal flooding, the storm surge (rise of seawater level above the predicted astronomical tide) caused by strong winds coming from hurricanes or northeasters is simulated by a computer model which uses historical data (wind speed, direction and air pressure) to obtain and calibrate surge elevation and the respective probabilities for each event. The model itself, only gives Stillwater flood elevations, hence, the wave action has to be included separately to account for maximum water elevation, wave run-up and wave setup. This is done by a hydraulic analysis, in which the bathymetry and topography of the area are used in order to determine the wave characteristics above the storm surge in the coastal basin. With this result, the BFE can be determined as the Stillwater elevation (storm surge) plus the wave run-up or the wave crest elevation.

For coastal areas, the high hazard areas are mainly determined based on exposure to wave effects and they normally are located between the shoreline and certain points, where for example the computed wave heights for the base flood are three feet (~ 1 m approx.) or more, or where the inland limit of the primary dune system ends or where the eroded ground profile is three feet below the original run-up elevation. The approximation of three feet wave was used because this is the threshold to break a wall panel. The areas located in the previously described floodplains are designates as “VE” zones and they have a different flood insurance rate due to their exposure to risk, other zones outside the “VE” areas are mapped as “AE” zones as can be seen in Figure 12.

Is important to notice that both flood studies (riverine and coastal) are performed separately as explained before and that the NFIP until know, doesn’t contemplate compound flooding produced by both storm surge and high precipitation in the area.

2.3.3 Insurance rates in the NFIP- Flood Risk Approach

When the flood studies have been performed either for coastal or riverine flooding, the results are compiled graphically on FIRMs (see example on Figure 11), which show flood zones, BFE and flood hazard areas amongst other information. The classification of flood zones according to the NFIP for both coastal and riverine flooding is given in Table 2. Depending on the classification showed in the FIRM, the insurance rates are assigned either on a risk based policy (actuarial rates for Post-FIRM structures) or a subsidized value (for Pre-FIRM structures) as depicted in Table 3.

Table 2. NFIP Flood Zones. Source:(National Research Council, 2015)

Hazard Level	Zone	Description
Special Flood Hazard Areas		
High	A	Areas subject to inundation by the 1 percent annual chance exceedance flood. Because detailed hydraulic analyses have not been performed, no base flood elevations (BFEs) or flood depths are shown.
	AE, A1–A30	Areas subject to inundation by the 1 percent annual chance exceedance flood determined by detailed methods. BFEs are shown within these zones. Zone AE is used on new and revised maps in place of zones A1–A30.
	AH	Areas subject to inundation by 1 percent annual chance exceedance flood (usually areas of ponding) where average depths are 1–3 feet (shallow flooding). BFEs derived from detailed hydraulic analyses are shown within this zone.
	AO	Areas subject to inundation by 1 percent annual chance exceedance flood (usually sheet flow on sloping terrain) where average depths are 1–3 feet (shallow flooding). Average flood depths derived from detailed hydraulic analyses are shown within this zone.
	AR	Areas that result from the decertification of a previously accredited flood protection system that is determined to be in the process of being restored to provide base flood protection.
	A99	Areas subject to inundation by the 1 percent annual chance exceedance flood, but which will ultimately be protected upon completion of an under-construction federal flood protection system. In these areas, enough progress has been made on the construction of a protection system, such as dikes, dams, and levees, to consider it complete for insurance rating purposes. Zone A99 may be used only when the flood protection system has reached specified statutory progress toward completion. No BFEs or flood depths are shown.
	V	Areas along coasts subject to inundation by the 1 percent annual chance exceedance flood with additional hazards associated with storm-induced waves. Because detailed coastal analyses have not been performed, no BFEs or flood depths are shown.
	VE, V1–V30	Areas along coasts subject to inundation by the 1 percent annual chance exceedance flood with additional hazards due to storm-induced velocity wave action. BFEs derived from detailed hydraulic coastal analyses are shown within these zones. Zone VE is used on new and revised maps in place of zones V1–V30.
Other Areas		
Moderate	B, X (shaded)	Moderate risk areas within the 0.2 percent annual chance exceedance floodplain, areas of 1 percent annual chance exceedance inundation where average depths are less than 1 foot, areas of 1 percent annual chance exceedance inundation where the contributing drainage area is less than 1 square mile, and areas protected from the 1 percent annual chance exceedance flood by a levee. No BFEs or flood depths are shown. Zone X (shaded) is used on new and revised maps in place of Zone B.
Minimal	C, X (unshaded)	Minimal risk areas outside the 1 percent and 0.2 percent annual chance exceedance floodplains. No BFEs or flood depths are shown. Zone X (unshaded) is used on new and revised maps in place of Zone C.
Undetermined	D	Unstudied areas where flood hazards are undetermined, but flooding is possible.

The insurance rates for Post FIRM buildings, was intended to reflect the risk of flooding depending on the structure elevation and other significant factors, while for pre-FIRM properties (properties usually below the BFE and seen in Figure 13) the rates are subsidized to avoid a dropping in the value of the property and to encourage communities to participate in the NFIP. Nevertheless, due to the slow disappearance or replacement of Pre-FIRM buildings, in 2012 the Biggert-Waters Flood Insurance reform Act was passed in order to replace subsidies by premium to reflect the real risk of these properties, which represents 20% of the NFIP portfolio (National Research Council, 2015). Those premiums increments were substantial when compared to the previous rates; therefore, in 2014 the Home owner Flood Insurance Affordability act restricted the annual policy increment to a maximum value of 18%.

2.3.3 NFIP Insurance rates

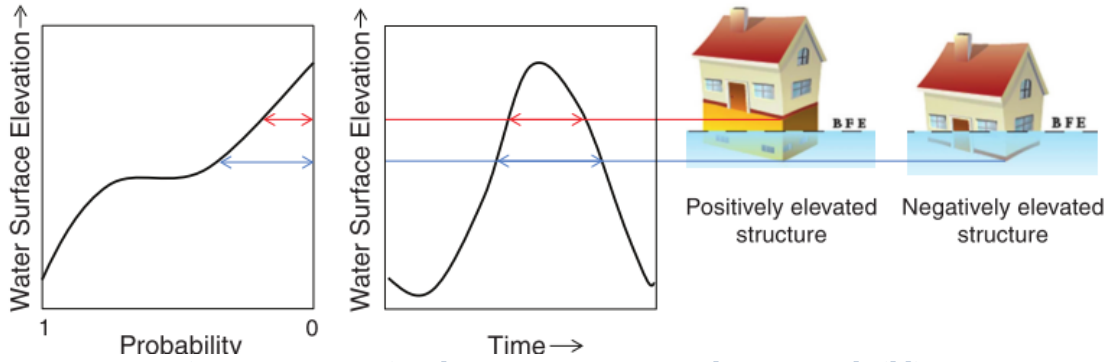

Figure 13. Comparison between Post-FIRM and Pre-FIRM buildings. Negative elevated structures will experience floods of longer duration than those constructed above the BFE. Source: (National Research Council, 2015)

As it can be seen from Table 3 the actuarial rates are computed based on an estimation of the average annual loss (in dollars) from flooding and on some correcting factors (Integration of right graph on Figure 14). The RATE formula gives a price per unit of insurance for each $100 of property coverage, this mean that the rate is multiplied by the amount of insurance purchased to determine the Premium that an owner will pay.

Table 3. Insurance Rate calculation in the NFIP. Source: (National Research Council, 2015)

Actuarial Rates	Subsidized Rates
** $RATE = [\sum_{i=\min}^{\max} (PELV_i \times DELV_i] \times \frac{LADJ \times DED \times UNIS}{EXLOSS}$ ***Where,*** $PELV$ is the annual probability of exceedance of a given depth relative to the BFE. $DELV$ is the damage to the property, expresses as % of the total property value, resulting from that level of flood water $LADJ$ is a loading factor to account for loss adjustment expenses DED is a factor to eliminate the portion of loss that will be borne by the policy holder through his deductible $UNIS$ is a factor of adjustment for how much a policy holder has underinsured his property $EXLOSS$ is the expected loss ratio *Min* is the Minimum elevation relative to the lowest flood at which flood damage occurs *Max* is the elevation relative to the lowest flood at which flood damage approaches a maximum ** *means that this formula is a simplified version of how the NFIP estimates insurance rates.* ***Whom?*** • Post-FIRM structures in all flood zones • Pre-Firm structures in area of moderate to minimal flood hazard	***Based on,*** • Flood Zone • Occupancy • Construction • Contents location • Subjective consideration (e.g. public policy, political reasons, etc.) • Objective processes (e.g. comparison with amount needed to meet NFIP premium income targets, etc.) ***Whom?*** • For pre-FIRM Structures primarily located in SFHA where insurance purchase in mandatory • Certain Post-FIMR structures for which protective structural measures are under construction ***Fact:*** • Pre-FIRM Subsidized premium are 5 to 60% lower that their true flood risk

The average annual loss is estimated by adding up the probability weighted estimate (PELV) of damage amount (DELV) for each inundation depth possible within the structure (See damage exceedance probability function in Figure 14). The PELV value is based on the NFIP hydrologic and Hydraulic Analysis and the DELV (See Figure 14 left and center graphs) value is based on NFIP claims for similar inundation

depths, which means that actual damage is not computed. In addition, the NFIP uses factors such as, flood zone, occupancy, construction, number of floors, type of foundation and elevation relative to the BFE, to group buildings into classes to then determine the average annual loss for each class, meaning that damage is not computed for each household and hence individuals will pay sometimes higher or lower values compared to the cases in which individual flood risk was assessed. Moreover, FEMA considers that in their calculation of the estimated annual losses there is a high degree of uncertainty, reason why they increase the inundation levels (double them) for all depths less frequent than 0.2% annual probability of exceedance (National Research Council, 2015). This metric doesn't have a proper justification other than coping with the uncertainty of the method. Furthermore, it is Important to understand that FEMA's flood insurance pay-outs are capped at $250,000 and have multiple limits such as exclusion of basements in the insured property. The aforementioned facts implies that damages involving more than $250,000 have not been used to construct the damage curves and therefore the most critical real damages are not accounted (e.g. wealthy properties) in the methodology.

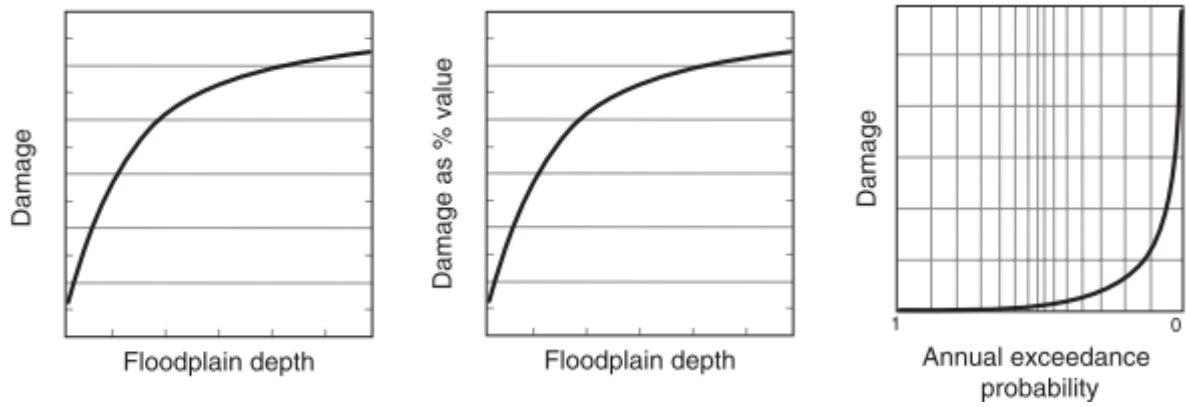

Figure 14. Damage functions Risk FEMA.
Left hand side image: Inundation depth-damage curve. Center image: Generic inundation depth-percent damage function scales by total value of the asset. Right hand side image: Damage – exceedance probability function. Source: (National Research Council, 2015)

To conclude this section on the preview of the NFIP program, is important to mention that insurance is available for both residential and commercial buildings and it can be purchased through representatives of FEMA or through the "Write Your Own Program" with a private insurer. Nevertheless, in the SFHA where is mandatory to buy insurance when the property is being bought through a federal regulated lending institution, lenders have been biased to believe that private insurance is not trustworthy, decreasing the participation of private parties in this process.

2.3.4 Discussion on NFIP setbacks in coastal cities prone to hurricane impact

As explained in section 2.3.2, the NFIP until know doesn't contemplate compound events to delineate floodplains in coastal cities. This issue makes under the author's opinion, that hazards in delta cities (especially those exposed to hurricane events) are highly underestimated and therefore, an increase in flood losses over time is observed due to either a poor management or a lack of regulations in the regions as it can be clearly seen in Figure 15 (in which also the development of the area has played an important role in the increase of damages over time). Likewise, as the floodplain maps produced by FEMA's NFIP are the primary tool to assess flood hazards and these maps are not the most accurate tool in coastal cities prone to hurricane events, this has led to a false sense of security for communities living outside the SFHA (Ray et. al., 2011a).

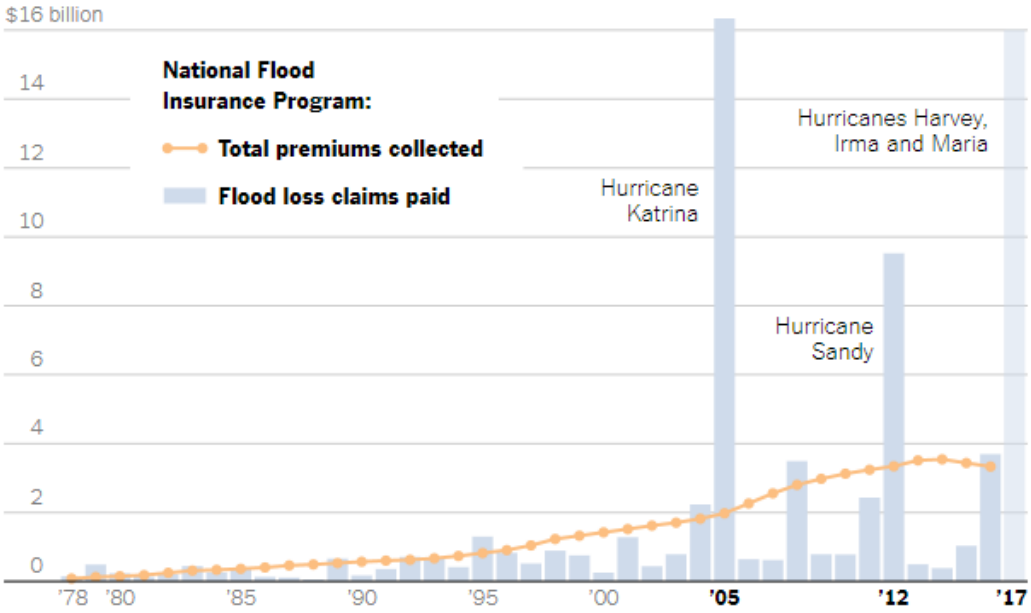

Figure 15. Flood loss claims paid and total premium insurance collected by the NFIP. The 2017 numbers are estimated values. The figure is reported in 2005 U.S Dollars. Source:(Williams, 2017)

The previous situation becomes even more relevant in places such as the Houston-Galveston Region which has been catalogued as the largest metropolitan region of the Gulf coast and the fifth largest city in the U.S (Sebastian, 2016). This area due to its close relationship with the Oil and Gas industry has been growing at a faster pace than any other region in the U.S. Additionally, there has been a cultural and governmental aversion to zoning policies, which has add up to the extensive development of the area. According to the Houston-Galveston area council, the population of the 8 main counties in 2016 was approximately 6.7 million people (H-GAC, 2017b). The previous number is expected to rise in 2.8 million by 2040, and by 2035 is estimated that 2.3 million people will reside within the coastal hurricane evacuation zones (Sebastian, 2016). This situation increases the exposure to risk and makes more crucial that the dynamics between storm surge and precipitation induced by tropical cyclones are understood in order to develop more sustainable and effective flood mitigation strategies. Besides, the Gulf coast region has 41% of all the flood insurance policies in the U.S, but they account for more than 80% of the claim pay-outs between 1978 and 2017 (Sebastian et al., 2017) making imperative to focus research efforts in this areas in order to make the NFIP more effective.

As it has been stated before, FEMA has been facing problems since Katrina flooded New Orleans in 2005. Until now, the NFIP is virtually the only source for flood insurance for more than five million households in the United States (Williams, 2017) and after Harvey hit Texas, the discussion was once again opened to

see if the program should be continued or not. Some of the criticisms or arguments that the NFIP has been facing over the years are:

- The main objective of the program has not been achieved; taking off the burden from taxpayers. This means that the program was created with the aim of collecting monetary funds from people continuously exposed to the hazard to decrease the amount that the government has to take from the National treasury to respond to flood emergencies
- The NFIP has enabled the construction in flood-prone coastlines, since the premium rates (Post-FIRM policies) are too low when compared to the true cost of building in these zones
- The generated floodplain maps are quickly becoming obsolete since they are a static tool that does not reflect new changes in the land use that could impact the estimation of the hazard itself. This means that urban development advances at a higher velocity than the updates on flood maps published by FEMA
- The program continues to reimburse residencies that are constantly inundating (e.g. case in Texas that has received $912,732 for 19 claims for repairs, when the value of the property is estimated at $42,024 (Williams, 2017)) which means there are not effective mitigation policies
- The program needs to assign subcontractors when floods of big magnitude occur to determine payments and normally this causes that claims of policyholders are often rejected, lengthening the entire process to receive the compensation
- FEMA has written until now more than 5 million policies but this doesn't come near to the number of households within the floodplains, so there is a lack of coverage in the most relevant zones

Discussion around the topic has agreed on the fact that the NFIP needs a major reform in order to cope with the new scenarios of more frequent storms and increased urban development. Proposals include not only providing more financial means (Debt relief), but also letting private companies to write flood insurance policies, stop giving coverage for post-FIRM buildings since essentially they should be designed as resilient structures, cut off the insurance for Severe Repetitive-Loss Properties (SRLP) since according to the Natural Resources Defense Council they account for more than 10% of the insurance claims. One alternative proposed for the SRLP, is that they are bought by the NFIP in order to relocate owners in safer locations, but this process involves other government agencies increasing substantially the complexity of the problem. In addition, there is also a discussion to change flood risk regulations into a range of possibilities instead of binary state (inside or outside the floodplain) as it is done at the present time. This will help to improve decision making in the area and people outside the floodplain could also identify the risks and be prepared in case a flood occurs.

A national study to see the economic effect of charging actuarially based premium rates for pre-Firm structures (PriceWaterHouseCoopers, 1999) concluded than from 1978 to 1996, 23% of the insured losses occurred outside the 100-year floodplain. A similar study from 1999 to 2009 estimated that the value increased to 25%, and that when the research was done for coastal jurisdictions, the value could easily escalate further (almost doubled to 47%) probably due to the sensitivity of the area to experience complex flood drivers and also to quick changes on the landscape that cannot be captured by the floodplain map updates carried out by the NFIP(Brody et al., 2013).

In 2009 and 2012 FEMA has gone through a series of transitions (Risk Map Program) that aimed to transform the mapping efforts and the flooding identification into a more integrated process in order to better address risk and implement mitigation strategies. This process involved the update of the flood risk maps to increase their accuracy and also the implementation of FEMA's community rating system which offers communities participating in the NFIP discounts of premium insurance in exchange for implementing mitigation activities (Brody et al., 2013) and although the strategies help in certain extent to understand more clearly the hazards, the maps still fail to recreate adequately flood conditions when there is a constant change in the development patterns and most importantly the fail to depict the flood hazard of compound events which are in most cases the worst case scenario for coastal cities.

2.4. Compound flooding

According to the IPCC special report on Managing the Risks of Extreme events and Disasters to Advance climate change adaptation(SREX) (Seneviratne et al., 2012), compound events (CE) in climate science are defined as:

> *"**(1)**Two or more extreme events occurring simultaneously or successively, **(2)** combinations of extreme events with underlying conditions that amplify the impact of the events, or **(3)** combination of events that are not themselves extremes but lead to an extreme event or impact when combined*"

A more recent general definition by Leonard et al. (2014), stated that *"A compound event is an extreme impact that depends on multiple statistically dependent variables or events"*, while during a compound event workshop held in Zurich on April 2017, the participants agreed on the following statement *"Compound weather or climate events refer to multiple drivers that combine to affect hazards contributing to societal or environmental risk"* (Eilander, 2017)

When referring to CE leading to flooding in coastal cities, the events are normally related to an increase in flooding levels due to sea level surge and precipitation-induced high river discharge as can be seen in Figure 16. The occurrence of extreme CE can be correlated due to a common external forcing factor that changes the probability of the two events (Regional warming, cyclones and hurricane formation, etc.), but also due to positive feedback processes between the events or actual conditional dependence between them (e.g. precipitation extremes and soil moisture levels).

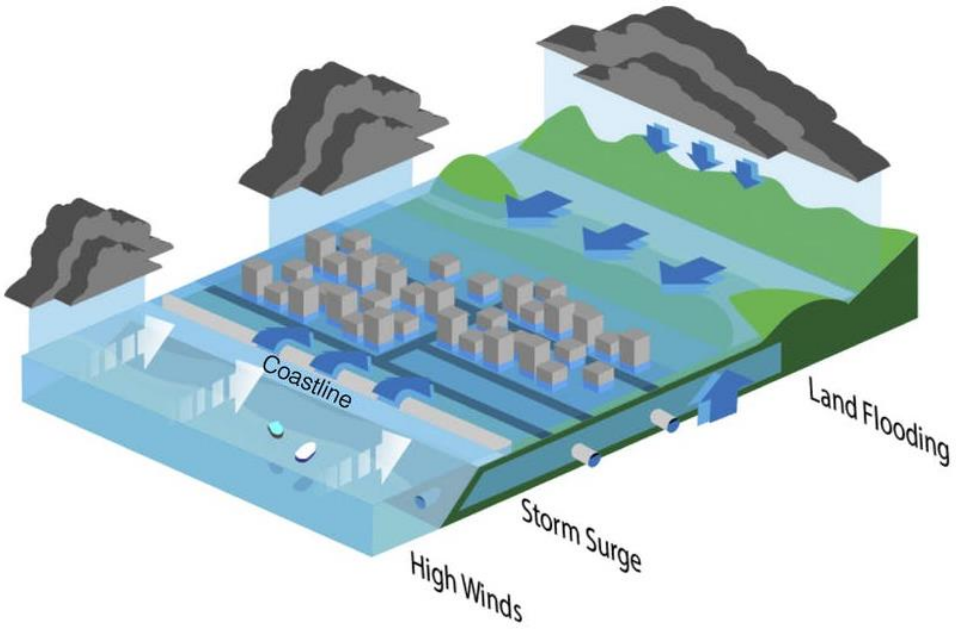

Figure 16. Compound flooding schematics. Source:(Wahl & Jain, 2015)

The complex relationship between storm surge and precipitation can increase the impacts of flooding in coastal zones through 3 general mechanisms (which gain or lose relevance according to the local watershed characteristics) according to (Wahl et al., 2015):

> *"**(1)** In estuarine regions, the joint occurrence of both events may elevate water levels to a point where flooding is initiated or its impacts exacerbated, **(2)** When a destructive storm surge already causes widespread flooding, such that any significant rainfall on top of this — even if it is not an extreme event on its own — increases the flood depth and/or extent of the inundated area, or **(3)** when a moderate storm surge occurs which does not directly cause flooding, but is high enough to*

fully block or slow down gravity fed storm water drainage, such that precipitation in more likely to cause flooding"

In some coastal regions of the world, tropical cyclones (as stated before) are one of the main external forcing factors for triggering compound events. As stated by the IPCC SREX report (Seneviratne et al., 2012) each year around 90 tropical cyclones (TCs) occur around the globe. Moreover, IPCC findings state that is likely that the TCs rainfall rates will increase with greenhouse warming and is also expected that the TCs maximum wind speed will follow the same trend, increasing implicitly the possible storm surge levels at the bays also due to the trend of sea level rise (SLR). In addition, it was also found that is more likely that the frequency of the most intense storms will increase substantially in some ocean basins. All of these facts and possible combination of scenarios make that estimation of compound flooding becomes a relevant discussion since it highlights the importance of shifting from a univariate flood condition to a more realistic approach in deltaic regions which takes into account the complexity of the flooding mechanisms in the area. The understanding of compound flooding will allow a better representation of what in some regions can be the "worst case" flooding scenario (see Figure 17) in determined seasons of the year, and it can help to adequately determine the hazards and risks associated with this type of events improving the flood risk management strategies for low lying deltaic areas.

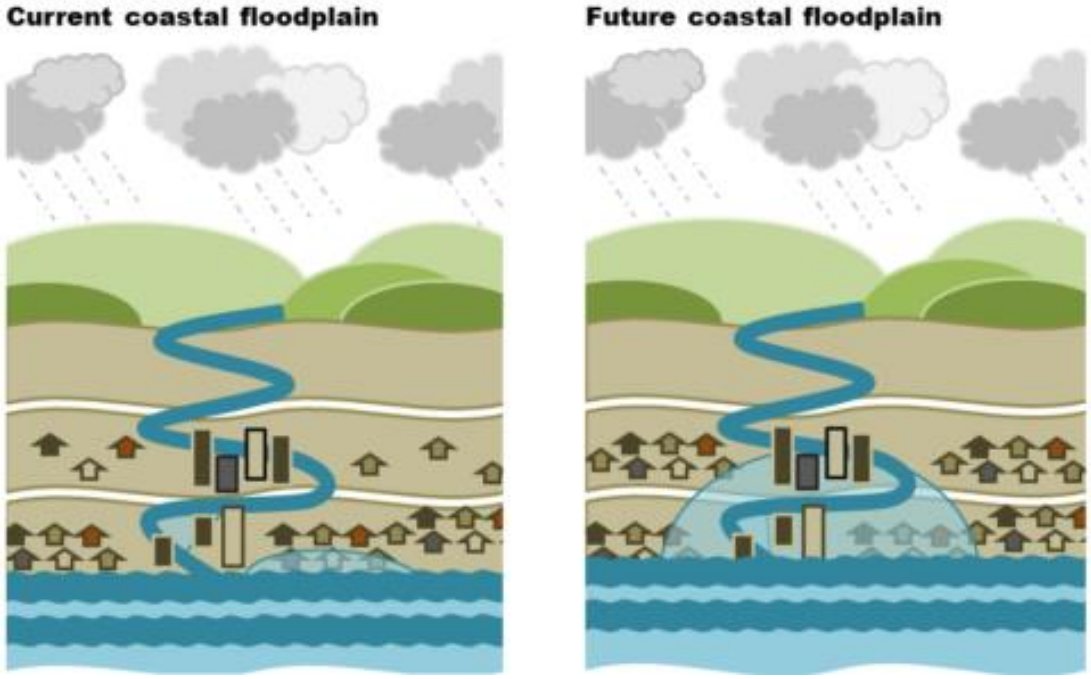

Figure 17. Current and future flooding: interaction between rainfall - storm surge and urbanization. Source: (Sebastian, 2016)

For this M.Sc. Research, the definition that is going to be adopted regarding compound flooding is the one generated by mechanism number 1 in which both storm surge and precipitation happen at the same time or in close succession exacerbating the impacts of flooding. This definition is going to be adopted since the study case for this research includes a region that is exposed to hurricane impact; a well-known phenomenon that is associated with extreme wind occurrence, but also with co-occurrence of storm-surge[2] and extreme rainfall causing a tremendous impact in terms of damages and loss of life. In addition, the specific watershed that is being analyzed in this research has characteristics (such as topography, land use, soil composition, etc.) that make that the response of the catchment is almost immediate, reason why mechanism 1 seems the most appropriate case to analyze in the region.

2 "Storm surge is the abnormal rise in seawater during a storm, measured as the height of water above the normal predicted astronomical tide. The amplitude of the surge depends on orientation of the coastline with respect of the storm track, storm intensity, size, speed and local bathymetry."(NOAA, 2017)

2.4.1 Compound flooding in the Galveston Bay

Focusing on the U.S Gulf coast, specifically in the state of Texas; according to the National Oceanic and Atmospheric administration (NOAA) approximately 64 hurricanes have hit the area since 1851 (Jones, 2017) and 20 of them have been catalogued as major hurricanes (between category 3 and 4) including hurricane Harvey in 2017. This represents 22% of the total recorded hurricanes in the U.S history since 1851, making Texas one of the most vulnerable states regarding this type of events. Hurricanes along the U.S gulf coast region have claimed the lives of approximately 15.000 people and damages rise up to more than 10's of billions of dollars (Ray et al., 2011a).

In the case of U.S coastal cities, 40% of the total U.S population resides in these areas (Wahl et al., 2015), making them densely populated and in most of the cases with a high degree of urbanization and development. The previous description is the case of the Galveston bay (see Figure 18), which is a low lying-coastal area that in addition is generally more susceptible to experience multiple flood drivers such as storm surge and precipitation (Brody et. al., 2013). In this context, the estimation of flood risk results quite complex due to the combined effects of the previously mentioned flood drivers, given the fact that a combination (not necessarily of extreme events in each category) often results in extreme impact (due to value of the assets exposed) when compared to a single variable flooding (Moftakhari et al., 2017). Moreover, it has been found that in small catchments where the response (rainfall-runoff) of the system is almost immediate (Case of the water system in the Clear Creek catchment), the joint occurrence of storm surge and discharge is more likely to happen (Klerk et. al., 2015), signalizing that the joint event has to be considered when determining hazards and risks in the area.

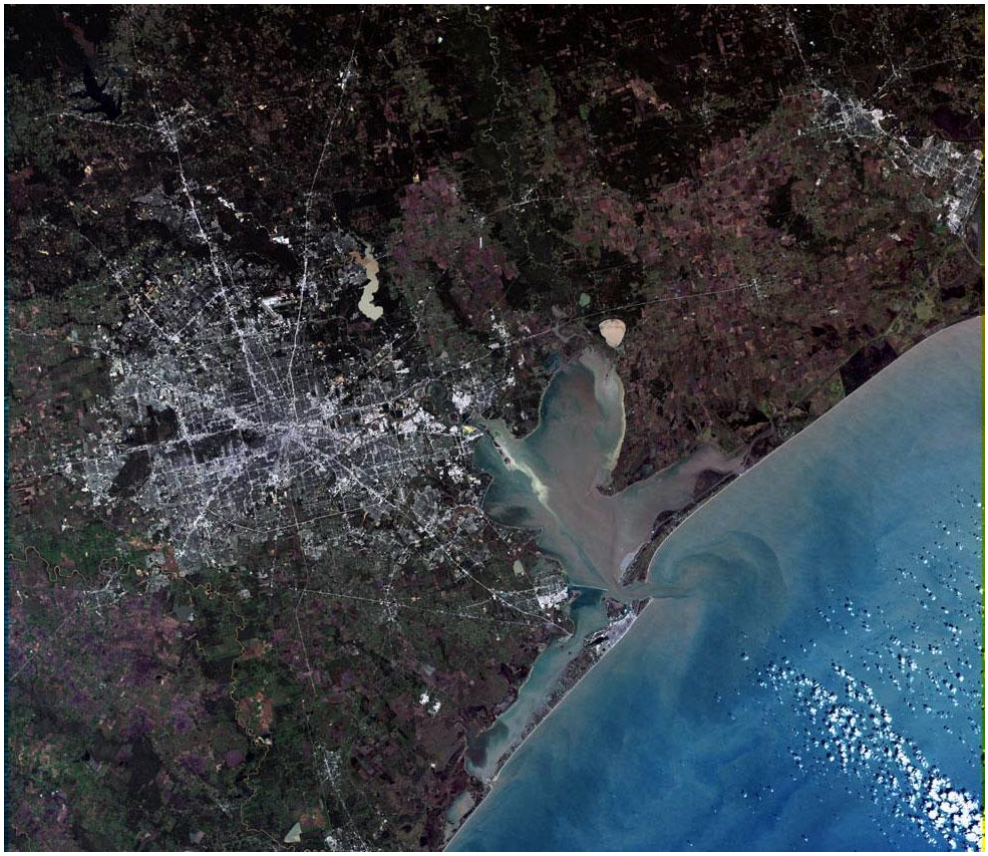

Figure 18. Galveston Bay Landsat Image. Source:(USGS, 2006)

Only taking into account the hurricanes making landfall in the latest century near the Galveston region, this area has suffered due to "The Galveston hurricane" what has been catalogued as the worst natural disaster in the United States in terms of fatalities (8.000 casualties- see Figure 20). Additionally, according to the Texas hurricane history (Roth, 2010), hurricanes such as Debra (1959) producing damages near the $6.7million, hurricane Claudette (1979) causing 15.000 homes to be flooded, hurricane Alicia (1983)

producing over $3 billion in losses, Allison (1989) topping $500 million in damages, and hurricanes Frances (1998), tropical storm Allison (2001), Ike (2008) and recently Harvey (2017) with damages of $10 million, $5 billion, $29 billion and $125 billion and 88 casualties respectively, have continuously affected the region and will with high probability continue to produce increasing damages since the value of the assets in the area is continuously increasing as a result of socio-economic development.

When speaking about tropical cyclones or hurricanes, storm surge is often the deadliest aspect of the phenomenon. Nevertheless, depending on the response of the system and the residence time of water in the watershed, often when there is a hurricane there are "compounding effects of ocean flooding – surge – and terrestrial flooding" according to Amir AghaKouchak (Professor at the University of California, Irvine) in an interview with The Washington Post (Harvey, 2017). Looking into the most recent hurricanes making landfall on Texas, in the case of hurricane Ike, (see Figure 21), the overall effect of the storm surge was greater than the effect of the precipitation (Berg, 2009), creating the 2nd mechanism of compound flooding described in the previous section, while tropical storm Allison (Figure 19) and hurricane Harvey (Figure 22) triggered a dominant precipitation over the storm surge, which coincides more with the definition of the 3rd mechanism of compound flooding. In the case of Harvey, the actual sea surge was about 0.91 meters but the actual water surge was approximately 2.7 meters due to the amount of rainfall falling in the area in short time (Fischetti, 2017).

Figure 19. Flooding in Tropical storm Allison 2001. Source:(Harris County Flood Control District, 2016)

Figure 20. Illustration of the Galveston hurricane. Source: (Kurz & Allison, 1900)

Figure 21. Hurricane Ike making landfall in Galveston island. Source:(Phillip, 2016)

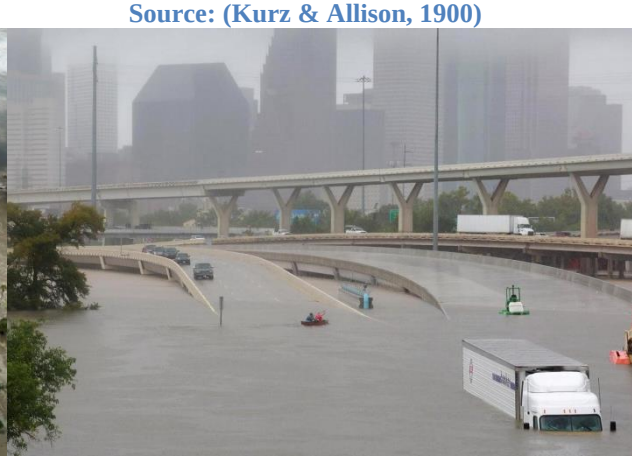

Figure 22. Hurricane Harvey flooding in the Interstate Highway 45. Source: (Carson, 2017)

A research carried out in the U.S (Wahl et al., 2015) found that actually the Atlantic/Gulf coast of the country (where Galveston in located) presents a higher risk of compound flooding than the pacific coast. The study provides evidence that the number of compound events has increased over the last century, pointing out the importance of revaluating the way in which risk and delineation of floodplains has been estimated in

the U.S. With respect to the Galveston Bay, all the previously mentioned evidence is exacerbated since due to the bathymetry and characteristics of the basin (Shallow and sloping coastline), the zone provides the natural conditions for storm surge to develop easily when compared to other locations. Besides this, recent research to understand the attribution of extreme rainfall from hurricane Harvey (Van Oldenborgh et al., 2017) has found that global warming (caused by anthropogenic greenhouse gas emissions) made the precipitation 15% more intense and that extreme precipitation events along the Gulf coast are indeed on the rise. These situations combined with the flat topography of Galveston, subsidence due to oil and gas extraction, soils with slow infiltration rates, SLR and continuous erosion of the barrier island makes that inundations due to storm surge and precipitation in the area are more prone to happen (Ray et al., 2011a). As a result of the previously mentioned facts, is highly important to quantify properly the probability of compound flooding in Galveston in order to properly mitigate the risks.

2.4.2 Main methodologies used to address compound events in coastal areas

Different methods to express the joint probability of storm surge and associated rainfall as a response of TCs or other CE drivers have been developed in the previous years in order to improve the risk estimation in coastal areas susceptible to this type of events. In the following section an overview of the methodologies is going to be explained as well and some limitations and shortcomings of each approach.

2.4.2.1 Surrogate modelling of joint flood risk

The study developed by Bass & Bedient (2018) made use of a surrogate model in order to represent peak inundation levels due to the joint occurrence of storm surge and rainfall produced by TCs. A surrogate model was chosen for the research, since they are computational efficient models that can approximate the multivariate input or output behavior of a complex system, based on a limited set of computational expensive simulations (Faculty of Engineering and Architecture - Ghent University, 2018). In the case of the research, the surrogate model was based on supervised machine learning and the computational high-fidelity simulations were taking from ADCIRC +SWAN for storm surge and waves and they were coupled with a hydrological and hydraulic model to represent the TC rainfall-runoff relations as it can be seen in Figure 23. The surrogate model itself requires the basic landfall TC characteristics (minimal central pressure (C_p), radius to maximum winds (R_{max}), 6-hour forwards speed (V_f), angle of approach (*from due north* θ_l) and landfall location (*longitude- lon*)) in order to make an approximation of the peak joint flood levels. The landfall characteristics were obtained from 223 synthetics wind and pressure-fields developed for FEMA and they include the full range of TC storms that could impact the north Texas coast (Bass & Bedient, 2018).

The supervised machine learning methods implemented to train the surrogate model were Artificial Neural Networks (ANN) and Kriging, for which regarding the joint flooding, Kriging proved to be more accurate than ANN since the estimation of flooding levels in Kriging directly takes into account the spatial structure of each storm floodplain by considering the covariance of input training features and flood response (Bass & Bedient, 2018). With the training of the surrogate model and the hurricane landfall characteristics, the model was able to return water levels for a determined storm within a few seconds which presented great advantages in terms of computational time.

Some of the limitations of the project were the uncertainty of the precipitation model, since the model used allows capturing broad scale TC rainfall and its asymmetric distribution, but it fails to represent other precipitation events such as rainfall produced by convection within the eyewall of TC or mesoscale rainfall bands[3]. Another limitation is that the hydraulic model used was a 1D model, making that the representation of flow direction and inundation levels less accurate than when using a 2D model. Finally, the wind speeds included in the input of the surrogate model only included values higher than 29.8m/s leaving out slow moving tropical storms that can result in sudden downpour like the ones seen in Allison (2001) and Harvey (2017). Nonetheless, given the explained limitations, the results showed an increase in risk in the Texas area when the compound effect of storm surge and precipitation is taken into account, showing that indeed a joint event analysis is needed when analyzing the flood risk in coastal areas prone to TC.

3 Mesoscale Rain bands (5 – 50km in average width) have been found in extratropical Cyclones according to studies developed by (Houze, Hobbs, Biswas, & Davis, 1976)

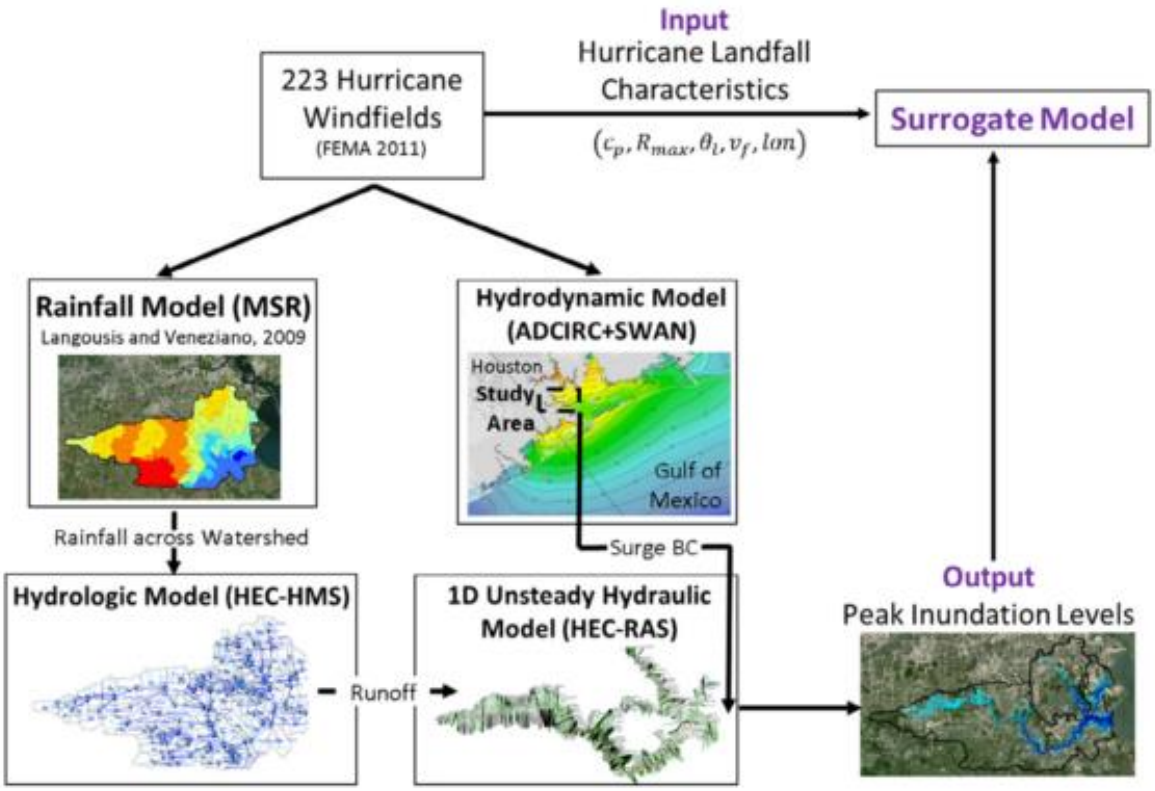

Figure 23. Coupled numerical models and input data utilized to train the surrogate model. Source: (Bass & Bedient, 2018)

2.4.2.2 Copulas and Bivariate dependence Analysis

A bivariate dependence analysis between river flow and coastal water level was proposed by Moftakhari et al. (2017) with the aim of characterizing flood hazards if there are compound effects. The study focus more in Sea Level Rise (SLR) effect rather than in storm surges since SLR is one of the trending effects of anthropogenic global warming that will increase the frequency of flood events in coastal cities. The research focused in the United States due to the fact that 8 out of the 20 most vulnerable cities in the world regarding annual losses due to flooding are located in this country (Hallegatte et. al., 2013).

The bivariate analysis used as data the largest freshwater inflow to the lower estuary and its corresponding largest observed hourly water level (WL) within ±1day. For the construction of the bivariate model, copulas were used to represent the joint dynamics of both variables.

In order the explain dependence between variables, copulas represent an advantage against traditional bivariate methods in the sense that they are not restricted to assume the same parametric family of univariate distributions for both of the individual variables contemplated in the analysis (Genest & Favre, 2007). This is essential in the analysis since it represents better the nature of each variable and therefore the joint behavior can be explained more accurately. The definition of a copula is a distribution on the unit square with uniform marginal distributions. If the case is restricted to a bivariate analysis, Sklar (1959) theorem dictates that random variables X and Y are joined by copula C, if their joint distribution $F_{XY}(x, y)$ can be written as:

$$F_{XY}(x, y) = C(F_X(x), F_Y(y)) \qquad \textbf{(2.4.1)}$$

Where $F_X(x)$ and $F_Y(y)$ are the marginal distributions and $C:[0,1]^2 \rightarrow [0,1]$ represents the copula. This means that there is always a unique copula that corresponds to a given continuous joint distribution. Due to their mathematical definition, copulas are highly flexible when compared with other methods and they are in most of the cases computational feasible (taking into account that as dimensionality

grows, dealing with copulas can become substantially more challenging) making them an attractive tool to model the joint behavior of natural hydrological variables.

In this specific case of Compound effects of sea level and discharge, 24 copulas were fitted to the data from 5 different families (Archimedean, Elliptical, Extreme value, Farlie-Gumbel-Morgenstern and Plackett). These copulas were tested using non-parametric Goodness-of-Fit tests and were compared between each other by means of the Akaike Criterion[4] in order to select the best copula describing the data.

In this case, the compound effect of the two described variables may result in hazardous occurrences, even though none of the single variables have extreme values. This approach is commonly known as OR analysis in which is enough that only one of the variables is large enough to produce damage and not necessarily both of them; the approach was implemented by delineating some Hazard scenarios (HSs) regions in the joint distribution of the variables as it can be seen in Figure 23.This was a key item in the study since it approaches the natural dynamics of coastal flooding.

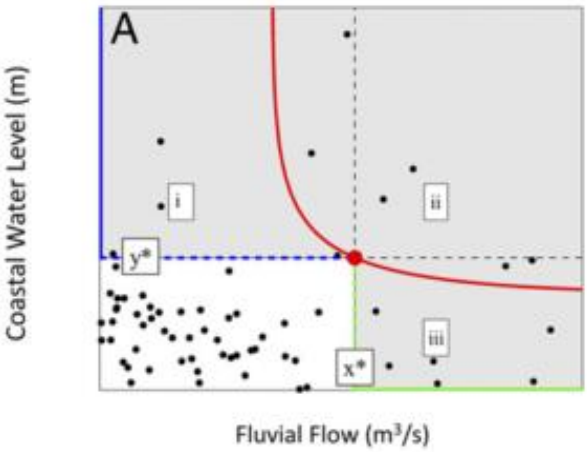

Figure 24. Bivariate Hazard Scenarios. Source: (Moftakhari et al., 2017)

With the best fitted copula and the HSs delineation, the return periods for the bivariate joint distribution could be computed. Afterwards, the failure probability was calculated as the probability of an event lying in a specific HS region at least once in a given lifetime. The results showed that when a Bivariate analysis is taken into account, the probabilities of failure increased if compares to a univariate analysis (only coastal or only fluvial). Another conclusion was that if SLR was taken into account, the failure probability for the same return period increased even more, showing that given the actual trend of increasing sea water levels due to climate change, a bivariate approach assuming dependency is the most appropriate methodology to assess impact of coastal cities.

In addition to the research carried out by (Moftakhari et al., 2017), there are other studies that have used Copulas and Bivariate analysis to determine the likelihood of compound events when dependency between flood drivers is taken into account. Studies like the one performed for flood analysis in Ravenna, Italy (Bevacqua et. al., 2017) showed that ignoring the dependency between sea and river levels lead to an underestimation of risk (higher return periods were obtained if independency was assumed). In this project Pair-Copula-constrictions (PCCs) were used for modelling multivariate dependencies since not only the two main variables were analyzed (Sea and River levels) but also some meteorological predictors that influenced the main variables were included as well. Similar results were obtained in an analysis in Fuzhou City, China (Lian et. al., 2013) where the Gumbel Copula presented the best fit to the joint distribution of rainfall and tidal level and in which the effect of working pumps in decreasing flood impact was analyzed in the case of CE flooding. Applications regarding bivariate analysis include a research carried out for the Australian Coast (Zheng et. al., 2013) in which a bivariate logistic threshold-excess (BLTE) model was used to analyze the dependency between rainfall and storm surge events. The results once again showed significant dependency even though when the distance between tide and precipitation gauges was in the order of hundred ok kilometers. The previous finding indicates that the correlation itself exists due to the large scale meteorological forcings affecting the entire area. According to the methodology described by Zheng et al. (2013),the BLTE implemented in the study is equivalent to an approach using Copulas. The main difference between approaches lies in how the margins are estimated; in the case of BLTE the margins are assumed as standard Fréchet, while in Copulas the margins are transformed to the unit Hypercube via the cumulative distribution function (CDF).

4 The Akaike information Criterion (AIC) is a technique based on sample fit to estimate the likelihood of a model to predict future values. (Arabnia & Quoc Nam, 2015)

2.4.2.3 Non- Parametric Bayesian Networks (NPBN)

Bayesian networks (BY) are graphical probabilistic methods that can express the joint distribution of multiple variables. The BN consists of directed acyclic graphs and a set of conditional distributions. Variables in the BN are represented by nodes while arcs connecting nodes represent a direct qualitative dependence relationship (Hanea et. al., 2015) between the variables. If certain node has no predecessors it is known as a parent node, while a predecessor is known as child. For each parent node a marginal distribution has to be specified and for each child an association with a conditional distribution has to be made. Traditional applications of BNs make use of discrete random variables, while many of the engineering applications require the joint behavior of continuous variables. To cope with this limitation, the NPBN was proposed as an alternative to deal with continuous data.

NPBN differ from normal BNs in the fact that there is not an assignment of a marginal distribution and the arcs are characterized by one-parameter copula, parametrized by Spearman's rank correlations (Hanea et al., 2015). This means that each node is represented by its empirical distribution and the dependence between parameters is determined only by the copula of one parameter. This type of BNs has multiple advantages since they can capture non-linear behavior and the graphical representation is explicit and visible for the user, which is not necessarily the case with regression methods. NPBN require that the chosen copula has the zero-independence property; this means a copula in which zero-correlation means independence. This property is needed since it allows assigning additional conditional independence statements that are not necessarily represented in the graphical arrangements and it allows the network to run faster.

Regarding the application of NPBN to compound flooding, a model was built based on Gaussian Copulas to model hydraulic boundary conditions for hurricane flood risk analysis in the Clear Creek watershed (Sebastian et al., 2017). In this specific study the flooding levels due to compound effects were not studied, but instead the dependency between the variables was analyzed. The NPBN was used to generate a group of synthetic TCs which were then used in an empirical wind setup model to simulate different storms in the Galveston bay and finally use the combination of storm surge and precipitation to make an estimation of the joint exceedance probabilities in the region (Sebastian et al., 2017). The NPBN constructed for the research can be seen in Figure 25 where the conditional rank correlations can be seen in the arcs, whereas in the nodes the histograms showing the distribution of each of the variables can be observed. In order to use the wind set-up model the NPBN needed to be conditioned to a fix angle of approach to the bay due a configuration of the program.

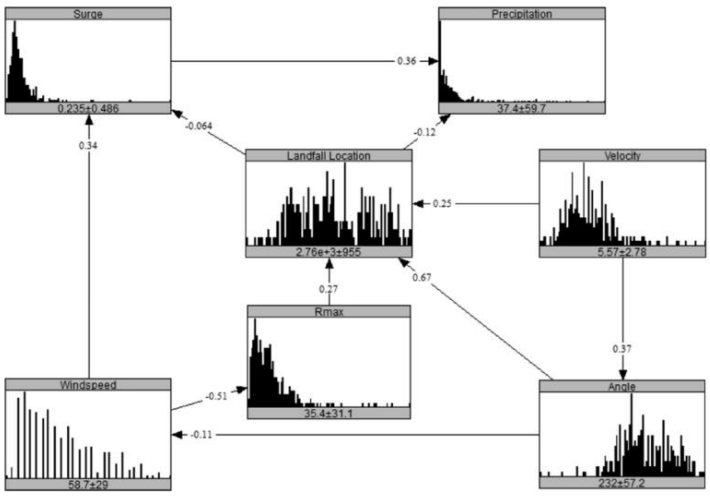

Figure 25. BN structure for TCs in Galveston Bay Region. Source: (Sebastian et al., 2017)

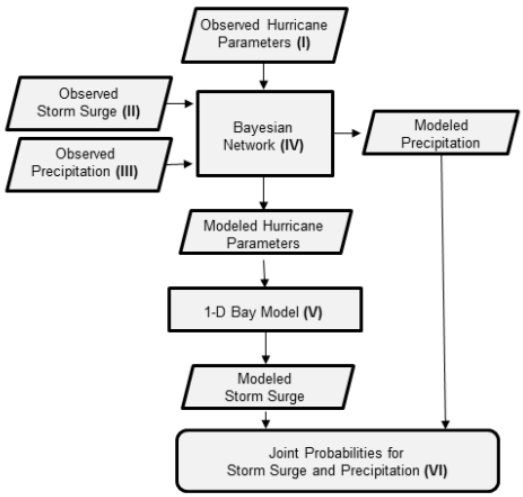

Figure 26. Work flow for joint exceedance probabilities. Source:(Sebastian, 2016)

The wind set-up model tracks the synthetic TC's created by the NPBN along a perpendicular trajectory through the coast taking into account a parametric wind filed built from the main characteristics of the hurricane itself. The storm surge at the coast is determined by solving the 1-D depth integrated SWE and then this value is translated to a storm surge within the bay by means of a parametric equation relating surge

and wind set-up. With the previous sea water levels, the joint probability can be computed using the cumulative precipitation in the area. This gives the first estimation of compound events in the Clear Creek watershed and determines the hydraulic boundaries that could be used in a hydraulic model to analyze flooding due to CE in a low-lying coastal watershed draining into a semi-enclosed tidal bay (Sebastian et al., 2017).The diagram process of the study can be observed in Figure 26.

Some of the limitations of the study were that the storm surge in the low frequency area was underestimated; this is partly due to uncertainty in historical data, change in topographic conditions and accumulated errors due to general assumptions used in the models (Selection of Gaussian copula, main variables selected for characterizing a TC, assumption for landfall direction). An additional improvement recommended in the study was to incorporate the relation between intensity and timing of rainfall to the one from storm surge since this will contribute to a worst cases scenario flood for the watershed.

2.4.2.4 Dynamic Modelling and Global Coupled Models

Dynamic models represent the behavior of a certain variable overt time. In the case of compound flooding, the variable that is being analyzed is the inundation levels over time in a specific watershed due to the combined effect of storm surge and precipitation. This type of modelling has been already introduced for a Texas coastal floodplain (Ray et al., 2011a) in which a HEC-RAS[5] 1-D model was run for both steady and unsteady states to study the effect on flood plains if CE were taken into account. The model was specifically run with data from hurricane Ike (2008) in the Horsepen Bayou near the Galveston bay.

The unsteady state model was run in order to capture the time-dependent nature of rainfall and storm surge, while the steady state was used to combine different scenarios contemplating design rainfall and storm surge levels to delineate floodplains in each one of the cases. The study took previously implemented hydrologic (TSARP HEC-HMS) and Hydraulic (TSARP HEC-RAS) models for the regions and made certain updates to be able to run the available HEC-RAS model in unsteady state. The HEC-HMS model was calibrated using tropical storm Allison (2001) and the 10-year and 100-year peak channels flows were extracted from this model to set them as input for the HEC-RAS hydraulic model. In the latest mentioned model, the storm surge was modeled as a downstream boundary condition that could vary from 0 to 6.10 meters according to the range of storm surge registered in the Galveston Bay. With the previous input and the rainfall fall estimation a backwater calculation was run to find the floodplain scenarios for the 10 and 100-year storms. The model and its different scenarios showed that in fact a large surge could influence and control the floodplain more than the rainfall itself; therefore, in order to evaluate flood risks in coastal communities is highly important to take into account the effect of CE in order to implement adequate floodplain management strategies.

The unsteady case was run afterwards to allow the dynamic input of rainfall and storm surge in the model. This allowed a more accurate representation to the hurricane data (Ike) and a better approach than the steady state to represent the dynamics of CE. This type of model showed a potential to be implemented as a predictive tool for flooding in deltaic areas based on meteorological and surge predictions. The late application could serve to predict rainfall-surge levels that could aid in the implementation of emergency plans in the regions. Future improvements for the results obtained with the dynamic 1-D modelling will consist on implementation on a 2-D model to incorporate better the effect of topography on the floodplain delineation during CE.

In addition to this study, another 1-D steady state hydraulic model has been implemented in order to analyze the influence of compound events on flooding in the downstream reach of the Houston Ship Channel (HSC) (Liu, 2017). The result of this study underestimate the influence of CE in the HSC due to assumptions made on the boundary conditions and inaccuracies of the hydraulic model, but following some recommendations and improvements, the effect of CE could be potentially estimated in the HSC and most importantly, the effectiveness of measures proposed to reduce the impact of storm surge in the area (Storm surge barrier near Fred Hartman Bridge proposed by the SSPEED center) could be evaluated.

5 HEC-RAS is a hydraulic model developed by the US Army Corp of Engineers that calculates the water depth in river cross sections given a flow rate input. (Ray et al., 2011a)

Most of the previously described methods used to model the compound risks of having fluvial and coastal flooding affecting simultaneously a watershed, have been limited to applications at small scales. Due to this limitation and the necessity to evaluate the impact at a large scale, a global couple river-coast flood model has been proposed (Ikeuchi et al., 2017) and its applicability has been tested in Asian mega delta regions.

The research focused in mega-deltas since in these areas more than 500 million people are settled and therefore the impacts area magnified when compared to other coastal smaller regions. The southeast of Asia was of interest since this zone is highly prone to heavy precipitation from the monsoon season and also cyclones could enhance the probability of significant storm surge at the coast. Moreover, global flood projections indicate that this phenome will increase in this region due to impacts of climate change and socio-economic development (Winsemius et al., 2016).

The methodology coupled the global river routing model (Catchment-bases Macro scale Floodplain model CaMa-Flood) with the global tide and surge reanalysis(GTSR) data set (Ikeuchi et al., 2017). The river model integrates the runoff generated from a Land-surface model along the river network to obtain the flood inundation levels and area, whereas the GTSR calculates surge by forcing the atmospheric pressure and wind speed and it superimposes the data with tide levels calculation. In this case each river mouth cell in the CaMa-Flood model was connected to the nearest output of the GTSR model (Ikeuchi et al., 2017) and the effect of storm surge on rivers was studied in detail for the Ganges-Brahmaputra-Meghna delta. The results showed that inundation levels increased considerably at the mouth of the river (>3m surge) and flooding depths could increase even 0.7m at a distance of approx. 200km inland from the river mouth when surge effect is taken into account. This again reflected the importance of assessing CE in deltaic regions since their effect could be potentially more devastating than when either of the events occurs individually.

Some of the limitation of the coupled global system included the fact that water flow via artificial canals or small channels cannot be modeled and this can reduce the impact of the storm surge. In addition, the GTSR doesn’t take into account the non-linear effect between tides and surge which has been proven to cause significant increase in sea levels, again underestimating flood level at the coast in certain regions. Finally, global bathymetry data has also a great deal of uncertainty and errors which affect the ultimate result of the coupled model.

2.5. Research gap selection

In the previous section an overview of the methodologies implemented until now to model compound flooding have been addressed briefly. It is clear that there is still a lot of research that needs to be done regarding compound flooding and that the topic is becoming each day more relevant for coastal cities given the predicted scenarios for climate change.

Focusing specifically in the Clear Creek watershed, it was seen that several studies focused on determining the boundary conditions of precipitation and storm surge in order to analyze the effect of compound flooding in the catchment (Sebastian et al., 2017). Initial use of some of these "compound events" in the area have been tested by means of a 1D model (see Ray et al. (2011b) & Sebastian, (2016)) and results show that in fact compound flooding should be included for the delineation of the flood hazard zones since not doing so will underestimate flooding extents.

In this M.Sc. thesis, the research gap that is going to be addressed is the use of a two-dimensional (2D) model to improve the results for dynamic modeling of compound events (Ray et. al., 2011b), which as mentioned before in its current state-of-the art method, uses a simplified HEC-RAS 1-D model to compute the effect on flooding extent due to storm surge and precipitation in coastal areas. The 1-D steady state hydraulic model used by Ray et al.(2011b) considers the storm surge as a static boundary condition that is changed in every single run to see the backwater effect in the watershed each time the downstream water level is changed. The result from this model shows already that there is an effect on the floodplain delineation if storm surge is considered together with the rainfall estimates. Some improvements to the model have been made by running the HEC-RAS model in an unsteady-state but further enhancement will mainly consist in translating the model to a 2-D version since this will allow incorporating the time dependent variability between storm surge and precipitation besides the fact that the overland flow will be better represented, reason why a 2-D model has be chosen in order to simulate compound flooding for this this research project

This approach presents an advantage towards the current method, since 2D finite difference and finite-element models (FEMs) could cope with some of the limitations of 1-D models. Such limitations include the fact than for instance in 1D hydraulic models, flow is assumed to be along the length of the stream and perpendicular to channel cross sections. This assumption underestimates or leaves out local ponding and flooding outside of the main channel potentially caused by small variations in both topography and LULC, causing that the predicted extent of the floodplain contains large inaccuracies. This is the particular case along the Gulf coast, in which there is little topographic relief and small changes in the water surface profile can lead to large errors in the estimation of the floodplain extent (Blessing et al., 2017), in addition the conventional methods make use of lumped hydrologic models (HEC-HMS) that average soil, LULC and topographical characteristics over large spatial areas which results in the loss of local variability in the runoff estimates at the watershed scale.

Studies have suggested that in order to cope with the limitations of lumped models , fully distributed hydrological models are an alternative when there is high resolution spatial data available (Ray et al., 2011a). These models capture more effectively the extent of floodplains, but most of them are only suitable to simulate rainfall-runoff and therefore are only suitable for precipitation based flooding (e.g. *Vflo* Hydrological modeling software) and not storm surge (Blessing et al., 2017). As a consequence, there is still the need of a 2-D model who could also include spatially distributed input for inland flooding, but that could also include the effects of storm surge and wind-setup on the coast in order to represent more accurately compound events in coastal watersheds.

One of the main concerns in the use of 2-D models instead of 1-D models is the increase in computational costs, which sometimes becomes so expensive that the accuracy obtained doesn't justify the investment. Therefore there is also the need for a fast computational 2-D model who balances accuracy and efficiency. Advanced 2D and 3D models for coastal (ADCRIC, SWASH, SWAN, etc.) and inland flooding (HEC-RAS, SOBEK) are available in the market, but just few of them can compute the joint effect (Delft 3D, D-Flow FM, MIKE 21/3, SFINCS) of inland precipitation flooding and storm-surge flooding (See comparison between models in Table 15 of the Appendices section). Most of the previously mentioned Software's are

computational expensive when the resolution of the model is increased, nevertheless there is one of the aforementioned models (SFINCS) that could be used for compound flooding at a low computational costs since it was designed under a simplified version of the shallow water equations which reduced significantly the computational time required by the model.

The SFINCS model was initially thought as a 2-D simplified fast coastal model that could be potentially used for forecasting purposes and Early warning systems (EWS) in dissipative beaches[6] prone to wave driven inundation. The model has been adapted through the years to include as well inland flooding processes and as a consequence, SFINCS was the model selected for the study case proposed in this M.Sc. research as it is an attractive 2-D model that could be used to analyze compound flooding in the Galveston Bay, particularly in the Clear Creek watershed.

In the Appendices (Section 9.1), an overview of the SFINCS model is given including its assumptions, implementation, limitations and some study cases that have been already performed using this model. Is important to mention that the SFINCS model has not yet been made publicly available since is still considered by Deltares to be in a phase of improvements and development. Nevertheless, under the politics of the Company, the long –term plan is that this model becomes an Open Source Model.

Finally, based on the content of this chapter, is concluded that indeed there is an increase in flood hazard due to the interaction between rainfall-runoff and storm surge as compared to the current FEMAs NFIP estimated hazard (Bass & Bedient, 2018), reason why (and taking into account the history of catastrophes in the gulf coast region) is imperative to delineate new hazard areas that correspond to what today is known as the worst case scenario in locations where there is constant susceptibility to TCs, which often produce strong onshore wind and changes in the pressure field that trigger both extreme storm surge and high precipitation on the nearby catchments (Zheng et al., 2013). Is clear that in order to implement flood reduction strategies that are more effective including improvements to the actual National flood insurance program, is necessary not only to improve hazard estimates but also to move from a hazard to a risk approach in order to inform better the communities and prepare them in case a flood hazard materializes. This is the reason why creating risk maps for the Clear Creek watershed is a topic that needs to be explored and hence is part of the research gap that was found throughout the literature review of the present M.Sc. thesis.

6 Dissipative beaches are characterized as being high energy beaches with a wide surf zone. Source: (NIWA-Taihoro Nukurangi, 2016)

3

Case Study & Model Validation

In this chapter an introduction to the main case study is going to be presented in order to introduce the reader to the characteristics of the watershed being analyzed and to show the current drawbacks of the floodplain delineation in the area. In addition, a detailed description of the two last storms (Harvey and Ike) that have affected significantly the area is presented with the intention of showing two storms that triggered compound flooding in the area but which had different dominant flood drivers. Afterwards, using the aforementioned storm characteristics, the SFINCS model is going to be run and validated for these cases with the intention of showing that this 2D model can be used for compound flooding analysis.

3.1. The Clear Creek watershed – Background information

The Clear Creek watershed was selected for this research due to the fact that it has been already used in studies involving compound flooding (Sebastian et al., 2017). This watershed is situated at 32km from the south-east of the city of Houston, Texas on the west side of the Galveston Bay as it can be seen from (see Figure 27). The catchment encompasses portions of 4 Texas counties, including Fort Bend, Brazoria, Galveston and Harris and 17 cities are partially within the watershed boundaries. The main stream (Clear Creek) flows from west to east and it ends in the in the Clear Lake which is connected to the Galveston Bay. The Clear Creek is tidally influenced from its confluence with the Clear Lake. The watershed covers approximately 500 km^2 including the Armand Bayou which is the largest tributary of the primary waterway (Clear Creek). In general the Armand Bayou in considered a separate watershed but for this study is going to be considered as part of the Clear Creek watershed (see Figure 27). The development of the region has been historically concentrated near the Clear Lake and other small located in the upper and middle parts of the catchment. In 2010, the population was of 164,172 people (excluding the Armand Bayou population (Survey & Data, 2009))which represented a 39% increase compared to the last decade. Reports of the 1990's for the regional flood control plan (Dannenbaum Engineering Corporation, 1991) already gave estimates for 2020 that the population might increase up to 530,000 people.

Figure 27. Galveston Bay Satellite Image with location of the Clear Creek watershed. Green stars are tide measurement gauges.

3.1. The Clear Creek watershed – Background Information

According to an USACE (2012) public report, the Clear Creek watershed presents on its upstream end a fairly shallow floodplain, while on its path downstream the floodplain becomes narrower and deeper. The catchment itself has natural and man-made characteristics (depicted in the bullets below) that have increase the risk of flooding during storm events.

- The area has a flat topography which delays the drainage of water in the watershed: Elevations ranging from 23 m at the western end to less than 1.5m above mean sea level near the Clear Lake with a seaward slope of approximately 0.03%
- The soils composition of the catchment is dominantly dark coloured clayey and loamy soils with poor infiltration capacity and high runoff (Lake Charles Clay and Bernard Clay Loam (USDA, 2018b)
- Approximately 2/3 (up to 1991) of the main channel has been channelized which has led to an increase of the development of the area and therefore an increment of exposure and risk

Historical flooding in the area triggered some flood damage reduction projects in the area which were authorized in 1982 and which resulted in an outlet structure and a second outlet channel (as seen in Figure 28 to Figure 30) that were thought to maintain the water levels at the lake and to minimize changes of the hydraulic conditions between the bay and the lake. The gates do not provide tidal protection for the lake side, but on 2013 the HCFCD agreed on operating the structure to reduce flood levels mainly from rainfall runoff. In addition, projects such as the South Belt Storm Water detention Basin and the Mud Gully (Beamer Ditch) have been started to reduce flood risk and damages along this watershed. The projects are in phase of construction and design and haven't been fully completed (HCFCD, 2018b). All of the previously mentioned projects are part of the Clear Creek Federal Flood Damage Reduction Project in which the USACE is the lead agency.

Major flooding in the area normally has coincided with hurricane activity, being Tropical Storm "Claudette" the storm which triggered the projects along the watershed since it caused more than 5,000 structures to flood and generated total damages that exceeded $90 million (1982 present value estimation by USACE).

Figure 28. Second outlet Channel (Downstream outlet Clear Creek watershed) (USACE, 2012)

Figure 29. Second outlet channel structure view (USACE, 2012)

Figure 30. Second Outlet Structure (Gate). Source: (USACE, 2012)

Due to the fact that the watershed encompasses several counties (see Figure 31), different Flood Control Districts (FCD) function in the area such as the Harris county FCD, the Fort Bend County Drainage District, the Brazoria County District No.4 and the Clear Creek Drainage district. This situation makes that coordination between different agencies is crucial to approve new projects and accept new standards.

Studies developed from 1999 to 2009 in the Clear Creek watershed (see Figure 31) determined that development in exposed areas in the region resulted in property damage of $356 Million (only accounting for the insured losses) (Brody et al., 2013) due to flooding hazards. Moreover, 75% of the flood losses claimed during this period of time were associated to hurricane Ike (2008) and tropical storm Allison (2001), which were two proven events that caused storm surge and rainfall flooding across the Harris County and its surroundings (Harris County Flood Control District, 2018). In hurricane Ike the storm surge was stronger, making the coastal flooding more critical (Ike was associated with a slightly larger 100-year return period for compound flooding see Figure 82), while for storm Allison (associated with a return period smaller than 10 years for compound flooding see Figure 82), the generated precipitation was dominant causing higher damages in the inland areas of the watershed. From all the losses claimed during the study, more than 40% of them occurred outside of the 100-year floodplain delineated by FEMA (see Table 4). This is highly problematic since structures outside of this area are not subjected to any flood regulation even though some of them are only a couple of feet away from the SFHA. This generates also a shift in development towards these areas that still are at a hazardous location.

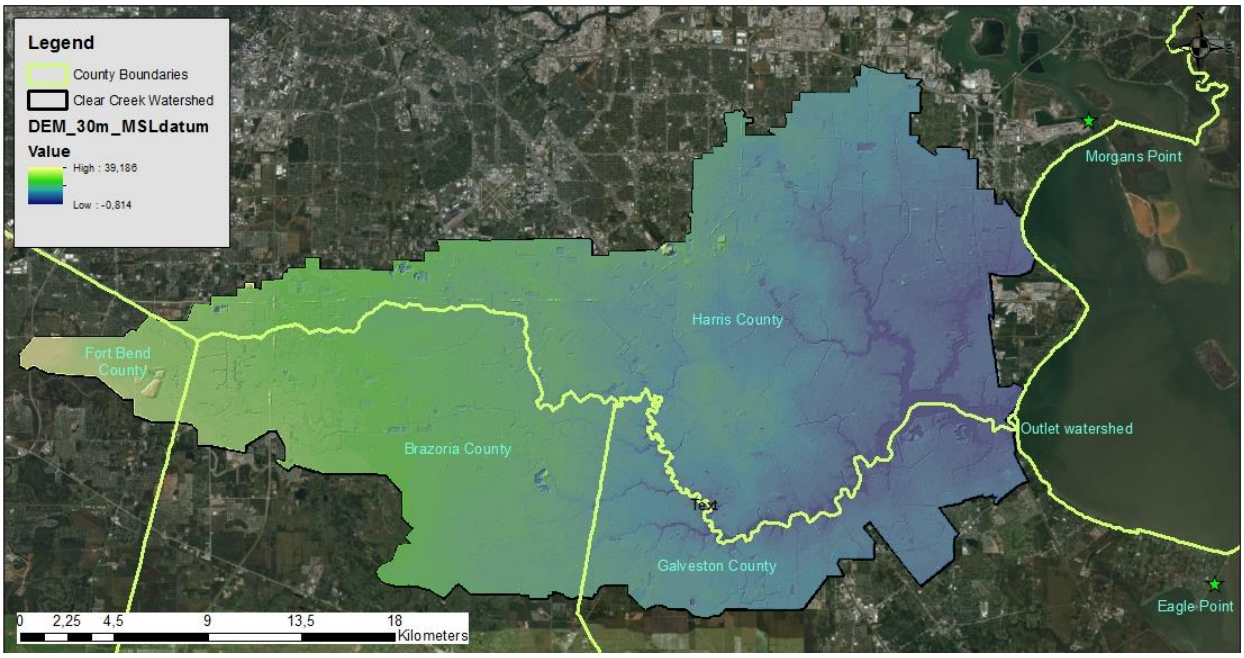

Figure 31. Digital Elevation Model of the Clear Creek.
30x30m resolution model of the Clear Creek watershed & location of tide gauges and county division

Table 4. Flood loss descriptive statistics as presented by Brody et al., (2013)

Descriptors	Claims (number)	Distance (ft) Floodplain	Content damage (U.S. dollars) Stream	Coast	Mean	Sum	Building damage (U.S. dollars) Mean	Sum	Total damage (U.S. dollars) Mean	Sum
All Claims	9,792	755	3,183	30,177	9,683	94,246,756	26,902	261,839,627	36,585	356,086,384
Inside Floodplain	4,427	0	3,422	25,604	13,184	58,090,334	34,999	154,209,886	48,184	212,300,221
Outside Floodplain	5,365	1,378	2,985	33,951	6,787	36,156,422	20,204	107,629,741	26,991	143,786,163
Hurricane Ike	4,241	604	2,689	15,650	10,998	46,206,425	32,442	136,289,984	43,441	182,496,410
Inside Floodplain	2,183	0	2,685	7,125	14,329	31,065,439	42,728	92,636,004	57,057	123,701,443
Outside Floodplain	2,058	1,245	2,695	24,694	7,447	15,140,986	21,472	43,653,980	28,920	58,794,967
Tropical Storm Allison	3,622	756	3,532	43,087	11,357	41,025,079	27,039	97,665,694	38,397	138,690,773
Inside Floodplain	1,585	0	4,165	46,168	15,341	24,269,810	33,119	52,394,319	48,460	76,664,129
Outside Floodplain	2,037	1,344	3,040	40,690	8,253	16,755,269	22,301	45,271,374	30,554	62,026,644

Note: Damage figures are in 2009 U.S. dollars.

Research like the one performed by Brody et al. (2013), concluded that the 100-Year floodplain is not enough to delineate flood risk in coastal watersheds since statistically speaking it is failing to capture almost half of the actual claims related to flood damage in the area. The boundaries stipulated by FEMA's 100-year flood plains, normally drive residents and local government to make decisions regarding mitigation strategies against hazard impacts. Nonetheless, areas not included in FEMA's floodplains are totally disregarded and considered as safe locations since risk is not computed for those areas. This is a dangerous approach since it is considering only a binary or discrete state of flooding which doesn't correspond to what happens in nature. In order to make flood control strategies successful there is a need to look beyond the regular floodplain boundaries and look into the whole area risk panorama, emphasizing the need to go from a hazard to a risk approach.

In Figure 32 the actual Floodplain delineation produced by FEMA can be observed in which different categories are shown for the area. These categories correspond to the description in Table 5. The 100-year floodplains delineated in Figure 32 by categories A, AE, AO and VE are mainly the areas that are going to be compared with the new hazard areas determined with the SFINCS model considering compound flooding. The actual floodplains are also going to be compared against the output obtained with SFINCS for a single flood driver event (design rainfall event delineated by the boundary conditions explained on section 4.2 and 4.3).

Table 5. Clear Creek Flood Hazard Zones according to FEMA.

Hazard Zones	Description
A	Areas subjected to the 1% annual chance exceedance of flooding. No detailed hydraulic analysis performed – No information about BFE
AE	Areas subjected to the 1% annual chance exceedance of flooding determined by detailed methods – BFE's shown for the area
AO	Areas subjected to the 1% annual chance exceedance of flooding with average depth between 0.3 and 0.9m
VE	Coastal areas subjected to the 1% annual chance exceedance of flooding and with additional hazard due to storm-induced waves – No detailed coastal analysis
X500	Moderate risk areas with 0.2% annual chance exceedance of flooding – No BFE's shown

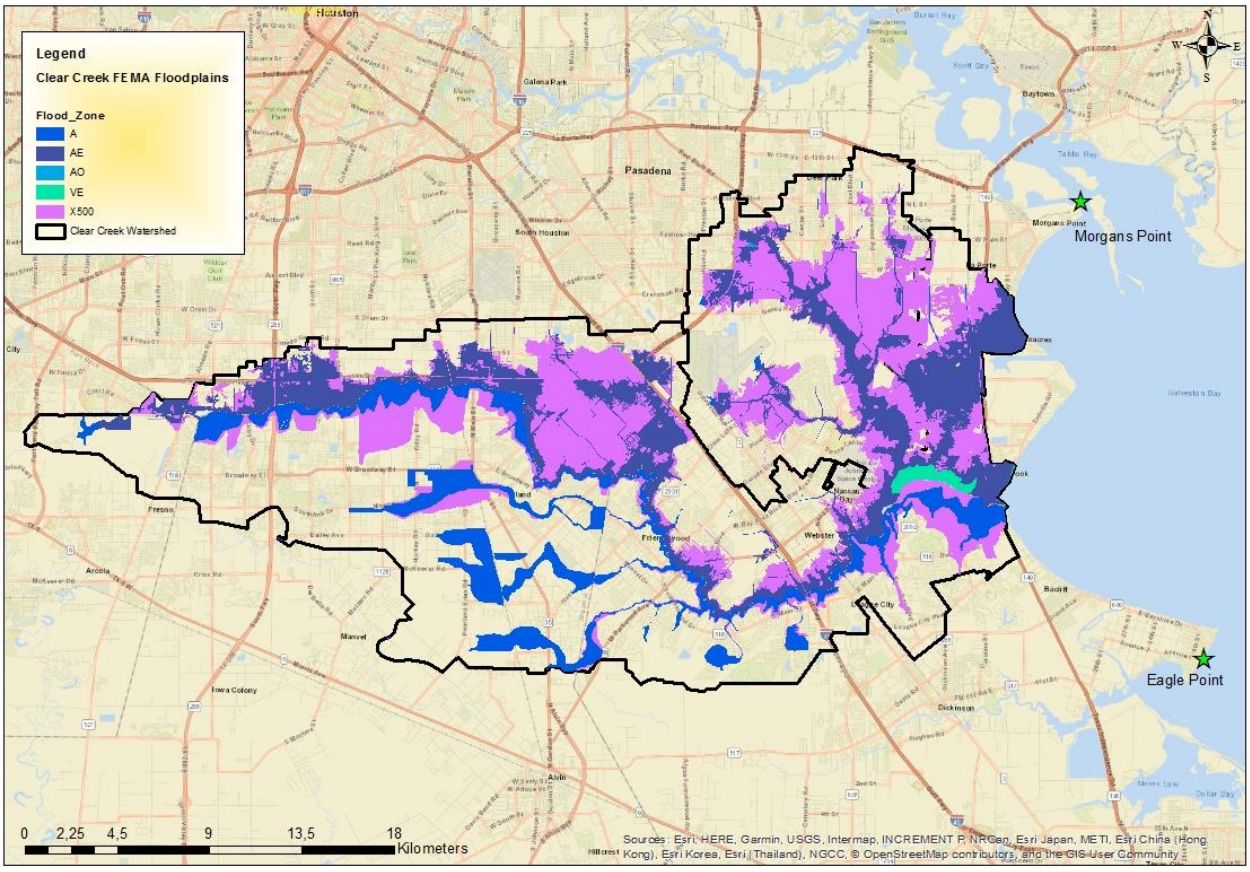

Figure 32. Clear Creek watershed - FEMA's Floodplain delineation.
Source (Risk MAP6, 2018)

3.2. Overview of past events

In the following section an overview of the 2 latest storm events hitting the Galveston Bay area are going to be described. The two events are Hurricane Ike and Harvey occurring in September 2008 and August 2017 respectively. Apart of being the two latest big magnitude events affecting the area and having more reliable data (events occurred in the past 10 years) these two storms were significantly different regarding the main driver event of flooding, reason why it was interesting to choose them as the main cases to validate the SFINCS model (see chapter 4). In the case of Hurricane Ike, the storm surge was dominant over the precipitation and in Hurricane Harvey the opposite situation occurred. Nevertheless, in both storms co-occurrence of precipitation and storm surge was observed, reason why both events are valuable for a compound flood analysis.

3.2.1 Hurricane Ike (2008)

In September 2008, hurricane Ike caused nearly $29 billion in damages and took the lives of 21 people in Texas, Arkansas and Louisiana. The hurricane prompted the largest search-and-rescue operation in the United States history at the time.

Ike made landfall on the Texas coast on September 13, 2008 and it was catalogued in 2010 as the third costliest storm in the U.S (Bedient, 2012). The hurricane reached a category 4 storm with sustained winds of 233 km/h and a minimum central pressure of 935 mbar. The wind fields spanned 724 km at landfall covering the entire Texas state and part of Louisiana and causing cascading effects such as a power outage that lasted until early October (Bedient, 2012). The eye of the storm passed north of downtown Houston and it triggered a 5.4m storm surge at the coast (Bolivar Peninsula – see Figure 27) with registered high water marks of 5.3m, 16 km inland from the coast at Chambers County (Berg, 2009).

Ike began as a tropical wave formation off the coast of West Africa on August 28, 2008, but it was only until the afternoon of September 9 that the hurricane entered the Gulf of Mexico. During its path toward Texas, the intensity of the storm increased and by the 11th of September the effects of the hurricane were started to be felt along the Texas coast when waves began to hammer at the Galveston Sea Wall (See hurricane path on Figure 33). One day after and 24 hours before Ike made landfall, the surge levels reached 3m on Galveston Island (See Figure 34). On the landfall day (September 13) the wind speed had decreased to 177km/h, but the storm surge couple with the high tide led to storm surge level of 4.6 to 6.1m along the Bolivar Peninsula (Harris County Flood Control District, 2018).

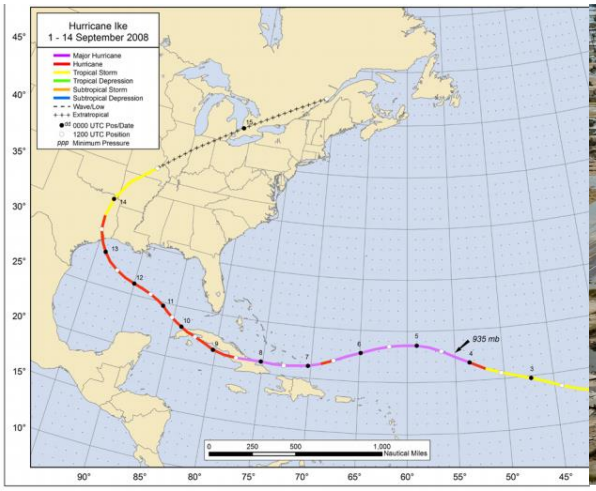

Figure 33. Hurricane Ike Track September 2008. Source:(Berg, 2009)

Figure 34. Hurricane Ike on September 14 in Gilchrist, Texas (Bolivar Peninsula). Source: (CNN, 2017)

3.2.1.1 Storm surge –Hurricane Ike

Regarding the Clear Creek watershed itself, apart from the reports from the Harris County Flood Control District, is important to visualize which was the storm surge level registered at the nearest measuring points

from the watershed outlet. From Figure 31 it can be seen that the nearest tide gauges are located on the west side part of the Galveston Bay both on the North and South East part of the catchment outlet (Clear Lake). The northern station is Morgan's Point, while the southern gauge is identified as Eagle point. In the following graphs, the tide and storm surge is going to be depicted for both stations, using the information consulted from NOAA's Tide prediction product (NOAA, 2018).

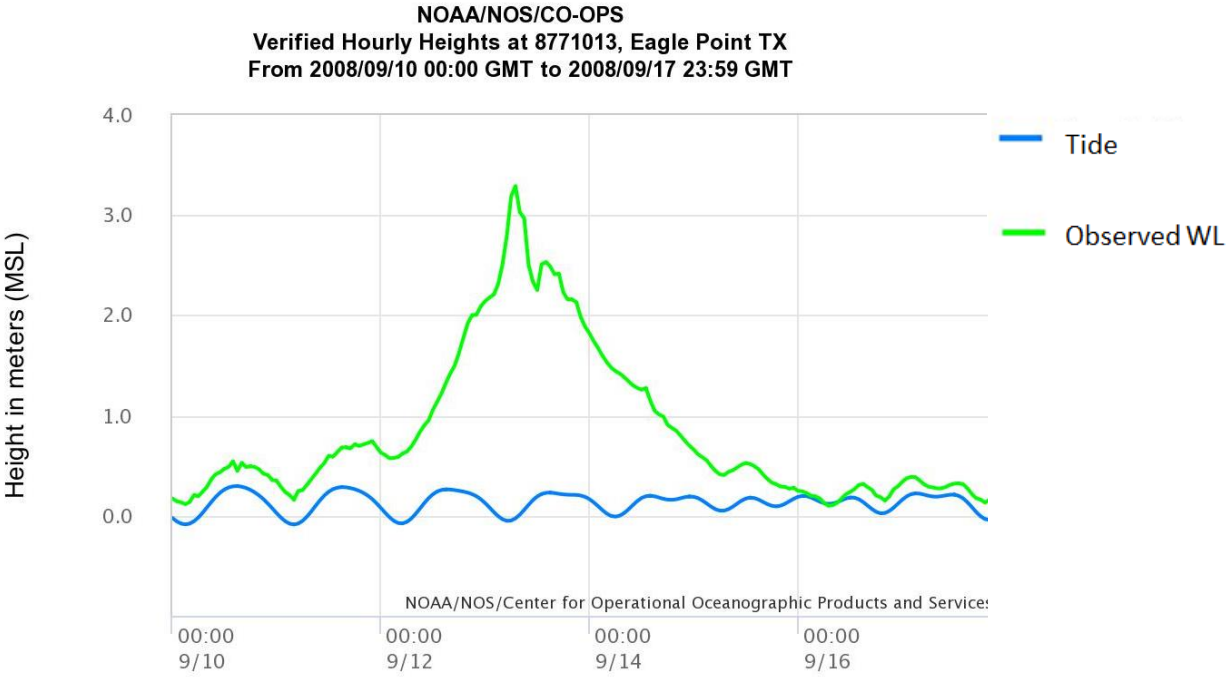

Figure 35. Eagle Point measured Water levels & Tide - Hurricane Ike.
Source: (NOAA, 2018)

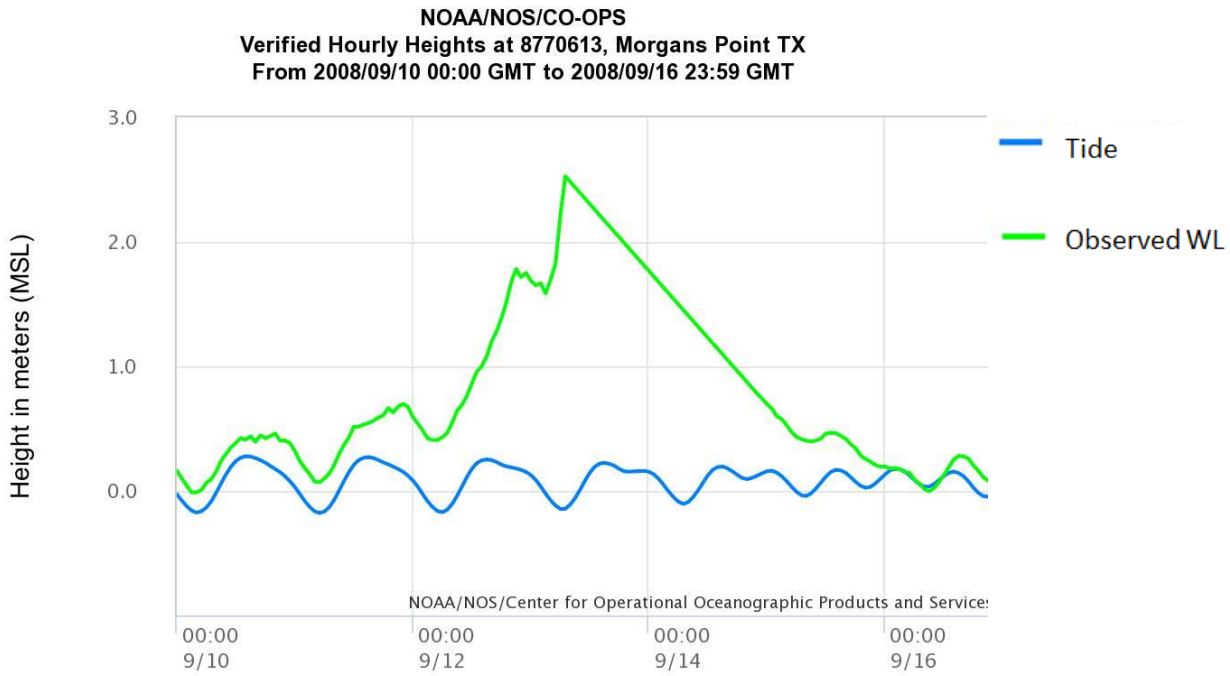

Figure 36. Morgan's Point measured Water levels & Tide - Hurricane Ike.
Source: (NOAA, 2018)

From Figure 35 and Figure 36 it can be seen that inside the Galveston Bay the maximum water level registered during Ike was 3.3 meters above mean sea level (on Eagle point) on September 13th, one day before the hurricane made landfall on Galveston Island and 2.5 meters above mean sea level at Morgan's Point. It can be observed that the storm surge lasted from the 12th of September to the late hours of the 15th

of September. It can be seen that from Figure 36 there is a sudden linear decrease of the storm surge, but this corresponds to a lack of data during the storm at Morgan's Point station due to the fact that some sensors failed from salt water intrusion and large wave action (Berg, 2009). From the Tropical Cyclone Report of hurricane Ike created by the National Hurricane Center, it was estimated that at the West part of the Galveston Bay the surge levels might have reached values between 3 and 4.5 meters above mean sea level.

Figure 37. Flooded road as hurricane Ike approached Galveston, Texas (12/09/2018). Source:(Phillip, 2017)

3.2.1.1 Precipitation –Hurricane Ike

The precipitation generated by the storm was comparatively low, meaning that for this particular hurricane, the storm surge was the dominant event. Nevertheless, according to the HCFCD, Ike generated during landfall a precipitation event that resulted in 15 to 26 cm across Harris County (see Figure 31) and a second event on September 14 that resulted in an additional 8 to 20 cm in the northwest part of the aforementioned county. The second event triggered severe street flooding since there were already some debris from the hurricane clogging the draining system (see Figure 41). According to the reports 1300 homes flooded from rainfall and the events along the coastal area where catalogued on average between a 10%(10-year) and 1%(100-year) frequency (Harris County Flood Control District, 2018).

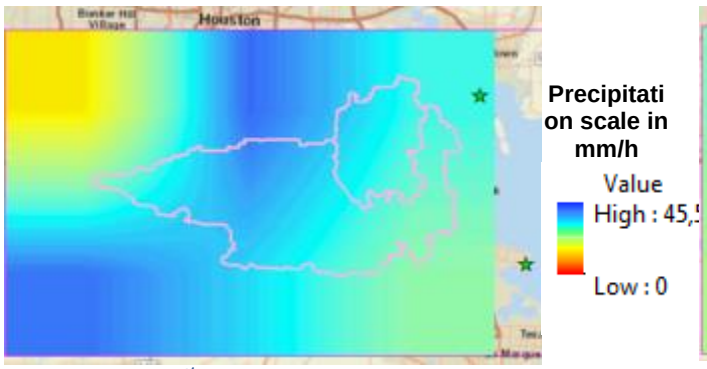

Figure 38. 1st Precipitation event rate distribution on the Clear Creek watershed. (Period from 22:30 -12/09/2008 to 01:30 - 13/09/2008).
Source: (Earth Data - NASA, 2018)

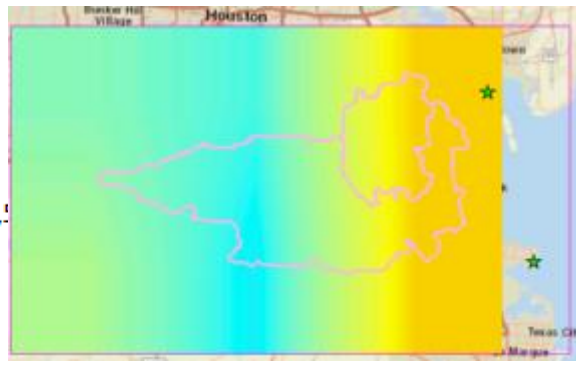

Figure 39. 1st Precipitation event rate distribution on the Clear Creek watershed (Period from 07:30 -13/09/2008 to 10:30- 13/09/2008).
Source: (Earth Data - NASA, 2018)

3.2.1 Hurricane Ike

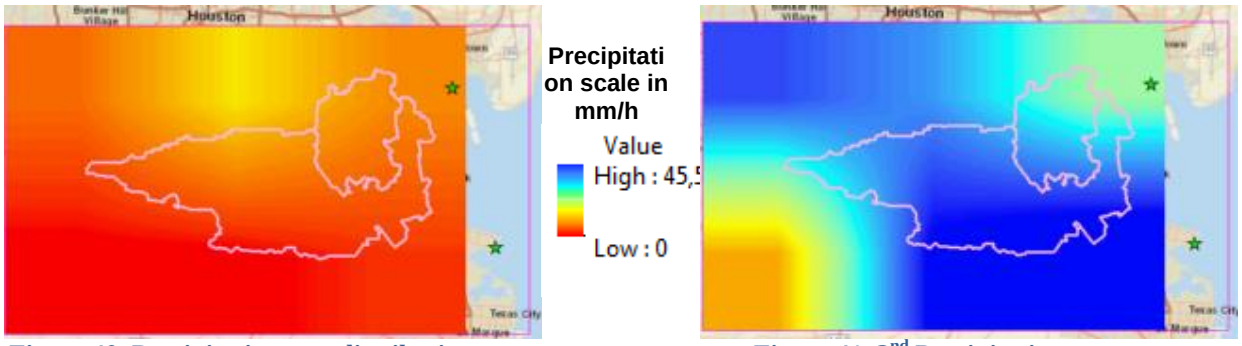

Figure 40. Precipitation rate distribution on the Clear Creek watershed Period between events (from 19:30 - 13/09/2008 to 22:30 -13/09/2008). Source: (Earth Data - NASA, 2018)

Figure 41. 2nd Precipitation event rate distribution on the Clear Creek watershed (Period from 10:30 - 14/09/2008 to 13:30 - 14/09/2008). Source: (Earth Data - NASA, 2018)

Using NASA's Web-based application: Giovanni© (Version 4.25), an overview of the spatially distributed rainfall over the area was obtained using the TRMM Near Real-Time precipitation 3 hourly data (Version 7). These data is the output from the TRMM Multi-Satellite Precipitation Analysis and it includes three-hour period of rainfall rate in [mm/h] with a resolution of 0.25°x 0.25° degrees which is relatively coarse when compared to the extent of the watershed (see polygon on Figure 38 to Figure 41), but it already shows spatial variations within the area of interest. The spatially distributed rainfall can be observed from Figure 38 to Figure 41 in which the two aforementioned rainfall events can be seen. Is important to mention that the observations do not reflect the total accumulated rainfall in the area for the events, but only 3-hourly time lapses of the storm, reason why the maximum scale only reaches values around 4.5cm/h.

Figure 42. Hurricane Ike- Warehouse in Downtown Houston (2008). Source:(Harris County Flood Control District, 2018)

3.2.2 Hurricane Harvey (2017)

On August 2017 hurricane Harvey made landfall at the Texas Coast as a Category 4 hurricane. The storm stalled after landfall remaining with its center near the Texas coast for four consecutive days, triggering a historical downpour of more than 1.5 meters at the Southeastern part of Texas (Kimberlain et. al., 2018). Harvey registered maximum sustained winds of approximately 200 km/hour as well as a storm surge on the coast causing severe damage to the region, however, the flood related damages associated to the record-setting rainfall were the most critical part of the event (Sebastian et al., 2017), cataloguing Harvey as the second-most costly hurricane un U.S history behind Katrina. This storm took the lives of 68 people (direct effects of the hurricane) being this the largest number of fatalities occurring due to a TC since 1919 (Kimberlain et al., 2018).

Harvey started as a weak tropical storm that dissipated over the Central Caribbean Sea but it reform over the Bay of Campeche and intensified on its path towards the Gulf of Mexico. The hurricane made its first landfall at 03:00 UTC on the 26th of August 2017 (see Figure 44) on the northern end of San Jose Island and after 12 hours of landfall the northwestward motion of the cyclone stopped due to the fact that Harvey was embedded in steering currents between the Four Corners region and the northern part of the Gulf of Mexico, afterwards, the storm made slow loops in the region going offshore and landward as it can be depicted in Figure 43 (Kimberlain et al., 2018). Overall until August 29th the eye of the storm never moved more than 90 km offshore of the Texas coast which in response generated the extreme rainfalls observed in the area. The hurricane finally transformed into an extratropical cyclone on the 1st of September on the Tennessee Valley and the next day it fully dissipated on northern Kentucky.

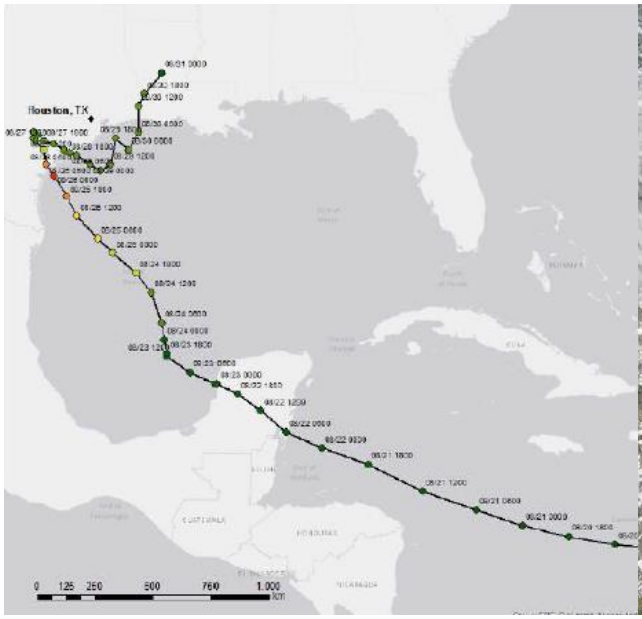

Figure 43. Hurricane Harvey's Track. Source:(Sebastian et al., 2017)

Figure 44. Hurricane Harvey making landfall in Texas (28/08/2018). Source:(Sebastian et al., 2017)

The storm was responsible for 36 casualties in the Harris County within the Houston Metro Area (see Figure 46 and Figure 47), from which 33 of the casualties were attributed to inland rainfall flooding and none could be attributed directly to storm surge (Kimberlain et al., 2018). According to NOAA, Harvey's damage estimation is around $125 billion in 2017 dollars with a 90% confidence interval. 300,000 structures in the area were flooded, 360,000 customers lost power supply and an estimated of 40,000 victims were evacuated or rescued and transported to shelters across Texas or Louisiana.

Record water levels were registered on the buffalo Bayou, the Clear Creek, Dickinson Bayou and Cypress Creek due to the extreme rainfall events. In addition, the levels of the Addis & Barker reservoirs (located near the eastern part of Houston and north from the Clear Creek watershed) reached high levels

during Harvey, which forced the controlled release of high volumes of water to prevent dam failure and caused further flooding of the region (HCFCD, 2018a) (see Figure 45).

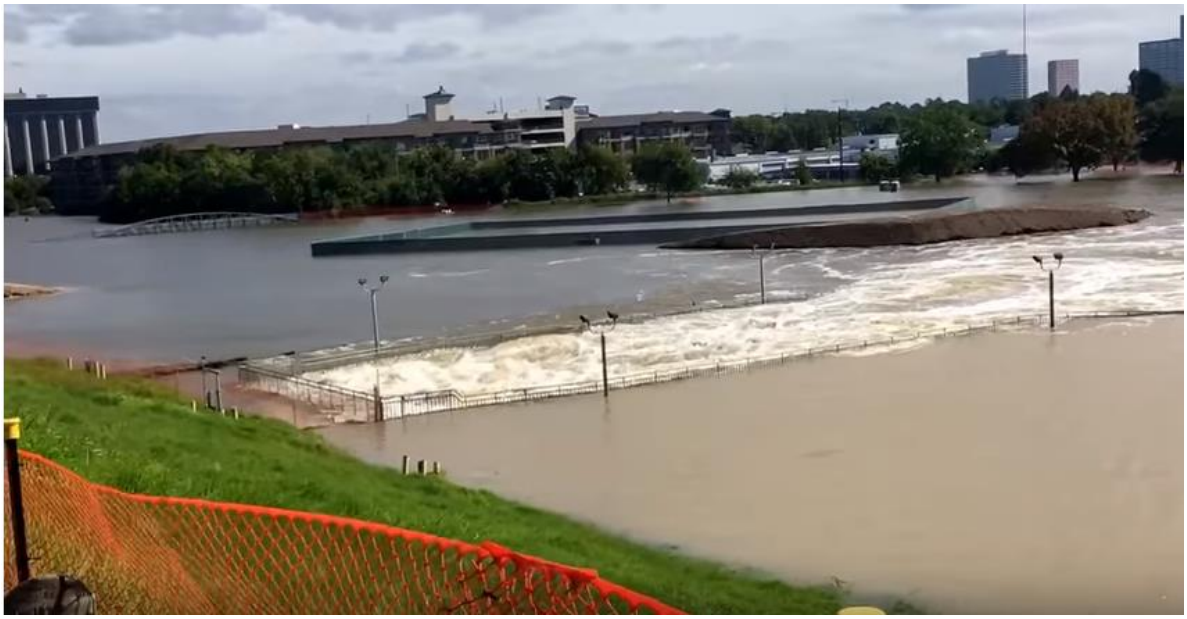

Figure 45. Release of Water through Barker's Dam Spillway - 30/08/2017. Source:(Graham, 2017)

Figure 46. Houston Texas (31/08/2017). Source: (Sebastian et al., 2017)

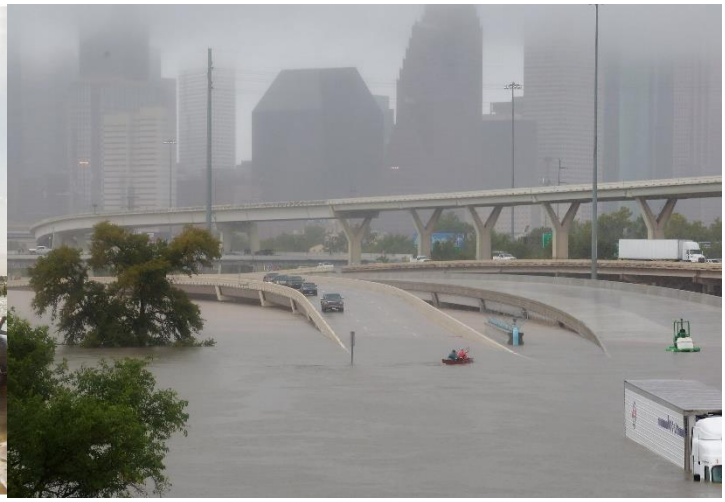

Figure 47. Houston Downtown Harvey flooding. Source:(Carson, 2017)

3.2.2.1 Storm surge –Hurricane Harvey

The combination of surge and tide triggered coastal flooding maximum water levels ranging from 1.8 m to 3m above ground level in the back bays between Port Aransas and Matagorda (Kimberlain et al., 2018). According to the USGS storm tide sensor data, the highest inundations from Harvey were from 2.4m to 3m above ground level. Is important to realize that the tide gauges near Houston recorded peak water levels that were significantly affected by rainfall runoff from Harvey, nevertheless is difficult to separate the signals and define the exact levels caused only by storm surge (Kimberlain et al., 2018). For hurricane Harvey the same tide stations depicted on Figure 31 are going to be presented in this section as they are the closest to the Clear Creek watershed. In the following graphs, the predicted tide and observed water level (as storm surge cannot be fully differentiated in this observations) is going to be presented for Eagle Point and Morgan's Point using the information consulted from NOAA's Tide prediction product (NOAA, 2018).

From Figure 48 and Figure 49 it can be observed that for both Eagle and Morgan's Point the highest water level registered was approximately 1.25 meters above mean sea level. The Water level signal in both graphs presents several fluctuations during the period from the 24th till the 31st of August presumably

suggesting that readings were partially affected by inland rainfall, but also due the track of the hurricane which moved inland and offshore causing several fluctuations in the area. According to NOAA the most affected gauges were two TCOON gauges at the east side of Houston (Kimberlain et al., 2018) while no information is reported for the station on the West side of the City which is where Eagle and Morgan's Point tide stations are located.

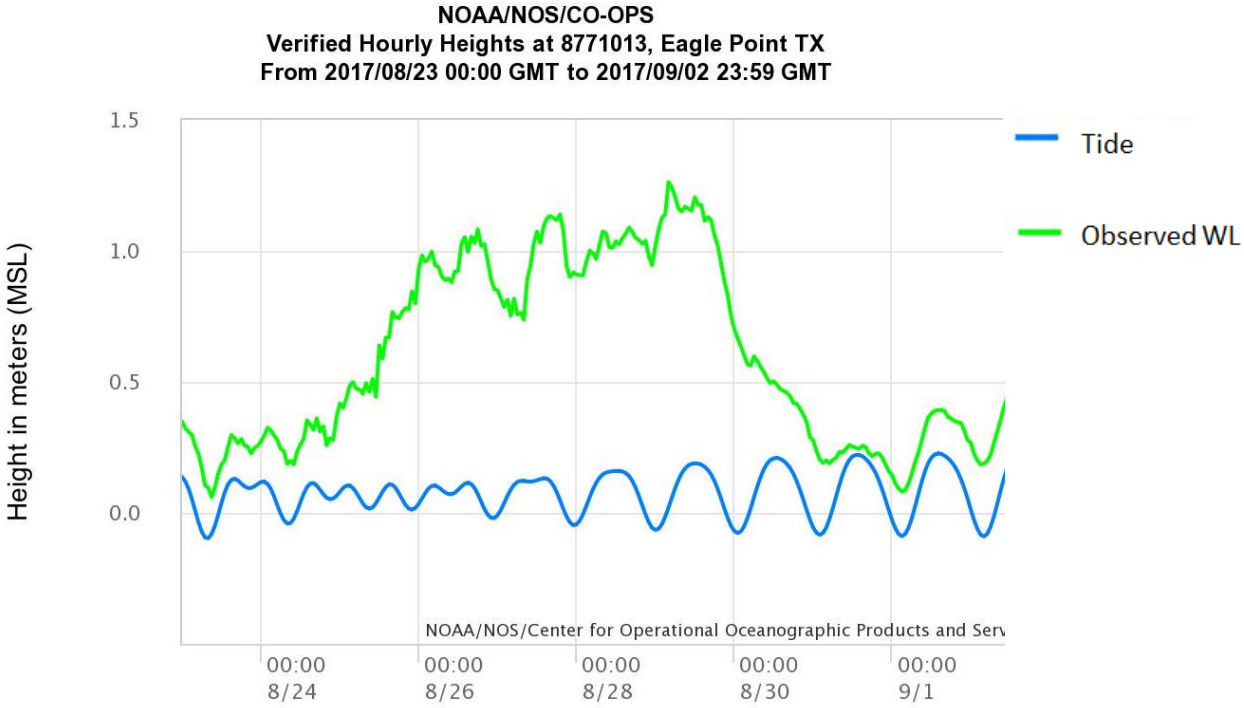

Figure 48. Eagle Point Station-measured Water levels & Tide - Hurricane Harvey. Source: (NOAA, 2018)

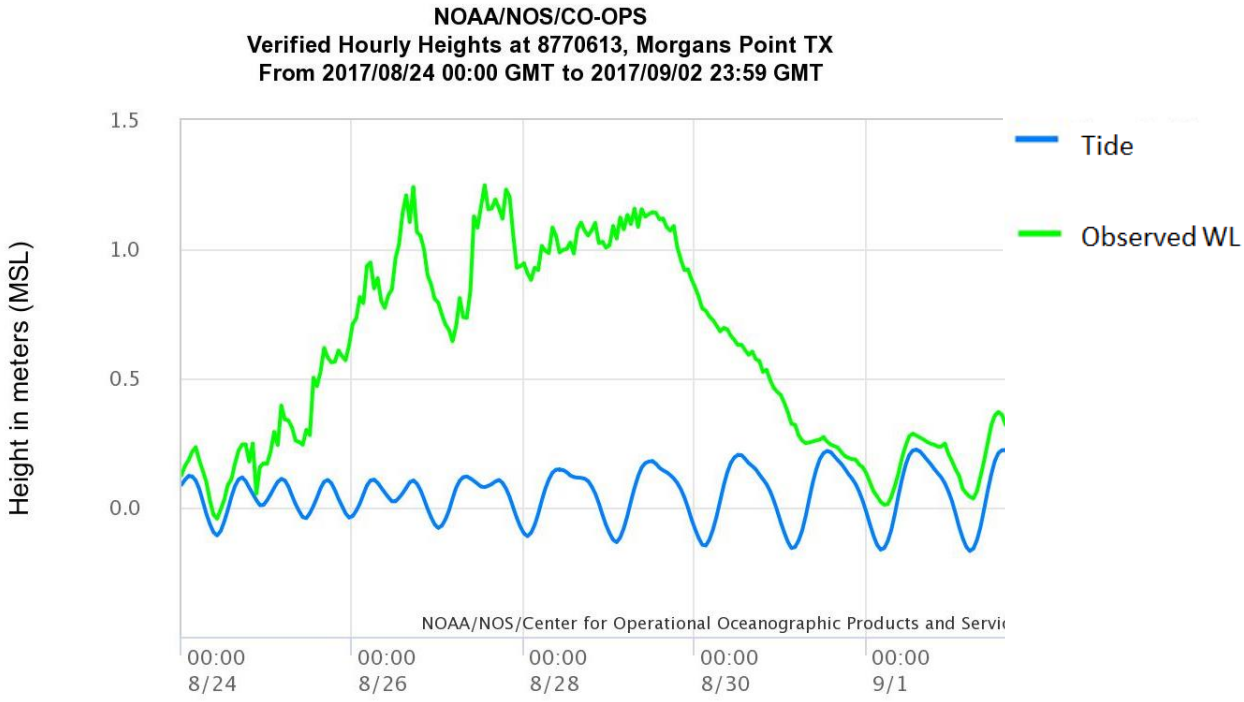

Figure 49. Morgan's Point Station -measured Water levels & Tide - Hurricane Harvey. Source: (NOAA, 2018)

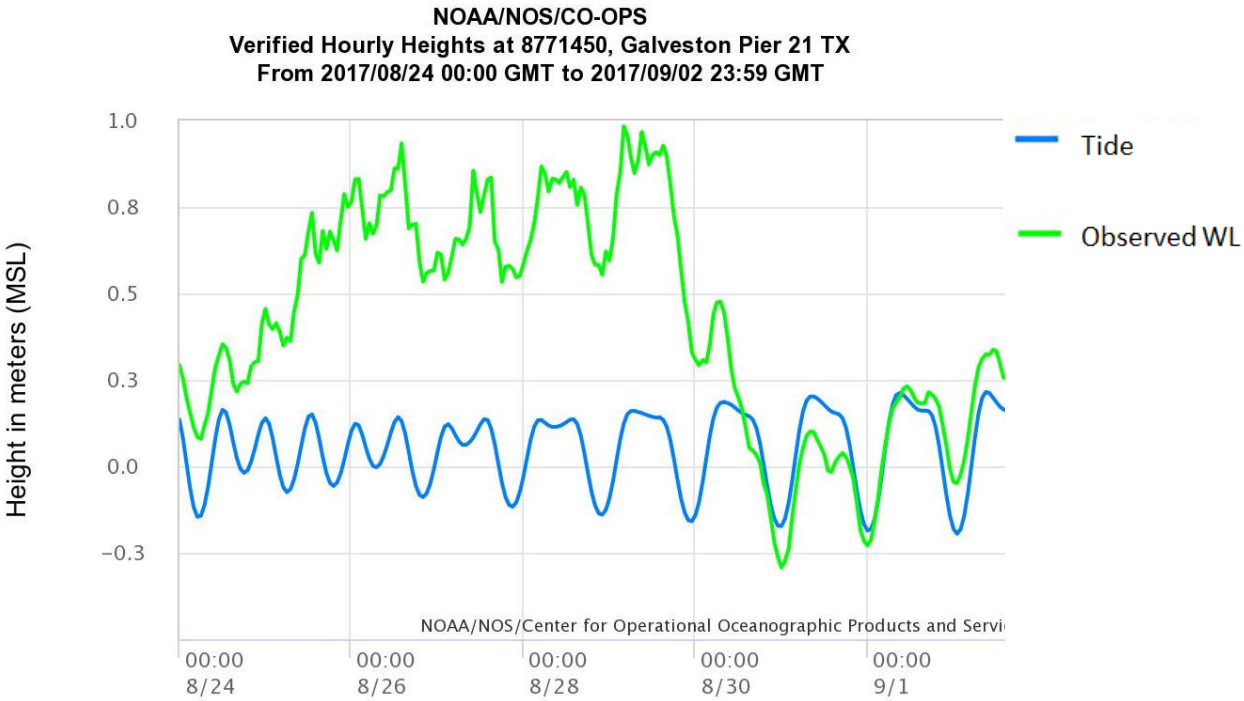

Figure 50. Galveston Pier 21 Station - measured Water levels & Tide - Hurricane Harvey.
Source: (NOAA, 2018)

In Figure 50 the water level data from Galveston Pier 21 station is shown since this station in located outside of the Galveston bay (Galveston Island) and it can show the differences in readings inside and outside the bay. It can be seen that even though many fluctuations can be seen in Figure 50, when there is a comparison for example with Morgan's Point station (Figure 49 –closest station to Houston, TX) on the last days of the storm (27th till late 30th of August) there is a significant increase on the water levels when compared to the ones at the entrance of the bay. The slow decrease of the water levels inside the bay (in Figure 49 for almost 3 days) does not match with the normal behavior of storm surge which only lasts for a couple of hours as it can be seen on the 29th august 2008 in Figure 50. This again suggests that rainfall-runoff affected the tide-gauge readings in the zone. In addition, according to Harvey's best track data (Weather Underground, 2018) in august 27th 2008 the pressure and wind speed combination coudnt have possibly created a considerable surge as seen in Figure 48 and Figure 49.

3.2.2.1 Precipitation –Hurricane Harvey

As mentioned before, Harvey's Rainfall made that this storm was catalogued as the most significant TC rainfall event in the U.S history. The highest precipitation report was 1.54m near Nederland and Grove, Texas. During Harvey 18 values over 1.2m were registered on Southeastern Texas with similar values ranging from 0.9 to 1.2 m in the Houston metro area (Kimberlain et al., 2018).

Most of the standard precipitation gauges have a maximum reading height of 0.3 meters and they couldn't be emptied due to the limitations imposed by the hurricane itself, therefore, the most accurate precipitation estimator are radar images (see Figure 51). According to an extreme exceedance analysis performed by NOAA the downpour in Southern Texas generated a flooding equivalent to a 1000-year event, a situation that has never been seen before in the United States.

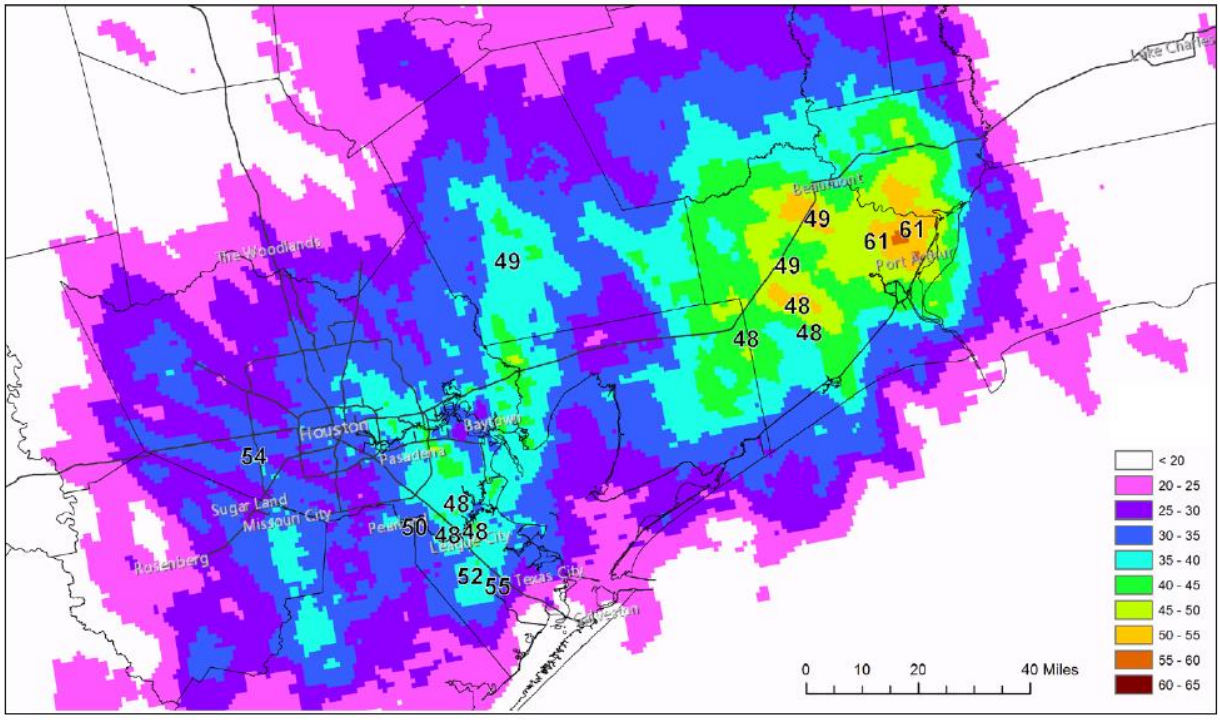

Figure 51. NOAA gauge-corrected, multi-sensor quantitative precipitation estimation for Harvey(Inches). From the 25th till the 1st of September. Black numbers are actual rain gauge values. Source:(Kimberlain et al., 2018)

As in the case of Ike, the NASA's Web-based application: Giovanni© (Version 4.25) was used to obtain an overview of the spatially distributed rainfall over the area in order to maintain the same data base of information. In the case of Harvey, a new satellite mission was launched replacing the one that obtained the TRMM Near Real-Time precipitation 3 hourly data (Version 7), thus, for this hurricane the data set used was the GPM IMERG Final Precipitation half hourly data set (Version 5). This data set is the unified U.S algorithm that provides satellite precipitation for the U.S GPM team which reports the combined precipitation computed from different satellite passive microwave sensors after calibrating the data 12 hours after observation time and re-calibrating once after the monthly gauge analysis is obtained.

The rate of precipitation is reported in [mm/h] with a resolution of 0.1°x 0.1° degrees equivalent to a 10km grid and is reported in half-hourly intervals. For sake of visualization, it was better to use NOAA's report to represent the total cumulative precipitation nearby the Galveston Bay as shown in Figure 51, nevertheless, some hourly precipitation obtained from NASA's tool is presented below from Figure 52 to Figure 55 in which the spatial distribution is shown for the 26th, 27th and 29th of August, 2018. It can be seen that through the Clear Creek watershed there was a constant change in the rainfall distribution and that in some cases the hourly precipitation reached values of 6.38 cm in 1 hour which is significantly higher than the values reached by Ike in the region which only sum up to 4.5 cm in 3 hours.

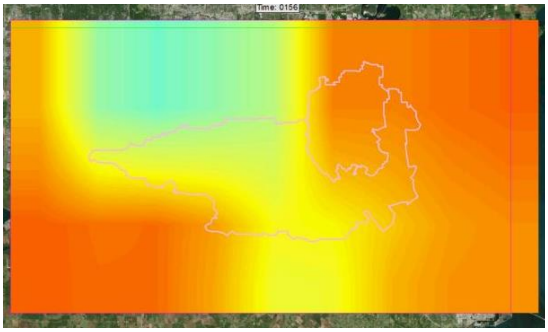

Figure 52. Precipitation rate distribution on the Clear Creek watershed.
Hourly period (from 11:00 -26/08/2017 to 11:59 -26/08/2017).
Source:(Earth Data - NASA, 2018):

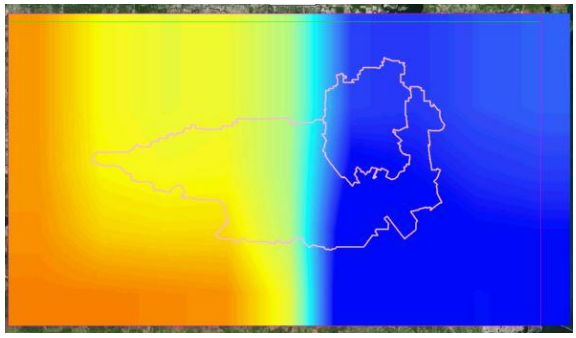

Figure 53. Precipitation rate distribution on the Clear Creek watershed.
Hourly period (from 02:00 -27/08/2017 to 02:59 -27/08/2017).
Source: (Earth Data - NASA, 2018):

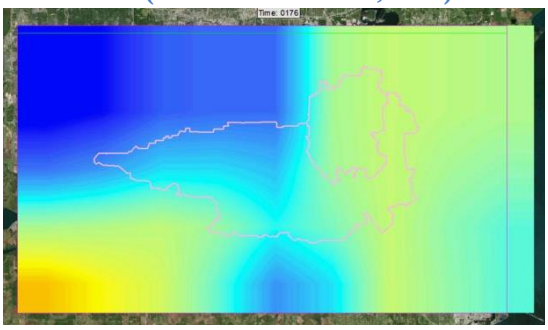

Figure 54. Precipitation rate distribution on the Clear Creek watershed.
Hourly period (from 07:00 -27/08/2017 to 07:59 -27/08/2017).
Source:(Earth Data - NASA, 2018)

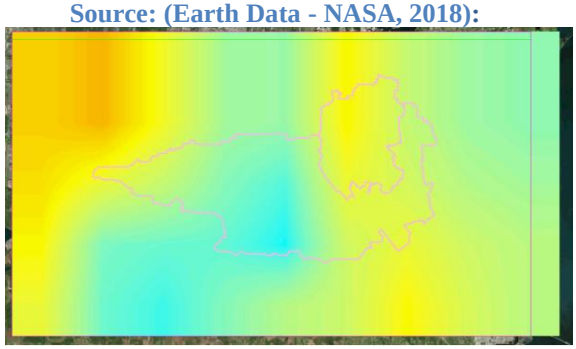

Figure 55. Precipitation rate distribution on the Clear Creek watershed.
Hourly period (from 03:00 -29/08/2017 to 03:59 -29/08/2017).
Source:(Earth Data - NASA, 2018)

Figure 56. Harvey's flooding and rescue activities. Source: (Borenstein, 2018)

3.3. SFINCS Model validation using previous storm events

In this section both Harvey and Ike storms are going to be modeled using SFINCS. The characteristics described for both storms regarding precipitation and storm surge on Section 3.2 are the ones that are going to be used as input for the model. In the appendices of this report (Section 9.1) an overview of SFINCS was given including details about its numerical implementation and particular set-up for this particular study case, therefore in this section only the model results are going to be described.

Is important to mention that in this particular research, SFINCS is not going to be coupled with any other advanced model to get the offshore input, therefore, the tested configuration doesn't include any wave-relevant process (wave-run up, setup, short period waves, etc.) that might influence flooding in coastal regions. For this specific configuration (historical storms) of the model, SFINCS is going to be forced instead with the water level observations at Morgan's and Eagle point (see Figure 31) according to the respective water level records on each one of the studied storm events. Since this approach was selected, it was decided that no additional forcing due to wind input was going to be included since the water level observations on the tide gauges have already implicitly included the effect of a possible wind-setup at the bay. In addition, no advection terms are going to be included in the model (see Appendices, Section 9.1.4).

As mentioned in the Appendices (Section 9.1.3), the infiltration rate in SFINCS is considered as a constant value across all the model space which acts throughout the entire time domain, therefore this parameter was set to a value of 1 [mm/h] which corresponds to a very low value of infiltration rate for clayish soil types. Normal values of infiltration rates for this type of soils on unsaturated conditions are on the range of 1 to 10 mm/h (FAO, 2012), therefore assuming there are some partial saturated conditions during TC events the infiltration rate was selected as the lower boundary. This specific value was used to model both Harvey and Ike, and is also going to be used when the compound boundary conditions are tested in chapter 5.

3.3.1 Hurricane Ike SFINCS model

In the case of hurricane Ike, as mentioned in section 3.2.1, the spatial distributed precipitation was obtained from NASA's Web-based application: Giovanni© (Version 4.25) using the TRMM Multi-Satellite Precipitation Analysis which includes three-hour period of rainfall rate in [mm/h] with a resolution of 0.25°x 0.25° degrees An example of three hourly data precipitation grid for the 12th of September from 13:30 till 16:30 pm is shown in Figure 57 where it can be seen that the resolution of the precipitation is much coarser than in the case of hurricane Harvey (see Figure 71).

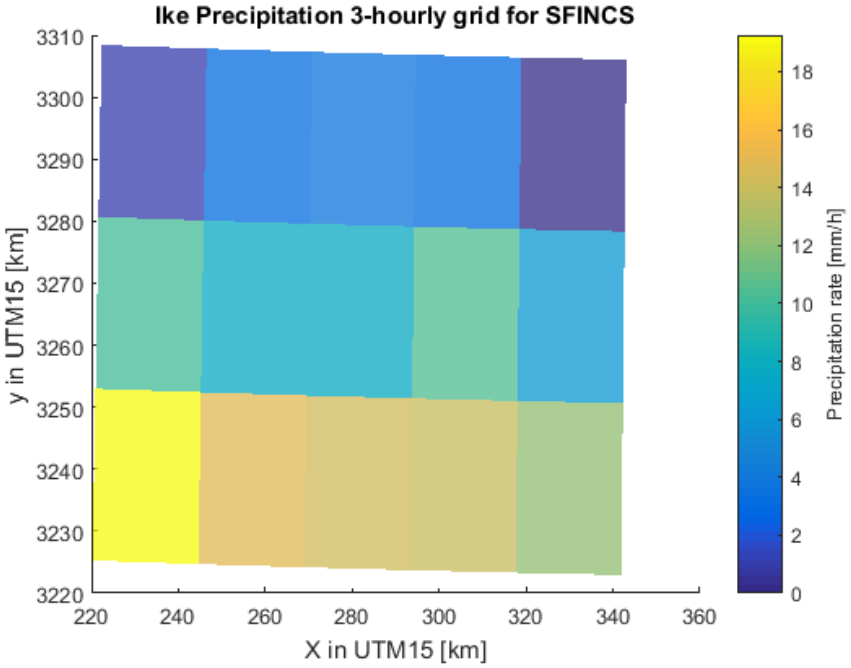

Figure 57. Three Hourly Ike precipitation grid for SFINCS.

In Figure 58, the water levels corresponding to Ike storm for the two tide gauges located nearby the Clear Creek watershed are shown and Figure 59 shows the observation points in where HWL's were recorded by FEMA during hurricane Ike. In total, the SFINCS model was run for 7 consecutive days from the 11th of September 2008, till the 17th of September 2008, taking 1.69 hours to run the full simulation.

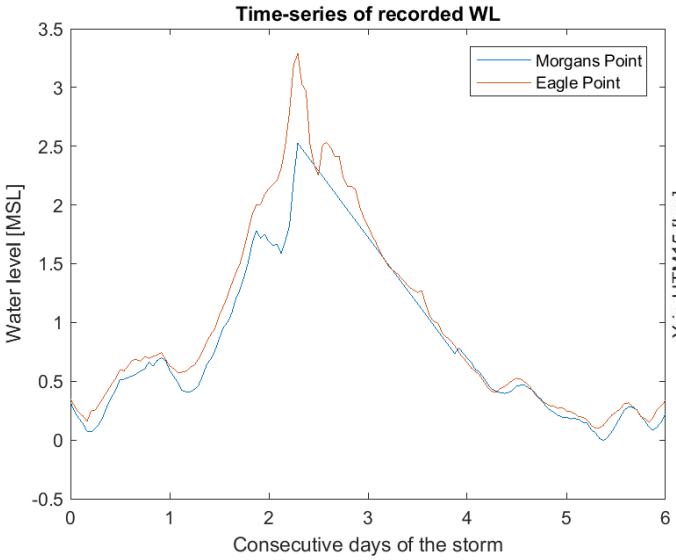

Figure 58. Water levels in tide gauges for Ike storm

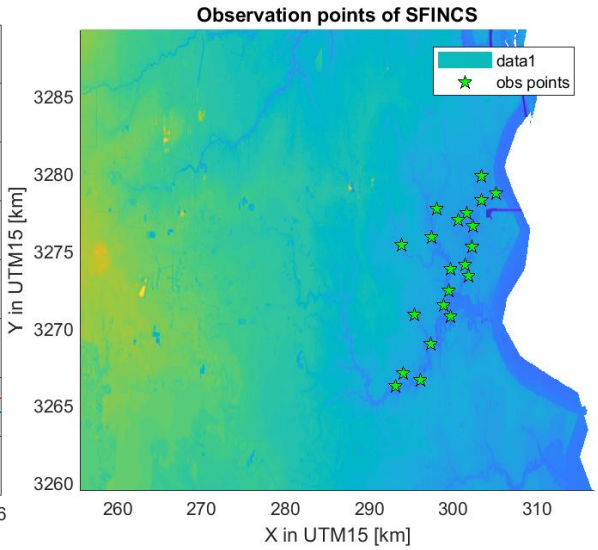

Figure 59. High Water Marks registered for Ike. Source:(FEMA, 2008)

The cumulative precipitation for hurricane Ike can be observed in Figure 60 in which the highest precipitation depth is located in the middle and southern part of the watershed with values around 0.55m and 0.65m respectively. The predominant values for the rest of the watershed are around 0.45m

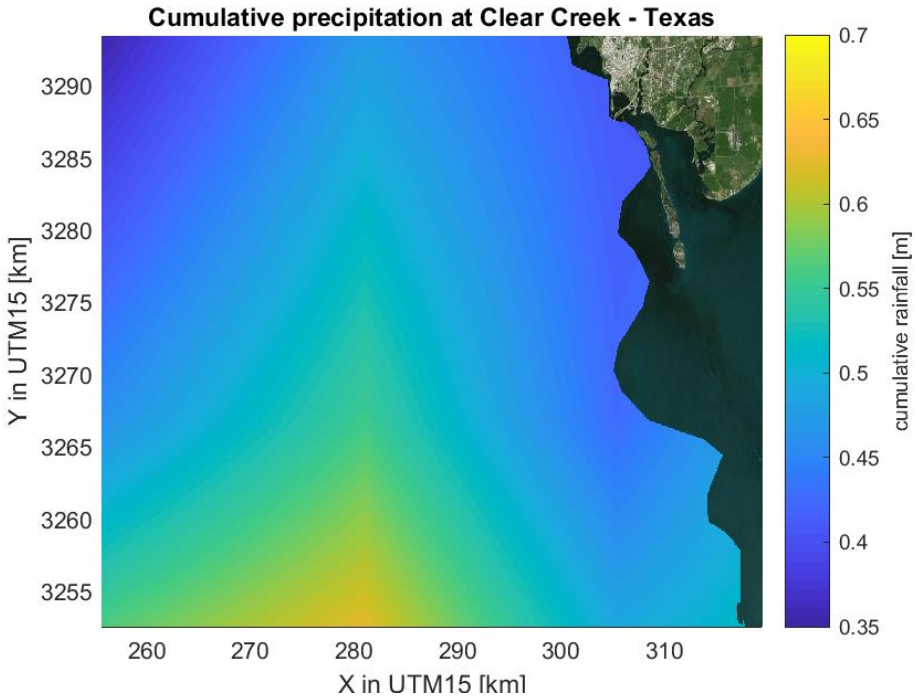

Figure 60. Cumulative rainfall (m) spatial distribution over the Clear Creek during hurricane Ike.

In Figure 61 the maximum flow velocity computed by SFINCS for hurricane Ike for the nearby region of the Clear Creek watershed can be observed. The values in this figure were limited to a maximum velocity of 0.5m/s since according to a study published on 2006 by the Department for Environment Food and Rural affairs of the UK (DEFRA), for this velocity and for water depths higher than 0.75m some adults might already have trouble to stand (see Figure 62). In this case the maximum velocities are shown clearly on the coast rather than on inland locations (opposite to Harvey's case see Figure 75) and this show how SFINCS can

capture both relevant processes for compound flooding. In this case, given the input, storm surge was clearly the most dominant process (see red values on the coast for Figure 61).

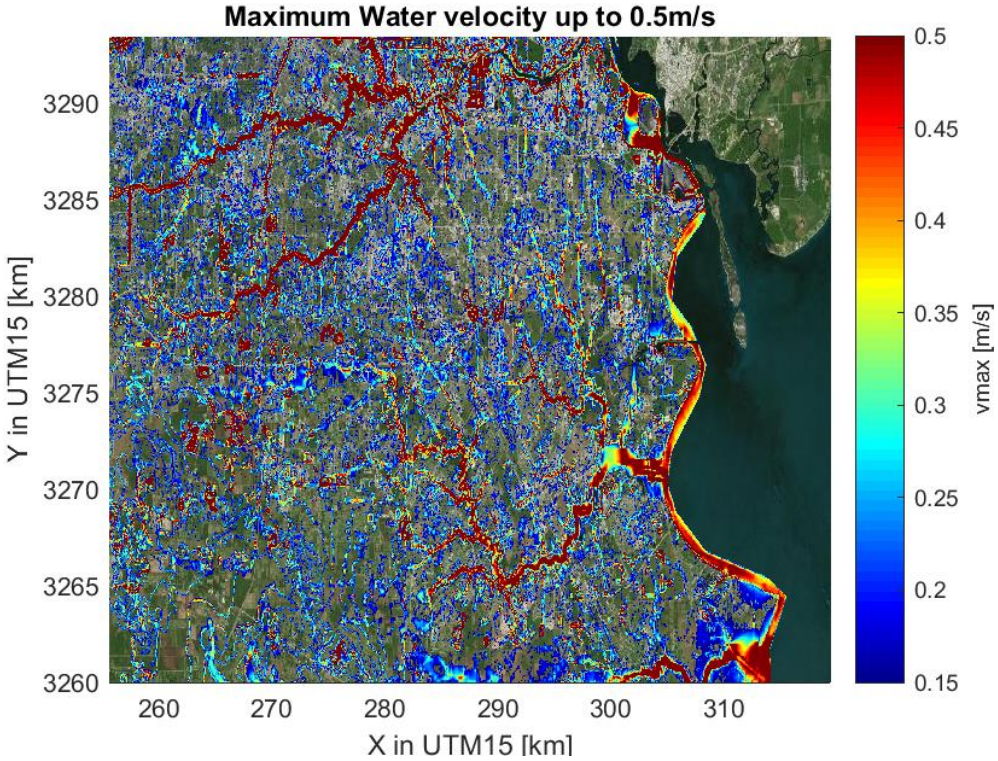

Figure 61. Maximum Water velocity up to 0.5m/s during Ike Storm according to SFINCS model

d * (v+0.5) + DF

Velocity \ Depth	0.25	0.50	0.75	1.00	1.25	1.50	1.75	2.00	2.25	2.50
0.00	0.13	0.25	0.38	0.50	0.63	0.75	0.88	1.00	1.13	1.25
0.50	0.25	0.50	0.75	1.00	1.25	1.50	1.75	2.00	2.25	2.50
1.00	0.38	0.75	1.13	1.50	1.88	2.25	2.63	3.00	3.38	3.75
1.50	0.50	1.00	1.50	2.00	2.50	3.00	3.50	4.00	4.50	5.00
2.00	0.63	1.25	1.88	2.50	3.13	3.75	4.38	5.00	5.63	6.25
2.50	0.75	1.50	2.25	3.00	3.75	4.50	5.25	6.00	6.75	7.50
3.00	0.88	1.75	2.63	3.50	4.38	5.25	6.13	7.00	7.88	8.75
3.50	1.00	2.00	3.00	4.00	5.00	6.00	7.00	8.00	9.00	10.00
4.00	1.13	2.25	3.38	4.50	5.63	6.75	7.88	9.00	10.13	11.25
4.50	1.25	2.50	3.75	5.00	6.25	7.50	8.75	10.00	11.25	12.50
5.00	1.38	2.75	4.13	5.50	6.88	8.25	9.63	11.00	12.38	13.75

Categories of flood hazard:

	From	To	
Class 1	0.75	1.50	Danger for some
Class 2	1.50	2.50	Danger for most
Class 3	2.50	20.00	Danger for all

Note: The table gives values of flood hazard (= d·(v+0.5) +DF)

Figure 62. Depths and velocities generating risk during flooding
In the formula of hazard, d represents flow depth, v is flow velocity and DF is a debris factor that depends on the land use. Source:(Defra/ Environment Agency, 2006)

In Figure 63, the maximum water depth registered in each cell of the SFINCS model during the entire simulation of hurricane Ike is presented. It can be observed that in this case coastal flooding is a major issue; especially in the area of the Clear Lake (outlet of the watershed) in which it can be seen that water has spread along the coast and in the nearby inland regions reaching high water levels. This can also be observed on the Armand Bayou (see last tributary into the Clear Lake) in which the effect of the surge nearby by one of the port mooring places is clearly affected. The effect of the surge can also be seen in the Southeastern corner of Figure 63 in which water has flooded this region entirely when compared to the case of hurricane Harvey (see Figure 76); this can also be validated with Figure 64 (see yellow circled area), which shows a Landsat image of the aftermath of hurricane Ike and it shows in red color the flooded areas. This coincides with the southern areas shown by the SFINCS simulation in Figure 63 (see yellow circle). Regarding the inland inundation, it is seen that some significant flooding and ponding can still be observed due to the rainfall generated by hurricane Ike. As an additional material, SFINCS was used to run hurricane Ike turning off each one of the flood drivers, to see the individual effect of each input. Both scenarios can be seen in Figure 65 and Figure 66 where only the storm surge and only the precipitation are shown respectively. From these last figures it can

be said that the effect of surge goes as far as 17 to 20 km inland from the outlet of the watershed on the Clear Creek and around 10km inland on the Armand Bayou. It can be seen as well that the precipitation had a higher effect on the upper stream part of the catchment and on the upper region of the Armand Bayou. In addition, precipitation also had an effect on the regions nearby the Clear Lake and only when both effects are taken into account (Figure 63) the maximum flood extent can be obtained, pointing out again that Ike hurricane trigger indeed compound flooding and that it was not solely a storm surge event.

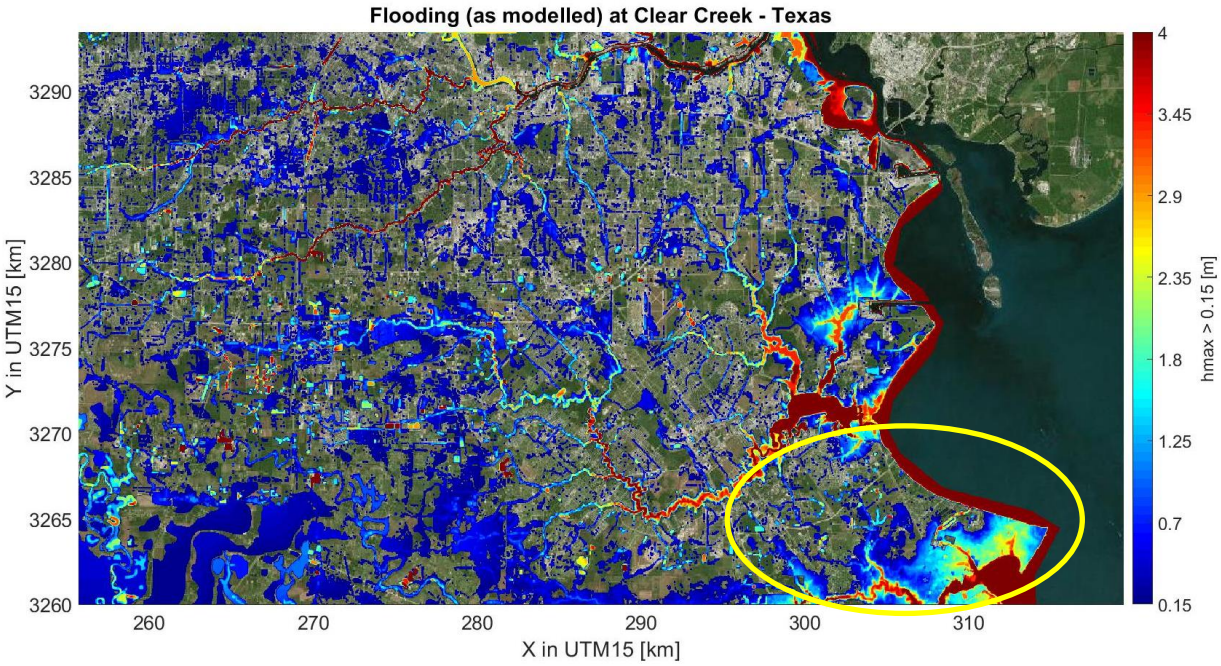

Figure 63. Maximum Flood Depth as modelled in SFINCS at Clear Creek during hurricane Ike. Maximum water depth illustrated corresponds to a value of 1m and flooding was considered only above a value of 15cm

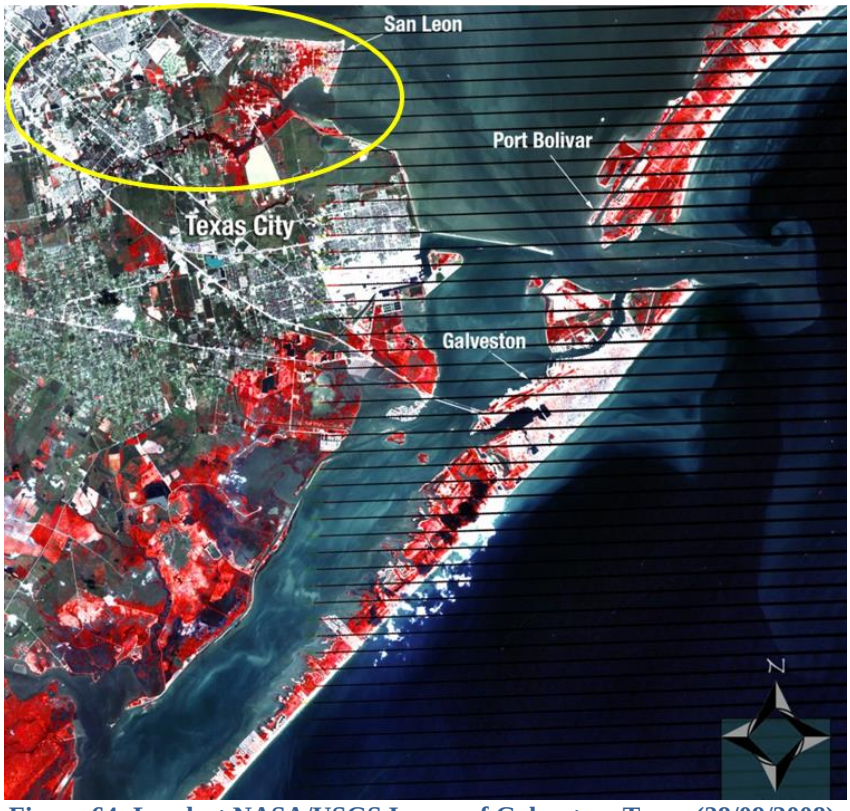

Figure 64. Landsat NASA/USGS Image of Galveston, Texas (28/09/2008). Source: (NASA, 2008)

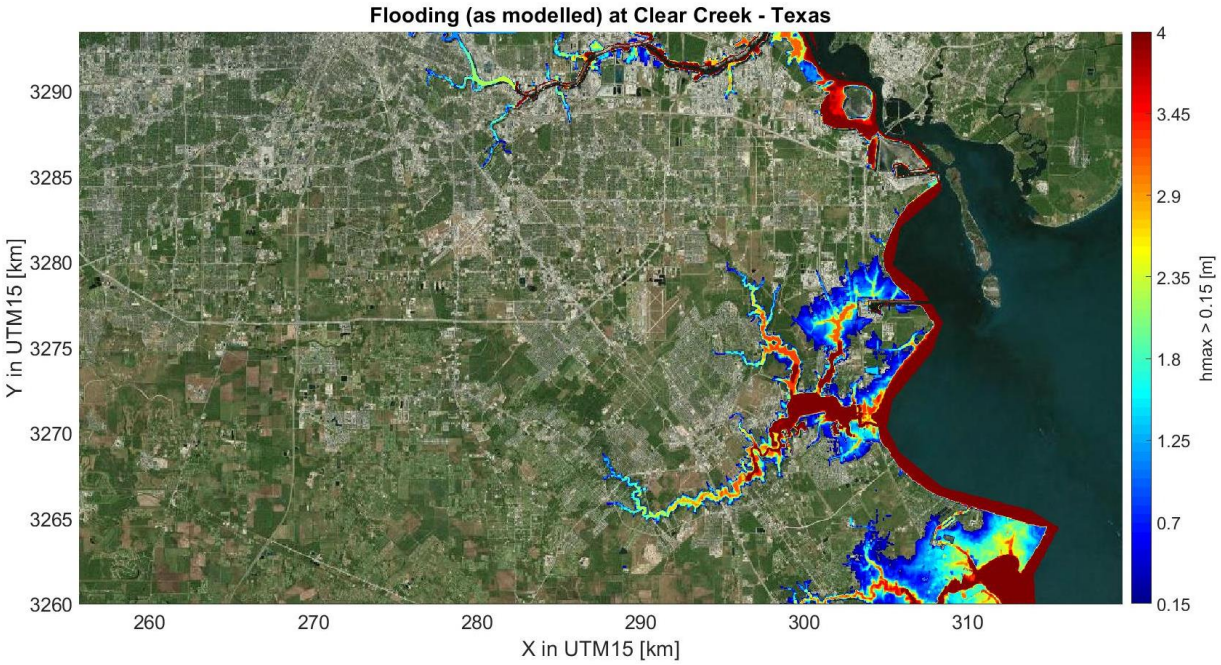

Figure 65. Hurricane Ike modelled Storm surge extent according to SFINCS (No rain Input).

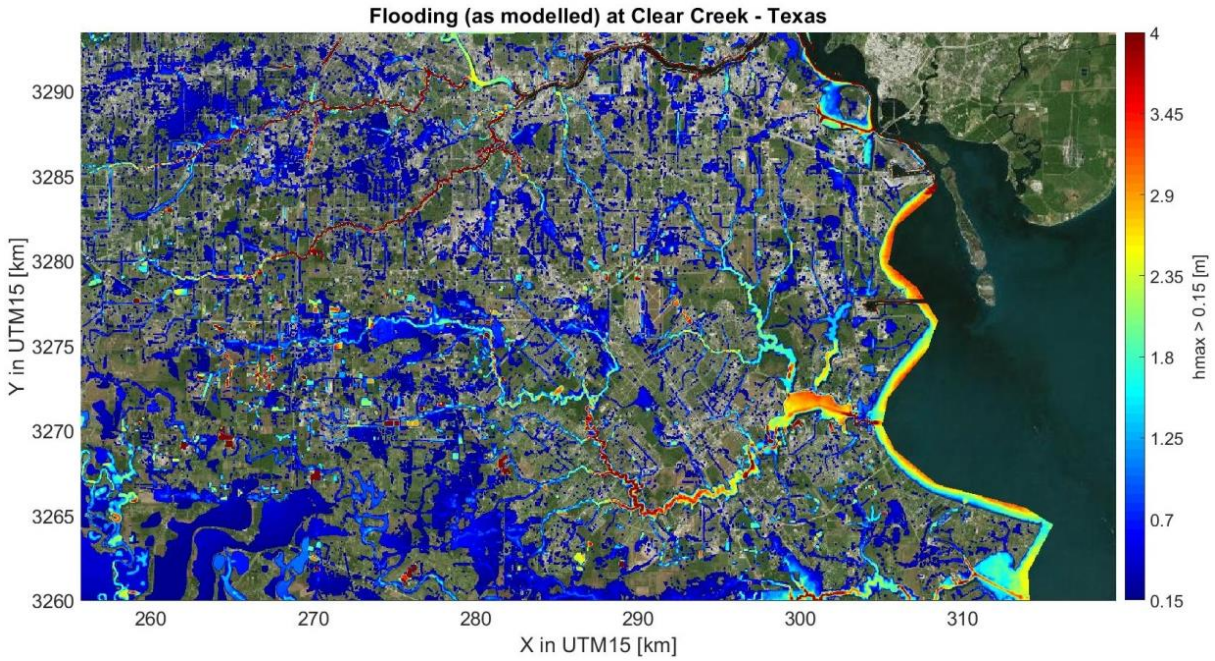

Figure 66. Hurricane Ike modelled precipitation extent according to SFINCS (Storm surge 0m).

3.3.1.1 Validation for Ike

In order to see the accuracy of the SFINCS model and to partially validate the results, the observation points where high water marks were registered by the FEMA (2008) were also included in SFINCS (see Figure 68) in order to obtain the maximum water depth at these locations and hence have a value of comparison between SFINCS and some real observations.

Initially, the values reported by FEMA were elevation data with vertical datum NAVD88, therefore, the original FEMA data was transformed to have the same datum as the one used in SFINCS (MSL). In addition, as the main output of SFINCS is the maximum water depth, these values had to be added with the bottom elevation at that specific point in order to get the same order of magnitude as the values reported by the FEMA. The result of the last operation can be seen in Figure 68 where additionally, the USGS locations evaluated in SFINCS are shown.

In Figure 67 each of the 21 FEMA points along the watershed were labeled in order to use them in Table 6 to compare them with the output of the SFINCS model using different threshold levels (h=5cm & h=2.5cm) (the threshold level in SFINCS act as a flooding or drying mechanism as explained in Appendix A).

Table 6 shows that generally, differences are less than 40cm which can be considered acceptable given all the simplifications made in the model (same as described in Section 3.3.2.1). In almost all the upper stream locations of the main waterway of the Clear Creek catchment and also in the upper part of the Armand Bayou the registered differences are less than 25cm. The highest difference registered is around 0.6m for location 2 nearby one of the port entrances near Morgan's point tide station. This is probably because SFINCS is linearly interpolating the water levels between the 2 tide stations along the whole coast which can give unrealistic values; especially considering the "heart shape" of the Bay at this location (this also explains the deviations on observation points 4 to 6).

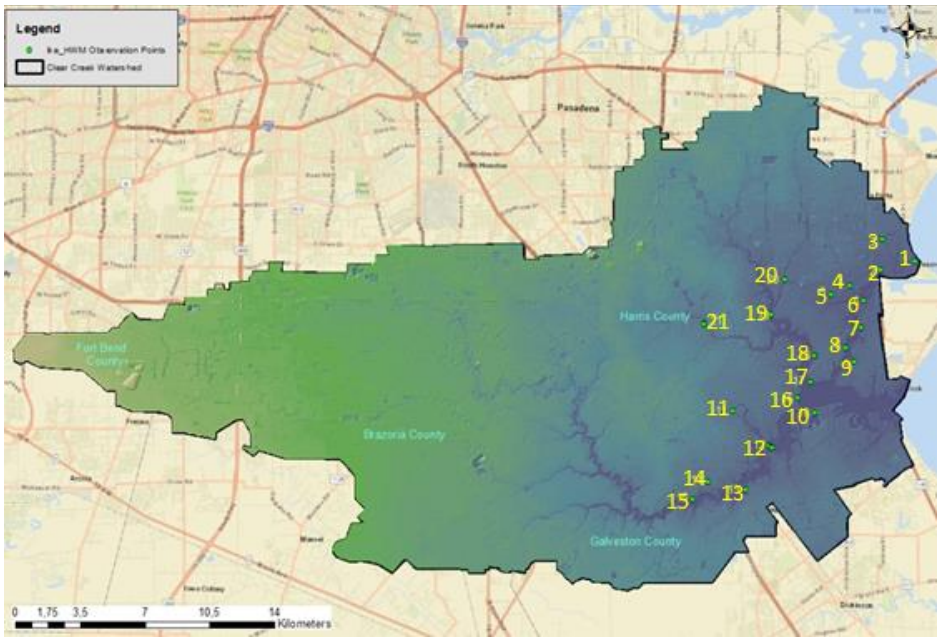

Figure 67. Labeled USGS locations of HWM for hurricane Ike. Source: (FEMA, 2008)

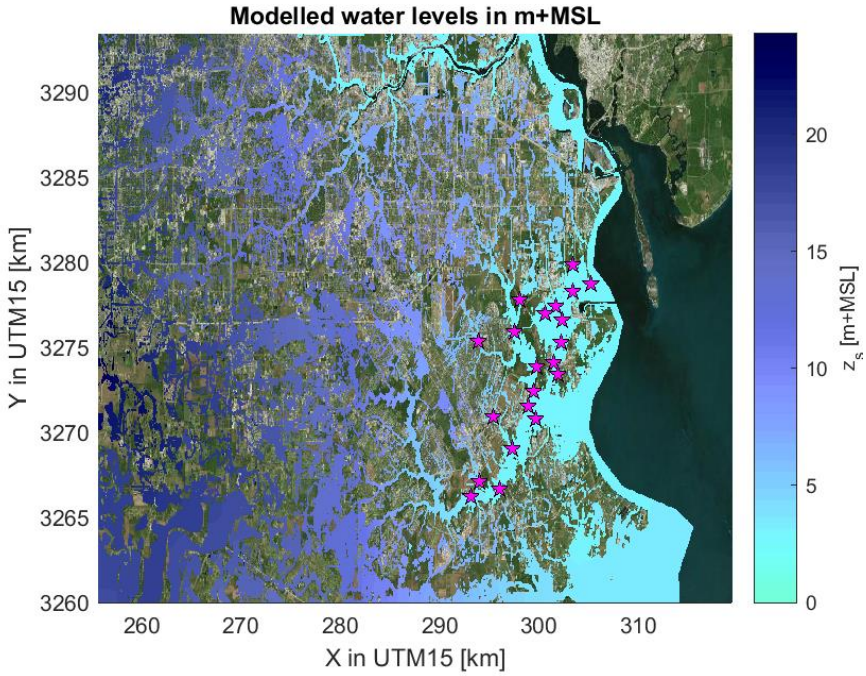

Figure 68. Simulated Water levels in m+MSL during Ike according to SFINCS. (Data containing topography details)

Table 6. Comparison between SFINCS and FEMA HWM (H) and Water depths (d) for hurricane Ike

Obs. Point	FEMA H (m+MSL)	SFINCS H (m+MSL)		FEMA d (m)	SFINCS d (m)		Diff. H & d FEMA/SFINCS		Flood Est.
		h.5cm	h.2.5cm		h.5cm	h.2.5cm	h.5cm	h.2.5cm	
1	3.501	3.144	3.119	1.534	1.177	1.152	-0.357	-0.382	Under
2	3.410	2.842	2.85	1.896	1.328	1.336	-0.568	-0.560	Under
3	3.410	3.624	3.606	1.528	1.742	1.724	0.214	0.196	Over
4	3.349	2.91	2.921	2.137	1.698	1.709	-0.439	-0.428	Under
5	3.349	2.914	2.923	1.48	1.045	1.054	-0.435	-0.426	Under
6	3.349	2.907	2.917	3.751	3.309	3.319	-0.442	-0.432	Under
7	3.258	2.901	2.91	4.154	3.797	3.806	-0.357	-0.348	Under
8	2.892	2.837	2.84	1.621	1.566	1.569	-0.055	-0.052	Under
9	3.227	2.904	2.912	2.218	1.895	1.903	-0.323	-0.315	Under
10	3.288	2.913	2.918	1.099	0.724	0.729	-0.375	-0.370	Under
11	3.806	3.94	3.928	1.276	1.13	1.141	0.134	0.122	Over
12	3.227	2.946	2.954	3.245	2.973	2.965	-0.281	-0.273	Under
13	3.471	3.009	3.034	1.667	1.205	1.23	-0.462	-0.437	Under
14	3.593	3.521	3.51	1.026	0.944	0.954	-0.072	-0.083	Under
15	3.684	3.414	3.428	0.378	0.123	0.109	-0.270	-0.256	Under
16	2.892	2.914	2.918	1.661	1.688	1.683	0.022	0.026	Over
17	3.471	2.944	2.955	2.797	2.27	2.281	-0.527	-0.516	Under
18	3.349	2.963	2.975	1.569	1.183	1.195	-0.386	-0.374	Under
19	3.258	3.012	3.028	3.496	3.25	3.266	-0.246	-0.230	Under
20	3.593	3.405	3.38	0.872	0.684	0.659	-0.188	-0.213	Under
21	5.422	5.61	5.606	2.832	3.02	3.016	0.188	0.184	Over

Table 7. Relative Bias and RMSE for Ike SFINCS Model given HWM and water depths from FEMA

Threshold model value	Relative Bias H	RMSE H	Scatter H (S.I)	Relative Bias d	RMSE d	Scatter d (S.I)
$h_{u,tresh} = 0.05m$	-7.11%	0.338	9.65%	-11.67%	0.337	15.06%
$h_{u,tresh} = 0.025m$	-7.03%	0.331	9.45%	-11.56%	0.332	14.82%

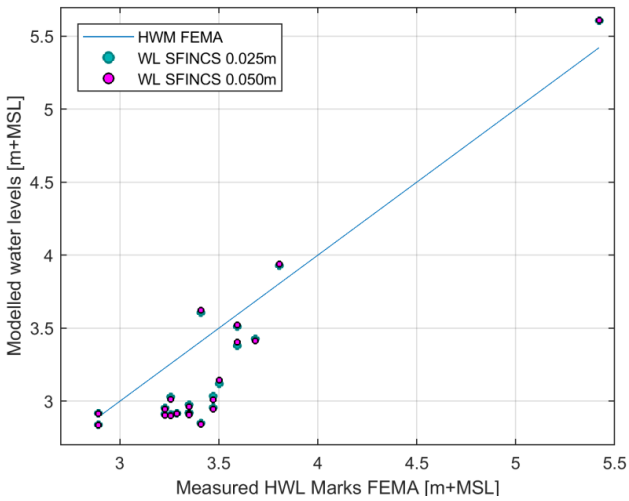

Figure 69. Scatter of SFINCS modelled water levels when compared to FEMA's HWM for Ike storm

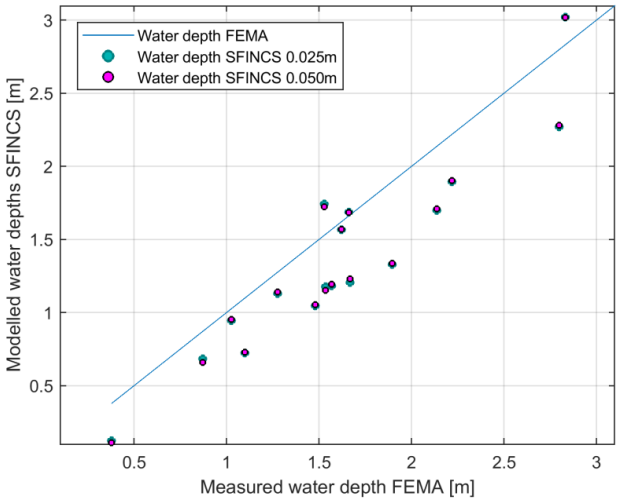

Figure 70. Scatter of SFINCS modelled water depth when compared to FEMA's recorded depth for Ike storm

In addition, in Table 7 some additional statistical definitions were computed (see equations 3.3.1 to 3.3.3) between the water levels and water depths predicted by SFINCS and FEMA HWM's and also a comparison was made between 2 different threshold values ($h_{u,tresh}$) for flow in the SFINCS model: One of 2.5cm and another one of 5cm. The results show that having a threshold of 2.5cm is slightly better than one of

5cm since the Scatter Index, the RMSE and the relative bias present lower values. In the case of Ike, SFINCS has a negative relative bias for the water levels of 7.1% and for water depths of 11.6%, meaning that overall, the model is under estimating around 7% and 12% (systematic error) the water levels and water depths respectively with a Root Mean Square Error (RMSE) of 0.33cm (approx. 20 cm lower than in the case of Harvey) which can attributed partially to the fact that the roughness is being wrongly attributed to certain locations. Nevertheless, the results can be considered as an acceptable approximation. Furthermore, the scatter of the modelled water levels is around 9.5% while for water depths it increases to a value of 15% which can also be considered as an acceptable result given that as was mentioned before, a grid of 50m probably cannot resolve punctual high water level measurements.

Systemic error relative to the Mean

$$rel.Bias = \sum_{i=1}^{N}(\text{ComputedWL} - \text{MeasuredWL}) / \sum_{i=1}^{N}(\text{MeasuredWL}) \quad \textbf{(3.3.1)}$$

Difference between values predicted by model and values observed

$$RMSE = \sqrt{\frac{1}{N}\sum_{i=1}^{N}(\text{ComputedWL} - \text{MeasuredWL})^2} \quad \textbf{(3.3.2)}$$

Standard deviation relative to the mean value of the measured signal

$$S.I = \frac{RMSE}{\frac{1}{N}\sum_{i=1}^{N} MeasuredWL} \quad \textbf{(3.3.3)}$$

3.3.2 Hurricane Harvey

In the case of hurricane Harvey, apart from the settings listed on the previous section, the spatially distributed rainfall over the area had to be included. As mentioned in Section 3.2.2, the spatial distributed precipitation was obtained from NASA's Web-based application: Giovanni© (Version 4.25) using the GPM IMERG Final Precipitation half hourly data set (Version 5). The rate of precipitation is reported in [mm/h] with a resolution of 0.1°x 0.1° degrees equivalent to a 10km grid and is reported in hourly intervals for Harvey storm. An example of one hourly data precipitation grid for the 25th of August from 23:00 till 23:59 pm is shown in Figure 71.

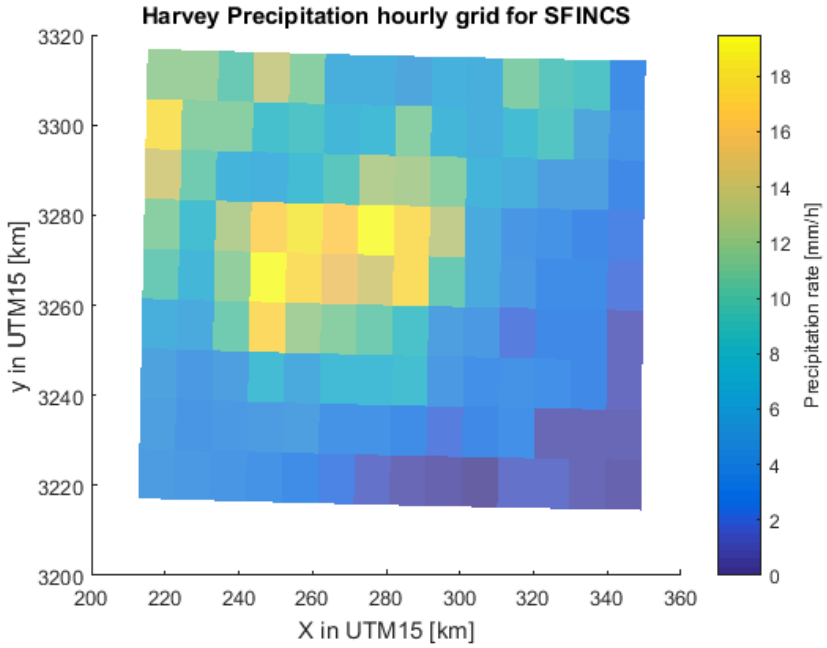

Figure 71. Hourly Harvey precipitation grid for SFINCS

In addition, Figure 72 shows the water levels corresponding to Harvey storm for the two tide gauges located nearby the Clear Creek watershed and Figure 73 shows the observation points registered in SFINCS, which correspond to the locations in which a high water mark (HWM) were registered by the USGS during the event (USGS, 2018). In total, the SFINCS model was run for 10 consecutive days from the 24th of August 2017, till the 2nd of September 2017. The time taken by the model to run the entire storm was 2.64 hours and the results of the simulation are shown from Figure 74 till Figure 76.

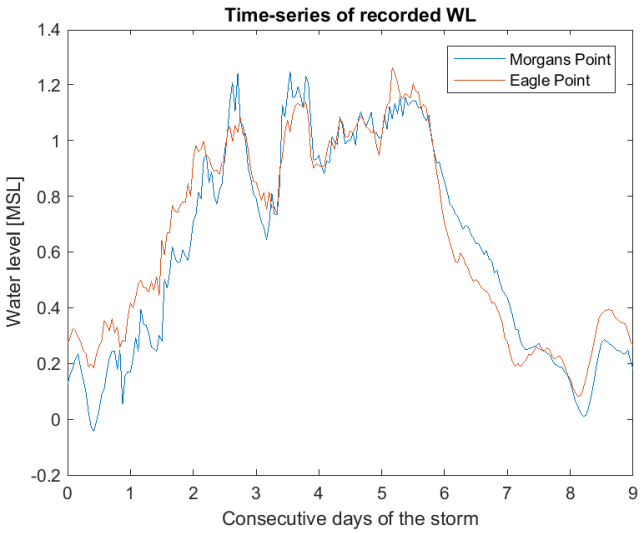

Figure 72. Water levels in tide gauges for Harvey storm

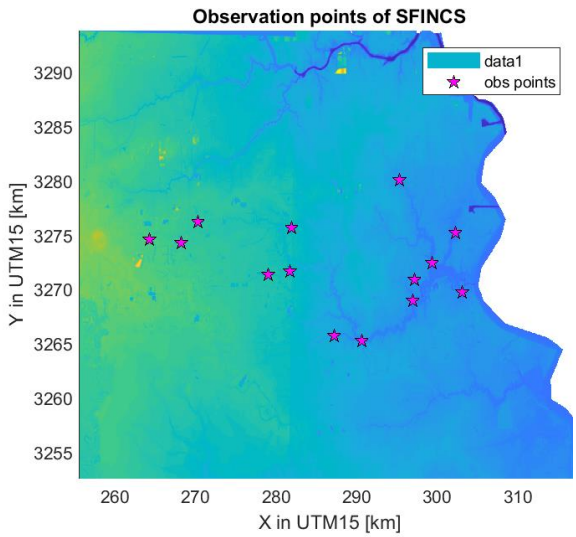

Figure 73. High Water Marks registered for Harvey in the Clear Creek watershed. Source:(USGS, 2018)

In Figure 74 the cumulative rainfall computed by SFINCS for hurricane Harvey for the nearby region of the Clear Creek watershed can be observed. It can be seen that the highest precipitation depth observed is on the south of the watershed with values around 0.8m of accumulated rainfall in 10 consecutive days of storm.

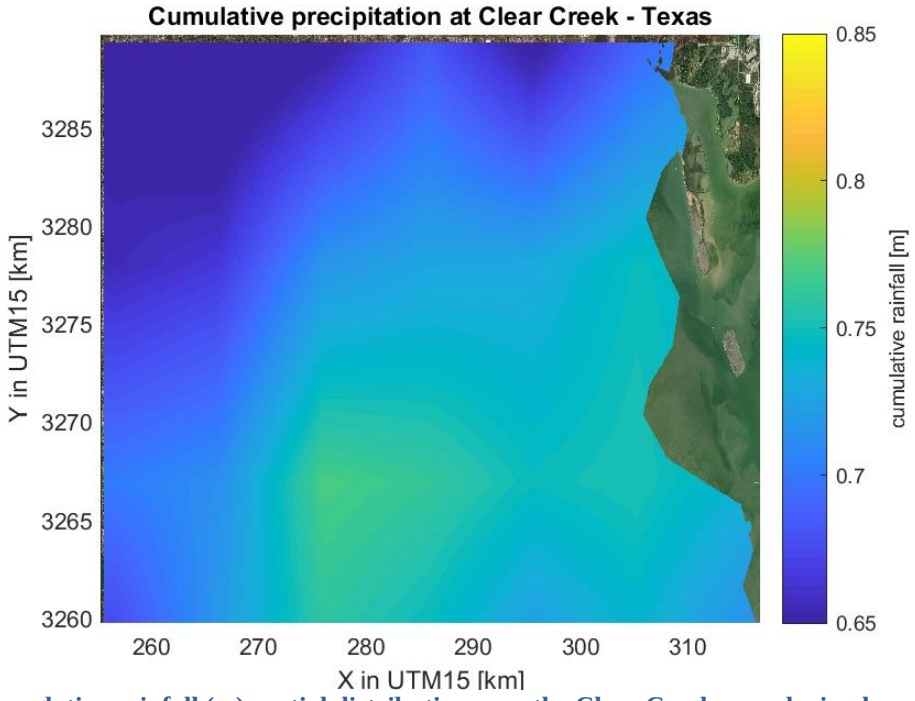

Figure 74. Cumulative rainfall (m) spatial distribution over the Clear Creek area during hurricane Harvey

In Figure 75 the maximum flow velocity computed by SFINCS for hurricane Harvey for the nearby region of the Clear Creek watershed can be observed. The values in this figure were limited to a maximum velocity of 0.5m/s as it was done before for hurricane Ike. The maximum velocities are shown clearly on the streams and also at the outlet of the watershed. Some inland locations also register the maximum velocity meaning that in this case precipitation was more relevant than the surge as it is also shown by the low velocities registered at the coast.

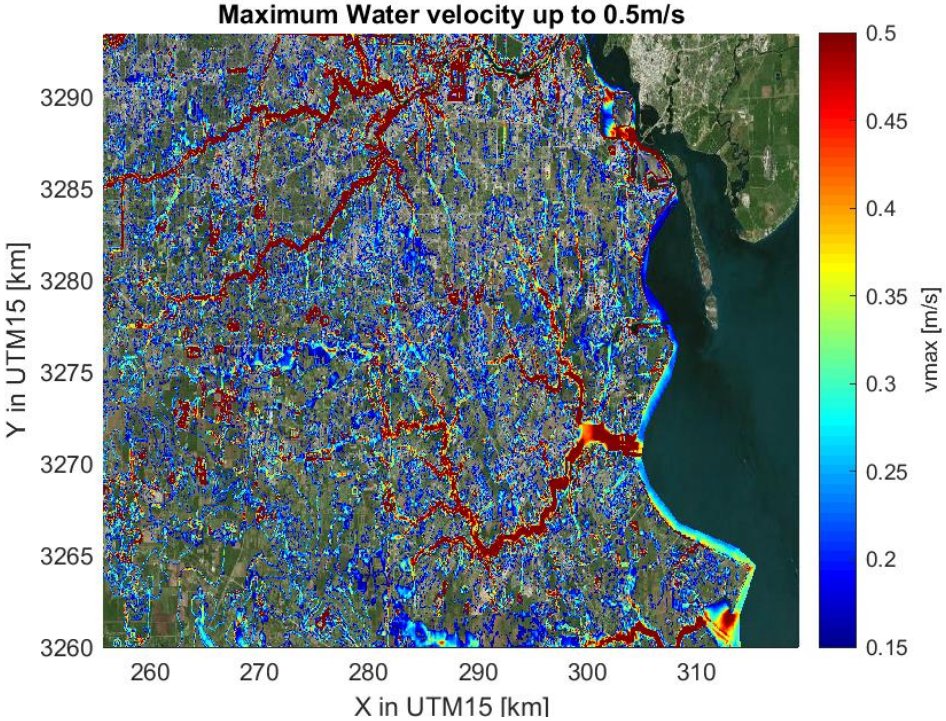

Figure 75. Maximum Water velocity illustrated up to 0.5m/s during Harvey Storm according to SFINCS model

In Figure 76 the maximum water depth is shown for each cell of the SFINCS model during the entire simulation of hurricane Harvey. For visualization reasons, the depth was limited to a maximum value of 1m for which it can be seen that the areas that suffered the most severe flooding were those located nearby Houston (upper west region) and also in the western part of the catchment demonstrating again that the main flood driver in this case was the precipitation event. The southern regions also register some significant flooding and it can be seen that in all the coastal boundaries the flood depth remain relatively low. The effect of the DEM used in SFINCS can be observed especially in the region nearby of the Clear Lake (outlet of the watershed) and also in the Armand bayou where it is seen that the flood spread through the residential areas.

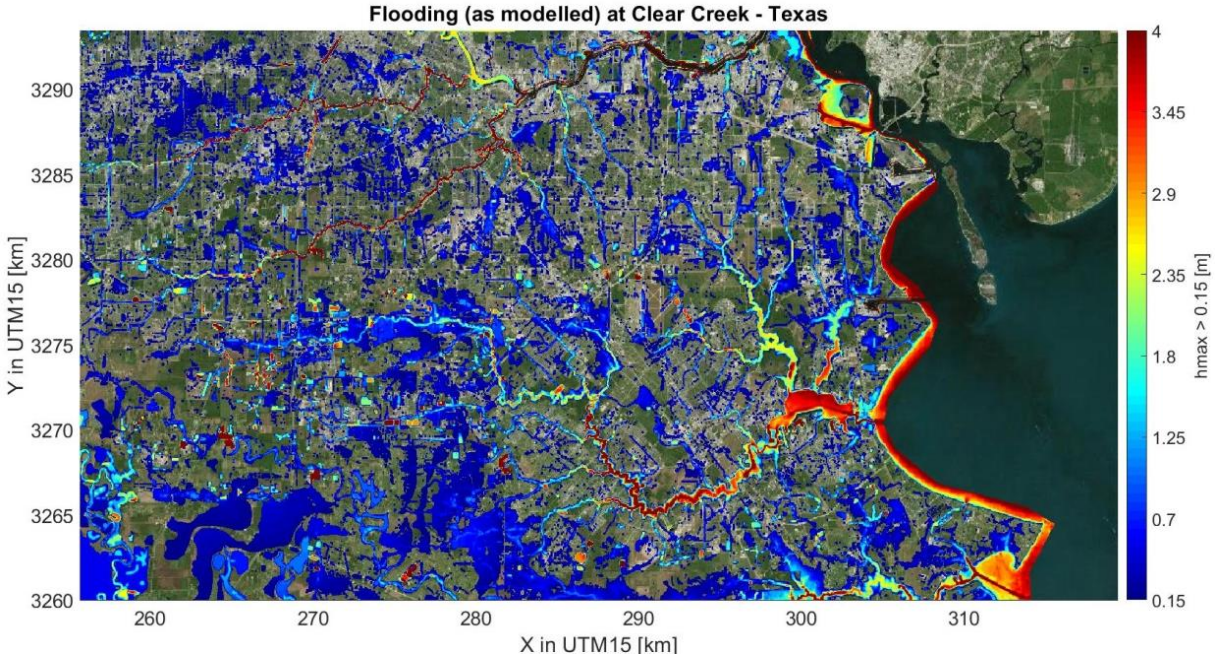

Figure 76. Maximum Flood Depth as modelled in SFINCS at Clear Creek during hurricane Harvey. Maximum water depth illustrated corresponds to a value of 1m and flooding was considered only above a value of 15cm

3.3.2.1 Validation for Harvey

Following a similar process as in the case of Ike, HWM's were used in order to see the accuracy of the SFINCS model and to partially validate the results. In this case, the information source of the HWM's was USGS (2018). The final results of the modelled water levels and the comparison between the USGS values (14 observation points) and the ones obtained in SFINCS are shown in Figure 77, Figure 78 and Table 8.

From Table 8 It can be seen that the 2 locations nearby the coast have the largest errors assuming that the USGS values are the real water levels. It can be observed that at location 1 and 2, the forcing of the model through the tide gages using the recorded levels (Figure 72) at the bay results in an over estimation of the flooding depth. This was expected since SFINCS is assuming this is the tide surge level coming from the bay but in reality, the tide gauges records were increased by the runoff precipitation and what SFINCS is doing is doubling the effect of the rainfall at these locations and hence reporting differences of even 1m. Since there is not a trustworthy estimation of what was the real surge of Harvey at the west side of the Galveston Bay, these errors have to be accepted. Locations 7 and 8 (located in the main waterway of the catchment) present differences of similar magnitude (1m) but in this case SFINCS is underestimating the flood depth, probably due to the fact that if the coordinates of these locations are looked closely and they are compared to Figure 144, at these locations the roughness associated was too high and didn't correspond to the roughness of the waterway, which may lead to an underestimation of flooding. All the locations in the Armand Bayou and in the west upstream part of the Clear Creek watershed present a difference in water depth less 35cm between SFINCS and the records of the USGS. Is important to mention that the depth values reported in Table 8 were computed taking the elevation point from SFINCS at the specific USGS coordinate since there is no reliable reference of flood depths in the USGS dataset and is more interesting to look at the simulated water depths rather than the water levels.

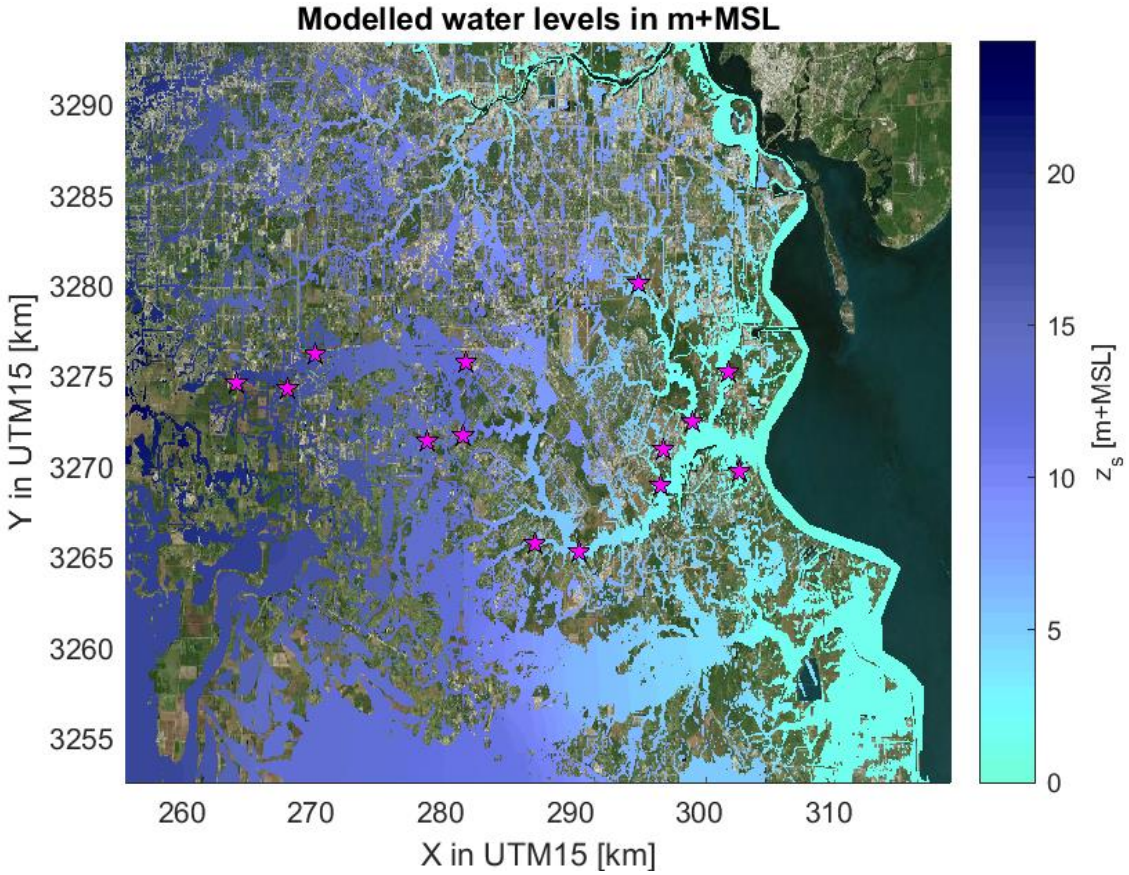

Figure 77. Maximum simulated water levels in m+MSL during Harvey according to SFINCS. (Data containing topography details)

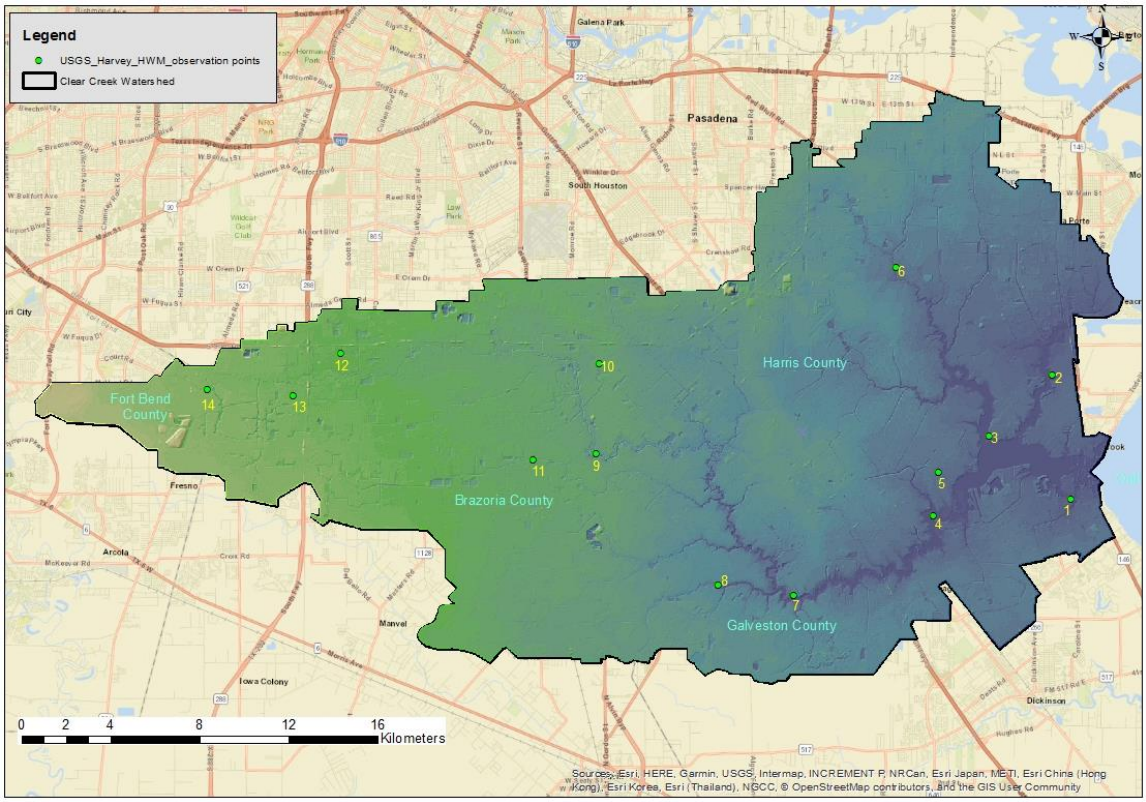

Figure 78. Labeled USGS locations of HWM for hurricane Harvey.
Source: (USGS, 2018)

Table 8. Comparison between SFINCS and USGS HWM (H) and Water depths (d) for hurricane Harvey

Obs. Point	USGS H (m+MSL)	SFINCS H (m+MSL)		USGS d (m)	SFINCS d (m)		Diff. H & d USGS/SFINCS		Flood Est.
		h.5cm	h.2.5cm		h.5cm	h.2.5cm	h.5cm	h.2.5cm	
1	2.605	3.608	3.607	2.443	3.446	3.445	-1.003	-1.002	Over
2	2.651	3.533	3.536	3.757	4.639	4.642	-0.882	-0.885	Over
3	1.706	1.757	1.767	2.109	2.160	2.170	-0.051	-0.061	Over
4	2.014	2.344	2.354	1.049	1.379	1.389	-0.33	-0.34	Over
5	4.157	3.914	3.918	0.31	0.072	0.068	0.243	0.239	Under
6	5.041	5.160	5.179	2.408	2.527	2.546	-0.119	-0.138	Over
7	6.049	5.089	5.097	5.476	4.516	4.524	0.96	0.952	Under
8	7.275	6.188	6.211	3.819	2.732	2.755	1.087	1.064	Under
9	12.310	12.358	12.350	2.533	2.581	2.573	-0.048	-0.04	Over
10	13.401	13.377	13.392	0.033	0.025	0.01	0.024	0.009	Under
11	14.264	14.447	14.448	0.986	1.170	1.169	-0.183	-0.184	Over
12	16.724	16.434	16.436	0.66	0.372	0.37	0.29	0.288	Under
13	17.629	17.320	17.325	1.05	0.747	0.742	0.309	0.304	Under
14	18.818	18.914	18.914	0.918	1.014	1.009	-0.096	-0.096	Over

Table 9. Relative Bias and RMSE for Harvey of SFINCS Model given HWM (H) and water depths (d) from USGS

Threshold model value	Relative Bias H	RMSE H	Scatter H (S.I)	Relative Bias d	RMSE d	Scatter d (S.I)
$h_{u,tresh} = 0.05m$	-0.140%	0.554	5.13%	-0.49%	0.553	22.35%
$h_{u,tresh} = 0.025m$	-0.007%	0.550	5.10%	-0.40%	0.550	22.24%

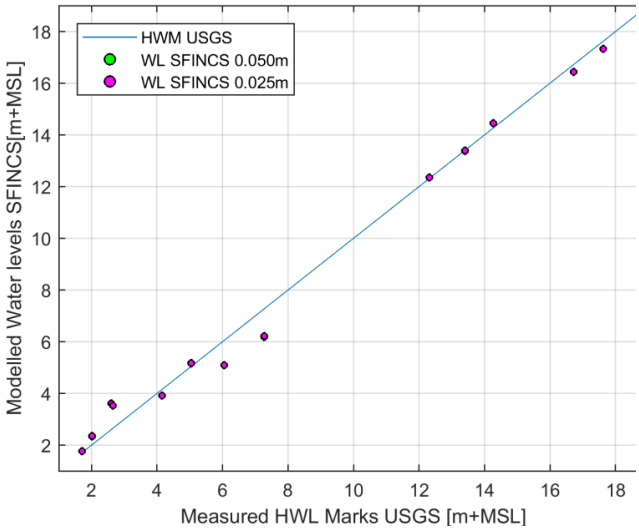

Figure 79. Scatter of SFINCS modelled water levels when compared to USGS HWM for Harvey storm

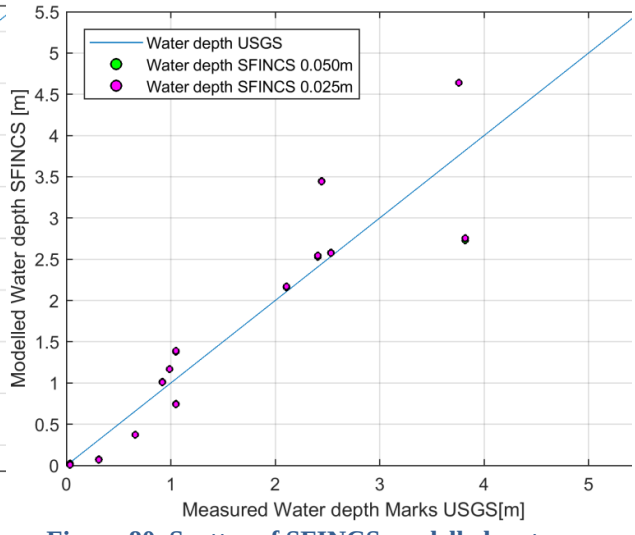

Figure 80. Scatter of SFINCS modelled water depths when compared to USGS water depth for Harvey storm

In addition, in Table 9 some additional statistical definitions were computed (see equations 3.3.1 to 3.3.3) for the water levels and water depths predicted by SFINCS and the USGS HWM's. In addition, a comparison was made between the 2 different threshold values ($h_{u,tresh}$) for flow in the SFINCS model: One of 2.5cm and another one of 5cm. The results of Table 9 show that there is not a significant difference between the output water levels or water depths of the model if the threshold is varied between these two numbers. In general, SFINCS has a negative relative bias of 0.20% for the water levels and water depth meaning that overall, the model is under estimating around 0.2% (systematic error) the water levels and water

depths with a Root Mean Square Error (RMSE) of 0.55cm which can be considered high but this can be attributed to the observation points near the coast which were doubling the effect of the precipitation. Furthermore, the scatter of the modeled water levels is around 5.1% while for the water depth the scatter increases to 22% (see Figure 79 and Figure 80), which says that there is more variation in the estimation of the water depths but this can be attributed to the outlier points near the coast and the 2 inland points underestimating the flooding. It is also seen that when Figure 80 is compared to Figure 70 from the scatter in water depths for hurricane Ike, it can be seen that there is a better agreement for hurricane Harvey and this can be partially attributed to the resolution of the precipitation input which is better in the case of Harvey; therefore, in can be said that for this particular case SFINCS is resolving better the precipitation than the surge in the catchment.

Taking into account that the measurement of HWM is also a process that carries a lot of uncertainty and that HWM's are more local situations that potentially could not be entirely represented by a 50m resolution grid, it can be said that given the results of Table 8 and Table 9, SFINCS is performing adequately and that due to some of the assumptions made (e.g. water levels at the coast are being forced by observation and not by the dynamic wave conditions near the bay, there is not any wind forcing, the additional water coming from the Addicks and Barkers reservoir was not included, etc.) the errors obtained only comparing with a small sample of 14 points are acceptable and therefore the use of SFINCS can be recommended for a compound flooding analysis, especially since almost all inland points are being well resolved by the model.

3.3.3 Conclusions

According to the results obtained by SFINCS when modelling hurricanes Harvey and Ike, it can be said that the accuracy obtained with SFINCs is acceptable and that this model could be used to model compound flooding since it is capable of resolving both processes (Storm surge and Precipitation) even when several restrictions and limitations (see below) are included in the setup of the model

- Shore forcing: Water levels from Morgan's and Eagle Point tide stations. No wave dynamics included
- Water levels linearly interpolated between stations disregarding shape of the bay
- No wind accounted in the model: this influences the extent of flooding

Ways to improve the limitations of the setup of SFINCS would be to include more forcing points along the coast or couple the model boundaries (located at 2m of depth in the coast) with a 2D model of the Galveston Bay (e.g. XBeach or Delft3D Model) and include the wind forcing along the hurricane track. Due to the scope of this research, this is out of reach, but the intention of modeling Ike and Harvey using the aforementioned restrictions and limitations was to show the power of the model, which showed that the model errors were most of the time underneath 20% when compared to punctual High Water Level Marks. Is important to mention, that the methodology of recording HWL marks is sometimes really subjective and dependent on who is taking the records, therefore uncertainty around this values also make possible that the error of the model is reduced.

It is clear that only few georeferenced water marks in approximately 500 km^2 is not enough to show the full accuracy of the model, but it is a first index that was used due to the fact that this was free available data and no major post processing of the data was required. Further validation for these two storms include a comparison with aerial extents of flooding in the area, nevertheless this information is not readily available and sometimes even satellite images have low quality since the storm itself generate obstructions that cover the inland regions (clouds). In addition, it was seen that in the **southern** part of the SFINCS model a strange behavior is occurring (see lower region of Figure 63, Figure 66 and Figure 76), in which there is an accumulation of water that is not happening due to the natural topography, but more due to the fact that the southern boundary is behaving like a closed boundary wall in which water piles up. A way in which this was tried to be solved was by lowering the southern boundary so that this effect is not seen in the Clear Creek watershed. This has to be applied as well for running all probabilistic scenarios; otherwise flooding will be unrealistically overestimated by the model.

Likewise, if the results from Ike and Harvey flooding are observed, and special focus is given to Figure 144 which shows the manning roughness values used in SFINCS, it can be seen that SFINCS is not differentiating any water bodies upstream of km 15 from the outlet of the watershed. This happens of course because the threshold value for manning is based on a height above mean sea level and at these locations, the main channels easily surpass this threshold, assigning to every region a roughness coefficient for land. The previous assumption will have an effect on the flooding depths and flooding extents, since using the same high uniform roughness value will create that in the upstream reaches of the catchment water is conveyed to the channel in a much quicker way than it would be in reality, due to the fact that manning will be underestimated on the overland part of the catchment. Nonetheless, once water arrives to the main stream, it would move at a slower pace since the roughness is overestimated for the creek. This process will create in the upper stream reaches an overestimation of the water depth by the model, and in the downstream part of the catchment a delay on the backwater effect between discharge and surge level that will possibly underestimate flooding in those areas. The current version of SFINCS doesn't allow changing the input for a spatially varying manning which would be the most appropriate way of solving the overland flow; nevertheless, possible improvements of SFICNS should try to include these variations in order to have better results without compromising the computational speed of the model. For the purposes of this research is enough to know the limitations and setbacks of the current version of SFINCS.

Finally, as a conclusion from changing the threshold value for flow (wet and dry condition of SFINCS) in both storms, it was decided that a value of 0.025 cm would be the appropriate choice for running the synthetic compound events (see chapter 5) since it doesn't increase significantly the computational time and it slightly improves the results.

4

Boundary conditions for compound flooding

In this chapter a description of the synthetic data set used to generate the boundary conditions for a compound flooding analysis of the Clear Creek watershed is going to be presented. This chapter will include the relevant details in order to determine the joint probability between peak storm surge and cumulative precipitation for the catchment as well as the final selection of compound flooding scenarios that are going to be used for the flood risk assessment of the Clear Creek watershed.

4.1. Definition of Boundary Conditions for Compound flooding in the Clear Creek watershed

As explained partially before in chapter 2 (Section 2.4.2.3), a NPBN has been used before in order to stochastically simulate large number of combinations of cumulative precipitation and peak storm surge given that a hurricane makes landfall on the Galveston Bay region. The study performed by Sebastian et al. (2017), constructed a NPBN (see Figure 81) to generate 100,000 synthetic storm events that may enter the Gulf of Mexico and potentially make landfall nearby the Galveston Bay.

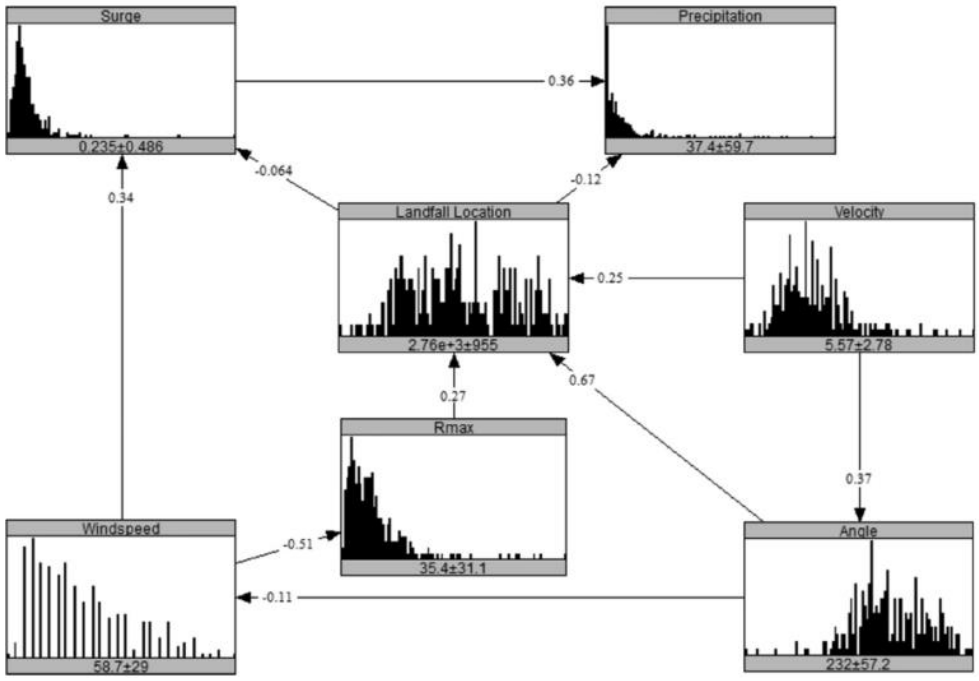

Figure 81. NPBN structure for TCs in Galveston Bay Region. Source: (Sebastian et al., 2017)

The NPBN was fed with data from 114 years of observations in the Gulf of Mexico, in which the main variables observed form the data were TC's characteristics in the entire Gulf of Mexico area, residual water levels (near the entrance of the Galveston Bay) and peak cumulative precipitation (on the Clear Creek watershed area). The NPBN was based on Gaussian Copulas in order to explain the correlation between

related variables (see arrows connecting boxes in Figure 81). After conditioning the NPBN to a specific angle at landfall (Perpendicular to the coast (Sebastian et al., 2017)), a suite of TC characteristics (angle, wind speed, etc.) was obtained in order to use it as input in an empirical wind setup model to simulate storm surge specifically at the outlet of the Clear Creek watershed (see location at Figure 31). Finally, with the estimated peak storm surge (from the wind setup model) and the peak cumulative precipitation (5-consecutive days from the NPBN) a data set was created for the Clear Creek watershed which represented the possible boundary conditions of storm surge and cumulative precipitation given landfall of a hurricane in the region.

Is important to mention that the observed TC's characteristics were based on 596 storms that entered the Gulf of Mexico and made landfall on the Gulf Coast. Only 32 of those storms made landfall nearby Galveston Bay. The hourly verified water levels collected from tide stations were adjusted for sea-level rise and reported relative to NAVD88 based on the actual National Tidal Datum Epoch (NTDE) (see Sebastian et al. (2017) for more details on the methodology).

The boundary conditions obtained from the research are highly important since they could be potentially used for a compound flooding analysis in which both variables occur at the same time or in close succession. For this reason, the results of the aforementioned study are going to be used in the present research in order to perform a flood risk assessment of the Clear Creek watershed considering compound event.

4.1.1 Joint Probability for cumulative precipitation and peak storm surge

The research done by A. Sebastian et al. (2017) also included a joint probability estimation (based on return periods) of the variables analysed from the synthetic data and it presented the results in joint probability contours as depicted in Figure 82.

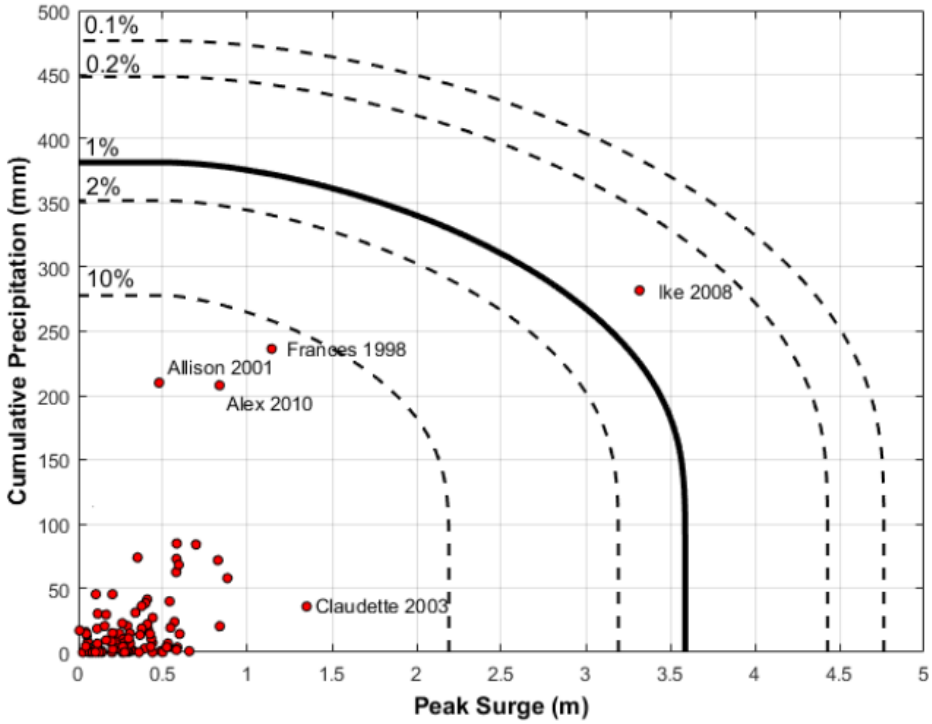

Figure 82. Joint probability for cumulative rainfall and peak storm surge at the outlet of the Clear Creek. Red dots are observed points of surge at Eagle point and cumulative precipitation in the Clear Creek watershed. Source: (Sebastian et al., 2017)

The calculation of the joint probability of peak surge and cumulative precipitation is based on the following steps:

1. Fitting of the marginal distributions (Surge and rainfall separately) based on the synthetic data

2. Fitting of a Copula[7] to explain correlation between variables
3. Computation of Iso-probability lines in the copula space corresponding to each return period being analysed (e.g. 100, 200. 1000 years)
4. Transformation of the Iso-probability lines from the Copula Space to the real space values by means of the inverse cumulative distribution function (ICDF) associated with each marginal

The following assumptions were made by Sebastian et al. (2017) in the aforementioned research in order to successfully construct Figure 82.

1. **Marginal distributions:**
    - **Precipitation:** Exponentially distributed
    - **Storm Surge:** Generalized Pareto Distribution (GPD With a minimum threshold of 0.55m)
2. **Copula:** Gaussian Copula Selected – Main reason for selection was that the NPBN was based also on Gaussian Copulas
3. **Iso-probability lines Copula space:** The AND (see (Salvadori & De Michele, 2004)) approach was used in order to compute the associated copula value related to a specific return period
4. **Transformation of Iso-probability lines:** Using the ICDF for the exponential distribution and the GPD for each respective variable

Figure 82 was obtained in 2014, and it shows all the possible scenarios along the return period curve that is being considered (e.g. 100-year, 500-year, etc.). In particular, the 100-year joint probability curve for the Clear Creek watershed shows that the maximum peak surge associated with a 100-year flooding event will be around 3.6m while for cumulative precipitation is around 380mm. Is important to mention that as the NPBN was used and calibrated before Harvey, the rainfall observations didn't include the extreme precipitation triggered by this particular storm (and other storm events that have occurred since 2014 until the present time) and therefore is worthy to explore in the future, a possible re-run of the NPBN in order to get an updated synthetic dataset including the effects of the increased precipitation values coming from storms in the last 4 years. As running again the NPBN is out of the scope of this particular project, the regular synthetic data is going to be used in order to determine the hydraulic boundary conditions that are going to be used in the SFINCS model in order to perform the flood risk assessment of the catchment considering compound events. Since the 100,000 synthetic data is available and for running SFINCs we need to choose appropriate points along each return period curve in order to run compound flooding scenarios, it was decided that the curves of the joint probability between the two interest variables was going to be performed again following the four steps mentioned above since the results and pairwise data of the curves in Figure 82 are not available for direct use. The steps and alternatives chosen are explained in the following section including the selection of the points along each curve that will represent each return period together with the most likely design realization along the curve as described by Corbella & Stretch (2012).

4.1.1.1 Fitting of Marginal distributions

In order to determine which is the distribution that better fits the data, several distributions were tested and compared to the synthetic data. For simplicity, only the distributions included on the Statistics and Machine Learning Toolbox of Matlab© (Version R2016b) were used. The following sub-sections present the final results of the probabilistic analysis performed for the synthetic data set, however all the process behind the final selection can be consulted in the appendices of this report (see Section 9.2).

4.1.1.1.1 Storm Surge

For determining the distribution that better describes the storm surge data a reduced number of the distributions included in Matlab© (Version R2016b) were tested. In the case of the storm surge only the

7 A copula is a function that joins multivariate distribution functions to their one dimensional marginal distributions functions. They are used to describe dependence between random variables and they allow to separate the marginal distributions from the dependence structure and model each one separately without meaning that the variables are independent (Rayens & Nelsen, 2000)

continuous distributions that included positive values (including the zero [0,∞)) were used for the analysis. In Figure 83 the synthetic data for storm surge is presented and plotted as a histogram. This data represents the empirical probability distribution (PDF) of the storm surge and is against this data that other distributions were compared (see Appendices Section 9.2). The final distribution selected to represent the storm surge data can be observed in Figure 84.

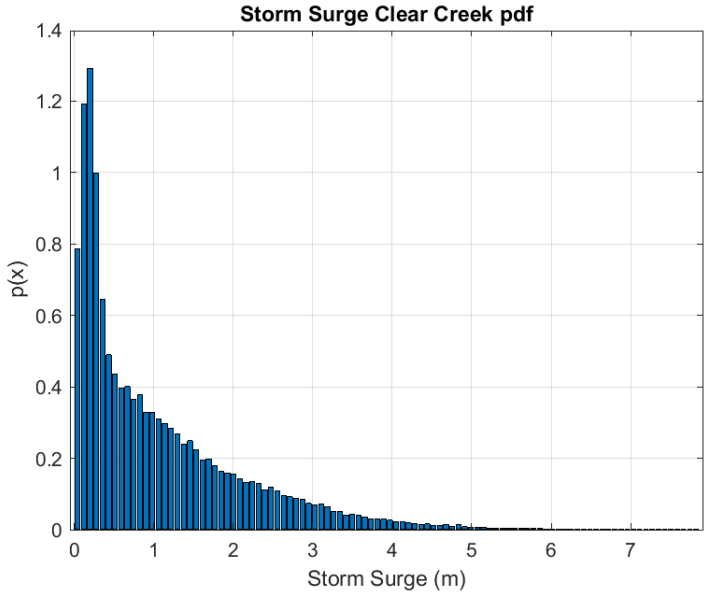

Figure 83. Storm surge in the Clear Creek watershed - Empirical PDF

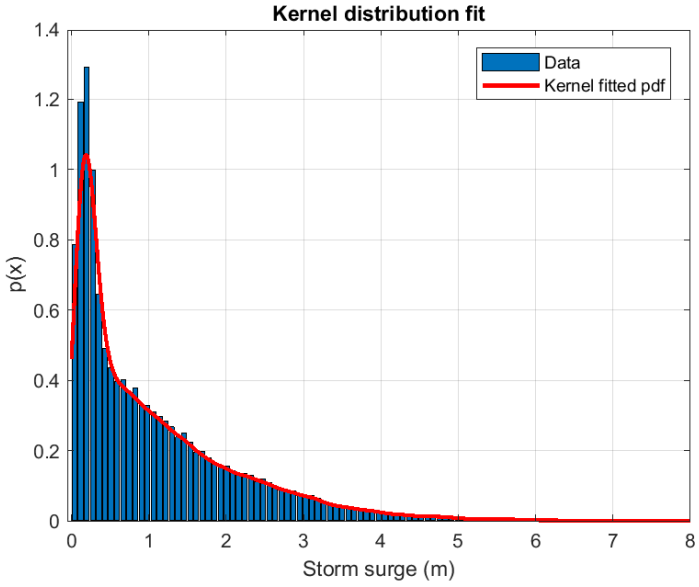

Figure 84. Selected Kernel PDF distribution fitted to Storm Surge Data

The Kernel distribution is a non-parametric representation of the PDF of a random variable. This is normally used when no other parametric distribution has a better fit to the data and no assumptions are want to be made regarding the distribution of the data. This distribution works as a smoothing function which is controlled by a bandwidth value. The smoothing function can be selected using different shapes such as the normal Gauss shape, a rectangular box or even a triangle. In this case looking into the data, a normal shape was the most indicated smoothing function. For this case the Generalized Pareto distribution was not tested (original assumption made by Sebastian et al. (2017)) since the storm surge data obtained from the NPBN included surge estimations with a zero value which cannot be included by the GP distribution (valid only for (0,∞) values).

4.1.1.1.2 Precipitation

For determining the distribution that better describes the precipitation data almost the full number of the distributions included in Matlab© (Version R2016b) were tested. Only the continuous distributions that included negative values were excluded from the analysis. In Figure 85 the synthetic data for precipitation is presented and plotted as a histogram. This data represents the empirical probability distribution (PDF) of the precipitation and is against this data that other distributions were compared. (See Appendices, Section 9.2). The final distribution selected to represent the precipitation data can be observed in Figure 86.

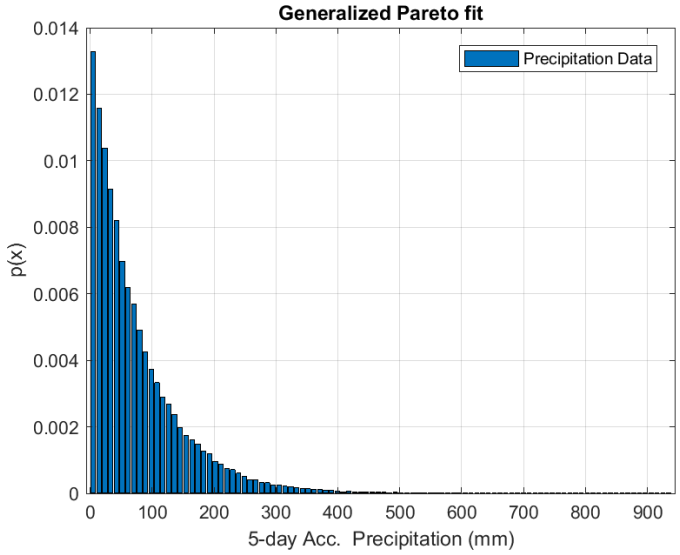

Figure 85. Accumulated precipitation in the Clear Creek watershed - Empirical PDF

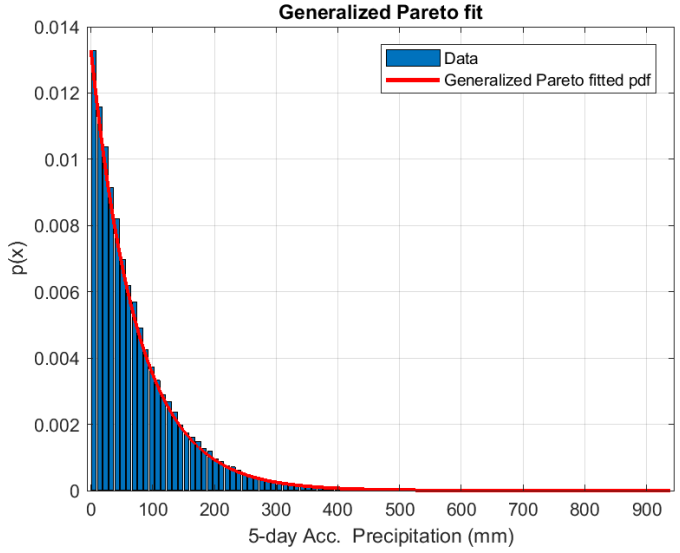

Figure 86.Selected GPD distribution fitted to Precipitation Data

The PDF of a GPD is described by means of equation 4.1.1 in which three parameters can be observed; the shape parameter $K \neq 0$, the scale parameter sigma (σ) and the threshold parameter theta (θ)

$$y = f(\mathrm{x} \mid \mathrm{k}, \sigma, \theta) = \left(\frac{1}{\sigma}\right)\left(1 + k\frac{(x-\theta)}{\sigma}\right)^{-1-\frac{1}{k}} \qquad \textbf{(4.1.1)}$$

$$for\ \theta < x, when\ k > 0, or\ \theta < x < \theta - \frac{\sigma}{k}\ when\ k < 0$$

For the fitted GPD to the precipitation data, the three parameters were the following:

- K = 0.0046
- σ = 75.2138
- θ = 0

For this case the exponential distribution was not chosen since in the Goodness-of-Fit test it ranked below the GDP (see Appendices Section 9.2). Nevertheless the value of K close to 0 shows that that actually the data could be also represented by an exponential distribution.

4.1.1.2 Fitting of Copulas to Joint Data

In order to estimate the return period in a bivariate analysis, two methodologies can be executed depending on the nature of the problem being analyzed. This two cases are known in literature (e.g. (Salvadori & De Michele, 2004),(Salvador et. al., 2011),(Gŕaler et al., 2013)) as the OR & AND cases (see Figure 87 and Figure 88 respectively) and they represent different regions carrying probability masses.

The OR case is given by the following expression and it represent the shaded region of Figure 87.

$$p_{\widetilde{u,v}} = P\{U > u \ \vee V > v\} = 1 - C(u,v) \qquad \textbf{(4.1.2)}$$

While the AND case is case is given by the following expression and it represent the shaded region of Figure 88.

$$p_{\widetilde{u,v}} = P\{U > u \ \wedge V > v\} = 1 - u - v + C(u,v) = \ C(1-u, 1-v) \qquad \textbf{(4.1.3)}$$

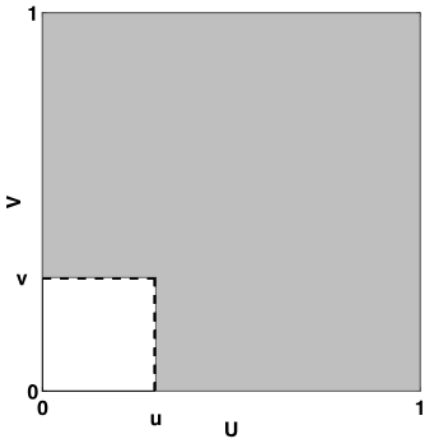

Figure 87. OR case as depicted by (Salvadori & De Michele, 2004)

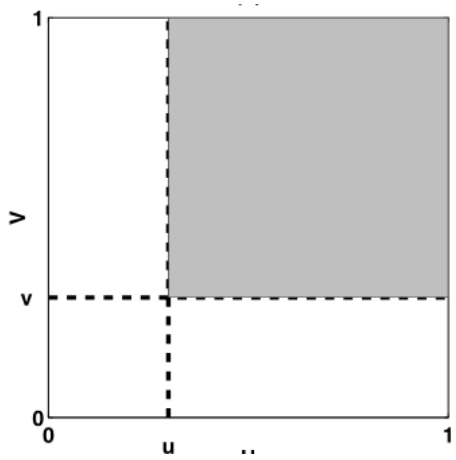

Figure 88. AND case as depicted by(Salvadori & De Michele, 2004)

Due to the selected definition of compound flooding stated in chapter 2 (Section 2.4), the joint probability will be delineated using the "AND analysis" (see formal definition on Salvadori & De Michele (2004)), since the area of interest is mainly the region in which both variables happen at the same time or in close succession. The "AND" case requires as seen from equation 4.1.3 the use a copula $C(1-u, 1-v)$ which in this specific case is known as the **survival copula** since it has marginals described by:$(1-u), (1-v)$. In the following section the results of the fitting of the survival copula to the data are going to be shown.

4.1.1.2.1 Survival Copula

In this section the regular definition of copula is going to be used in which according to Sklar (1959) theorem the random variables X and Y are joined by copula C, if their joint distribution $F_{XY}(x,y)$ can be written as:

$$F_{XY}(x,y) = C(F_X(x), F_Y(y)) \qquad \textbf{(4.1.4)}$$

Where $F_X(x)$ and $F_Y(y)$ are the marginal distributions and $C:[0,1]^2 \rightarrow [0,1]$ represents the copula.

As shown before, the copula space only exists for values between 0 and 1 therefore a transformation of the data (x, y) is required (see original data on Figure 89) in order to construct the empirical copula (see definition on Appendices Section 9.2). This transformation is done in the case of the Survival Copula by subtracting from one (1) the ranked data and dividing afterwards by the number of samples plus one as depicted below. With this transformation the copula can be represented as $C(1-u,1-v)$ and the data from Figure 89 is transformed to the one represented in Figure 90.

$$\left(1-\frac{R_i}{n+1},1-\frac{S_i}{n+1}\right) \qquad \textbf{(4.1.5)}$$

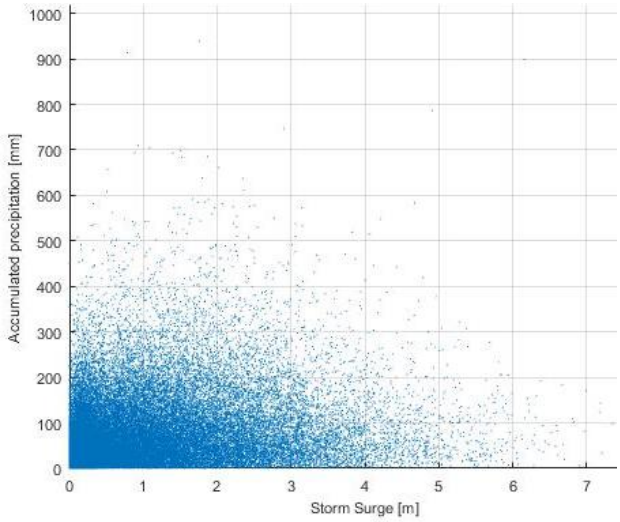

Figure 89. Storm and Surge Data from Synthetic data (100,000 data from the NPBN)

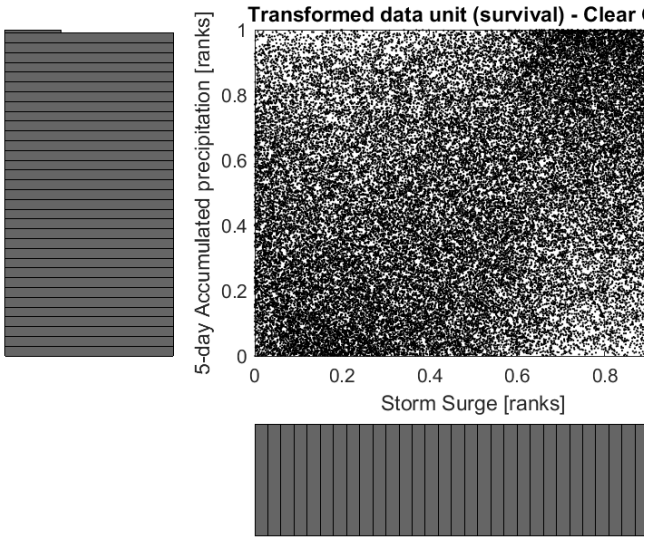

Figure 90. Transformed data to copula space with uniform marginal

In order to find the best copula that fits the original data transformed to the copula space $[0,1]$, five (5) copula families were tested (see families below). As in the previous section, this was done since these families are implemented in the Statistics and Machine Learning Toolbox of Matlab© (Version R2016b) and they are the most common copulas used in engineering applications.

- Gaussian
- Gumbel
- Frank
- t-student
- Clayton

The results from the fitting analysis according to the Crámer-von Mises criterion and the Semi-correlations analysis (see Appendices Section 9.2) state that the appropriate survival copula is the Frank copula which is described by the following expression:

$$C(1-u,1-v)=-\frac{1}{\theta}\ln\left[1+\frac{(e^{-\theta(1-u)}-1)(e^{-\theta(1-v)}-1)}{e^{-\theta}-1}\right] \qquad \textbf{(4.1.6)}$$

In which the θ parameter fitted to the synthetic data is equal to 1.7604 according to the fitting analysis (see Appendices Section 9.2). In Figure 91 and Figure 92 the theoretical CDF and PDF of the selected copula can be observed.

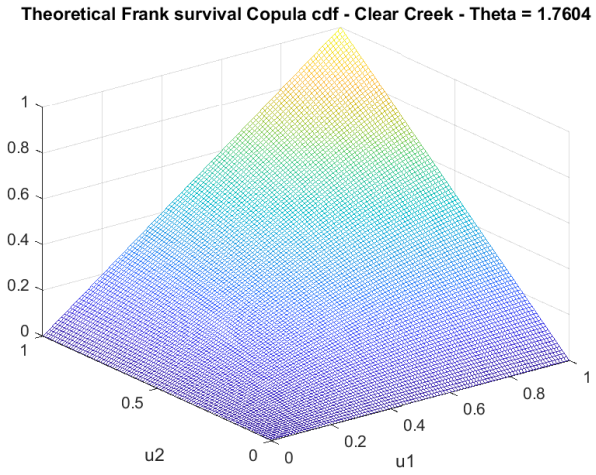

Figure 91. Theoretical CDF -fitted Frank Copula and Theta parameter

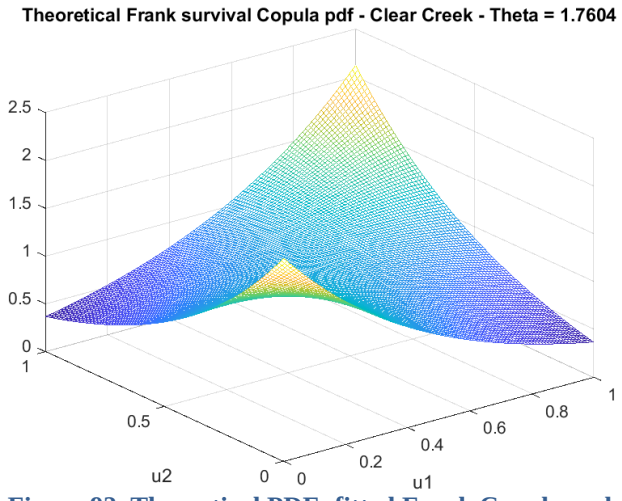

Figure 92. Theoretical PDF- fitted Frank Copula and Theta parameter

4.1.1.3 Joint Return period estimation

As mentioned in the previous section on copulas, in order to estimate the multivariate return period for the specific analysis of this research the AND case (see Figure 88) was chosen and therefore, equation (4.1.3) was used in combination with the Wald equation (Salvadori & De Michele ,(2004)) in order to estimate the return periods according to the following expression:

$$Return\ Period\ (RP) = \tau_{\widehat{u,v}} = \frac{\mu_T}{p_{\widehat{u,v}}} = \frac{\mu_T}{C(1-u,1-v)} \qquad \textbf{(4.1.7)}$$

Where $\boldsymbol{\mu_T}$ represents the inter-arrival time between storms (in years) which represents the time between each storm arrival into the system (in this case the arrival of a tropical cyclone into the gulf of Mexico or the Galveston bay) , $p_{\widehat{u,v}}$ represents the joint probability of having precipitation and storm surge at the same time (which is at the same time represented by the survival copula) and $\tau_{\widehat{u,v}}$ represents the return period being analysed (e.g. 10, 20,100 years), which should not be confused with the inter-arrival time since the return period represent the *"average time elapsing between two successive realizations of a prescribed event* (Salvadori & De Michele, 2004)*"* in which the prescribed event is the compound event itself (storm surge and precipitation) and not the triggering phenomena (the tropical cyclone).

If equation 4.1.7 is used and the return periods are stablished beforehand, the survival copula values ($\boldsymbol{C(1-u,1-v)}$) for a specific inter-arrival time can be computed as shown in Table 10, in which 2 different inter-arrival times were used for the analysis

The inter-arrival times shown in Table 10 were calculated taking into account that the synthetic data was computed based on observed storms during a period of 114 years (Sebastian et al., 2017). In those 114 years, **596 storms** were observed entering the Gulf of Mexico, giving a rate of **0.19 TC's per year**, while only **32 storms** were observed on the Galveston Bay in the same time lapse, suggesting that the inter-arrival time for Galveston is around **3.5 years.**

Table 10. Copula values for different inter-arrival times and specific return periods.

Inter-arrival time	0,191	3,563
Return Periods	$\boldsymbol{C(1-u,1-v)}$	
10	0,01913	0,35625
20	0,00956	0,17813
30	0,00638	0,11875
50	0,00383	0,07125
100	0,00191	0,03563

200	0,00096	0,01781
300	0,00064	0,01188
500	0,00038	0,00713
1000	0,00019	0,00356
1250	0,00015	0,00285

Taking into account the previous values and using the survival copula determined in the previous section, contour lines corresponding to the values in Table 10 were computed in the copula space for each inter-arrival time. As an example in Figure 93 the general contours in the Frank survival copula space are shown and a zoom-in into the specific values of the inter-arrival time of 0.19 years is showed in Figure 94.

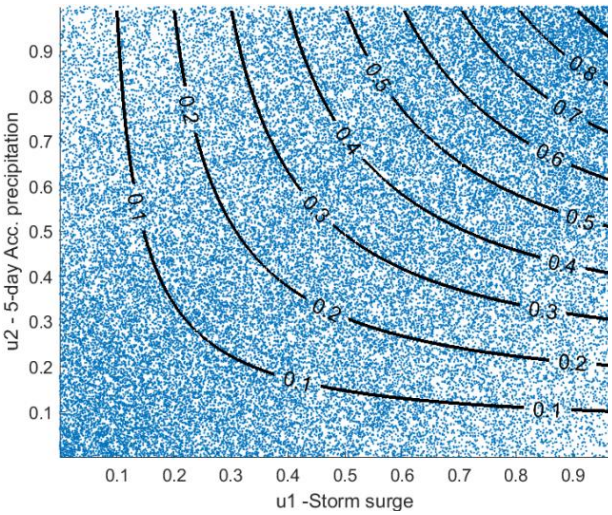

Figure 93. General Contours in Copula space- blue dots are random values of the size of the original data

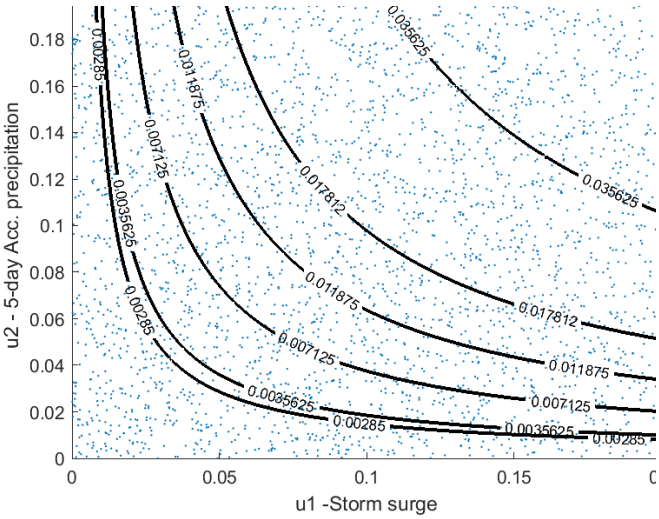

Figure 94. Zoom in AND Case –Inter-arrival time 0.19 years -

Using the Marginal distributions selected in Section 4.1.1.1 the inverse cumulative function of each marginal is applied to all the data along the curves presented in Figure 94 as shown in equation 4.1.8. The result of this transformation will generate a similar outcome than the one obtained by Sebastian et al. (2017) in Figure 82. The results for the Joint probability for cumulative precipitation and storm surge, assuming a Frank copula and considering the different inter-arrival times is presented below.

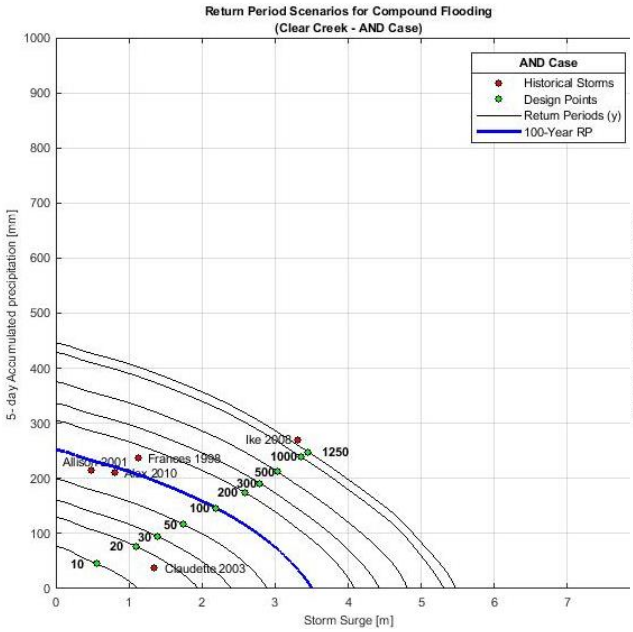

Figure 95. Joint return period for Inter-arrival time 3.56years

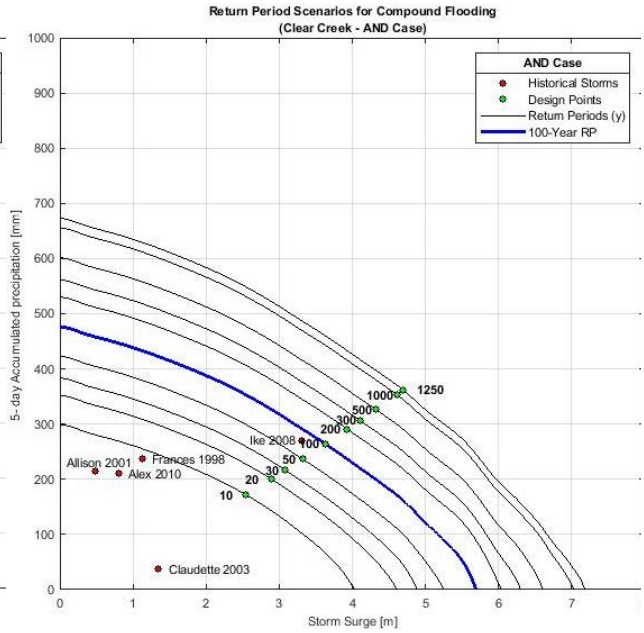

Figure 96. Joint return period for Inter-arrival time 0.19years

$$x = F_x^{-1}(u)$$
$$y = F_y^{-1}(v) \qquad \textbf{(4.1.8)}$$

For the purpose of this M.Sc. research and according to what was obtain in Figure 95 and Figure 96, it was decided that to delineate the boundary conditions for compound flooding in the Clear Creek watershed only Figure 96 was going to be used since it shows more resemblance with what was obtained originally in Figure 56. This means that the inter-arrival time that is going to be used corresponds to all hurricanes entering the Gulf of Mexico in 114 years of observations, which at the same time translates into the assumption that every hurricane that enters this area has the potential to make landfall nearby the Galveston Bay region and hence trigger compound flooding in the Clear Creek watershed.

4.1.2 Selection of scenarios on compound flooding

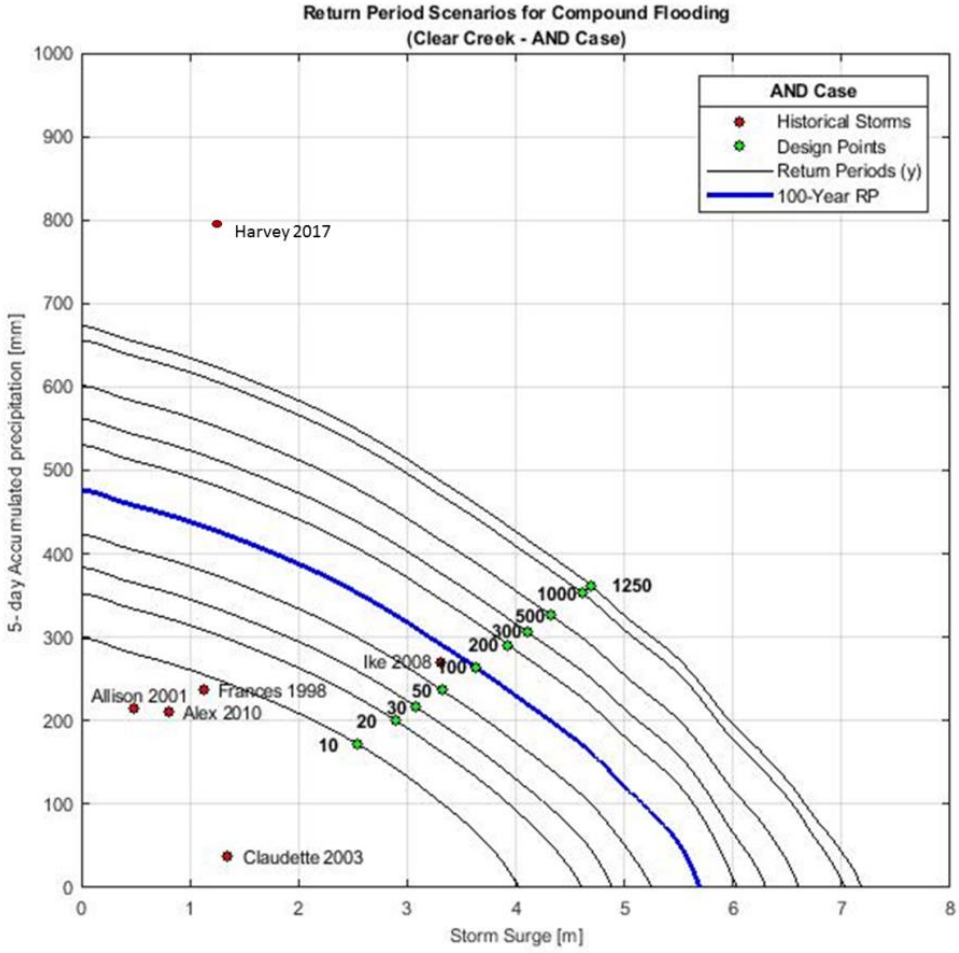

Figure 97. Updated joint probability for rainfall and peak storm surge in the Clear Creek watershed. Red dots are observed points in the watershed being analyzed.

As mentioned in the previous section, Figure 97 was selected in order to define the hydraulic boundary conditions for compound flooding in the Clear Creek Catchment. It can be seen from the previous figure that a so called “design point” (see green dots) was plotted along each return period curve. These points were selected as the points with the largest joint probability density along each return period curve as stated by Gľaler et al. (2013) in equation 4.1.9.

$$(u, v) = \arg\max\ f_{xy}\left(F_x^{-1}(u), F_y^{-1}(v)\right) \qquad \textbf{(4.1.9)}$$

This approach is known as the most likely design realization criterion as it identifies within each curve which pair of values occurs more frequently. This approach unfortunately only has a mathematical justification

but is not related to any physical processes and cannot be related to physical consequences along the watershed (Corbella & Stretch, 2012), for example, is clear that if the design point is shifted in Figure 96 towards the right, the downstream region of the catchment will experience a higher storm surge while the upper region won't see probably any effect. The opposite situation will occur if the design point is shifted to left, where probably the extent of flooding will dramatically change since precipitation is being dominant over the storm surge values. Looking into these scenarios, is clear that choosing a unique "design point" along this curve is probably not the best approach since basically at every location within the watershed there is a different combination of precipitation and storm surge along the curve that causes higher impacts and consequently what should be considered as the "design point" is constantly shifting according to the region. This discussion about the adequate selection of the design point from a bivariate joint distribution has been raised in the scientific community (e.g. (Gŕaler et al., 2013),(Corbella & Stretch, 2012),(Salvadori et al., 2011)) but a general consensus has not been achieved since it clearly depends on the nature of the problem being analyzed.

For the specific case of this research, it was decided that two approaches were going to be used in order to select the boundary conditions to delineate adequate floodplains considering compound events in the Clear Creek watershed. The first one will focus on selecting as much points as possible along the specific return period (e.g. 100-year blue line on) of interest in order to get the full hazard picture of flooding in the region. This method will allow computing the maximum flooding extent overlaying all scenarios (the envelope of the 100-year compound events) and hence, it will be only related to maximum areas that will flood but it won't be useful to determine the probable associated flood depth. The second approach, addresses the issue of the flood depth by selecting different scenarios along a uniform numerical grid independently from the associated return period, due to the fact that any compound event has the potential to generate at any location within the catchment the 100-year flood depth. The numerical grid was created taking into account the maximum values of precipitation and peak surge recorded in the initial synthetic data set for compound events created by Sebastian et al. (2017a) which was around 1000mm for the precipitation and 8m of storm surge. The proposed numerical grid can be seen in Figure 98; in which each green point corresponds to the corner of a cell in the numerical grid, and each red point corresponds to the scenario that better represents the specific cell (mid-point). In total 400 compound scenarios were selected as boundary conditions to be run in the SFINCS model.

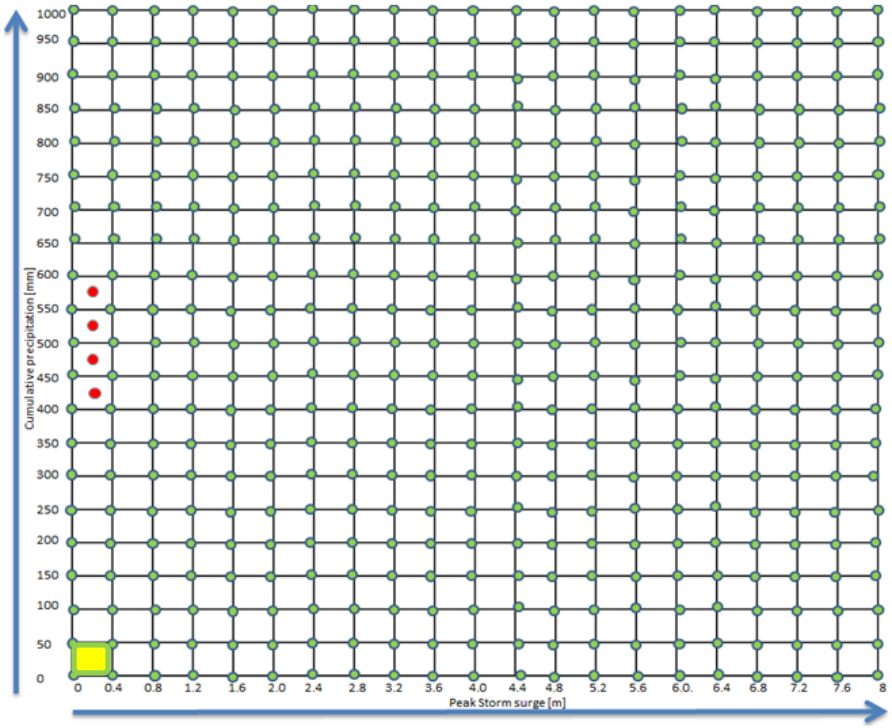

Figure 98. Grid of compound scenarios to determine the 100-year flood depth. yellow area represents the probability of the red point scenario occurring (see detailed explanation of chapter 5 and Appendix 9.2)

4.1.3 Time-series assigned distribution

As concluded from Section 4.1.2, several scenarios (Figure 97) for compound flooding are going to be run given a specific return period. If Figure 97 is observed closely, is clear that each point along the 100-year return period curve or along the numerical grid is a combination of single values of peak surge and total cumulative precipitation. This information solely is not enough to run a 2-D model of the catchment and therefore, a time-series has to be assigned to each variable of the pair that contains the information of peak surge and total cumulative precipitation.

4.1.3.1 Precipitation Time series

In the case of cumulative precipitation, several methods exist to do this, such as the SCS method (only valid for the US), the Triangular hyetograph or using IDF relationships. The most commonly used method in the US is the SCS method which was developed in the 1970's by the NRCS and which developed four synthetic 24-Hour rainfall distributions (I, IA, II and III as depicted in Figure 99) to represent various regions of the United States (USDA, 1986). In the case of Texas (See Figure 100) the distribution that applies specifically to the Galveston Bay is the SCS Type III distribution which represents the Gulf of Mexico and Atlantic coastal areas where TC's trigger large precipitation amount in 24-hours.

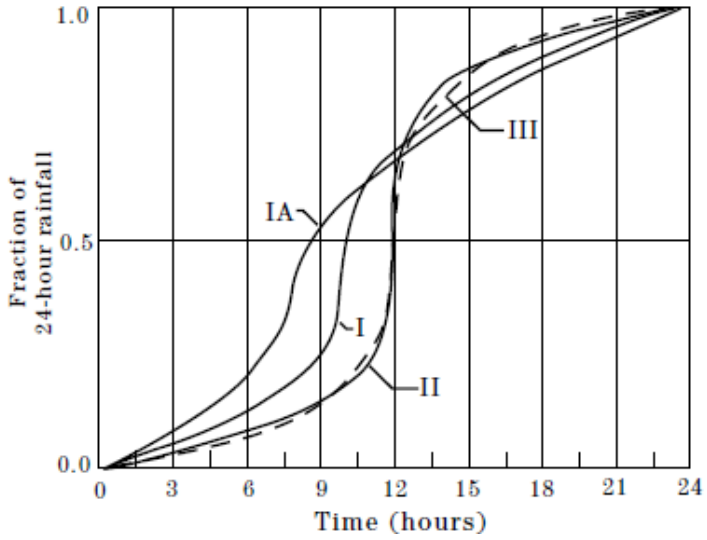

Figure 99. SCS -24-hour cumulative rainfall distribution types in the U.S. Source: (USDA, 1986)

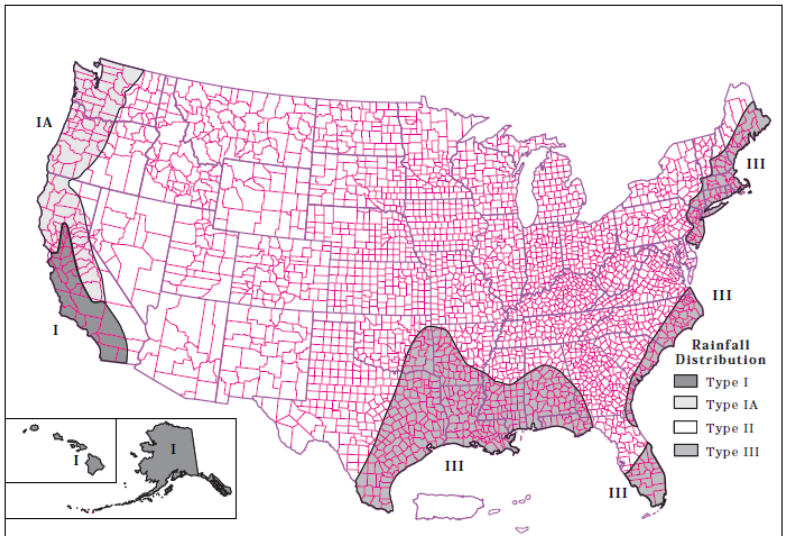

Figure 100.Geographic boundaries for NRCS (SCS) rainfall distributions. Source: (USDA, 1986)

The SCS curves are if the form of cumulative percentage mass for a 24-hour rainfall, therefore a scaling process has to be applied to the data if the duration of the storm is higher or lower. For this specific research, it was decided that for running the compound scenarios in SFINCS, the precipitation event was going to last 3 days since it was concluded by Sebastian (2016) that for the majority of the events that were used to construct the synthetic dataset, more than 90% of the total cumulative rainfall occurred during the first 72-hours after landfall: meaning that the two last days are not significant for the analysis.

The scaling process of the total cumulative rainfall coming from the synthetic data has to be applied to all precipitation points along each return period curve. This means that Figure 99 has to rescale by a factor of 3 since the new duration of the event is 72-hours. An example of this process is shown in Figure 99 for which an event of 975mm of cumulative rainfall was selected.

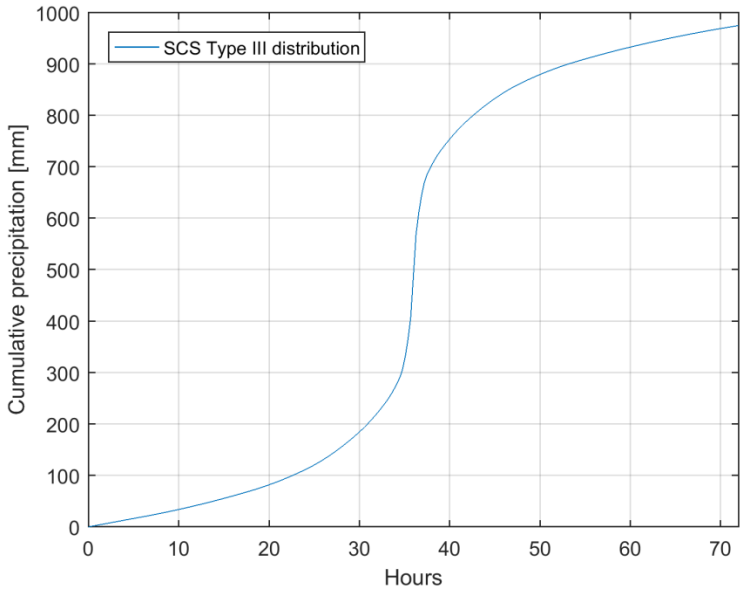

Figure 101. SCS Type III distribution for precipitation event.
Depth: 975mm of accumulated rainfall in 72-hours of storm duration.

After obtaining the cumulative distribution of rainfall given a certain final precipitation depth, the data has to be transformed once again to obtain the time series containing hourly data for the precipitation rate. This is shown in Figure 102 where the final time series of the rainfall is shown. This time-series distribution is the one that is going to be applied as a spatially uniform event across the Clear Creek watershed for the compound event analysis.

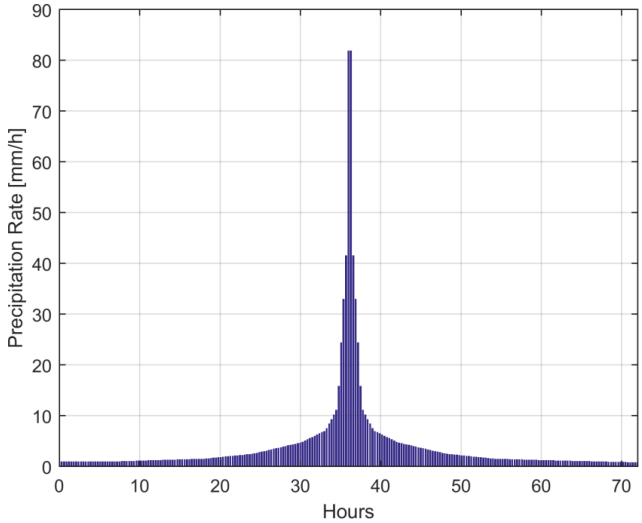

Figure 102. Time-Series of synthetic precipitation event based on a cumulative rainfall of 975mm

4.1.3.2 Storm surge Time series

In the case of storm surge, there is not an official guideline as in the case of the precipitation on how to assign a time-series based on a peak value. Therefore, it was decided that the storm surge behaviour registered in hurricane Ike at Eagle Point (see Figure 35) was going to be used to rescale the Peak surge observed in the synthetic dataset. Is important to mention, that only the storm surge was rescaled and afterwards the tide signal was added (see Figure 103) to obtain the observed storm tide level at the outlet of the Clear Creek watershed (see Figure 104). The peak surge levels in the synthetic data were reported in NAVD 88 datum, therefore a transformation of these levels to MSL was also necessary.

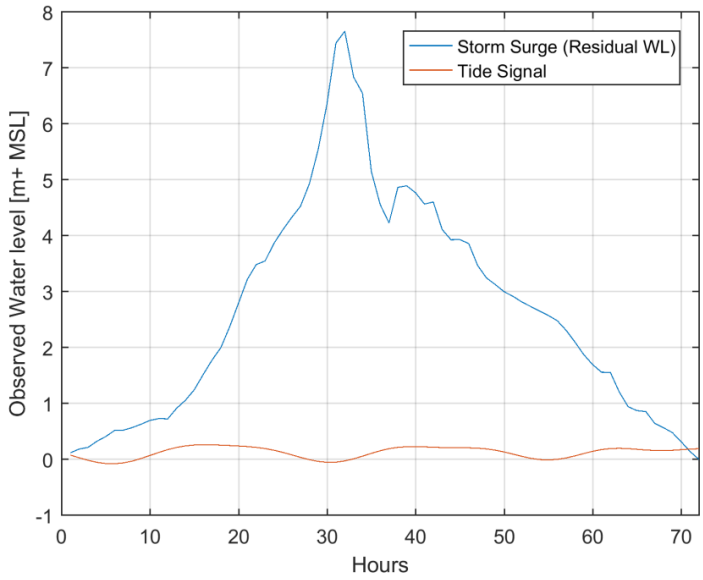

Figure 103. Storm Surge and tide signal in MSL datum at the outlet of the Clear Creek watershed Example of Peak storm surge event reported in the synthetic dataset of 7.75m

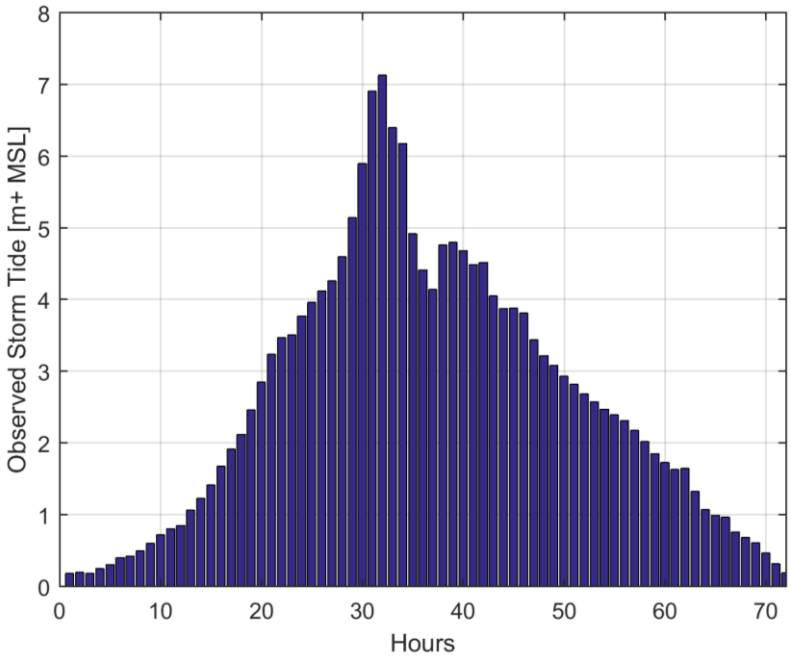

Figure 104. Observed Storm Tide in MSL datum at the outlet of the Clear Creek watershed. Example of peak storm surge event reported in the synthetic dataset of 7.75m

4.1.3.3 Overview of timing between storm surge and precipitation events

According to the results of the time-series distributions obtained in the previous sections, the peak rainfall will occur on hour 36 from a 72-hour event and the peak storm surge will occur around hour 32. This means that the events are happening almost at the same time with just 4 hours of lag between the peak events. An example of this overlay between the events can be seen in Figure 105 which was built using the same example events of the previous sections.

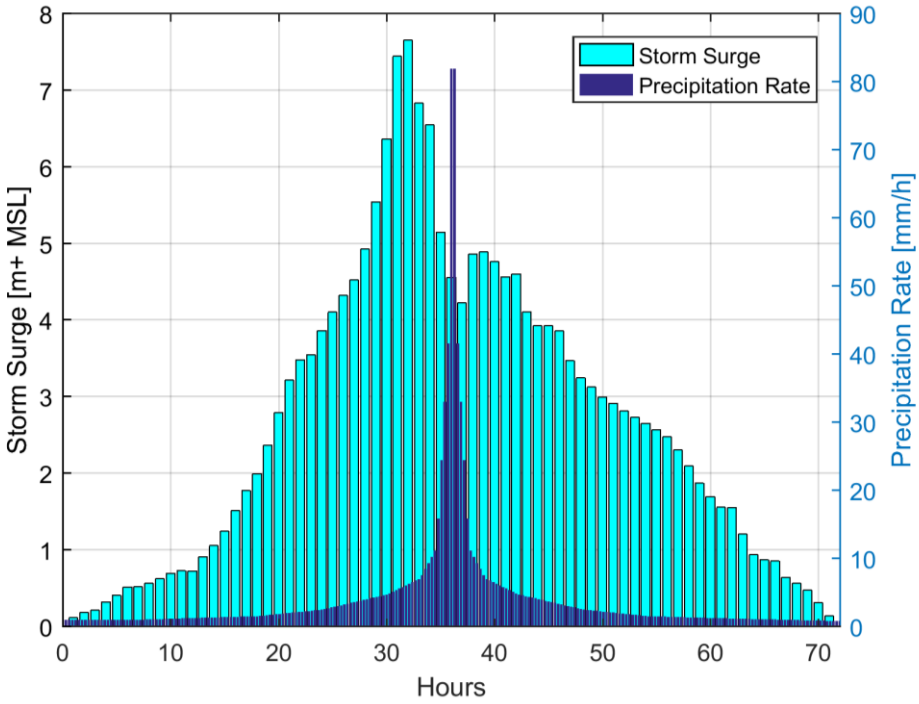

Figure 105. Synthetic compound events time-series for a 72-hour period in the Clear Creek watershed

5

Flood Risk assessment of the Clear Creek watershed

In this chapter, a comparison between the FEMA floodplain maps and the SFINCS outcome using an only rainfall flood driving event was included with the purpose of showing how much the floodplain estimation differs from one case to the other and identifying possible limitations and assumptions of each one of the methods. After this is done, the boundary conditions delineated in chapter 4 for the 100-year return period for compound events in the Clear Creek watershed were run within SFINCS. This was done with the aim of obtaining the maximum flooding extent corresponding to the overlay of all scenarios (the floodplain envelope of the 100-year compound events) in order to update the estimation of the flood hazard in the area. Afterwards, so as to go from a hazard to a risk approach, different scenarios along a numerical grid were used to cover all possible compound events in the catchment. These scenarios generate different water depths in each cell of the SFINCS model which were used afterwards in a frequency analysis to determine the 100-year water depth hazard map. Subsequently, with the corresponding probabilities of each scenario happening and with the associated damage generated from the scenarios extracted from the numerical grid, the risk map of the Clear Creek watershed due to compound events was obtained.

5.1. SFINCS Vs. FEMA comparison

5.1.1 Boundary conditions

For the **100-year design rainfall event** in the Clear Creek watershed, the Hydrology & Hydraulics Guidance Manual (HCFCD, 2009) was used in order to determine the rainfall depth duration frequency relationship in the area. These relationships were based on the Atlas of depth-duration frequency of precipitation annual maxima for Texas developed by (Asquith & Roussel, 2004).

The Hydrology & Hydraulic manual of the HCFCD shows all the watersheds covered by the Harris County (see Figure 106) and it also shows a division of the total county area in 3 hydrologic regions as depicted in Figure 107 in which it can be seen that the Clear Creek watershed belongs to region 3 of the Harris County. For region 3, the manual establishes the precipitation depth in inches for different exceedance probabilities and storm durations. This can be seen in Table 11 for which it can be seen that the 4-day design –rainfall depth that should be adopted if an exceedance probability of 1% is being considered is 16.9 inches or 0.429m.

Taking into account the previous information, and considering that FEMA delineates the 100-year floodplains considering precipitation design events with durations that are considered to be large enough to provide reasonable runoff and sediment volumes (FEMA, 2009) , a duration of 4 days was chosen to run a case in SFINCS in which precipitation is the only flood driver in the region.

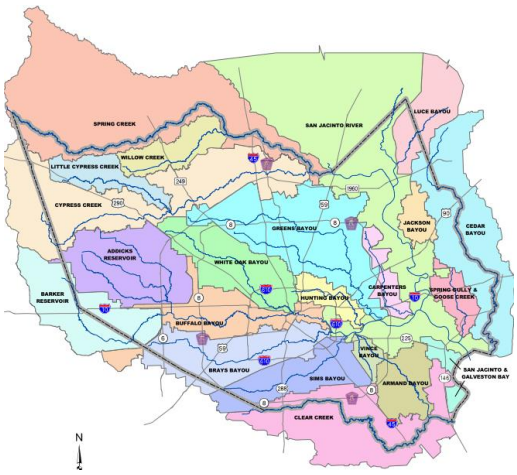

Figure 106.watershed Boundaries and primary drainage systems on Harris County. Source: (HCFCD, 2009)

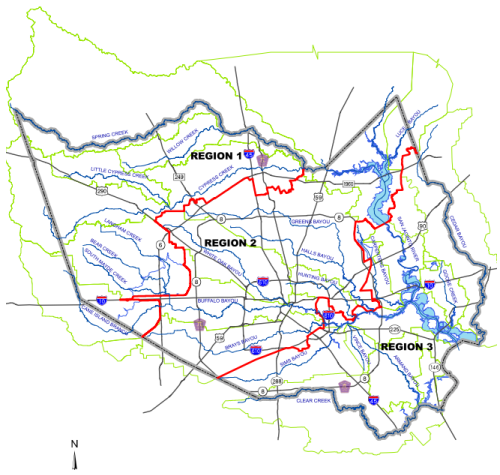

Figure 107. Harris County Hydrologic Regions. Source: (HCFCD, 2009)

Table 11. Harris County Hydrologic Region 3: Rainfall (inches). Source: (HCFCD, 2009)

Duration	Exceedance Probability (Frequency)							
	50% (2-Year)	20% (5-Year)	10% (10-Year)	4% (25-Year)	2% (50-Year)	1% (100-Year)	0.4% (250-Year)	0.2% (500-Year)
5 Minutes	0.7	0.8	0.9	1.0	1.1	1.2	1.3	1.4
15 Minutes	1.1	1.4	1.5	1.7	1.9	2.1	2.3	2.5
30 Minutes	1.5	1.9	2.1	2.4	2.7	3.0	3.4	3.7
60 Minutes	2.0	2.5	2.9	3.4	3.8	4.3	5.0	5.5
2 Hours	2.4	3.1	3.7	4.4	5.0	5.7	6.8	7.7
3 Hours	2.7	3.5	4.2	5.1	5.9	6.8	8.2	9.4
6 Hours	3.2	4.4	5.3	6.6	7.7	9.1	11.2	13.1
12 Hours	3.8	5.3	6.4	8.0	9.5	11.1	13.6	15.9
24 Hours	4.5	6.4	7.8	9.8	11.6	13.5	16.6	19.3
2 Days	5.3	7.5	9.0	11.2	13.1	15.1	18.1	20.7
4 Days	6.2	8.7	10.5	12.9	14.8	16.9	19.8	22.3

As mention in Section 4.1.3, SFINCS needs a time series for the precipitation in order to run the simulation. The same approach used in Section 4.1.3.1 was used to generate the time series for the design precipitation which can be observed in Figure 108 and Figure 109. For the downstream boundary conditions, the water level was considered to be at 0+MSL to reflect that there is not any surge at the coast that could trigger flooding in the region.

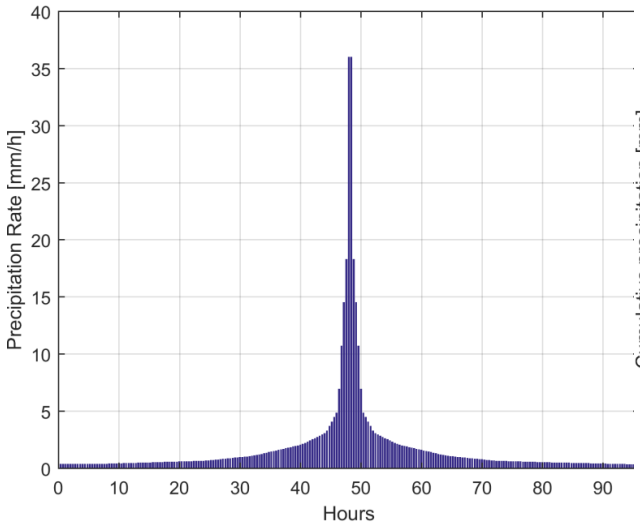

Figure 108. Time-Series distribution of 4-day 100 year design rainfall event - Clear Creek watershed

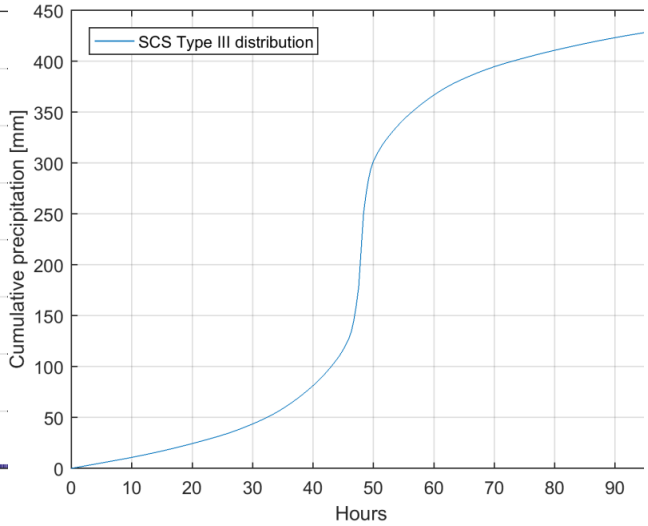

Figure 109.Accumulated 4 day 100 year design rainfall event - Clear Creek watershed

5.1.2 Flood maps SFINCS Vs. FEMA– Riverine flooding

The final results for the simulation using the boundary conditions defined in the previous section can be observed in Figure 110, in which the maximum water depth can be observed overlaying the Clear Creek region. As the aim of this section is to compare if SFINCS is giving similar results to the flooding extents presented by FEMA, Figure 111 was created to show the overlay of the SFINCS output with the FEMA floodplain. Figure 111 shows in pink the regions that are considered to be the 100-year flood plains and they are clearly wider than what is obtained with SFINCS. Nevertheless, the patterns are similar and they follow the main waterways of the catchment, presenting higher water depths in regions nearby the channels. In general, SFINCS shows a lot of ponding in the Clear Creek area and this is basically the result of changing from a 1D model (FEMA) to a 2D model which takes into account possible flooding happening outside of the main channels potentially caused by small variations in topography. This is highly important since at it is shown in Figure 111, FEMA doesn't cover this areas, but potentially a 100-year precipitation event can affect the region. Relevant ponding areas (Higher than 0.5m occur in the upper west part of the catchment and also SFINCS is capturing an additional expanded flooded area around coordinate (280km,3265km) in the map.

Is important to mention that a complete agreement between the SFINCS model running a 100-year precipitation event and the FEMA floodplains was not expected since not necessarily a 100-year storm causes a 100-year flood. In reality, there are many factors that can influence the relationship between rainfall and streamflow (such as the extent of the rainfall events, soil saturation before storm and relation between size of the catchment with duration of the storm) which is actually the measure that is used in a frequency analysis to determine the so called "100-year flood".

Normally, the process undertaken by the federal agency is that a historical analysis of the annual peak streamflow values recorded at different stream gauges is performed and based on this historical data, the 1% annual exceedance probability flood is determined on specific cross-sections of the stream; afterwards, the flood elevations are connected from cross section to cross section to obtain the full flood profile of the river or main waterway being analyzed. This also explains the reason why FEMA maps don't include any area located far away from the mains stream since flooding for the agency is only a direct consequence of high streamflow overtopping the natural or artificial banks in any reach of the stream (USGS, 2010) and therefore ponding due to rainfall outside of the main waterways is also not considered.

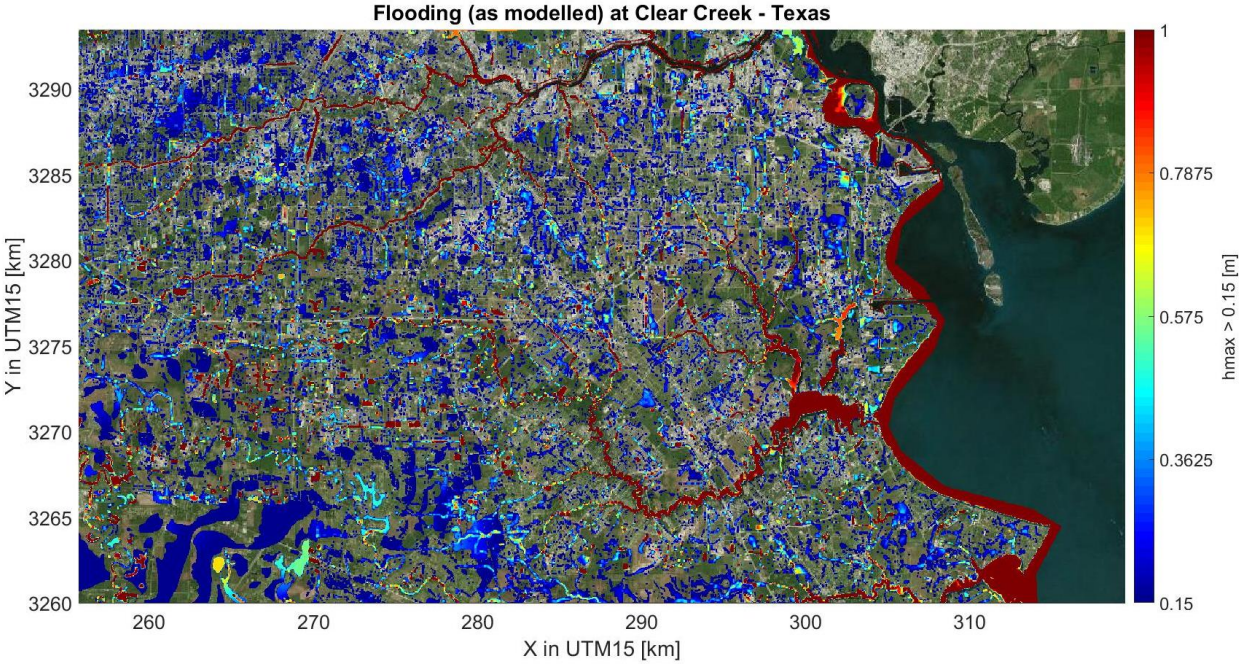

Figure 110. Maximum Flood Depth as modelled in SFINCS during 4 days design precipitation event. Maximum water depth illustrated corresponds to a value of 1m and flooding was considered only above a value of 15cm

In Figure 111 is important to mention that a flow depth delimiter of 15cm was used to plot the maximum water depths since given the fact that spatially uniform rain is being used, all cells within the model

will be potentially wet at a certain instant of time during the simulation. In FEMA's approach, the flow depth delimiter is tuned to a value of 0cm and this can explain partially the bigger extent areas nearby the main streams.

In order to do a better comparison between SFINCS and FEMA's approach, the specific point discharges used by FEMA along each mainstream as stipulated on the Flood Insurance Study (FIS) of the Harris County (FEMA, 2017) for an exceedance probability of 1% should be used instead of using a spatially distributed rainfall. Nevertheless, this was considered to be out of the scope and relevance of this research since the compound events that are going to be used for the Clear Creek watershed are based on peak rainfall depth and not in peak discharge along the waterways.

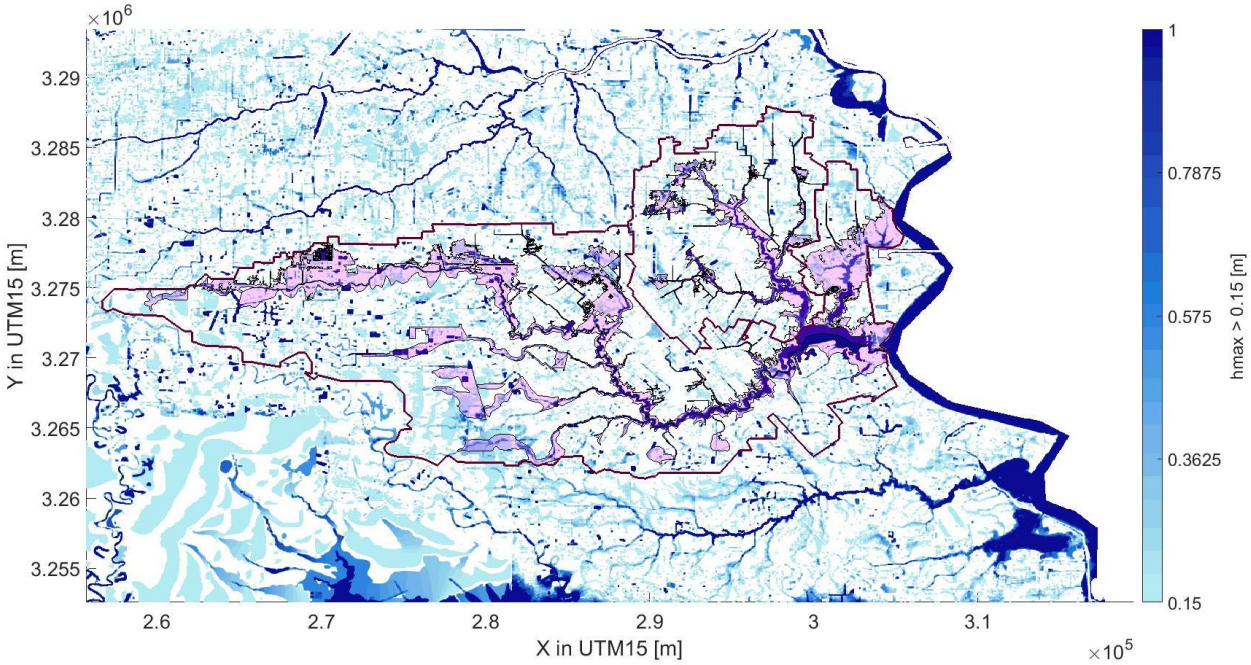

Figure 111. Flood extents between FEMA (Pink Polygon) and simulated flood on SFINCS (blue marks). Dark red polygon represents boundaries of the Clear Creek watershed. Maximum water depth illustrated corresponds to a value of 1m and flooding was considered only above a value of 15cm

5.1.3 Discussion on differences between FEMA and SFINCS

As seen from the previous section, is clear that the current FEMA methodology to delineate floodplains differs in essential concepts from the approach that is being proposed in this research (use of a semi-advanced 2D model considering compound events). Therefore, a full agreement between them was not expected but some conclusions and discussion can be opened regarding where the main differences lie between the methods so that the final method used by FEMA can be enhanced

The main reasons for disagreement between flood extents between the two methods can be summarized on the 4 points below, organized from top to bottom according to their relevance.

1. Discharge Vs. Rainfall
2. Grid Size of the model used
3. Roughness
4. Over dimensioning of FEMA (Cross Section based and 1D model)

The first reason for having large differences is mainly due to the fact that the variables used to trigger flooding are different. In the FEMA approach as explained before, the trigger for flooding is extreme historical discharge on the main channels, while the approach used in this research uses design rainfall rates over entire extent of the model. The first hypothesis is that the rainfall used in SFINCS is not producing the historical discharge used by FEMA, and therefore the flooding extents will be much lower when compared to those ones computed by FEMA. If a punctual value for discharge used by FEMA is extracted from the Flood

Insurance Study of the area, and this is compared to a value extracted from SFINCS at the same reach upstream reach location, it can be seen that the difference is highly significant (see values on Table 12). If similar extents want to be achieved, is recommended that a uniform discharge rate is applied in SFINCS to simulate the steady flow state behavior of the FEMA approach instead of using the peak rainfall rates. In this way a direct comparison can be done between the 2 methodologies since the values reported on Table 12 for SFINCS are coming from an unsteady approach (running the boundary conditions stated in section 5.1.1) and not a steady state flow approach as is the case of FEMA.

Table 12. Comparison of estimated discharge values between SFINCS and FEMA. (For 3 upstream locations of the clear creek watershed. (Upstream locations only for the clear creek tributary))

Location	FEMA Discharge [m^3/s]	SFINCS Discharge [m^3/s]
1	30.49	12.87
2	67.45	14.62
3	120.17	32.98

The second reason that induces differences between the flooding extents of the two approaches is the grid size chosen for the SFINCS model. As it was shown in Appendix 9.1, a model grid size of 50 m was chosen since with this size SFINCS could still run fast enough to perform some probabilistic calculations. Nevertheless, when Figure 111 is observed, it was seen that not much flooding is occurring nearby the mainstreams in the upper part of the catchment. This can be partly attributed to the fact that if a zoom in is performed in these areas, the coarse grid has flattened out too much the topography in these areas and actually the streams are partly lost. If the same model was run with a higher resolution (say 10m: same as the DEM) more flooding can be captured. Ideally this would be the resolution of the SFINCS model that needs to be used to improve the flood hazard results in the upper part of the catchment, however, the computational time increases from 15 minutes to 4 days of computation since the number of cells in the model increase almost 20 times which makes this approach impractical if several scenarios want to be run (probabilistic method). By using the current version of SFINCS a sacrifice need to be done between the resolution and the computational efficiency of the model. In this research as a probabilistic method needed to be applied in order to delineate risk, it was decided to remain with the 50m resolution, already consciously knowing that the flood depth in the upper part of the catchment will be underestimated.

The third reason can be the use of a spatially uniform manning value in SFINCS. This reason was already explained on the conclusions of chapter 3 and therefore, not any additional information is going to be added in this section.

Finally, the last reason for differences between FEMA and SFINCS, is that actually FEMA interpolates the flooding results from cross section to cross section and it can happen that at certain locations this technique overestimates the flooding extents. If the FEMA map is observed (see Figure 32) some abnormal geometrical shapes area observed in the floodplain delineation, which are solely the result of interconnecting flood depth between cross sections in a 1D model that doesn't reflect the reality of how water flows in an area. In this sense the use of the SFINCS model is much better since this approach is not only using the topographic details of one specific location, but it uses the entire DEM to route water in 2 directions in order to drain water to the Galveston Bay.

Thus is concluded that given the results of SFINCS, its limitations, advantages and assumptions made within the model when compared to FEMA's approach, is expected that when using the boundary conditions defined in chapter 4 to generate the flood hazard and risk maps of the area, inland flooding is going to be underestimated in the upper part of the catchment, since the resolution of the model didn't allow to capture fully the main channels in this part of the regions and also because the precipitation rates used didn't generate high discharges as compared to the discharge rates of FEMA.

5.2. Delineation of flood hazard maps

In order to compute the flood hazard of the Clear Creek watershed, two approaches were used. The first one, a hazard map showing the maximum extent of flooding in the area (envelope of 100-year compound events) disregarding the water depth, and the second one a hazard map corresponding to the 100-year water depth induced by compound events in the Clear Creek area. The procedure to obtain both maps is explained below.

5.2.1 Maximum extent of flooded areas considering 100-year compound events.

Using the blue curve on Figure 97 corresponding to the 100-year return period for compound events in the area, it was decided that approximately 100 events along this curve were going to be used in order to cover all possible values of cumulative precipitation and peak storm surge corresponding to that return period. All selected scenarios were uniformly distributed over the curve and afterwards, using the pairwise data of accumulated rainfall and peak surge and the procedure explained in Section 4.1.3 of chapter 4, the time series corresponding to each event was computed in order to be used as an input in the SFINCS model.

In total, the SFINCS model was run 102 times using the time series of precipitation as a spatially uniform rate along the watershed and setting at the outlet of the catchment (see Figure 31) the corresponding surge tide level time-series. As explained before, the model was run for a duration of 72 hours with a phase lag of 4 hours between the peak intensities of both events (see example of Figure 105), The SFINCS setup for all scenarios follows the same general configuration depicted in section 4.2, nevertheless the only changes are both the precipitation and water levels at the outlet according to the respective scenario being simulated.

In order to get the maximum flooding extents, for each cell of the model, the maximum water depth registered during the entire simulation was stored. Afterwards, each of these scenarios were superimposed, an again, the maximum water depth at each model grid cell was determined. In this way, the maximum extent of flooding due to multiple 100-year compound events can be achieved in the area as in can be seen in Figure 112 and Figure 113. As an addition, Figure 114 and Figure 115 are shown with the intention of showing the most extreme events along the 100-year curve (blue line in Figure 97), which corresponds to an event with zero surge and 480mm of cumulative precipitation and an event with 5.6m of storm surge at the outlet of the watershed with almost zero rainfall respectively. It is relevant to point out once again, that the final products depicting flood hazard (Figure 112 and Figure 113) are not related to the 100 flood depth generated by compound events in the region; the maps only intend to show the possible maximum flood extent in the Clear Creek region if 100-year return period compound events are considered.

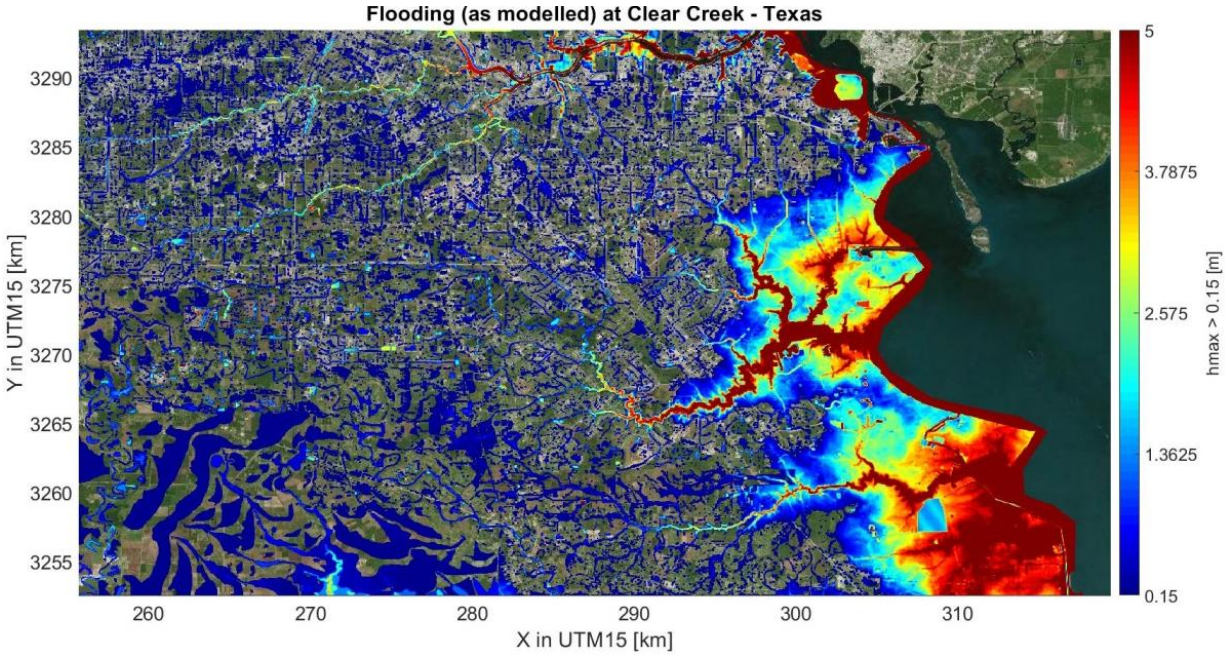

Figure 112. Maximum floodplain corresponding to ensemble of 100-year CE in the Clear Creek watershed.

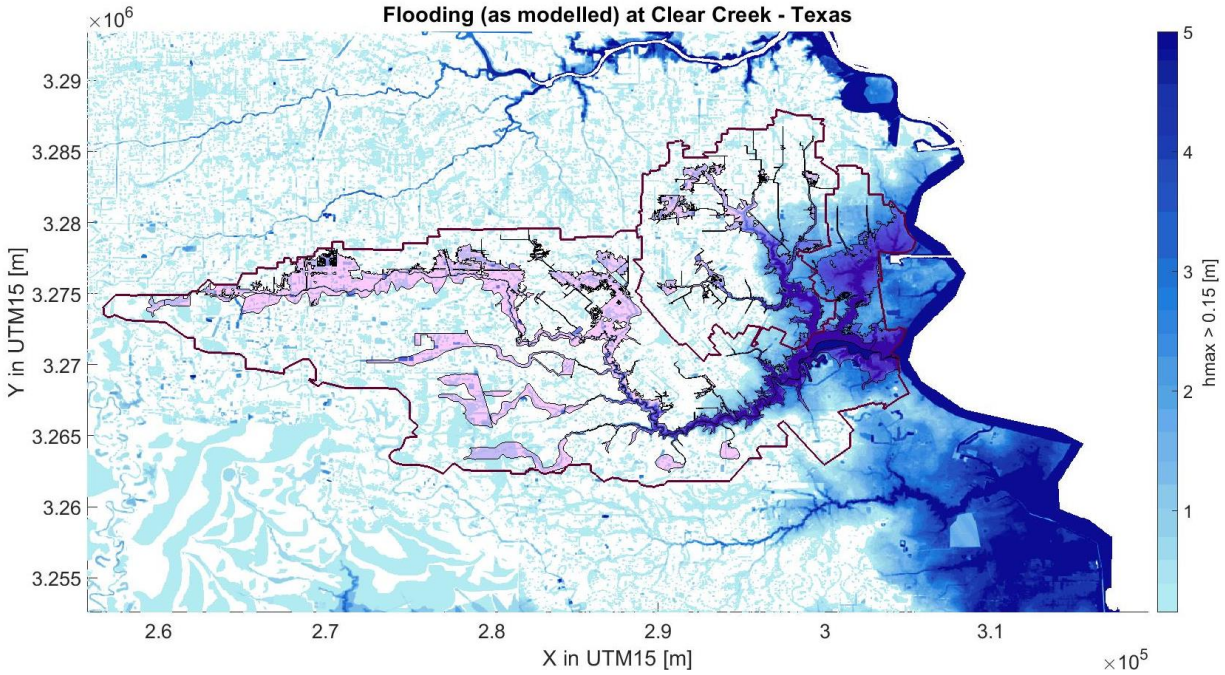

Figure 113. Maximum floodplain corresponding to ensemble of 100-year CE in the Clear Creek watershed Comparison with FEMA floodplains (pink polygon). Maximum Water depth shown is 5m and minimum scale corresponds to a value of 15cm.

It can be seen that Figure 113 is basically an overlay of the both extreme scenarios (see Figure 114 and Figure 115) and that when the results are compared to the extent of FEMA's floodplains (pink polygon on Figure 114 and Figure 115) , SFINCS is capturing **more coastal flooding** than the one that is originally presented by FEMA. It is important to mention, that if the zoom-in circle of Figure 115 is closely observed, only a small part of the Clear Creek Lake is considered to be affected by coastal flooding (VE Zone marked by small green area), while the results shown by SFINCS show that if 100-year compound events are considered, the effect of surge in the downstream part of the catchment is far wider than only the VE zone.

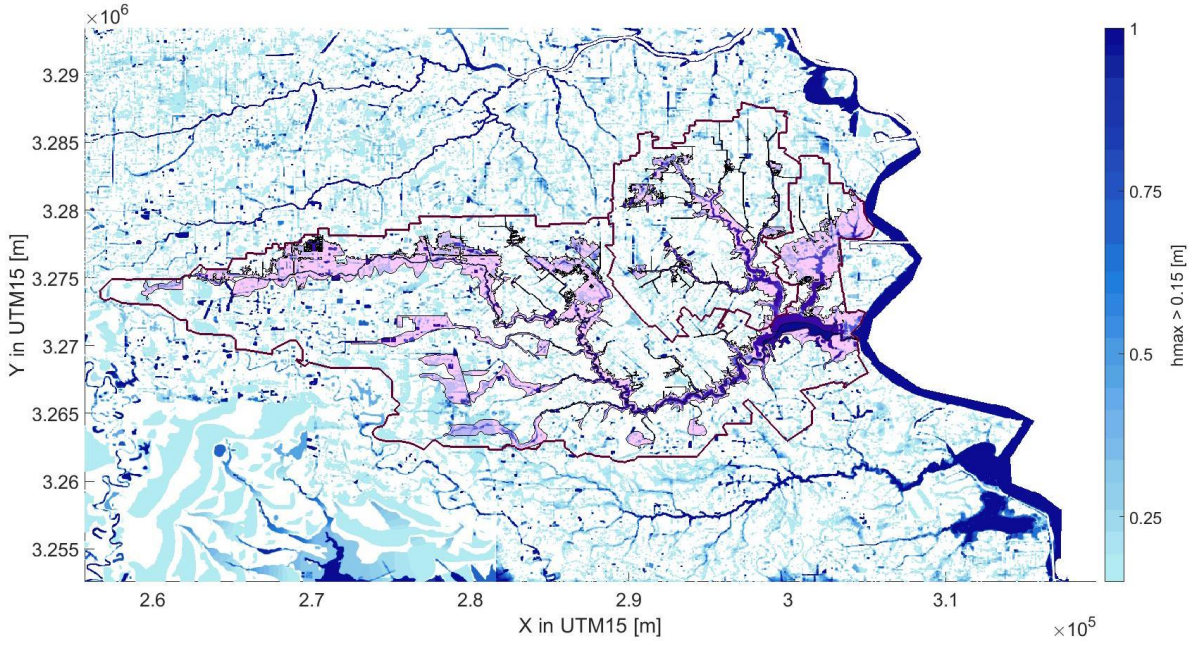

Figure 114. Compound flooding Scenario 1: ~480mm 3-day Precipitation event with ~0m of storm surge. Maximum flooding water depth shown corresponds to a value of 1m and minimum water depth is only shown above 15cm.

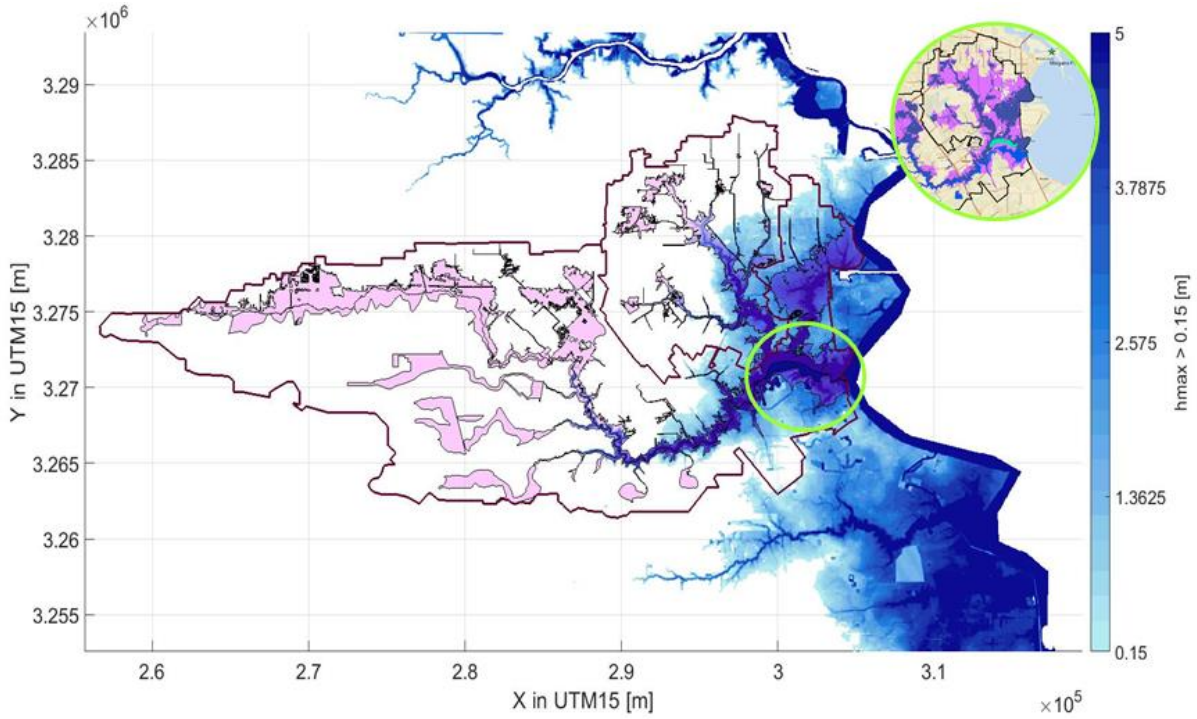

Figure 115. Compound flooding Scenario 2: ~0mm 3-day Precipitation event with ~5.6m of storm surge. Maximum water depth shown corresponds to a value of 5m and minimum water depth is only shown above 15cm. Zoom in corresponds to FEMA delineation

It is relevant to notice that inland flooding is being underestimated, mainly due to the reasons exposed in Section 5.1.2, for this reason and until SFINCS (which is still in phase of development) is able to incorporate a spatially varying manning, a high resolution grid and use as input similar discharges as the ones used by FEMA, is recommended to take the inland flooding nearby the streams from the latest Flood Insurance Study report for the area and combined it with the observed ponding from SFINCS in areas far away from the main channels since this is a more complete approach that the one that currently exists. Is it also important to mention, that the effect of surge goes as far as 17 to 20 km inland from the outlet of the watershed on the Clear Creek and around 10km inland on the Armand Bayou as seen also from the behavior of hurricane Ike, meaning that particularly for these regions, is highly important to consider in the flood analysis the co-occurrence of storm surge and precipitation since only by doing a compound flood analysis the maximum hazard can be obtained.

5.2.2 100-year flood depth in the Clear Creek watershed considering compound events.

In order to delineate the 100-year flood depth due to the occurrence of compound events in the Clear Creek watershed, it is necessary as mentioned in chapter 4 to run an ensemble of probabilistic compound events that cover all possible combinations (numerical grid as seen in Figure 116).

As shown on Figure 116; each **green point** corresponds to the corner of a cell in the numerical grid, the **red point** corresponds to the scenario that better represents the specific cell (mid-point) and the **yellow area** represents the probability of occurrence of each scenario (red point). In total 400 compound scenarios were selected (red points) to be run in the SFINCS model, each one with its associated probability of occurrence (yellow area).

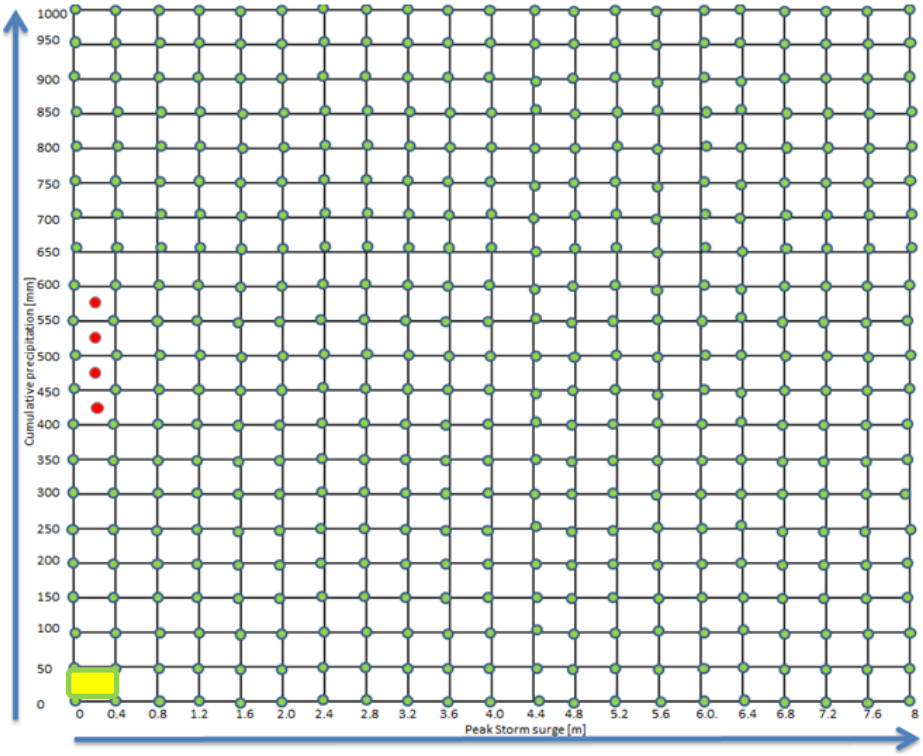

Figure 116. Grid of compound scenarios to determine the 100-year flood depth.

In order to compute the probability of occurrence of each scenario (yellow area), the fitted copula determined in chapter 4 was used following the detailed procedure presented in Appendix B, Section 9.2.3, which can be summarized as follows:

1. Add all the corner points (green points) from the numerical grid to the initial synthetic data used in this research (Sebastian et al., 2017) and transform the modified dataset to the copula space (0 to 1 values) by ranking the data explained in chapter 4, section 4.1.1

2. Determine the probability of each corner point (green dots) in the numerical grid by using the fitted Frank copula expression obtained in this research and its respective copula parameter:

$$P\{U > u \cap V > v\} = C(1-u,1-v) = -\frac{1}{\theta}\ln[1+\frac{(e^{-\theta(1-u)}-1)(e^{-\theta(1-v)}-1)}{e^{-\theta}-1}]$$

3. For each cell in the grid (formed by 4 green dots), denominate the South West corner as “I”, the South East corner as “II”, the North Western corner as “III” and the North Eastern corner as “IV”

4. Compute the probability for each cell in the numerical grid (yellow area) by means of the following equation:

$$for\ cell\ = i : 400$$
$$P_I + P_{IV} - P_{III} - P_{II} = P_{grid}$$

The previous approach means that each spatial grid cell of the SFINCS model will have 400 maximum flood depths. With this information a frequency analysis is performed by means of ranking the flood depths in each spatial grid cell and determining for each of the 645918 active cells of the model, what would be the corresponding 100-year flood depth (depth with 0.01 probability of exceedance). This process can be summarized in Figure 117 and the final map product can be observed in Figure 118 which depicts the 100-year flood depth in each cell of the model (corresponding to a 50m x 50m area) if compound events are considered in the region. As an addition, the 500-year flood depth was also computed (see Figure 119) since most of the time both the 100-year and 500-year floods are presented by FEMA.

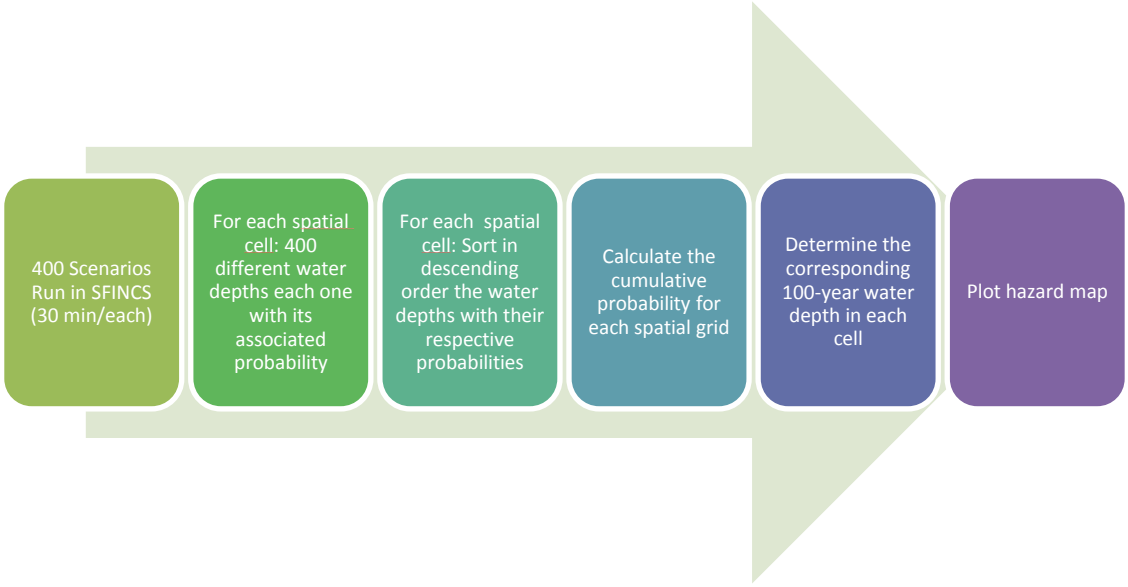

Figure 117. Flow chart for delineating flood hazard given compound flood analysis

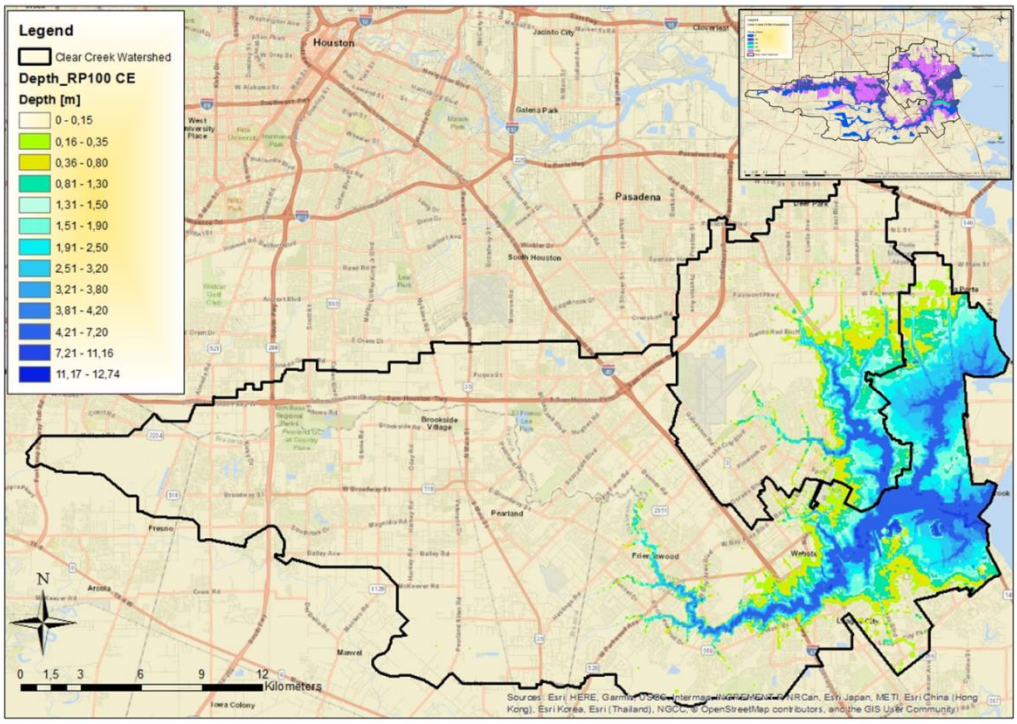

Figure 118.100 Year flood depth map of the Clear Creek watershed considering compound events.

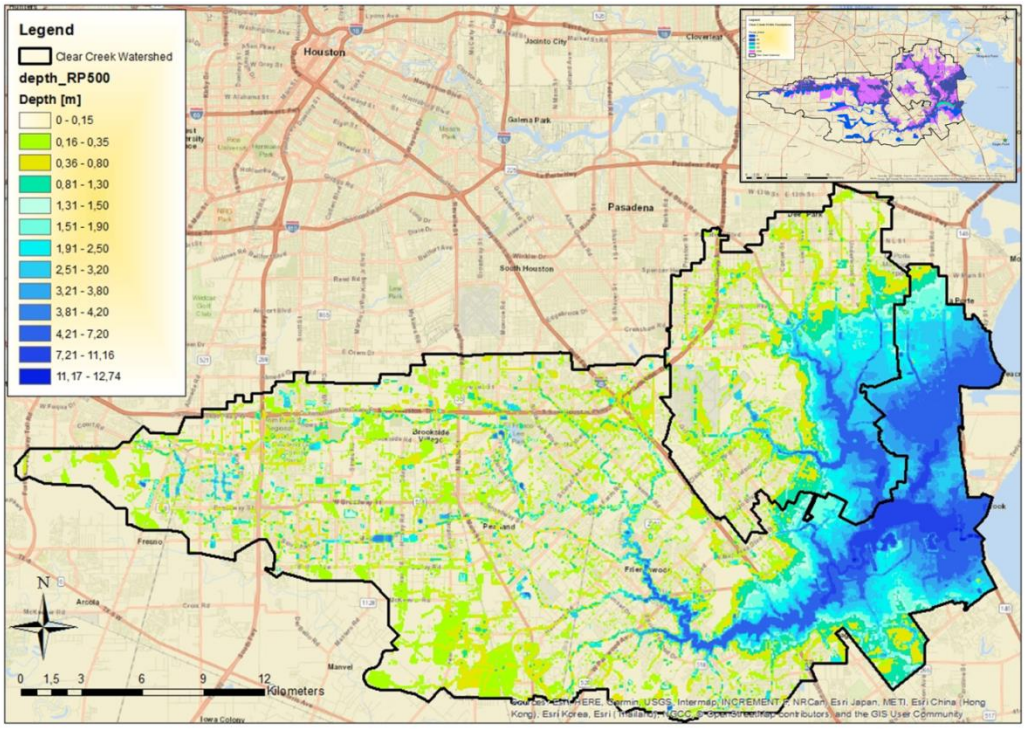

Figure 119. 500 Year flood depth map of the Clear Creek watershed considering compound events.

As it can be seen from both Figure 118 and Figure 119, the highest flood hazard is found nearby the coast on the outlet of the clear lake into the Galveston Bay. From the 100-year compound flood map (Figure 118) it can be seen that there is not much inland flooding, but as mentioned in the first section of this chapter, this was already expected since the resolution of the model was not high enough to capture the channels at these locations and also because the discharges generated by the precipitation are not that high when compared to the values used by FEMA.

It can also be seen that when compared to FEMA maps (see upper zoom right corner of Figure 118; blue areas), the 100-year compound flood map is capturing more area near the coastal region than what is classified as the 100-flood map for FEMA and even more, capturing areas classified as the 500-year flooded regions by FEMA (see purple are on Figure 118). It is also important to notice that the main driver for flood hazardous zones nearby the coast mainly comes from considering storm surge and therefore, what is shown by FEMA (see light green in upper right corner image of Figure 118) as coastal hazard, is highly underestimated showing again the necessity of doing a compound flood analysis to truly depict flood hazard in the area.

If Figure 118 is observed and compared to Figure 119, it can be seen that inland flooding and pounding starts to be relevant for the catchment when the 500-year water depth return period due to compound events is being considered, while for the 100-year water depth return period, the most relevant variable is storm surge. This is in agreement with the results obtained for hurricane Ike (see Figure 97) joint return period, which classifies the storm as a 100-year compound event, and therefore is a compound event in which the most dominant variable is storm surge. Similarly, the result for hurricane Harvey also agree with the compound flood hazard maps obtained in this research, since Harvey could be catalogued as a compound event with a return period larger than 1250 years (see Figure 97) making it a more extreme event in which rainfall starts to be relevant for the flooding in the catchment (more towards Figure 119). Is again important to mention that these maps are still underestimating inland flooding, and therefore only until the comparison of discharges with the FEMA approach is done a full conclusion can be determined.

Is essential to understand that a full agreement with the FEMA flood zones was not expected (as mentioned at the beginning of this chapter) since the two methods are fundamentally different; FEMA uses historical annual extremes for discharge in a 1D model and the proposed methodology uses rainfall design event rates and storm surge in a 2D model. The results show promising modifications that could be included

to improve hazard delineation in this coastal watershed, nevertheless some additional work has to be performed regarding improving the roughness input in the model and also increasing computational speed of SFINCS to be able to run probabilistic scenarios with high resolution.

Due to the fact that one of the purposes of this research is to see if with the newly proposed method there is an increase of coverage in historical claims, the damage density information (see Figure 120) constructed for hurricane Ike by Blessing et al., (2017) was compared to the results obtained in Figure 118 and Figure 119. If these images are compared, is clear that the new compound flood scenarios capture more flooding than what FEMA initially stablishes, especially the regions catalogued in Figure 120 with densities between 0.4 and 0.9 which contributes with the largest areas of claims in the Clear Creek watershed.

A quantitative analysis done only for hurricane Ike claims show that the FEMA maps capture 51% of the claims while SFINCS (Figure 118) capture 67% when comparing only the 100-year flood depth maps from both approaches. In addition, locations with high density of claims are covered a 100% by the SFINCS compound hazard maps and they coincide with the regions with higher flood depths, which demonstrate again the importance of considering compound flooding for this specific catchment

In addition, if the SFINCS model for Ike (see Figure 63) is compared to the historical claims of Ike (Figure 120) the results are further improved since the model is capturing 79% of the claims which is an improvement to the 51% covered by FEMA (see Table 4). The improvement in coverage comes from the inclusion of the real spatial precipitation rates in the hurricane event, while Figure 118 is only based on synthetic rainfall rates. In addition, when the results from the SFINCS model of Harvey are observed (Figure 76) and compared to the claims registered on November 2017 (data of this claims is not published in this report due to confidentiality reasons) for this hurricane, the results are covering 66% of the claims.

If additional historical claims as the ones registered for tropical storm Allison are evaluated (see Table 4 and Figure 121) and compared to the results obtained in SFINCS, is seen that there is a decrease in coverage of the claims when using SFINCS, mainly due to the fact that most of the density of the claims occurred in the inland part of the catchment (Allison storm was a rainfall dominant event). This was expected as explained before due to the assumptions made in the SFINCS model and the input used to generate the flooded areas. Overall it can be said that doing the compound flood hazard analysis using SFINCS gave a lower performance in the upstream tributaries of the catchment (Turkey Creek and Horsepen Bayou), whereas in the downstream portion of the watershed (where the interaction zone between precipitation and storm surge happens) the results were highly satisfactory covering almost 100% of the historical claims. Is relevant to mention that the boundary conditions of the SFINCS model for this study case only included tropical cyclone events and therefore the results might be under predicting regular flood events.

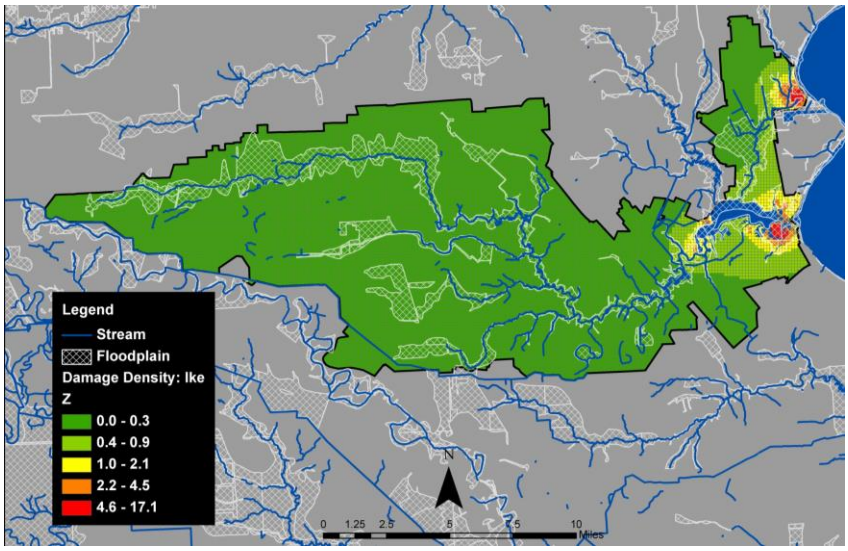

Figure 120. Damage density for hurricane Ike.
FEMA floodplains are showed in white rectangular grids
Source: (Blessing et al., 2017)

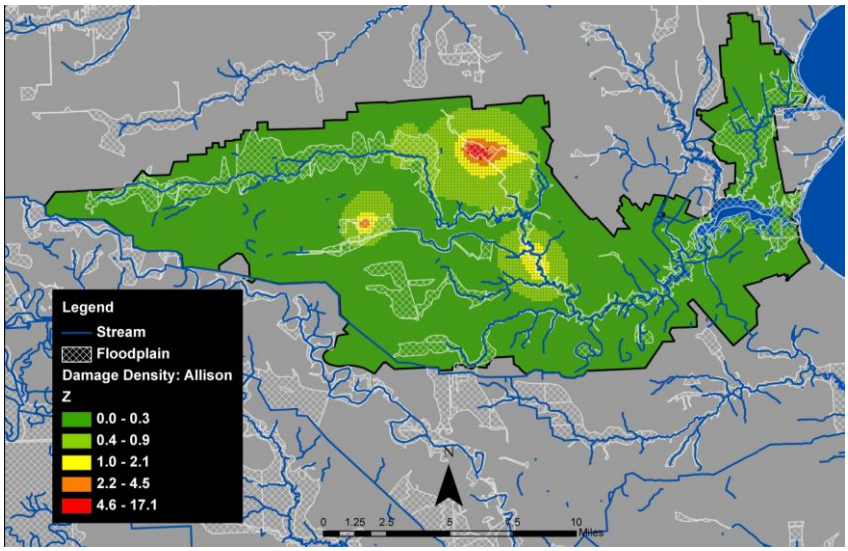

Figure 121. Damage density for tropical storm Allison. FEMA floodplains are showed in white rectangular grids Source: (Blessing et al., 2017)

As an additional validation, recent research done by Jonkman et. al. (2018) showed that during hurricane Harvey they were 70 fatalities associated directly with the event. Most of these locations occurred in the greater Houston area; nevertheless, some fatalities occurred also within the Clear Creek watershed area and therefore these locations were compared with the 100-year compound flood map and with the FEMA floodplains. The results are shown in Figure 122 and they demonstrate that if the 100 or 500-year compound flood hazard was used instead of the FEMA floodplains, these causalities would have been included in the hazardous zones of the new map.

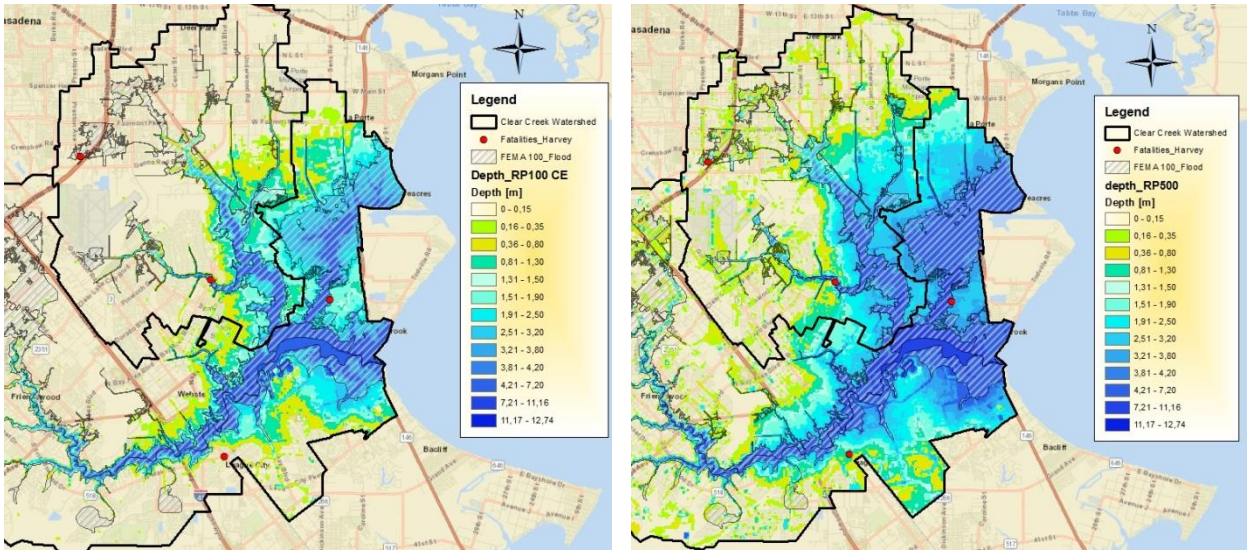

Figure 122. Harvey fatalities locations compared to the 100 and 500-year compound flood depth map

5.3. Delineation of flood Risk map

In order to translate the flood hazard map into a risk map, the damages for each scenario run in SFINCS needed to be computed. This was done using the flood impact model Delft-FIAT (see Appendix C for details) developed by Deltares and by using adequate exposure and vulnerability data of the area. In the following subsections a description of the datasets used to compute damages is shown, as well as an explanation of the process taken to compute the final risk map of the Clear Creek watershed.

5.3.1 Vulnerability and Exposure

In order to use Delft-FIAT some exposure data and vulnerability information of the area has to be provided. Even though a detail method exists in the U.S to compute damages due to hazards (HAZUS), it was decided that a simple and more general approach was going to be followed, since sometimes the exposure data is not publicly available due to privacy reasons and most of the time the required processing time of the exposure dataset to the level of detail that HAZUS requires can be quite extensive.

The approach that was taken to compute damage was to use global flood depth-damage functions based on land use type. These functions were published by the JRC in 2017 (Huizinga et al., 2017) with the aim of creating a globally consistent database of depth-damage curves which were normalized and developed for each continent and each country. The dataset includes damage curves depicting fractional damage as a function of water depth and also the maximum damage values for a variety of land uses classes. The damages are reported in 2010 euros or dollars.

In this particular case, the U.S was selected as the country of analysis to extract all the respective damage information from the JRC report (Huizinga et al., 2017). The global flood-depth damage functions included the following damage classes or land use types:

- Residential buildings
- Commercial buildings
- Industrial buildings
- Transport
- Infrastructure - roads
- Agriculture

It was decided that given the fact that only global functions but no detailed information for the U.S was given for land use classified as: “Infrastructure - roads or Transport”, these damage classes were going to be left out of this particular analysis. Moreover, checking the original dataset published by the JRC (Huizinga et al., 2017), it was observed that for North America, the damage functions estimate certain amount of damage when the flood depth is zero. This assumption is made by the JRC due to the fact that they contemplate the existence of basements below ground level. Nonetheless, for this research the previously mentioned assumption was considered to be wrong since as the SFINCS model is including a spatially uniform precipitation over the whole domain, the damages will be greatly overestimated due to the fact that eventually all cells from the model will experience a water depth higher than 0 due to the rainfall input. In order to correct for the previously mentioned error, the damage functions where shifted 30cm in order to have at zero flood depth, a damage equal to zero €/m^2. Additionally, the report also assigned a maximum damage value of agriculture of 1324 €/m^2 for the U.S, which is attributed also to damages caused to farms (buildings) and warehouses in what is considered to be agricultural land. The previous value was considered to be too high since the information obtained for agriculture land parcels in the Clear Creek watershed did not include information about buildings in these areas, reason why most probably, there will be an overestimation of damage. The previous reasoning made that the final adopted value for maximum damage in agricultural LU was taken from Australia rather than from the U.S with a final value of 4.85 €/m2. The final vulnerability information used for the Clear Creek watershed with all the modifications done to the initial JRC reported values can be seen in Table 13 and Figure 123.

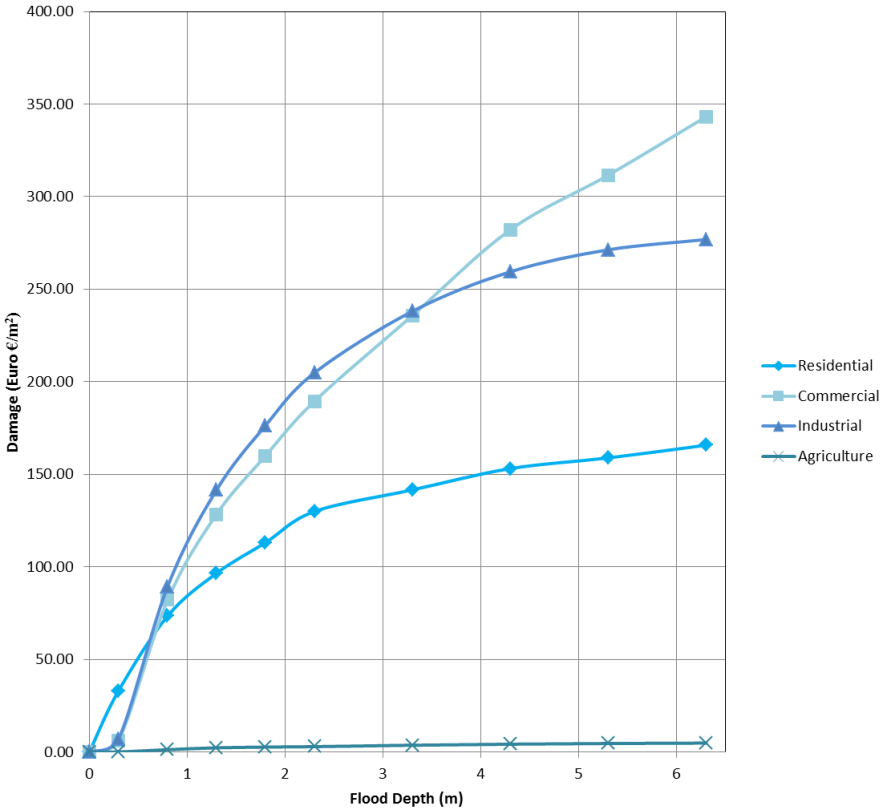

Figure 123. Modified JRC Depth- total damage functions for the U.S.
Adapter from Huizinga et al., 2017

Table 13. Depth-damage information according to damage class or land use type for the United States

Damage class	Flood depth, [m]	Total Damage Fraction	Max Damage Land-use based Total (€/m2, 2010)	Flood-Depth Damage estimation (€/m2, 2010)
Residential buildings	0	0.00	165.79	0.00
	0.3	0.20		33.16
	0.8	0.44		73.49
	1.3	0.58		96.62
	1.8	0.68		113.16
	2.3	0.78		129.98
	3.3	0.85		141.65
	4.3	0.92		153.14
	5.3	0.96		158.92
	6.3	1.00		165.79
Commercial buildings	0	0.00	343.26	0.00
	0.3	0.02		6.32
	0.8	0.24		82.13
	1.3	0.37		128.46
	1.8	0.47		160.05
	2.3	0.55		189.53
	3.3	0.69		235.86
	4.3	0.82		282.19
	5.3	0.91		311.67
	6.3	1.00		343.26
Industrial buildings	0	0.00	276.88	0.00
	0.3	0.03		7.12
	0.8	0.32		89.39
	1.3	0.51		141.60
	1.8	0.64		176.41
	2.3	0.74		204.89
	3.3	0.86		238.12
	4.3	0.94		259.48
	5.3	0.98		271.34
	6.3	1.00		276.88

Agriculture	0	0.00	4.85	0.00
	0.3	0.02		0.09
	0.8	0.27		1.30
	1.3	0.47		2.30
	1.8	0.55		2.67
	2.3	0.60		2.92
	3.3	0.76		3.69
	4.3	0.87		4.24
	5.3	0.95		4.63
	6.3	1.00		4.85

Since the vulnerability data presented before is related to specific land use types, an exposure data set containing this specific classification needs to be achieved. For this area of Texas, the Houston-Galveston Area Council developed a land use and land cover data set that has been updated until 2017 and that is publicly available for download in ESRI file geodatabase format (H-GAC, 2017a). The original data base included the following land use classes:

- Government/ Medical/ Education
- Multiple
- Other
- Parks/ Open Spaces
- Vacant Developable (includes Farming)
- Undevelopable
- Residential buildings
- Commercial buildings
- Industrial buildings
- Unknown
- Undetermined

As the found exposure data had more classes that the ones delineated in the depth-damage function, some modifications had to be done to group all classes into the 4 different types of land use needed to compute risk. Residential Buildings was mixed with “Other” and “Undevelopable” land use types; Commercial building was combined with “Multiple”; “Government/ Medical/ Education” was considered to be part of Industrial buildings, and the rest of the classes were considered to be part of the agriculture land use type. The final exposure data that was used for the area can be seen in Figure 124.

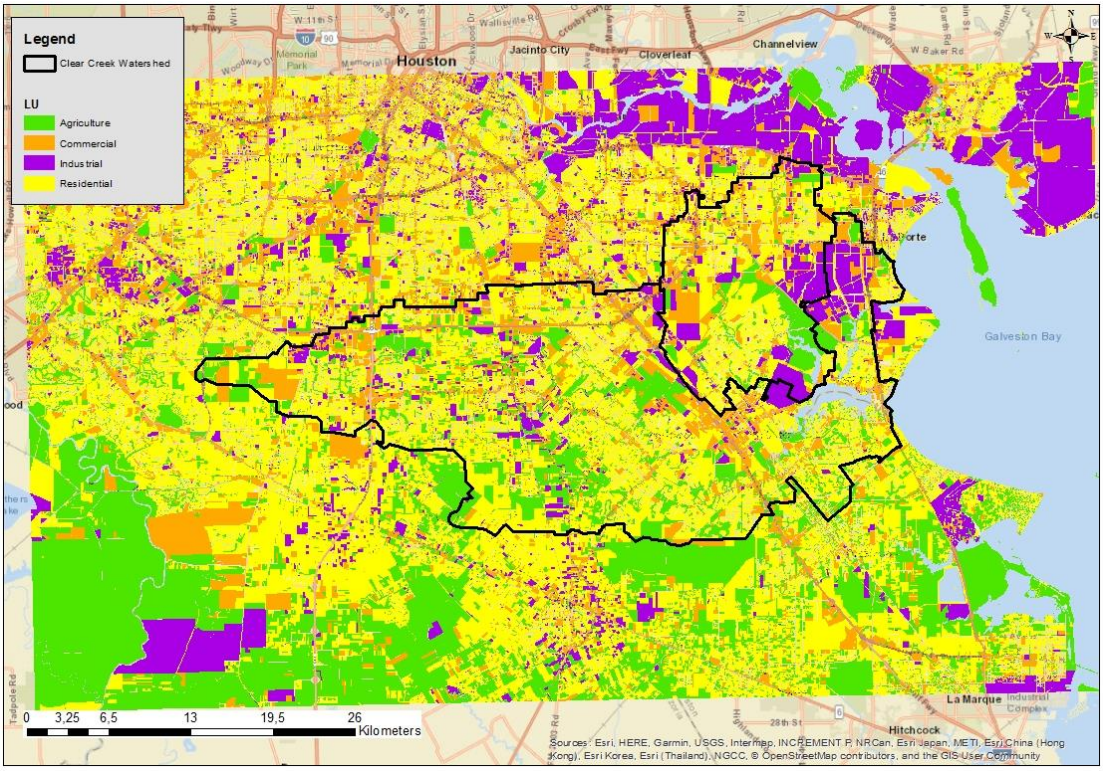

Figure 124. Modified LU exposure data set for the Clear Creek watershed. Source:(H-GAC, 2017a)

5.3.2 Risk delineation process

In order to obtain the final risk map of the Clear Creek watershed, a similar process as the one followed in section 5.1.2 to compute the 100-year flood depth map due to compound events had to be followed but this time focusing on the damage estimation rather than on the flood depth. The process followed to compute risk can be seen in Figure 125 and the final risk map can be seen in Figure 126 where the total risk in equivalent 2010 Euros per year for all type of land uses is shown. In addition, and individual risk map was created for each type of LU used in the exposure information (See Figure 127 to Figure 130).

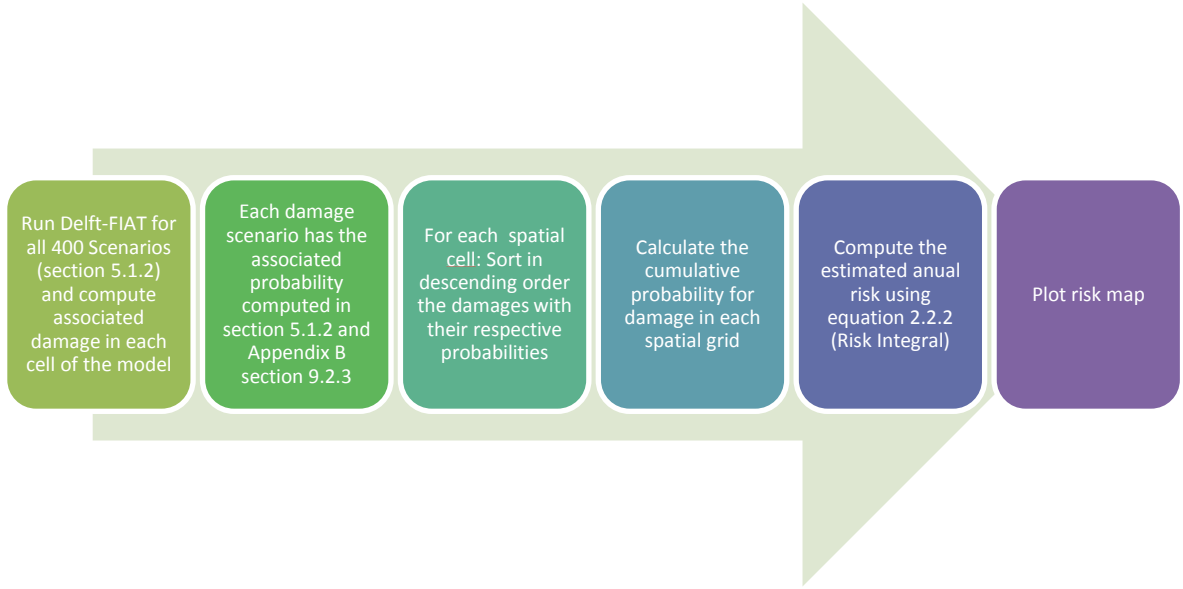

Figure 125. Flow Chart for delineating flood risk given compound flood analysis

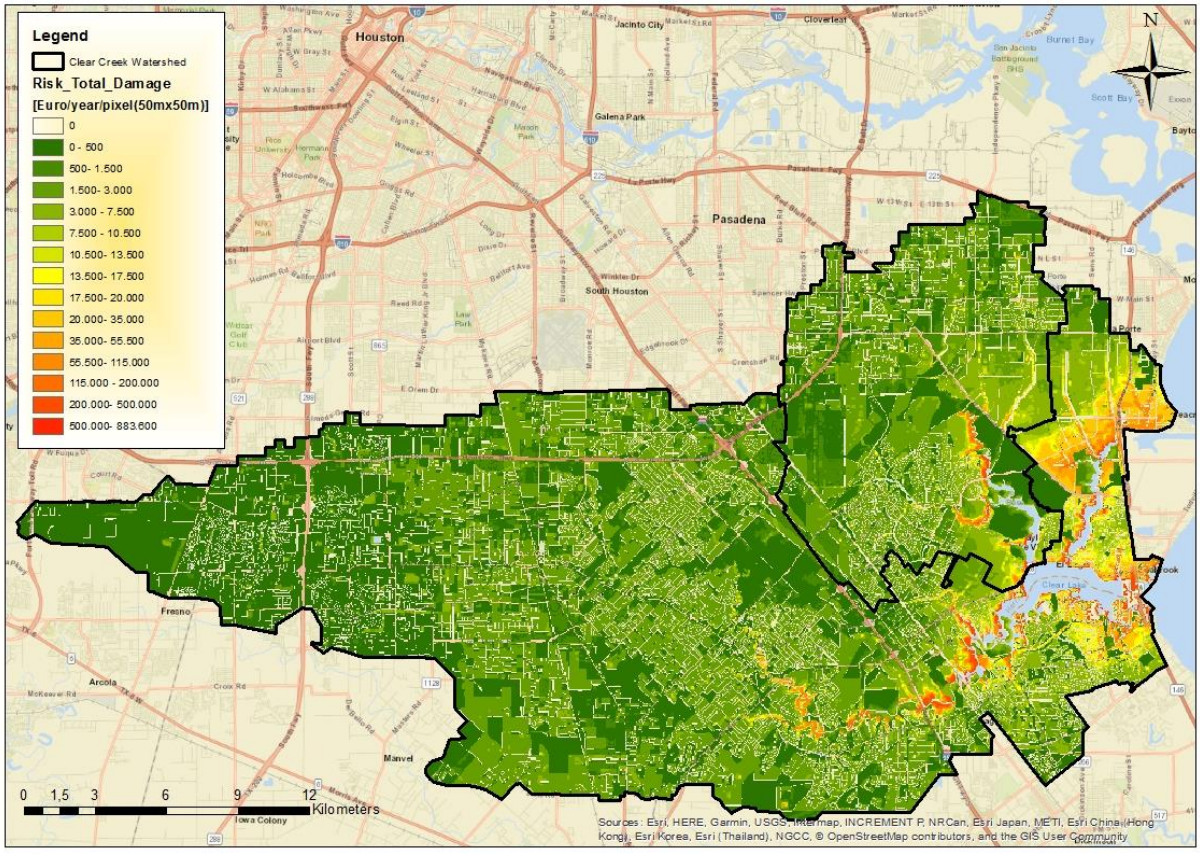

Figure 126. Total Flood Risk [€(2010)/year per pixel of 2500m^2] of the Clear Creek watershed.

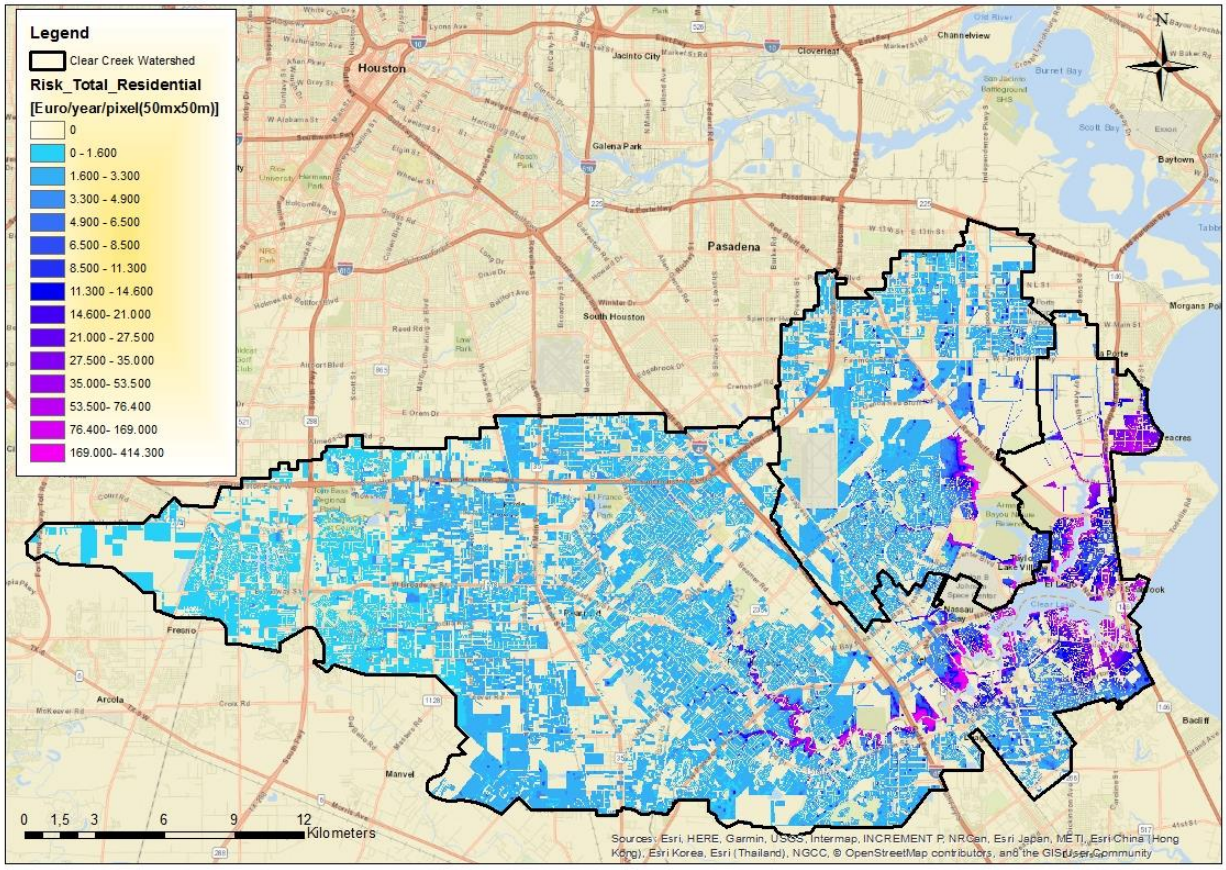

Figure 127. Flood Risk for Residential LU [€(2010)/year per pixel of 2500m^2] in the Clear Creek.

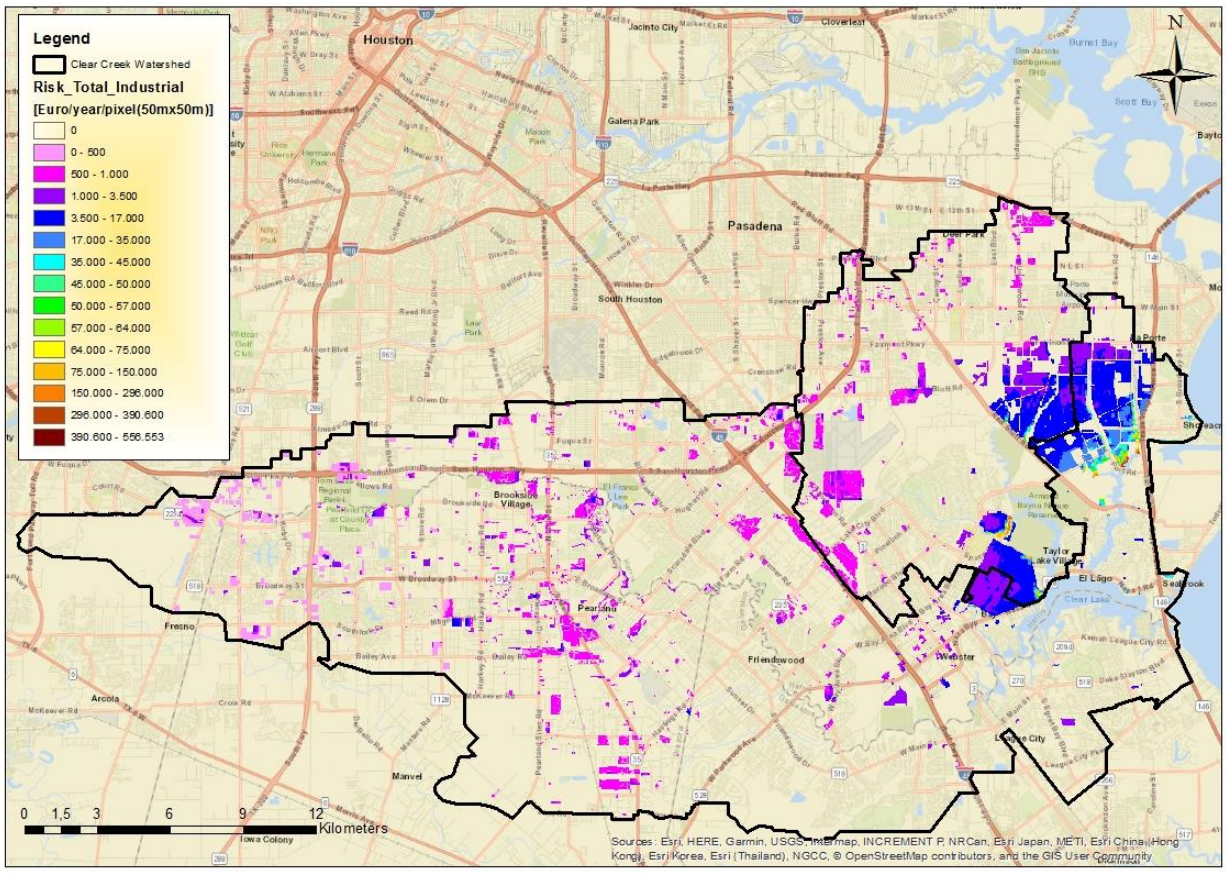

Figure 128. Flood Risk for Industrial LU [€(2010)/year per pixel2500m^2] in the Clear Creek.

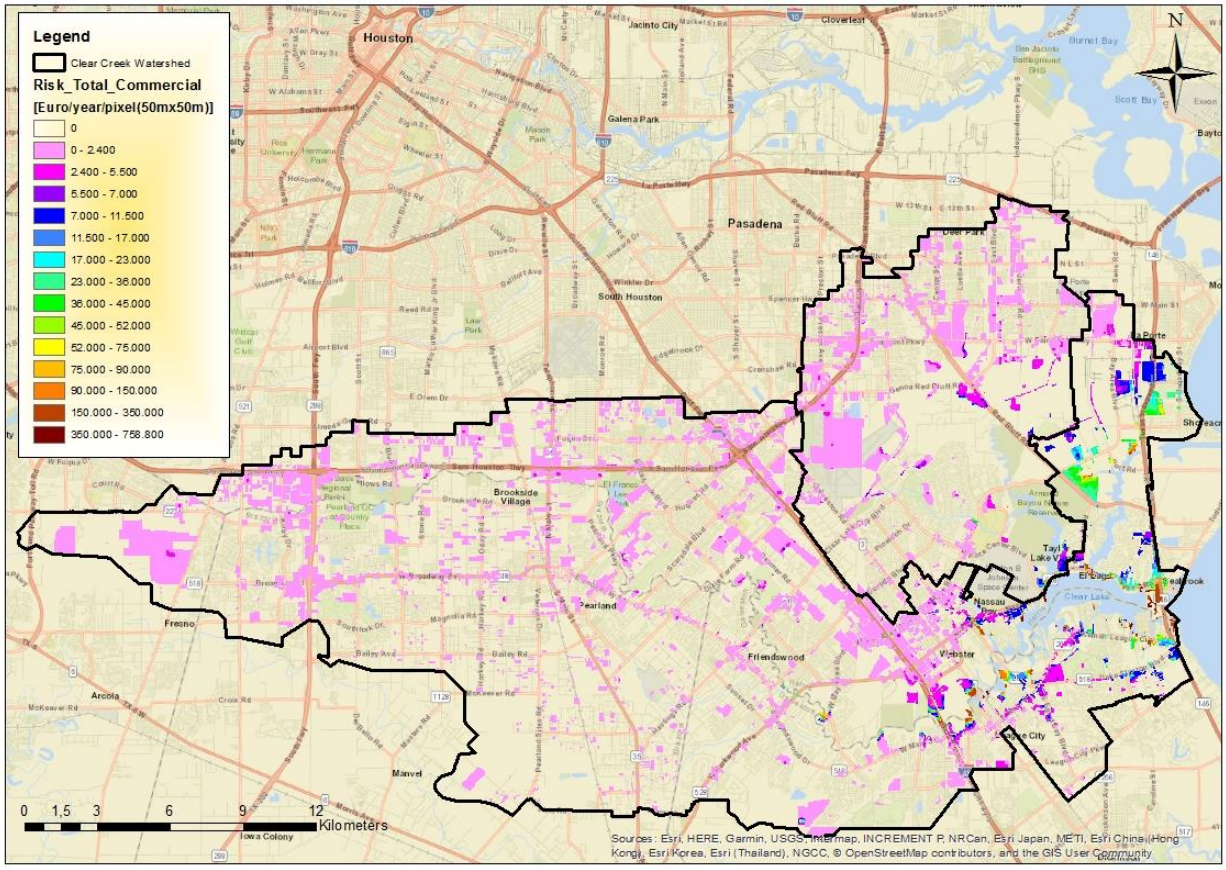

Figure 129. Flood Risk for Commercial LU [€(2010)/year per pixel of 2500m^2] in the Clear Creek.

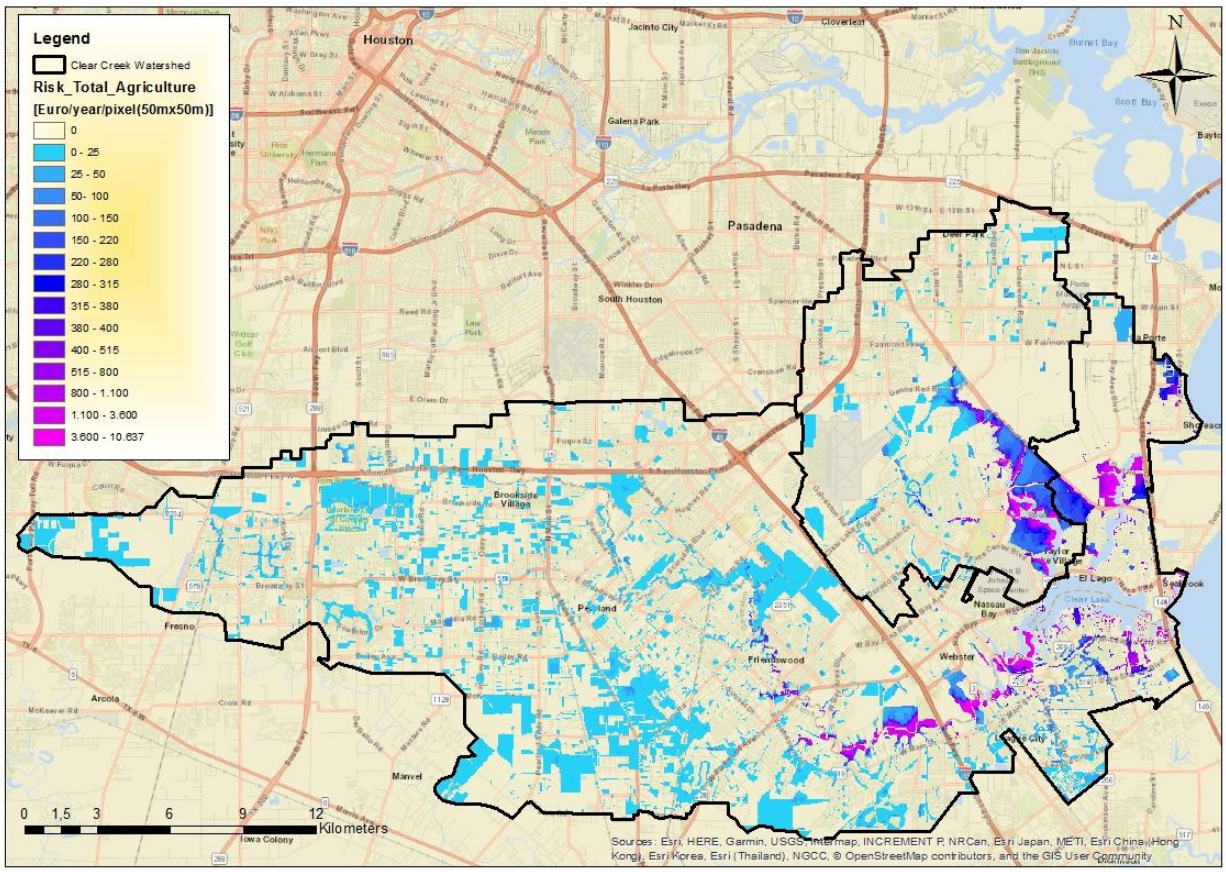

Figure 130. Flood Risk for Agriculture LU [€(2010)/year per parcel of land of 2500m^2] in the Clear Creek.

As it can be seen in Figure 126, the total risk of the Clear Creek watershed ranges from a value of 0 to a maximum of approximately 884,000.00 Euros of damage per year per parcel of land of 2500m^2 due to occurrence of compound events in the region. It was be seen clearly that the highest values are located nearby the coast and surround the downstream parts of the Clear Creek and the Armand Bayou. It can be seen that in general terms, the mean loss is between 3,000 and 10,500 Euros per year and that most of these losses come from residential damage (See Figure 127) located in the mid part of the watershed with some high estimated damages also nearby the outlet to the Galveston Bay. The highest registered damages belong to the commercial land use (see Figure 129) and the lowest values belong to the agriculture land use type with approximate maximum values of 10,600 Euros per year (Figure 130). The damages to industrial buildings have mean losses from 17,000 to 35,000 Euros per year (Figure 128) which can be considered low if for example these industries belong to the oil and gas sector. Probably in this case more detailed vulnerability information is needed to have more accurate damage information, since probably the global depth damage function for the United States will underestimate damages, especially if we are speaking of Texas; one of the richest states due to is oil and gas industry. Nevertheless, for a first approximation, the previously depicted maps are very useful in order to inform better the communities living in the Clear Creek watershed, since with a risk map is clear that flooding in not a binary state that can happen only to people living within regions close to the main waterways, but actually, even for people living far from the main channels, flooding can still affect them and potentially there are some damages that they could experience if a flood hazard materializes. Other potential uses of these maps consist of using these estimates for performing a Cost Benefit Analysis (CBA) of possible measures to reduce flood risk in the area, also, they could be used to improve the assignment of insurance rates by policy writers, as well as a tool to improve the decision-making strategies of communities to acquire flood insurance even though is not mandatory. Finally, the risk maps could be used for planning and development strategies for the area. All of these applications are going to be discussed in further detail in chapter 6 in the conclusions of this research.

6 Conclusions

In this chapter, the results obtained throughout this study are used in order to answer the main research objective and first research question formulated in chapter 1.

Develop a method to delineate compound flood hazard and risk analysis, applied to the Clear Creek watershed as a case study.

How can flood hazard estimates be improved in coastal watersheds by the inclusion of compound events in the analysis via the use a of a semi- advanced 2D model (SFINCS)?

The main methodology to delineate compound flood hazard and risk in the area is summarized in Section 6.1 which is thereafter followed by Section 6.2, which contains the conclusions derived from the new flood hazard maps considering compound events for the Clear Creek watershed.

6.1. Methodology to delineate compound flood hazard and risk

In this research new and previously used methodologies were explored in order to improve the delineation of floodplains in coastal watersheds considering compound events. The aim of the investigation was to contribute towards the understanding of flood behavior and its drivers in coastal areas (especially those subject to hurricane activity) in order to delineate flood hazard adequately and be able to identify the associated risks with the intention of implementing strategies for flood risk management that are more effective, cost-efficient and socially acceptable. The following methodology was applied successfully to the Clear Creek catchment but it can be potentially used for other coastal watersheds exposed to compound flooding.

1. **Generation of synthetic data set of pairwise data for compound events (CE):**
   In this case the synthetic data was generated through a NPBN and a 1-D Bay Model which was already constructed for the area and which proved to be a flexible and computationally efficient tool to generate cumulative precipitation and peak storm surge data (Sebastian et al., 2017). Other techniques could be explored to generate synthetic data sets for other coastal watersheds

2. **Estimation of Joint Probability of CE through the use of Copulas and the determination of return periods in a multidimensional environment:**
   By fitting a copula $[C(1-u,1-v)]$ to the synthetic dataset, and using the concept of multidimensional return period established by Salvadori et al.(2011), the joint probability of occurrence between precipitation and storm surge can be determined (see Figure 97), given that there is a common triggering factor (tropical cyclone) for the compound events so that the inter arrival time (μ_T) between compound events can be determined.

$$Return\ Period\ for\ Compound\ Events = \frac{\mu_T}{p_{\widehat{u,v}}} = \frac{\mu_T}{C(1-u,1-v)}$$

3. **Definition of Boundary Conditions to delineate flood hazard due to CE**
   The selection of boundary conditions for compound flooding can be done using two approaches; the first one is by selecting only scenarios with the same return period (e.g. 100-year return period of

compound flood pairwise scenarios), and the second one by generating a grid (see Figure 116) that covers all compound flooding scenarios portrayed on the synthetic data.

4. **Flood hazard delineation using boundary conditions in a 2D model (SFINCS)**
To delineate flood hazard, is recommended that both boundary conditions described previously are used since they will give different information that can be useful for communities and policy makers to reduce flood risk in the region.

The first approach is to use CE's with certain return period as an input within a 2D semi-advanced model (in this case SFINCS) to delineate the floodplains of the region. The overlay of all events with the same return period will generate a map showing the **maximum compound flooding hazard extent** in the catchment. This map will only show flood extent considering compound events, but it won't give statistical information about the flood depth occurring due to these events, other than the maximum flood depth registered at each location within the watershed. This information might be useful if FEMA for example continues to set mandatory insurance within the "100-year" floodplain, since in this case the 100-year compound floodplain will contain in addition, all those areas exposed to storm surge and all the areas outside the main streams that might get flooded due to ponding.

The second approach is more similar to the regular practice known worldwide, in which the floodplain delineation is associated with the **100-year flood depth.** In this case, the procedure explained in Figure 117 was followed, in which the ensemble of probabilistic compound scenarios in a numerical grid was used within SFINCS in order to determine what would be the 100-year flood depth at each single location of the watershed due to any compound event occurring in the area. In this case, the flood hazard map is more useful in terms of identifying what would be the associated annual damages and therefore an estimation of risk can be done if this approach is used which can drive decision making regarding flood risk reduction strategies in the area (see discussion on chapter 7)

5. **Risk delineation using ensemble of probabilistic CE hazard scenarios with their associated damage**
In order to delineate estimated annual damage in the area is not enough to follow the actual approach by FEMA in which the risk is only estimated based on few flood hazard scenarios defined by a return period (see FEMA approach below)

$$EAD = \sum damage(depth_{RP}) \cdot probability_{\text{depth}_{RP}}$$

Normally, no more than 5 return periods are evaluated which can lead to an underestimation of the total risk, and actually not all possible damages are being assessed.

With the new approach proposed in this research which allows the estimation of the joint probability of compound events via the use of copulas and a numerical grid in addition to the computational efficiency of SFINCS, it is possible to compute several scenarios (400 scenarios in this case study) that allow a full probabilistic description of all the damages occurring in the area, hence allowing the use of the truth definition of annual estimated damage as seen below

$$EAD = \int damage(\mathrm{p})\,\mathrm{dp}$$

In Table 14 a comparison between the newly proposed methodology to delineate flood hazard in the area and the currently approach used by FEMA is presented to understand clearly the main differences between methodologies.

Table 14. Main differences between FEMA and SFINCS approach

SFINCS with Compound Events	FEMA
Co-occurrence of flood drivers: Storm surge and Precipitation rates	Uses a single flood driver: historical discharge rates
Unsteady flow state - (flood wave traveling downstream)	Steady state (100-year discharge occurring infinitely)
Inland flooding: based on rainfall rates	Inland flooding: based on stream gauge measurements

100-year water depth for all locations within the catchment	Flooded areas with a range of depth values related to the steady discharge value. (not a specific value)
Coastal flooding: based on storm surge synthetic data	Costal flooded areas: based on wave height larger than 1m.

6.2. General Conclusions regarding flood hazard improvement

Based on the results obtained in this research (chapter 5) and by using a 2D semi-advanced coastal model in order to incorporate the interaction between co-occurrence of storm surge and precipitation in the Clear Creek watershed, it can be said (answering the main question) that for this specific case, compound flooding should be indeed incorporated for the analysis of flood hazard in the area since not doing so will highly underestimate the flood depth and extent in areas nearby the Galveston Bay.

It was seen that mainly for the Clear Creek, the effect of surge can go as deep as 17 to 20km inland from the outlet of the catchment and that for the Armand Bayou, the effect can go up to 10 to 12 km from the outlet meaning that in between these regions, if compound flooding is excluded from the analysis, flood hazard will be severely underestimated when compared to the actual FEMA approach which considers only one flood driver at a time. Moreover, it was found that the actual FEMA delineation, only considers a small region (VE green zone Figure 132) within the Clear Lake to be affected by coastal flooding, while the approach used in this research found that a much larger zone was influenced by storm surge. The VE area delineated by FEMA only reflects possible areas subject to wave heights larger than 1m, but it leaves out all areas affected by a coastal flood driver independently of the occurrence of waves. This information can be confusing for the users of these maps since it gives the wrong impression that elevated water levels at the coast won't affect certain locations, when in fact most of the flooding in the downstream part of the watershed is dominated by the conditions at the Galveston Bay.

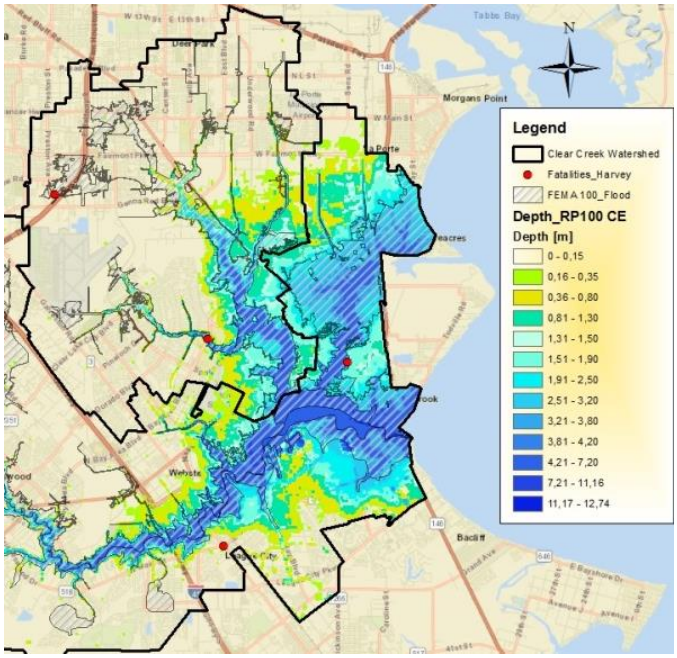

Figure 131. FEMA floodplains Vs. SFINCS 100 -year floodplain considering compound events. Dashed regions are FEMA SFHZ corresponding to 100-year flood events and green and blue areas correspond to the 100-year compound flood depth computed with SFINCS.

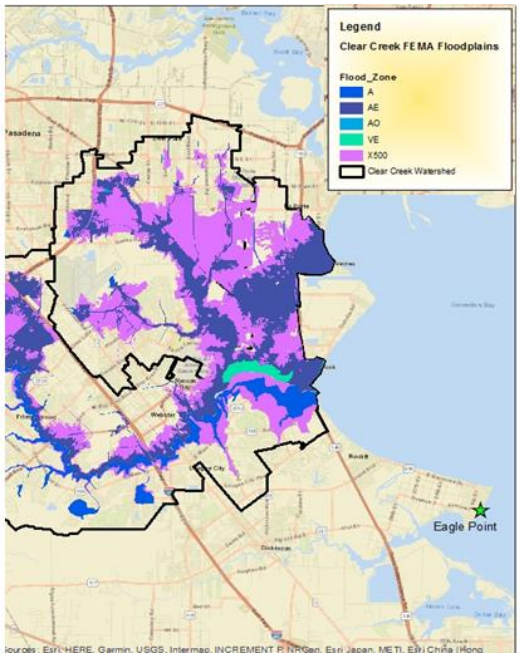

Figure 132. FEMA floodplain -Zoom in into nearest locations to the Galveston Bay.

Likewise, it is also seen than the **100-year compound flood** delineation (see Figure 131) covers almost as much as what is depicted by FEMA in the 500-year flood (see purple areas in Figure 132), pointing again that the new methodology followed in this research indeed covers more area (making it a more conservative approach) in the coastal areas than the traditional approach leading to the conclusion that FEMA

has been underestimating flood hazard in the area, mainly due to the effect of storm surge. Additionally, it is also seen that that for the 100-year compound floodplain, the dominant factor for flooding is mainly storm surge since not much inland flooding is observed (partly due to the fact that FEMA uses discharges instead of precipitation rate and since the precipitation used in SFINCS triggers a much lower discharge than the one used by FEMA)

Most importantly, as mentioned in chapter 5 (Section 5.1.2), the flood hazard maps are capturing more claims than what FEMA estimates when both maps are compared to the damage claim density triggered by hurricane Ike (see Figure 120) which shows that using the proposed methodology in this research indeed improves the delineation of flood hazard in this particular coastal watershed. In terms of area, FEMA was capturing 51% of the claims, while the new approach using SFINCS managed to capture 67% of the claims, going up till 79% of the claims when the direct SFINCS model of hurricane Ike is observed. Besides, when the location of fatalities happening during hurricane Harvey are overlaid with the new compound flood hazard maps (see Figure 122), these new maps cover all casualties in the watershed showing the relevance of considering compound events for the delineation of flood hazard maps in this specific coastal watershed, since the FEMA maps were not capturing all the casualties registered in the area.

Is also very interesting to notice that using the methodology of this research, there is not such a big change in terms of flood extent between the 100-year compound flood and the 500-year compound flood when they are compared to what is delineated by FEMA for different flood return periods (Compare Figure 118 and Figure 119 to Figure 32). What it is indeed changing considerably in the new approach is the flood depth in each cell, which becomes less or more critical depending on the return period being evaluated. The new approach makes much more sense since it stops contemplating flooding as a binary state in which if an asset is outside the floodplain it will not suffer any flooding. In reality, flood depths are transitional and is more useful to have maps depicting ranges of inundation depths within the total extent of flooding than simply an area which most of the time has not even an associated depth of inundation (FEMA Case of Zones A and AO).

In Addition, the use of a 2D model was one of the keys to improve the delineation of flood hazard, since SFINCS allowed to use all the topographic details of the region in order to route water in both directions all over the extent of the model, and not only focus on the routing through the main channels. This approach is very important since it reflects more closely reality, due to the fact that when there is a precipitation event, the rain doesn't fall only into the main waterways but it can be spatially distributed over the entire domain causing potential ponding in areas that are not even close to a draining channel. In addition, the use of SFINCS avoided the necessity of connecting water levels between cross-sections which can easily overestimate the flooding extent and can create strange patterns in the data that make that the flooding depths are not correctly continuous. This problem was solved by SFINCS in which due to the use of the entire DEM of the watershed and the 2D configuration of the physics of flooding, flooding extents can be computed outside of the surroundings of the main tributaries.

What is more, the use of the SFINCS model allows having quick hazard information due to the computational efficiency of the model and it doesn't require extremely detailed information other than the DTM of the area and the boundary conditions of the model (Rainfall rate, offshore water level, wind, etc.), thus making it an ideal and attractive alternative to compute flooding in coastal watersheds since it allows to go a step further in the modelling transitioning from a 1D model towards a 2D model without major computational effort and having as an advantage that the timing between variables can be also explored. If a 2D model can be easily set-up for a coastal watershed, it can reduce the effort of over simplifying a system in order to represent all the physics of flooding in a 1D plane. This most of the time can generate errors if the physics behind flooding are not fully understood.

Taking into account the results obtained in this study, is recommended that future researchers focus in improving further some of the features of SFINCS like the computationally efficiency when the resolution of the model is increased, or explore also the inclusion of different grid sizes for certain parts of the model. Some additional recommendations on how to improve the delineation of hazard can be found in more detail in chapter 8.

The purpose of this research is not to replace the methodologies followed by FEMA to delineate flood hazard, but to propose possible improvements to the actual methodology following the approach showed in this research. In the case of policy makers and possible users of the results published in this thesis (especially those obtained in chapter 5 regarding the flood hazard maps), is recommended that if an alternative to the FEMA maps is seek, especially in the regions nearby the Galveston Bay, the new proposed 100-year and 500-year compound flood maps can be used since they give more information than what is currently available to the public. Due to the results obtained with inland flooding in the upper part of the catchment for now is recommended that the flooding extends of FEMA are maintained until a full analysis with SFINCS is done using similar discharge values as the one used in the Flood insurance study of the area.

The methods presented in this M.Sc. thesis have important implications for the implementation of flood risk management strategies in coastal environments and they represent further improvements that could be considered in order to update the actual flood delineation strategies for coastal watershed in the United States. Similar approaches could be used as well in other coastal catchments outside the U.S to improve flood mitigation, prevention and adaptation measures in flood prone communities

7 Discussion

In this chapter, the second research question (see below) of this thesis is addressed in a discussion that focuses mainly on the implications of going from a hazard to risk approach taking into account compound events in the Clear Creek watershed.

What may be the implications of delineating new flood hazard maps considering compound flooding for flood risk assessment, implementation of flood risk management strategies and insurance rates in the Clear Creek watershed?

7.1. Discussion regarding inclusion of risk information

In terms of the implications for **flood risk assessment** of having delineated new flood hazard maps for the Clear Creek watershed considering compound events, is that actually, flood hazard has been improved using probabilistic methods that go beyond an extrapolation of historical extreme values of a single variable (discharge), and therefore, there is more representative information about the flood hazard than what is depicted by FEMA, in addition to the fact that the new maps are covering more flood claims than the actual approach.

The method presented in this report allows having a more complete picture of flooding in the area since it includes a bivariate analysis of flood drivers and due to the use of a 2D model it also permits having detailed information about flooding in the whole extent of the watershed which is vital for performing a risk analysis

When computing the risk for the watershed is important to mention that damages were estimated not only for few single scenarios corresponding to a return period water depth (as explained in the Conclusions chapter) but actually, the truth definition of risk was used, which computed the integral of the possible damages generated by certain scenario with a determined probability. In this way the estimation of the Expected Annual Damage (EAD) is done in a more consistent way covering all possible scenarios that could happen at a certain location and truly depicting in the initial risk map of the watershed which shows the average losses that any location within a parcel of land of 2500m^2 (50m x 50m cell of the flood hazard output) can expect in a year, only considering economic damages.

The relevance of this type of information is the amount of applications and flood risk management strategies that can be derived from a map like this. The main identified applications are listed below:

1. Preparation Strategies
2. Response Strategies
3. Recovery Measures
4. Mitigation Measures
5. Development of flood safety standards

The first 4 applications can be said to be part of the Disaster Management Cycle, in which having a good estimation of risk for an area can help in the **preparation phase** in the way that if property owners know the risk that they are exposed to, and an EWS alerts that a storm might be coming, local fast measures can

be taken by communities like installing temporary flood defenses such as inflatable barriers or even sand bags. Besides, if communities are aware, local measures can be taken as a merely preventive measure (raise buildings and facilities), which will turn a city into a much resilient place. In the **response phase**, if authorities know where the risky spots are (by using both the flood hazard and risk maps), it helps to organize where to send aid first. In the same way, if there is a reliable estimate of possible losses per year, during the **recovery phase** it can be partially estimated how much money has to be freed up for recovery of a region. Similarly, during the **mitigation phase** many possibilities can be explored since the risk map can be used to perform a Cost-Benefit analysis that helps in choosing between a set of measures (structural or non-structural) that effectively reduce the flood risk of the area. Also, it can be used for setting the first steps towards an adaptive delta management in order to integrate better planning for long-term development of coastal areas. In addition, as it was explained before, it can be used to set insurance premiums and it this particular study case, update the methodologies used by the NFIP of the Unites States.

Moreover, going from a hazard to risk approach can help to improve or create new safety standards for the region which nowadays at least in coastal watershed in the United States are wrongly associated to the 100-year flood criteria stipulated by FEMA for insurance purposes. This new approach can help towards answering the popular question: *How safe is safe enough?* Which involves the estimation of economic risk (done in general terms in this research), but also it needs an estimation of individual and societal risk as in can be seen in Figure 133. If the question is solved by estimating what is the acceptable risk for the region, modifications to the NFIP program can be made in terms of whom has to pay mandatory insurance and this decision will not depend anymore of being inside or outside a specific floodplain delineated by a flood return period. In addition, The total risk map (See Figure 126) obtained in this research can be even useful if the actual approach of FEMA remains the same, since it can be used to educate communities outside of the floodplain about the annual flood risk they are exposed to and can even serve as an encourager to be part of the NFIP if they considered the damages are too high compared to the annual cost of a flood policy. It can be used as well by policy writers to set the insurance rates inside and especially outside of the FEMA 100-year floodplains since more accurate information is available. Nevertheless, is recommended that more detailed vulnerability information is used for the damage estimation since the initial risk approach used in this research is still too general to propose accurate modifications to the rates, especially if the global damage functions have not been compared to the ones delineated by HAZUS to see if the simple approach could be used to propose modifications to the insurance rates

Figure 133. Flood Risk Framework to generating safety design standards.
Source: (Kok, 2015)

In this research, the gap of calculating risk based on total damage and not in maximum pay-out value ($250,000) was performed so that communities are better informed of actual losses. Is important that in order

to complete the economic risk estimates, damages to content are also included and that the analysis is done per object and not per land use as mentioned before. In the case of policy makers, is important that the shift from a hazard to a risk approach is done as quickly as possible since this method allows assessing and implementing flood prevention and mitigation strategies that are more effective and efficient in reducing flood risk in coastal watersheds.

8

Future Research

This chapter suggest future research directions that could be followed in order to improve the flood risk assessment of coastal watersheds considering compound events through the use of the semi-advanced 2D model: SFINCS. All the future research directions are given based on the discussion of the methodology that was used in this study for performing the flood risk assessment of the Clear Creek watershed and on the limitations, accuracy and uncertainty of the results found on the results of this research.

Initially, recommendations are given regarding the definition of boundary conditions for compound flooding and possible research regarding a lagged analysis between the compound events to determine when the strongest correlation is achieved and how sensitive is the flood extent to different lags between the main flood drivers. Thereafter, possible improvements to the SFINCS model based on the work presented in this thesis are given in order to capture more realistically flood hazards in coastal watersheds, especially in cases when tropical cyclones are the main triggering factor for compound events. Finally, some improvements are suggested in Section 7.3 to improve the damage estimation using more detailed vulnerability information.

8.1. Boundary conditions for compound flooding

As mentioned in chapter 4, the definition of the boundary conditions for this research were derived from a synthetic dataset derived from a NPBN and a 1D bay model of the Galveston Bay (Sebastian et al., 2017). This data set was derived in 2014 and therefore it doesn't include some extreme events recorded after this date which included Tropical Storm Dolly, Bill, Cindy and hurricanes Patricia and Harvey. The inclusion of these extremes will obviously generate a shift of the joint return period curves for compound events in the area towards higher values of precipitation and therefore, is recommended that an update of this information is performed to reflect the new conditions for compound flooding. Moreover, it would be also useful to generate synthetic data for other regions in the west coast of the Galveston Bay instead of only generating data for the outlet of the Clear Creek watershed, since this will allow representing better the changes of water level along the coast during the 2-D simulation of compound events in the area.

In addition, as it was mentioned in Section 4.1.3, the time lag between peak storm surge and maximum rainfall intensity was of 4 hours but this value was obtained directly from the SCS type III curves for precipitation and from the scaling of the storm surge using the values from hurricane Ike. The maximum duration of each event was considered to be 3 days since this was the time reference observed in the historical data used to feed the Bayesian Network. However, even though this approach is appropriate for the first estimation of risk due to compound flooding in the Clear Creek watershed, is recommended that future research explores more the timing between these events both in terms of finding which is the time lag between compound events that has the strongest correlation, and also how the flood extent changes if different timings are considered (e.g. one day between peak of events). The previous approach will allow the research to expand to include other definitions of compound flooding in which one event is dominant (e.g. elevated offshore water levels that slow down the run off drainage of the basin) or in which the combination of non-extreme events can lead to an extreme impact due to the timing of the events

8.2. The SFINCS model

As mentioned in chapter 3 and 4, many simplifications were done in the setup of the SFINCS model to run previous storms as Ike and Harvey and also to run the ensemble of probabilistic scenarios considering

compound events. Many of the simplifications included not using some features of the semi-advanced model, since the available input data was not as detailed as what SFINCS can resolve, therefore in the bullets below a summary is presented of the key points that could be improved to have more precise flood hazard maps.

- Regarding the validation of previous storms it would have been more precise to force the offshore water levels coupling the SFINCS model with the results of an advance model that could solve the water levels at the Galveston Bay (e.g. XBeach - Delft3D)

- For both the simulations of previous storms and the ensemble of compound flood scenarios, the inclusion of wind is something that should be considered since depending on the magnitude this can affect the flooding extent. In the case of previous storms the hurricane's track is well known so this can be included by a spider-web file in SFINCS, and in the case of the synthetic data set, the initial NPBN created by Sebastian et al. (2017) included details of the hurricane's wind velocity that could be introduced in SFINCS as a spatially uniform condition

- As mentioned on Section 4.4, SFINCS doesn't allow the introduction of a spatial varying Manning roughness coefficient and only sets a threshold for changing the manning value according to a depth parameter set at 0m + MSL to identify what is sea and what is land. This approach is appropriate for flat zones nearby the coast where the topography doesn't change too much, nevertheless for the upstream parts of a catchment, this approach assigns a high value of roughness (land value) to all water bodies causing and underestimation of the flow depth since water is not properly conveyed to the main channels. It will be worth to explore the inclusion of a varying input In order to capture also changes in land use roughness as well. The implementation will have to take into consideration the efficiency of the model so as to not increase the computational time

- For this specific watershed, it was seen that a grid resolution of 50m was too coarse to capture the upper part of the Clear Creek watershed and that due to this resolution, there was an increase in the amount of ponding and an underestimation of the flood extent nearby the main waterways. Nevertheless, decreasing the grid size to the same value of the DEM (10m grid) in order to capture the channels, increased the computational time from 15 minutes to almost 4 days (e.g. simulation of design precipitation event) which at the end was not viable to do, if the idea was to run an ensemble for 400 probabilistic events. Nevertheless, it is recommended that some research is performed regarding how to increase the computational speed for SFINCS in these cases, or as an alternative try to explore additional options to include different spatial resolutions within the model. This could also add value to the implementation of SFINCS as a tool for FEWS(see Leijnse (2018))

- Is recommended that if SFINCS is going to be connected to Delft-FIAT in the future, empty cells with the assigned value "NaN" are avoided since these values generate disagreements between the models. Final hazard outputs in GeoTiff format will improve the configuration of Delft-FIAT

8.3. Risk approach

As mentioned in chapter 5 and 6, a simple vulnerability and exposure approach based on global land-use damage functions was chosen in order to delineate risk in the Clear Creek watershed. This approach is general and is useful for first insight, however, is recommended than in order to have better estimations of risk, a more detailed methodology is used that takes into account damage per household in order to have improved recommendations for insurance rates across the area. Using HAZUS damage curves and detailed information about buildings and objects in the area will be a step forward in the quantification of risk at least for this particular study case.

In addition, moving a step forward in the risk approach, it should be worthy to explore the effect of flooding in this particular area to Critical Infrastructure (CI), since this has a close relationship with consequences for life and environment in an area. An initial risk map like the one produced in this research, leaves out the consequences for example of a power outage that could affect millions of people (see latest example of Puerto Rico with hurricane Maria), or for example the additional damages created by an interruption of CI such as Communication, transport systems or drinking water facilities that all have most of the time long-lasting societal impacts apart from the obvious economic losses. Using the risk map to identify

most critical affected infrastructure can be the first step, to later this use information with the participation of different stakeholders involved in managing these assets, to understand the complex relationship between the CI systems and society. This activity can allow seeing possible cascading effects that could harm the recovery of a city after a flood event and therefore, this should be included in a full risk assessment in order to create better policies that in effect turn a city more resilient against flooding. Such tools that allow different stakeholders to understand relationships between CI have been already explored by Deltares with the Circle Tool and therefore this could be potentially used in a next phase of this research.

Finally it would be worth to explore damage functions related to loss of life and in this way also estimate the individual risk of flooding in this particular area to contribute towards the construction of flood safety standards for the area. Recent research done by S. Jonkman, Godfroy, Sebastian, & Kolen (2018) for the most recent devastating storm hitting the area (Harvey), shows that 70 fatalities occurred due to the event and that most of them occurred outside of the designated 100-year floodplain by FEMA and most importantly due to drowning reasons. Therefore, next steps on research should be focus on constructing based on Harvey and other mayor storms, initial FN curves that could be used in combination with improved versions of the flood hazard estimated in this research to estimate the first societal or group risk map of the Clear Creek watershed. Such a map could also help in the design of potential evacuation and early response plans.

9

Bibliography

Amadeo, K. (2018). hurricane Katrina Facts: Damage and Costs. Retrieved March 22, 2018, from https://www.thebalance.com/hurricane-katrina-facts-damage-and-economic-effects-3306023

Arabnia, H. R., & Quoc Nam, T. (2015). Akaike Information Criterion - an overview | ScienceDirect Topics. Retrieved March 12, 2018, from http://www.sciencedirect.com/topics/pharmacology-toxicology-and-pharmaceutical-science/akaike-information-criterion

Asquith, W. H., & Roussel, M. C. (2004). Atlas of depth-duration frequency of precipitation annual maxima for Texas. *U.S. Geological Survey Scientific Investigations Report*, *5041*.

Bass, B., & Bedient, P. (2018). Surrogate Modeling of Joint Flood Risk across Coastal watersheds. *Journal of Hydrology*, *558*, 159–173. https://doi.org/https://doi.org/10.1016/j.jhydrol.2018.01.014

Bates, P. D., Horritt, M. S., & Fewtrell, T. J. (2010). A simple inertial formulation of the shallow water equations for efficient two-dimensional flood inundation modelling. *Journal of Hydrology*, *387*(1–2), 33–45. https://doi.org/10.1016/j.jhydrol.2010.03.027

Bedient, P. B. (2012). *Lessons from hurricane Ike* (1st Editio). Texas A&M University Press.

Berg, R. (2009). Hurricane Ike Report. *National Hurricane Centre*, (September 2008), 1–14. https://doi.org/10.1017/CBO9781107415324.004

Bevacqua, E., Maraun, D., Hobæk Haff, I., Widmann, M., & Vrac, M. (2017). Multivariate statistical modelling of compound events via pair-copula constructions: Analysis of floods in Ravenna (Italy). *Hydrology and Earth System Sciences*, *21*(6), 2701–2723. https://doi.org/10.5194/hess-21-2701-2017

Blessing, R., Sebastian, A., & Brody, S. D. (2017). Flood Risk Delineation in the U.S.: How much loss are we capturing? *Natural Hazards Review*, *18*(3), 1–10. https://doi.org/10.1061/(ASCE)NH.1527-6996.0000242.

Borenstein, S. (2018, January). Federal report shows punch of last year's hurricane Harvey. *Fox News*. Retrieved from http://www.foxnews.com/us/2018/01/25/federal-report-shows-punch-last-years-hurricane-harvey.html

Brand, N., Sebastian, A., Nillisen, A. L., & Jonkman, S. N. (TU D. (2015). Delft Delta Design Delft Delta Design Houston Galveston Bay Region, 136.

Brody, S. D., Blessing, R., Sebastian, A., & Bedient, P. (2013). Delineating the Reality of Flood Risk and Loss in Southeast Texas. *Natural Hazards Review*, *14*(2), 89–97. https://doi.org/10.1061/(ASCE)NH.1527-6996.0000091

Brody, S., Sebastian, A., Blessing, R., & Bedient, P. (2013). Where Will I flood? Identifying the impacts of residential location on flood risk and loss Journal: *Journal of Flood Risk Management*.

Carson, R. (2017, September 1). Houston under water. *Reuters*. Retrieved from https://www.reuters.com/news/picture/houston-under-water-idUSRTX3DNFZ

CNN. (2017). Hurricane Ike slams Texas in 2008. Retrieved May 20, 2018, from https://edition.cnn.com/2017/04/27/us/gallery/hurricane-ike-texas-2008/index.html

Congressional Budget Office. (2017). The National Flood Insurance Program: Financial Soundness and

Affordability, (September). Retrieved from www.cbo.gov/publication/53028

Corbella, S., & Stretch, D. D. (2012). Multivariate return periods of sea storms for coastal erosion risk assessment. *Natural Hazards and Earth System Science*, *12*(8), 2699–2708. https://doi.org/10.5194/nhess-12-2699-2012

Couasnon, A. A. O. (2017). *Characterizing flood hazard at two spatial scales with the use of stochastic models*. Delf University of Technology.

Dannenbaum Engineering Corporation. (1991). *Clear Creek Regional Flood Control Plan*.

de Moel, H., Jongman, B., Kreibich, H., Merz, B., Penning-Rowsell, E., & Ward, P. J. (2015). Flood risk assessments at different spatial scales. *Mitigation and Adaptation Strategies for Global Change*, *20*(6), 865–890. https://doi.org/10.1007/s11027-015-9654-z

Defra/ Environment Agency. (2006). *Flood Risks to People - Phase 2 - FD2321/TR2 Guidance Document*. London. Retrieved from http://randd.defra.gov.uk/Default.aspx?Module=More&Location=None&ProjectID=12016

Deltares. (2018a). Delft-FIAT. Retrieved July 17, 2018, from https://publicwiki.deltares.nl/display/DFIAT/Delft-FIAT+Home

Deltares. (2018b). Delft Dashboard. Retrieved June 11, 2018, from https://publicwiki.deltares.nl/display/DDB/Delft+Dashboard

Doocy, S., Daniels, A., Murray, S., & Kirsch, T. (2013). The Human Impact: a Historical Review of Events 1980-2009 and Systematic Literature Review. *PLOS Currents: Disaster*, *1*(October 2012). https://doi.org/10.1371/currents.dis.f4deb457904936b07c09daa98ee8171a.Authors

Earth Data - NASA. (2018). Giovanni - The bridge between Data and Science. Retrieved April 14, 2018, from https://giovanni.gsfc.nasa.gov/giovanni/#service=AcMp&starttime=2008-09-07T00:00:00Z&endtime=2008-09-07T11:59:59Z&bbox=-96.004,29.0094,-94.5099,30.0092&data=TRMM_3B42RT_7_precipitation&variableFacets=dataFieldMeasurement%3APrecipitation%3B

Eilander, D. M. (2017). *Modelling impacts and drivers of compound extremes in delta areas at a global scale*. VU University of Amsterdam.

European Parliament, & Council of the European Union. (2007). DIRECTIVE 2007/60/EC OF THE EUROPEAN PARLIAMENT AND OF THE COUNCIL of 23 October 2007 on the assessment and management of flood risks. *Official Journal of the European Union*, 27–34. Retrieved from https://eur-lex.europa.eu/legal-content/EN/TXT/PDF/?uri=CELEX:32007L0060&from=EN

Faculty of Engineering and Architecture - Ghent University. (2018). Surrogate Modeling Lab (SUMO)-Ghent University. Retrieved March 7, 2018, from http://sumo.intec.ugent.be/

FAO. (2012). Annex 2 Infiltration rate and infiltration test. Retrieved June 8, 2018, from http://www.fao.org/docrep/s8684e/s8684e0a.htm

FEMA. (1998). *Managing Floodplain Development Through The National Flood Insurance Program*. Illinois. Retrieved from https://www.fema.gov/pdf/floodplain/is_9_complete.pdf

FEMA. (2008). *Mitigation Assessment Team report - High Water Marks hurricane Ike*. Houston.

FEMA. (2009). *Guidelines and Specifications for Flood Hazard Mapping Partners - Appendix C*. Washington D.C. Retrieved from https://www.fema.gov/media-library-data/1387814760538-48140a90bd0462c31a686a957ad7ad7c/Guidelines_and_Specifications_for_Flood_Hazard_Mapping_Partners_Appendix_C-Guidance_for_Riverine_Flooding_Analyses_and_Mapping_(Nov_2009).pdf

FEMA. (2017). *Flood Insurance Study - Harris County, Texas and Incorporated Areas* (Vol. 1). Retrieved from ftp://ftp1.co.mecklenburg.nc.us/luesa/stormwater/Flood Insurance Study/FIS/37119CV001C.pdf

Fischetti, M. (2017, August). Hurricane Harvey: Why Is It So Extreme? Retrieved January 5, 2018, from https://www.scientificamerican.com/article/hurricane-harvey-why-is-it-so-extreme/

Genest, C., & Favre, A.-C. (2007). Everything You Always Wanted to Know about Copula Modeling but Were Afraid to Ask. *Journal of Hydrologic Engineering*, *12*(4), 347–368. https://doi.org/10.1061/(ASCE)1084-0699(2007)12:4(347)

Gomes, M. P., Pinho, J. L., Antunes do Carmo, J. S., & Santos, L. (2015). Hazard assessment of storm events for The Battery, New York. *Ocean and Coastal Management*, *118*, 22–31. https://doi.org/10.1016/j.ocecoaman.2015.11.006

Graham, R. (2017). Barker dam spillway on 30 Aug 2017 after hurricane Harvey. Retrieved May 21, 2018, from https://www.youtube.com/watch?v=Sqw9_4gqAQM

Gřaler, B., Van Den Berg, M. J., Vandenberghe, S., Petroselli, A., Grimaldi, S., De Baets, B., & Verhoest, N. E. C. (2013). Multivariate return periods in hydrology: A critical and practical review focusing on synthetic design hydrograph estimation. *Hydrology and Earth System Sciences*, *17*(4), 1281–1296. https://doi.org/10.5194/hess-17-1281-2013

H-GAC. (2017a). Land Use & Land Cover Data. Retrieved from http://www.h-gac.com/community/socioeconomic/land-use-data/default.aspx

H-GAC. (2017b). *Mid-Year Population Estimates for H-GAC Region Counties Source : U . S . Census Bureau Released : March 2017*. Houston. Retrieved from http://www.h-gac.com/community/socioeconomic/census/documents/Estimates_Total_Counties_Census.pdf

Hallegatte, S., Green, C., Nicholls, R. J., & Corfee-Morlot, J. (2013). Future flood losses in major coastal cities. *Nature Climate Change*, *3*(9), 802–806. https://doi.org/10.1038/nclimate1979

Hanea, A., Morales Napoles, O., & Ababei, D. (2015). Non-parametric Bayesian networks: Improving theory and reviewing applications. *Reliability Engineering and System Safety*, *144*, 265–284. https://doi.org/10.1016/j.ress.2015.07.027

Harris County Flood Control District. (2016). HCFCD - Tropical Storm Allison (2001). Retrieved March 13, 2018, from https://www.hcfcd.org/storm-center/tropical-storm-allison-2001/

Harris County Flood Control District. (2018). HCFCD - Hurricane Ike (2008). Retrieved from https://www.hcfcd.org/flooding-floodplains/storm-center/hurricane-ike-2008/

Harvey, C. (2017, August 27). Hurricane Harvey shows how we underestimate flooding risks in coastal cities, scientists say - The Washington Post. *The Washington Post*. Retrieved from https://www.washingtonpost.com/news/energy-environment/wp/2017/08/29/hurricane-harvey-shows-how-we-underestimate-flooding-risks-in-coastal-cities-scientists-say/?noredirect=on&utm_term=.5b147461bf90

Haverkort, J. W. (2009). Numerical Methods for time-dependent Partial Differential Equations, (April), 1–14. Retrieved from http://homepage.tudelft.nl/20x40/documents/NumMethPDEs.pdf

HCFCD. (2009). *Hydrology & Hydraulics Guidance Manual*. Houston. Retrieved from https://www.hcfcd.org/media/1999/hcfcd-hydrology-hydraulics-manual_03-2016.pdf

HCFCD. (2018a). Flooding impacts in connection with the Reservoirs. Retrieved from https://www.hcfcd.org/hurricane-harvey/flooding-impacts-in-connection-with-the-reservoirs/

HCFCD. (2018b). HCFCD - Second Outlet Channel and Gated Structure. Retrieved May 20, 2018, from https://www.hcfcd.org/projects-studies/clear-creek/second-outlet-channel-and-gated-structure/

Houze, R. a., Hobbs, P. V., Biswas, K. R., & Davis, W. M. (1976). Mesoscale Rainbands in Extratropical Cyclones. *Monthly Weather Review*. https://doi.org/10.1175/1520-0493(1976)104<0868:MRIEC>2.0.CO;2

Huizinga, J., Moel, H. De, & Szewczyk, W. (2017). *Global flood depth-damage functions: Methodology and database with guidelines*. Publications Office of the European Union. https://doi.org/10.2760/16510

Ikeuchi, H., Hirabayashi, Y., Yamazaki, D., Muis, S., Ward, P. J., Winsemius, H. C., … Kanae, S. (2017). Compound simulation of fluvial floods and storm surges in a global coupled river-coast flood model:

Model development and its application to 2007 Cyclone Sidr in Bangladesh. *Journal of Advances in Modeling Earth Systems*, *9*(4), 1847–1862. https://doi.org/10.1002/2017MS000943

Jones, S. (2017, August 25). Harvey Would Be 64th hurricane to Hit Texas Since 1851. *CNS News*. Retrieved from https://www.cnsnews.com/news/article/susan-jones/harvey-will-be-64th-hurricane-hit-texas-1851

Jonkman, S., Godfroy, M., Sebastian, A., & Kolen, B. (2018). Brief communication: Loss of life due to hurricane Harvey. *Natural Hazards and Earth System Sciences*, *18*(4), 1073–1078. https://doi.org/10.5194/nhess-18-1073-2018

Jonkman, S. N., Jorissen, R. E., Schweckendieck, T., Van Den Bos, J. P., Oosterlo, P., Delft, T., & Van Kooten, V. (2017). *Flood defences Lecture notes CIE5314*. Delft.

Kalyanapu, A. J., Burian, S. J., & McPherson, T. N. (2009). Effect of land use-based surface roughness on hydrologic model output. *Journal of Spatial Hydrology*, *9*(2), 51–71. Retrieved from http://spatialhydrology.net/index.php/JOSH/article/view/84

Kaplan, S., & Garrick, B. J. (1981). On The Quantitative Definition of Risk. *Risk Analysis*, *1*(1), 11–27. https://doi.org/https://doi-org.ezproxyegre.uniandes.edu.co:8843/10.1111/j.1539-6924.1981.tb01350.x

Kimberlain, T. B., Blake, E. S., & Cangialosi, J. P. (2018). *National Hurricane Center Tropical Cyclone Report: Hurricane Harvey*. *National Hurricane Center Tropical Cyclone Report*. https://doi.org/AL092017

Klerk, W. J., Winsemius, H. C., Van Verseveld, W. J., Bakker, A. M. R., & Diermanse, F. L. M. (2015). The co-incidence of storm surges and extreme discharges within the Rhine-Meuse Delta. *Environmental Research Letters*, *10*(3). https://doi.org/10.1088/1748-9326/10/3/035005

Kok, M. (2015). Economical Optimal Safety standards in Flood Risk. Delft.

Kulp, S., & Strauss, B. (2017). These U.S. Cities Are Most Vulnerable to Major Coastal Flooding and Sea Level Rise. Retrieved January 5, 2018, from http://www.climatecentral.org/news/us-cities-most-vulnerable-major-coastal-flooding-sea-level-rise-21748

Kurz & Allison. (1900). Galveston's awful calamity - Gulf tidal wave, September 8th 1900.

Leijnse, T. (2018). *Computationally Efficient Modelling of Compound Flooding due to Tropical Cyclones with the Explicit Inclusion of Wave-Driven Processes - Research into the required processes and the implementation within the SFINCS model*. Delft University of Technology.

Leonard, M., Westra, S., Phatak, A., Lambert, M., van den Hurk, B., Mcinnes, K., … Stafford-Smith, M. (2014). A compound event framework for understanding extreme impacts. *Wiley Interdisciplinary Reviews: Climate Change*, *5*(1), 113–128. https://doi.org/10.1002/wcc.252

Lian, J. J., Xu, K., & Ma, C. (2013). Joint impact of rainfall and tidal level on flood risk in a coastal city with a complex river network: A case study of Fuzhou City, China. *Hydrology and Earth System Sciences*, *17*(2), 679–689. https://doi.org/10.5194/hess-17-679-2013

Liu, F. (2017). *Analyzing the influence of compound events on flooding in the downstream reach of the Houston Ship Channel*. Delft University of Technology.

MIT. (2018). Chapter 14: Stability of Finite Difference Methods. Retrieved March 19, 2018, from http://web.mit.edu/16.90/BackUp/www/pdfs/Chapter14.pdf

Moftakhari, H. R., Salvadori, G., AghaKouchak, A., Sanders, B. F., & Matthew, R. A. (2017). Compounding effects of sea level rise and fluvial flooding. *Proceedings of the National Academy of Sciences*, *114*(37), 9785–9790. https://doi.org/10.1073/pnas.1620325114

NASA. (2008). Hurricane Season 2008.

National Centers for Environmental Information (NCEI & NOAA). (2018). Galveston, Texas Coastal Digital Elevation Model. Retrieved April 14, 2018, from https://www.ngdc.noaa.gov/metaview/page?xml=NOAA/NESDIS/NGDC/MGG/DEM/iso/xml/403.xml&view=getDataView&header=none

National Research Council. (2015). *Tying Flood Insurance to Flood Risk for Low-Lying Structures in the Floodplain*. The National Academies Press. https://doi.org/10.17226/21720

NIWA-Taihoro Nukurangi. (2016). 13 Beach Types. Retrieved March 20, 2018, from https://www.niwa.co.nz/coasts-and-oceans/nz-coast/learn-about-coastal-environments/beach-types/13-beach-types

NOAA. (2013). National coastal population report: Population trends from 1970 to 2010. *NOAA State of the Coast Report Series*, 22.

NOAA. (2017). What is Storm Surge? Retrieved March 13, 2018, from https://oceanservice.noaa.gov/facts/stormsurge-stormtide.html

NOAA. (2018). Meteorological Observations - NOAA Tides & Currents. Retrieved May 21, 2018, from https://tidesandcurrents.noaa.gov/met.html?id=9415102

NOAA & NHC. (2018). Costliest U.S. tropical cyclones tables updated. *NOAA Technical Memorandum NWS NHC-6*, 3. Retrieved from https://www.nhc.noaa.gov/news/UpdatedCostliest.pdf%0Ahttps://www.nhc.noaa.gov/pdf/nws-nhc-6.pdf%0Ahttps://www.nhc.noaa.gov/dcmi.shtml

Phillip, D. J. (2016). Hurricane Ike Sweeps Across the Gulf - Photo Essays - TIME. *TIME*. Retrieved from http://content.time.com/time/photogallery/0,29307,1840002_1764785,00.html

Phillip, D. J. (2017). A look back at hurricane Ike 9 years later. Retrieved from http://abc13.com/weather/a-look-back-at-hurricane-ike-9-years-later/2412026/

PriceWaterHouseCoopers. (1999). *Study of the Economic Effects of Charging Actuarilly Based Premium Rates for Pre-FIRM Structures*. Retrieved from https://www.fema.gov/media-library-data/20130726-1602-20490-9031/finalreport.pdf

Project Brays. (2018). Floodplains Explained. Retrieved July 13, 2018, from https://www.projectbrays.org/learning-center/floodplains-explained/

Ray, T., Stepinski, E., Sebastian, A., & Bedient, P. B. (2011a). Dynamic Modeling of Storm Surge and Inland Flooding in a Texas Coastal Floodplain. *Journal of Hydraulic Engineering*, *137*(10), 1103–1111. https://doi.org/10.1061/(ASCE)HY.1943-7900.0000398.

Rijkswaterstaat VNK Project. (2014). The National Flood Risk Analysis for the Netherlands.

Risk MAP6. (2018). Flood Information Portal. Retrieved May 28, 2018, from http://maps.riskmap6.com/

Roth, D. (2010). *Texas Hurricane History*. Camp Springs, MD. Retrieved from https://www.weather.gov/media/lch/events/txhurricanehistory.pdf

Salvadori, G., & De Michele, C. (2004). Frequency analysis via copulas: Theoretical aspects and applications to hydrological events. *Water Resources Research*, *40*(12), 1–17. https://doi.org/10.1029/2004WR003133

Salvadori, G., De Michele, C., & Durante, F. (2011). On the return period and design in a multivariate framework. *Hydrology and Earth System Sciences*, *15*(11), 3293–3305. https://doi.org/10.5194/hess-15-3293-2011

Sebastian, A. (2016). *Quantifying Flood Hazard and Risk in Highly Urbanized Coastal watersheds*. Rice University.

Sebastian, A., Dupuits, E. J. C., & Morales-Nápoles, O. (2017). Applying a Bayesian network based on Gaussian copulas to model the hydraulic boundary conditions for hurricane flood risk analysis in a coastal watershed. *Coastal Engineering*, *125*, 42–50. https://doi.org/10.1016/j.coastaleng.2017.03.008

Sebastian, A., Lendering, K., Kothuis, B., Brand, N., Jonkman, B., van Gelder, P., … Lhermitte, S. (2017). Hurricane Harvey Report: A fact-finding effort in the direct aftermath of hurricane Harvey in the Greater Houston Region. *Delft: Delft University Publishers*, 102.

Seneviratne, S., Nicholls, N., Easterling, D., Goodess, C., Kanae, S., Kossin, J., … Zhang, X. (2012). Changes in climate extremes and their impacts on the natural physical environment. *Managing the Risk of Extreme Events and Disasters to Advance Climate Change Adaptation (SREX)*, 109–230. https://doi.org/10.1017/CBO9781139177245.006

Survey, F., & Data, M. (2009). Clear Creek.

Torres, J. M., Bass, B., Irza, N., Fang, Z., Proft, J., Dawson, C., … Bedient, P. (2015). Characterizing the hydraulic interactions of hurricane storm surge and rainfall-runoff for the Houston-Galveston region. *Coastal Engineering*. https://doi.org/10.1016/j.coastaleng.2015.09.004

USACE. (2012). *Clear Creek, TX - Draft General Reevaluation Report and Supplemental Environmental Impact Statement*. Retrieved from http://leaguecity.com/DocumentCenter/Home/View/4784

USDA. (1986). *Urban Hydrology for Small watersheds*. Washington D.C. Retrieved from https://www.nrcs.usda.gov/Internet/FSE_DOCUMENTS/stelprdb1044171.pdf

USDA. (2018a). USDA-NRCS: Geospatial Data Gateway. Retrieved April 13, 2018, from https://datagateway.nrcs.usda.gov/GDGOrder.aspx?order=MBROrder

USDA. (2018b). USDA - Offical Soil Series Descriptions and Series Classification. Retrieved August 5, 2018, from https://soilseries.sc.egov.usda.gov/OSD_Docs/L/LAS_POSAS.html

USGS. (2006). USGS Landsat project, Investigations . Retrieved from http://landsat.usgs.gov/technical_details/investigations/index.php

USGS. (2010). *100-Year Flood – It's All About Chance: Haven't we already had one this century?* Retrieved from https://pubs.usgs.gov/gip/106/pdf/100-year-flood-handout-042610.pdf

USGS. (2015). National Elevation Dataset. Retrieved March 20, 2018, from https://lta.cr.usgs.gov/NED

USGS. (2016). NOAA. Retrieved March 20, 2018, from http://www.nhc.noaa.gov/data/

USGS. (2018). Harvey High Water Marks -HydroShare. Retrieved June 18, 2018, from https://www.hydroshare.org/resource/615d426f70cc4346875c725b4b8fdc59/

Van Engelen, T. E. (2016). Towards a rapid assessment flood forecasting system for the Southern California coast, (October). Retrieved from https://repository.tudelft.nl/islandora/object/uuid:cb904f76-8771-42ab-b069-d645f5c8f7d0?collection=education

Van Oldenborgh, G. J., Van Der Wiel, K., Sebastian, A., Singh, R., Arrighi, J., Otto, F., … Cullen, H. (2017). Attribution of extreme rainfall from hurricane Harvey, August 2017. *Environmental Research Letters*, *12*(12). https://doi.org/10.1088/1748-9326/aa9ef2

Van Ormondt, M. (2017). *Hurricane Harvey: Surge and flood modelling*. Delft.

Wagenaar, D. (2018). Flood Impact Modelling. Delft: Deltares.

Wahl, T., & Jain, S. (2015, July 27). Flood severity along US coastline has worsened. *The Conversation*. Retrieved from http://theconversation.com/flood-severity-along-us-coastline-has-worsened-45208

Wahl, T., Jain, S., Bender, J., Meyers, S. D., & Luther, M. E. (2015). Increasing risk of compound flooding from storm surge and rainfall for major US cities. *Nature Climate Change*. https://doi.org/10.1038/nclimate2736

Walsh Williams, M. (2017). A Broke, and Broken, Flood Insurance Program - The New York Times. *New York Times*. Retrieved from https://www.nytimes.com/2017/11/04/business/a-broke-and-broken-flood-insurance-program.html?hp&action=click&pgtype=Homepage&clickSource=story-heading&module=second-column-region&region=top-news&WT.nav=top-news

Weather Underground. (2018). Hurricane Harvey - Storm activity. Retrieved May 28, 2018, from https://www.wunderground.com/hurricane/atlantic/2017/hurricane-harvey?map=history

Winsemius, H. C., Aerts, J. C. J. H., Van Beek, L. P. H., Bierkens, M. F. P., Bouwman, A., Jongman, B., …

Ward, P. J. (2016). Global drivers of future river flood risk. *Nature Climate Change*, *6*(4), 381–385. https://doi.org/10.1038/nclimate2893

Zheng, F., Westra, S., & Sisson, S. A. (2013). Quantifying the dependence between extreme rainfall and storm surge in the coastal zone. *Journal of Hydrology*, *505*, 172–187. https://doi.org/10.1016/j.jhydrol.2013.09.054

Zheng, L., Weisberg, R. H., Huang, Y., Luettich, R. A., Westerink, J. J., Kerr, P. C., … Akli, L. (2013). Implications from the comparisons between two- and three-dimensional model simulations of the Hurricane Ike storm surge. *Journal of Geophysical Research: Oceans*, *118*(7), 3350–3369. https://doi.org/10.1002/jgrc.20248

9 Appendix A

9.1. SFINCS Model

The **S**uper **F**ast **I**nundation of **C**oast**S** (SFINCS) was a model developed initially by Maarten van Ormondt (Deltares) to model coastal floodplain inundation via shallow water flow phenomena in the near shore region of dissipative coastal environments (Van Engelen, 2016).

SFINCS was designed as an efficient inundation two-dimensional (2-D) storage inundation model which was based on the research developed by Bates et. al., (2010) on the LISFLOOD-FP model. The model efficiency comes from a series of justified simplifications made to the different solved processes within it (Leijnse, 2018). On its current version, SFINCS solves both the processes of the swash zone[8] and the land onshore region making it a powerful tool not only for EWS (due to its computational speed) during TC activity, but also as a tool to run probabilistic scenarios in order to analyze the effect of compound flooding in coastal watersheds.

SFINCS uses a decoupled system of quasi-linearized momentum equations derived from shallow-water theory (equation 9.1.2 and 9.1.3) in combination with a global continuity equation (equation 9.1.1) that links flow in both directions. This process-based hydrodynamics shallow water model does not account for morphodynamic phenomena, but it does include the effects of inertia, bottom friction and pressure gradients. The model is simplified for instance by parametrizing the surf zone or by excluding the viscosity effects. In addition, depending on the case analyzed[9], advection can be neglected as well.

SFNICS allows for dynamic simulation of coastal flooding at large spatial scales with very low computational effort when compared with other 2-D models making it an attractive tool, especially for ensemble coastal flooding forecasting purposes and quick hazard assessments (Leijnse, 2018). The model was originally built using the FORTRAN 90 programing language and recent changes have been implemented by Van Engelen (2016) and Leijnse (2018) to include a SFINCS setup script using Matlab© (Version R2016b).

The governing partial differential equations (based on mass and momentum conservation) in which SFNICS is based (neglecting the advection, Coriolis and viscosity terms and using linearized terms) are presented below:

$$\frac{\partial \zeta}{\partial t} + \frac{\partial q_x}{\partial x} + \frac{\partial q_y}{\partial y} = 0 \qquad \textbf{(9.1.1)}$$

$$\frac{\delta q_x}{\delta t} + gh\frac{\delta \zeta}{\delta x} + \frac{gn^2 {q_x}^2}{h^{7/3}} = 0 \qquad \textbf{(9.1.2)}$$

$$\frac{\delta q_y}{\delta t} + gh\frac{\delta \zeta}{\delta y} + \frac{gn^2 {q_y}^2}{h^{7/3}} = 0 \qquad \textbf{(9.1.3)}$$

8 The Swash zone referrers to the area in which the waves reach the coast and cause the waterline to vary in time (Leijnse, 2018)

9 In cases in which super-critical flow doesn't occur or when wave-driven flooding doesn't need to be taken into account (Leijnse, 2018)

Where ζ is the free surface elevation with respect to the reference level z=0 as seen in Figure 134, h is the water depth ($\zeta + d$), q_x and q_y are the fluxes per unit width [m^2/s] in *x*-*y* direction, n is the manning roughness coefficient [s/m$^{1/3}$] and g is the earths gravitational acceleration constant

The two last equations presented above are the result of neglecting the advection, coriolis and viscosity terms on the 1-D momentum SWE and the first equation is derived from the mass conservation principle The combination of the three equations results in a decoupled system (with ζ, q_x and q_y as unknowns) which solves the flux in *x* or *y* direction separately.

The first term on equations 9.1.2 and 9.1.3 represent the local acceleration in x or y direction, the second term denotes the water level gradient and the third term represent the effect of bottom friction. In this equations the surface elevation (ζ) replaced the water depth (h) since the bottom level is constant in time (no morphology is considered) (Leijnse, 2018)

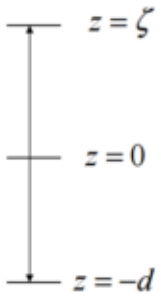

Figure 134. Free surface height and bed level w.r.t a vertical reference level (z). Source:(Van Engelen, 2016)

9.1.1 Numerical implementation

SFINCS uses a staggered equidistant rectilinear grid in Cartesian coordinates (*m, n*) in which the free-surface elevation and bed level are defined in the cell center, which provides an advantage for the implementation of boundary conditions (Van Engelen, 2016).In this system the flow velocities (*u, v*), flow depths (*h*) and fluxes (*q*) are defined on the cell edges as depicted in Figure 135, which implies an interpolation of water and bed levels to the cell edges for the computations of the flow depth difference between two adjacent cells (Leijnse, 2018)

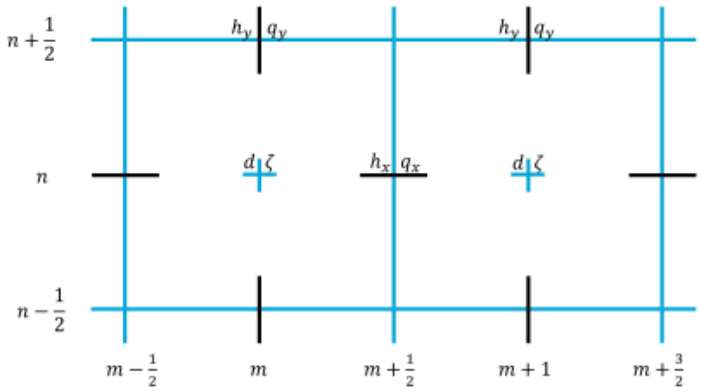

Figure 135. Staggered computation grid in SFINCS. Source: (Leijnse, 2018)

As it was mentioned before, the water depth is needed at all cell edges, reason why the first step of the model is to compute this by means of equation 9.1.4 (showed only for *x* direction, but *y* direction has similar structure) which is based on the implementation in the Delft3D-FLOW model and which calculates the depth based on the mean values of the adjacent cells.

$$h^{t-\Delta t}_{x,m+\frac{1}{2},n} = \frac{\zeta^{t-\Delta t}_{m,n} + \zeta^{t-\Delta t}_{m+1,n}}{2} - \frac{d^{t-\Delta t}_{m,n} + d^{t-\Delta t}_{m+1,n}}{2} \qquad \textbf{(9.1.4)}$$

After water depths have been defined at all cell edges, the momentum fluxes are computed by means of discretising equation 9.1.1 using a first order explicit time-stepping with a first order backward finite

difference approximation of the spatial derivative (FTBS- Scheme[10]) (see equation 9.1.5). In addition, equations 9.1.2 and 9.1.3 are also discretized (see equations 9.1.6 and 9.1.7), but this time using the methodology proposed by Bates et al. (2010) in order to improve the stability of the numerical solution (Van Engelen, 2016).

$$\zeta^{t}_{m,n} = \zeta^{t-\Delta t}_{m,n} - \Delta t \left[\frac{\left(q^{t}_{x,m+\frac{1}{2},n} - q^{t}_{x,m-\frac{1}{2},n} \right)}{\Delta x} + \frac{\left(q^{t}_{y,m,n+\frac{1}{2}} - q^{t}_{y,m,n-\frac{1}{2}} \right)}{\Delta y} \right] \tag{9.1.5}$$

$$q^{t}_{x,m+\frac{1}{2},n} = \frac{\overbrace{\left[\theta \cdot q^{t-\Delta t}_{x,m+\frac{1}{2},n} + (1-\theta) \cdot \frac{q^{t-\Delta t}_{x,m+\frac{3}{2},n} + q^{t-\Delta t}_{x,m-\frac{1}{2},n}}{2} \right]}^{A} - \Delta t \cdot g \cdot h^{t-\Delta t}_{x,m+\frac{1}{2},n} \left[\frac{\zeta^{t-\Delta t}_{m+1,n} - \zeta^{t-\Delta t}_{m,n}}{\Delta x} \right] + \tau^{t}_{x,m+\frac{1}{2},n} \cdot \Delta t - adv_{x} \cdot \Delta t}{1 + \Delta t \cdot g \cdot n^{2} \left[\frac{\left| q^{t-\Delta t}_{x,m+\frac{1}{2},n} \right|}{\left(h^{t-\Delta t}_{x,m+\frac{1}{2},n} \right)^{7/3}} \right]} \tag{9.1.6}$$

$$q^{t}_{y,m,n+\frac{1}{2}} = \frac{\overbrace{\left[\theta \cdot q^{t-\Delta t}_{y,m,n+\frac{1}{2}} + (1-\theta) \cdot \frac{q^{t-\Delta t}_{x,m,n+\frac{3}{2}} + q^{t-\Delta t}_{y,m,n-\frac{1}{2}}}{2} \right]}^{B} - \Delta t \cdot g \cdot h^{t-\Delta t}_{y,m,n+\frac{1}{2}} \left[\frac{\zeta^{t-\Delta t}_{m,n+1} - \zeta^{t-\Delta t}_{m,n}}{\Delta y} \right] + \tau^{t}_{y,m,n+\frac{1}{2}} \cdot \Delta t - adv_{y} \cdot \Delta t}{1 + \Delta t \cdot g \cdot n^{2} \left[\frac{\left| q^{t-\Delta t}_{y,m,n+\frac{1}{2}} \right|}{\left(h^{t-\Delta t}_{y,m,n+\frac{1}{2}} \right)^{7/3}} \right]} \tag{9.1.7}$$

In equations 9.1.6 and 9.1.7 the water level gradient is computed using a 1st order forward difference approximation, and the fluxes (q_x and q_y) in the next time step (*t*) are estimated using a weighted average of the previous time step ($t - \Delta t$) and the average of fluxes in the adjacent cells as it can be seen in the expression of A and B on equations 9.1.6 and 9.1.7. This averaging process smoothen the solution and limits the possible instabilities. In the previous equations, *m* and *n* are the grid indexes in Cartesian *x*- and *y*-direction, θ represents a weighting factor that should be near to 1 to allow a smoother solution (in SFNICS the default value is set to 0.9), $\tau^{t}_{x,m+\frac{1}{2},n}$ and $\tau^{t}_{y,m,n+\frac{1}{2}}$ represent the wind stresses in both directions acting on the water and an advection term ($adv_{(x\_or\_y)}$) is added when this is specified by the user (using the 1D or 2D version of SFINCS SSWE). It is important to mention that the advection term and the momentum fluxes are only updated if the water depth surpasses certain threshold value which is set as $h_{u,tresh} = 0.05m$. The previous criteria act as a flooding and drying mechanism (Leijnse, 2018).

The discretized equations presented above allow a separate computation of mass fluxes in both directions at each time step, which is later used in the 2-D depth averaged continuity equation for the

10 The Forward in Time, Backward in Space (FTBS) scheme is a finite difference method used traditionally to solve parabolic partial differential equations. It is in general a 1st order accurate in both space time and space (Haverkort, 2009)

computation of the updated water levels which are computed using equation 9.1.5 (Van Engelen, 2016). In case additional processes like precipitation, discharge or infiltration are specified (see Section 9.1.3), the changes on water level are added immediately after the momentum equations but before the continuity equation (Leijnse, 2018).

The model in addition uses an adaptive time-step that helps in the convergence and stability of the solution since the CFL[11] condition on its own is not enough to achieve this goal. This adaptive step was proposed by Bates et al. (2010) as follows:

$$\Delta t < \alpha \cdot \frac{\Delta x}{\sqrt{g h_{\max}}} \qquad \textbf{(9.1.8)}$$

Where α is a heuristic reduction factor that depends on the grid size and takes values between 0.1 and 0.75 (being 0.75 the default value), $h_{\max}$ is the maximum value of the water depth in the computational domain at that time-step, implying that the largest water depth dictates the time-step (Van Engelen, 2016). This means that in order for the solution to be stable, smaller grid sizes require smaller time steps.

9.1.2 Wave relevant processes

As in this specific research, SFINCS is not going to be used to model flooding due to wave relevant processes and instead the model is going to be forced either with water level observations at certain tide gauge locations or with the synthetic data at the outlet of the catchment, the waves relevant processes included in SFINCS are not going to be explained in detail in this appendix, but for further details the reader is referred to Leijnse (2018).

As general background on the wave-related processes included in SFINCS is important to mention that in this model the swash zone is modelled by forcing the system at an offshore boundary (set at 2m water depth (Van Engelen, 2016) since at this depth most of the incident wave energy is dissipated). At this point the system is forced with an incoming wave velocity u_b using a weakly reflective generating-absorbing boundary condition (see Figure 136 and equation 9.1.10)

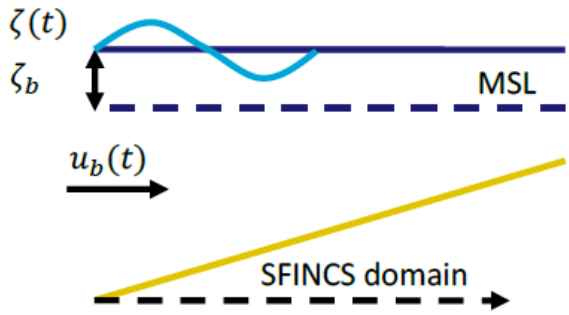

Figure 136. SFINCS wave-related processes forcing. Source: (Leijnse, 2018).

$$u_b(t) = 2u^+ - \sqrt{\frac{g}{h(t)}}\zeta(t) + \bar{u} \qquad \textbf{(9.1.10)}$$

For the boundary conditions on the rectangular grid used in SFINCS for both one- and two-dimensional simulations, the weakly reflective boundary condition (equation 9.1.10) is applied along all four boundaries of the rectangular grid. In this equation, u_b is the velocity at the boundary, u^+ is the velocity associated with the incoming wave components w.r.t the mean current and $\bar{u}$ is the flow velocity due to residual currents. The formula is derived from Linear wave theory and detailed description on the numerical

11 The Courant-Friedrichs Lewy (CFL) condition was implicitly applied in the FTBS- Scheme to allow convergence in the solution of the partial differential equations (PDE). This condition states that in order for the solution of a hyperbolic PDE to converge (using a finite difference method), the numerical domain of dependence has to contain the mathematical domain of dependence. Source: (MIT, 2018)

implementation on SFINCS can be found on chapter 4 of Van Engelen (2016) as well as wave related processes included in the model such as the inclusion of Infra-gravity waves[12], short waves, wave-induced setup, run-up, swash and overtopping (see chapter 2 and 3 of Leijnse (2018)).

9.1.3 Inclusion of relevant processes for compound flooding

As stated before, SFINCS was created initially with the aim of modelling coastal flooding in dissipative coastal environments. Nevertheless, due to its accuracy and low computational coasts, the model has been expanded to include certain processes and improve its flexibility in order to be able to use it in broader applications. One of these applications is to model compound flooding due to TCs in coastal watersheds, reason why the use and validation of the SFNICS model in this type of case studies is highly valuable. For this specific application, wind forcing, precipitation, infiltration and discharge points where added to the model. This was done through the common spider web formulation, corresponding with the functionality of the TC-Toolbox (Gomes, Pinho, Antunes do Carmo, & Santos, 2015), in which the frame of reference is not static , but it moves with the eye of the TC (Leijnse, 2018). In addition new updates to the model include the option of using a normal Cartesian grid to include spatially distributed rainfall over an area.

9.1.3.1 Wind-induced setup

$$\tau^{t}_{x,m+\frac{1}{2},\mathrm{n}} = C_d \cdot \rho_a \cdot u^2_{wind} \qquad \textbf{(9.1.11)}$$

SFINCS originally included wind input which could be included in the spiderweb-file implementation. However, recent updates included the option to add a spatially uniform wind forcing and an improvement of the definition of the drag force coefficient which is in agreement with the specification used in Delft3D. This adjustment included a threshold level for which the drag force coefficient (C_d) increased linearly if the value is below the threshold (25 *m/s*), and which decreases after the threshold is exceeded until it becomes constant after a value of 50m/s is reached (Leijnse, 2018). The wind forcing term is included in the momentum equations (9.1.6 and 9.1.7)

9.1.3.2 Precipitation

The precipitation in SFINCS is included by adding the water level per grid cell due to rainfall before the continuity equation as in can be seen below.

$$\zeta^{t}_{m,n} = \zeta^{t-\Delta t}_{m,n} + w^{t}_{prec} \cdot \Delta t \qquad \textbf{(9.1.12)}$$

The rainfall (w^{t}_{prec}) is specified in the input as *mm/hour*, which is converted afterwards to *m/s.* The rain input included in SFINCS can be spatially varying (using the common spiderweb approach or the spatial Cartesian grid) or can be set as uniformly distributed giving the model high flexibility and making it more adequate for compound flooding than 1-D models which only include uniformly distributed precipitation. The input is always time-varying as well (Leijnse, 2018).

9.1.3.3 Infiltration

The infiltration in SFINCS is included by changing the water level per grid cell due to infiltration before the continuity equation as in can be seen below.

$$if \quad \zeta^{t-\Delta t}_{m,n} - d_{m,n} > h_{u,tresh} : \zeta^{t}_{m,n} = \zeta^{t-\Delta t}_{m,n} + q^{t}_{\mathrm{inf}} \cdot \Delta t \qquad \textbf{(9.1.13)}$$

12 Waves with a lower frequency (Period between 30 seconds to 5 minutes) than those of wind-generated surface gravity waves. This waves have been proven to be dominant in the swash motion in dissipative beaches with a cut-off Irribaren number of ξ=0.3, making them important for modeling coastal flooding in those environments.(Van Engelen, 2016)

The infiltration rate ($q^t_{\inf}$) should be specified in m^3/s and using a negative value to allow the immediate infiltration water out of the model. In the case of SFNICS a limiter value is applied (threshold of $h_{u,tresh} = 0.05m$) in order to only allow infiltration in there is a minimum water depth value in the velocity points (Leijnse, 2018). The infiltration is included as a spatially uniform rate, which is not the optimum case when different soil types are found in an area and there is a constant change between urban and non-urban landscapes. In the case of the Galveston bay, this is not the case since the vast majority of the soils consist in clayish soils with very low infiltration capacity that can resemble in certain way to an almost impermeable surface.

9.1.3.4 Discharge points

The discharge points in SFINCS are implemented as follows:

$$\zeta^t_{m,n} = \zeta^{t-\Delta t}_{m,n} + \frac{q^t_{src} \cdot \Delta t}{\Delta x \cdot \Delta y} \qquad \textbf{(9.1.14)}$$

In this equation, a source point affects one cell by increasing the water level accordingly for every time-step. This step is done before the update of the water level by the continuity equation. This discharge points can be used to simulate river discharges and can be also used to model tributaries along a main stream.

9.1.4 Model Limitations

SFINCS has some limitations due to the theoretical basis under which it is constructed. As explained before, the model was based on a simplified case of the SWE, and this means that that the assumption of having hydrostatic pressure and negligible vertical variations of the horizontal flow are taken as true, which is valid in very shallow water in the case of short incident waves.

In addition, as mentioned before, the advective transport of momentum was neglected which is acceptable for flood waves in low land rivers with slow changes, since both the local and advective inertia terms are very small when compared to the resistance term. Nevertheless, the same assumptions is not valid for rapidly responding rivers (e.g. small catchment area, steep slopes) or for super-imposed wave phenomena (e.g. translatory waves) in which this term becomes more important and therefore the initial SFINCS assumption is no longer valid and the version of SFINCS SSWE is recommended instead. In the case of short incident waves the advective transport of momentum is important and this effect can only be taken into account if the version of SFINCS SSWE is used. Therefore one can say that the initial model is more suitable for waves with longer periods and larger wave length (such as infragravity waves, coastal tides or propagating tides in channels, etc.). In the case of flood waves, the advective acceleration term does play a role at a local scale (e.g. in locations where there is an abrupt change in elevation, etc.), however, when the entire scale of the flood wave is observed those local acceleration features can still be neglected even though they contribute to friction and energy loss.

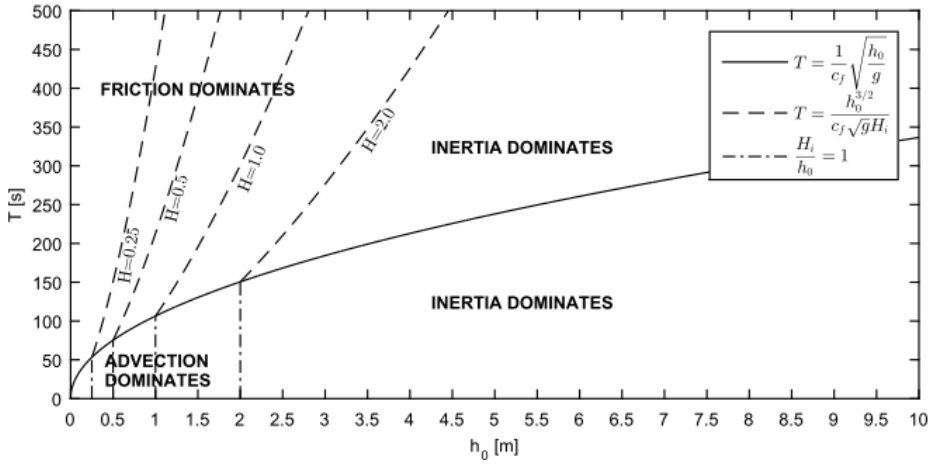

Figure 137. Dominant term in the 1-D depth averaged momentum equation for linear shallow- water waves. Source: (Van Engelen, 2016)

In Figure 137 it can be seen for different combinations of water depth (h_o), Wave Period (T) and Wave Height (H), the dominance of each term. It can be seen that for smaller water depths and short wave periods, advection is the dominant term, while for any other case the local inertia or the friction are the dominant processes.

Another limitation of the SFINCS model is that all the viscosity terms are neglected, meaning that there is not loss of momentum due to horizontal gradients in the velocity and the associated turbulent motions. In SFINCS the flow is coupled only through the 2-D mass balance. In addition, as the effect of short waves is being left out of the analysis, this means that SFNICS does not include any short-wave forcing terms (e.g. radiation stress gradients) which are responsible for the set-up and set-down of the mean water level and also can drive mean currents in cross-shore and along-shore direction.

In addition the Coriolis effect is also neglected in SFINCs since this model is only used for the nearshore region and as an inland model so at this scale indeed neglecting the Coriolis Effect is a good approach. In case large scale flows are going to be modelled before the coast and during a TC event, Coriolis should be included Leijnse (2018).

All the aforementioned limitations due to general assumptions made on the underlying equations of the model, have also an advantage in the fact that they all simplify the equations in a way that the computational time is significantly reduced. This is an advantage when the accuracy of the model is not compromised when compared to more advanced models which include all coastal and inland hydrological processes (D-flow FM, Delft 3D). Therefore it seems that for modelling coastal flooding triggered by tropical cyclones, SFINCS is a good alternative since the general assumptions can be valid under this framework and is a step forward from the 1-D only inland flooding, but is less complex than a 2-D or 3-D Coastal model. This can be seen in the comparison made between models carried out by Leijnse (2018) and presented in Table 15 of the appendices of this report.

9.1.5 SFINCS model Set-up - Harvey and Ike in the Clear Creek watershed

This section includes more information regarding the model setup of the Clear Creek watershed study case. The majority of the information included in this section also applies for the model configuration using the boundary conditions established for the compound flooding analysis (See chapter 4 and chapter 5).

9.1.5.1 Topography and Bathymetry details

In order to set-up SFINCS, the first thing that should be addressed is the size of the grid of the model. This grid is partially dependent on the resolution of the DEM/DTM of the area since the grid itself cannot be smaller than the resolution of the topography raster. For this research, the resolution used for the DEM was of 10m as described below, reason why this was the minimum size that the grid of the SFINCS model could have. Since this resolution is very high and it was intended that the model could run fast, the grid size selected was of 50m x 50m. The grid was created using the Delft Dashboard (Deltares, 2018b) which is a standalone Matlab-based graphical user interface developed by Deltares.

In the particular case of the Clear Creek watershed, the Geo Spatial Data Gateway of the USDA was used (USDA, 2018a) to acquire the National Elevation Dataset (NED) developed by the USGS at 10m resolution which uses as vertical datum the NAVD88 and as horizontal datum the World Geodetic system - WGS84 (see Figure 138). The NED found for this region in Texas didn't include information about bottom depths, especially those located within the Galveston Bay, therefore, an additional dataset was needed that included bathymetry information. This dataset was found in the National Centers for Environmental Information (NCEI & NOAA) (2018) and it included a high-resolution (10m) coastal DEM for Galveston, Texas, which integrates both bathymetric and topographic DEMS of the area and it uses as vertical reference the tidal datum of Mean High Water (MHW) and horizontal datum WGS84 (see Figure 138). As it can be seen from Figure 138 and Figure 139, the datasets do not share the same extent, reason why a combination of both DEM's was needed in order to get a final file (see Figure 140) that could be used by SFINCS with the appropriate information. This was done by transforming both datasets to a common reference vertical datum which was set as the Mean Sea Level (MSL) since the tidal gauge information at Morgan's and Eagle point used the same reference level.

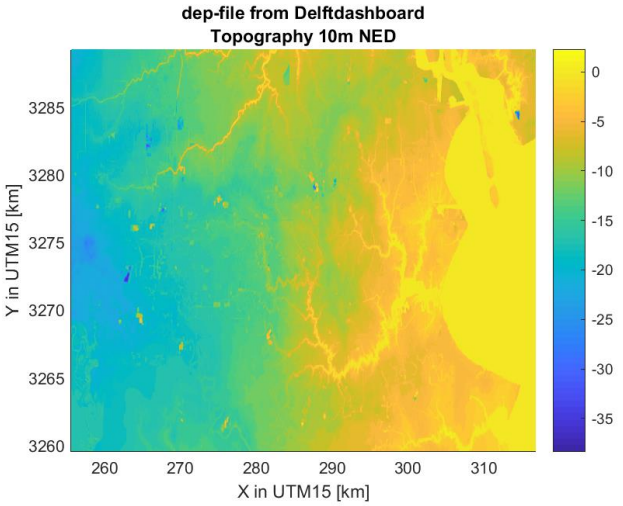

Figure 138.dep file showing the topography of the Clear Creek watershed. Based on the National Elevation Dataset with 10m of resolution and interpolated into the computational grid of SFINCS

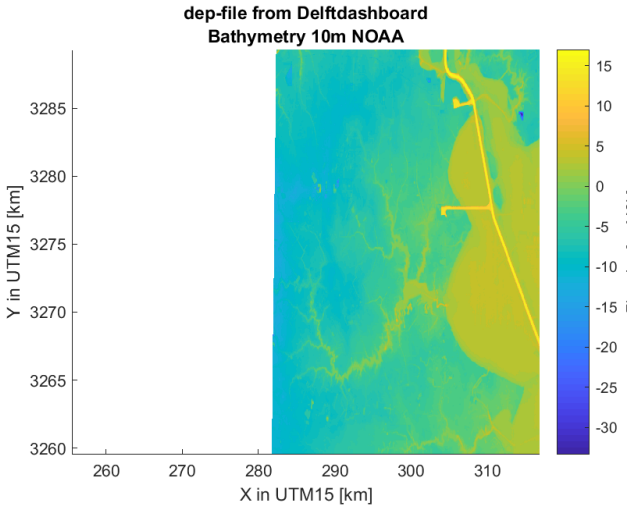

Figure 139.dep file showing the Bathymetry of the West Galveston Bay. Based on NOAA's Coastal DEM with 10m of resolution and interpolated into the computational grid of SFINCS

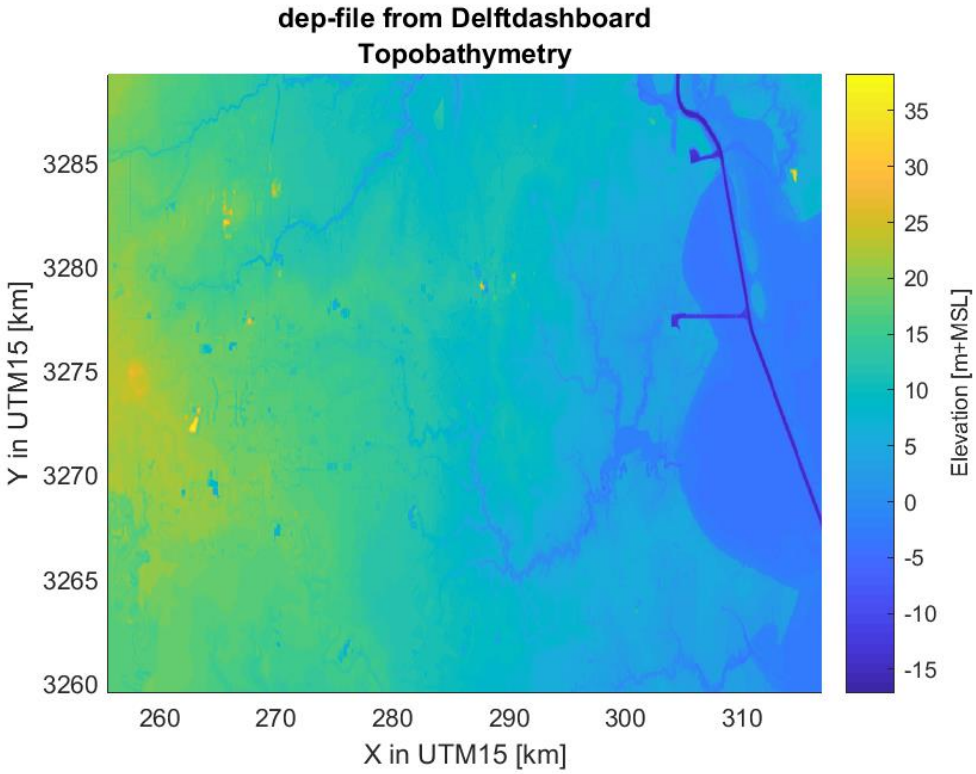

Figure 140. Final elevation details of the Clear Creek watershed.

Once the correct elevation file is obtained, a mask file (see Figure 141) is generated by delineating a polygon (created in Delft Dashboard) which aim is to exclude from the computation all points that are not necessary in the model (See blue region on Figure 141). In this particular case as the Galveston Bay was not going to be modelled, all points in this region were neglected (see Figure 142) since the water levels as mentioned before, are going to be forced at the location of the tidal gauges (see Figure 142). In addition, is possible to set some observation points in SFINCS which are locations within the model for which the variations in water level (or other hydraulic parameter) during the whole duration of the simulation can be recorded and written out in the output of the model. This tool is useful since it allows the user for example, to

compare the model results with observed water levels registered on precipitation or stream measurement gauges and it can serve as a validation mechanism. In Figure 143 some observation points are shown just as an example, but this observation points will vary in each case according to the available dataset. For both the cases of Ike and Harvey, the validation is going to be performed based on High Water Marks registered throughout the storm by the USGS or by FEMA.

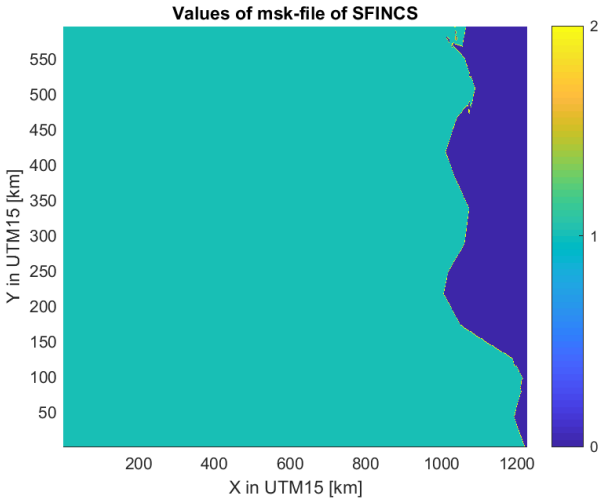

Figure 141. Mask file of SFINCs for the Clear Creek watershed.

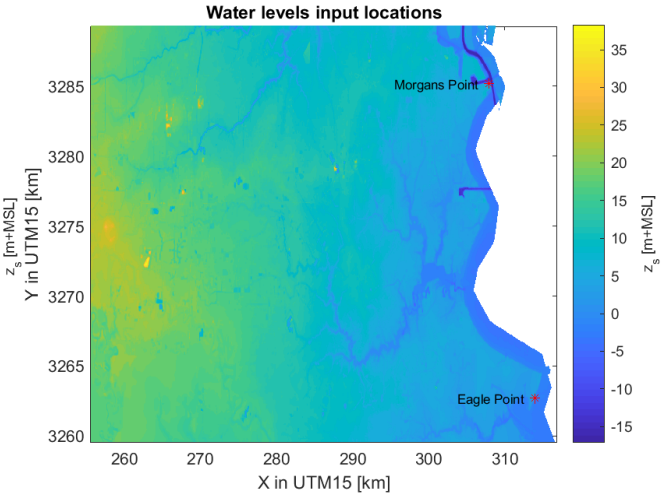

Figure 142.Water level forcing locations for the SFINCS model of the Clear Creek watershed

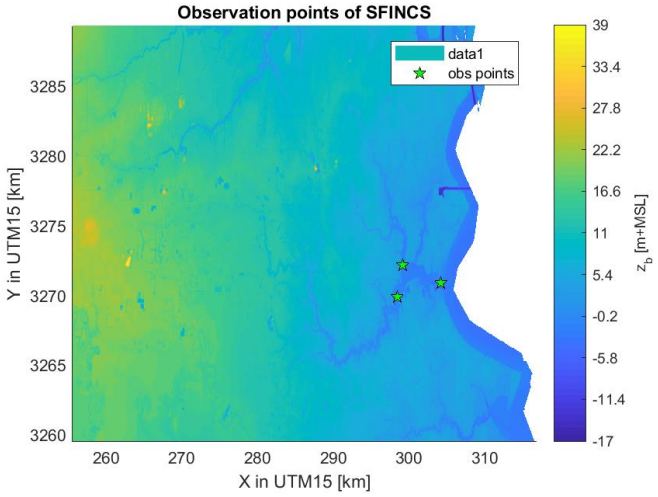

Figure 143. Observation points locations for the SFINCS model of the Clear Creek watershed

9.1.5.2 Manning roughness coefficient

Until the last version of SFINCS, the manning roughness coefficient can be included in two ways: either assigning a spatially uniform value or assigning a varying value that change with depth. For this specific setup, the second option was chosen by selecting two manning values, one for the land and another for the sea or open water. The value will change from one another depending on a threshold level that determines when the model is “dry” or “wet”.

For the constant manning coefficient for land, a value of 0.0678 $s/m^{1/3}$ was chosen that corresponds to the description of the National Land Cover Dataset (NLCD) of the U.S to the class known as “Developed - medium Intensity” which is described as an area with a mixture of constructed material and vegetation and for which the impervious surfaces account for 50 till 79% of the total surface. This value was extracted from a

study performed by Kalyanapu et. al. (2009) for which some manning values where determined for the Greens Bayou; a watershed located on the north side of Houston.

According to Zheng et al. (2013) coastal waters (continental shelves and estuaries) have manning coefficients that vary with a range of 0.02 to 0.045 $s/m^{1/3}$. This range agrees also with the values found by Kalyanapu et al. (2009) from the NLCD in the Greens Bayou and also with a general value used by Leijnse (2018) in the SFINCS model for a case study in Jacksonville, Florida, for which a manning coefficient of 0.024 $s/m^{1/3}$ was assigned to what was considered as water nearby the coast, and therefore the same value is going to be adopted for the case of the Clear Creek SFINCS model. In Figure 144 the initial manning coefficients of the SFINCS model are presented where:

$$n = 0.0678_{s/m^{1/3}} \rightarrow if \;\; bed \;\; level > 0m + MSL$$

$$n = 0.024_{s/m^{1/3}} \rightarrow if \;\; bed \;\; level < 0m + MSL$$

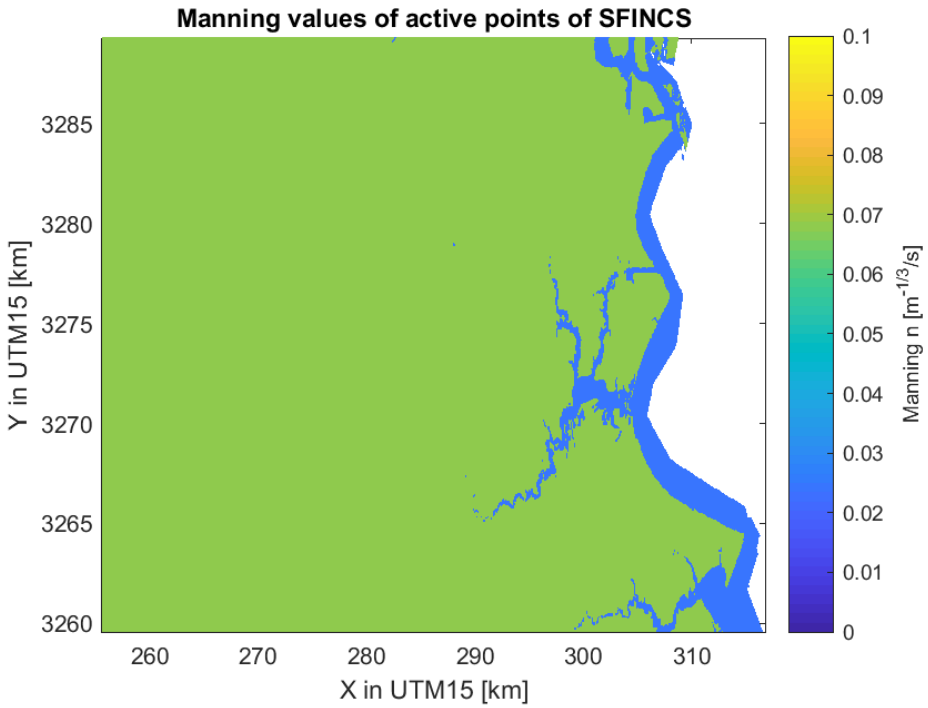

Figure 144. Manning values of active cells in SFINCS model for the Clear Creek watershed

9.1.5.3 General SFINCS configuration for the Clear Creek watershed

Detailed model:

- SFINCS LIE
- Shore forcing: Water levels from Morgan's and Eagle Point tide stations.
- Precipitation: spatially distributed using rectangular grid and resolution of each storm (Harvey and Ike details on chapter 3)
- Wind: Not account for
- Infiltration: 1 mm/h
- Bathymetry: NED+NOAA's DEM of the Clear Creek region
- Grid: equidistant, 50 x 50 m, 1226 x 596 cells, hereby the offshore point lower than 2m with respect to MSL are not used. Number of active cells 645918.
- Roughness: depth varying manning

$$n = 0.0678_{s/m^{1/3}} \rightarrow if \;\; bed \;\; level > 0m + MSL$$

$$n = 0.024_{s/m^{1/3}} \rightarrow if \;\; bed \;\; level < 0m + MSL$$

- Numerical settings: $h_{u,tresh} = 0.05m - or - 0.025m$ (Calibration tool), $\theta = 0.9, \alpha = 0.75$

9.1.6 SFINCS model – Case studies

Regarding compound flooding, SFINCS has been used (apart from this particular research) recently in 2 study cases. The first one, an additional case study regarding hurricane Harvey surge and flood modelling, and the second case: flooding due to hurricane Irma at Jacksonville, Florida.

9.1.6.1 Hurricane Harvey – Surge and flood modelling

This case was developed by Maarten van Ormondt (Deltares) in order to quickly assess the extent of flooding due to hurricane Harvey (Harvey made landfall on Texas in the 25th of August 2017 and the assessment was carried out on the 30th of August). The model was build using as an input the storm surge obtained from a Delft 3D model already built for the region (Matagorda/ San Antonio Bay/Corpus Christi and Galveston Bay~500*m* resolution model), and SFINCS was directly used for computing the inland flooding. The model was forced with a parametric wind model based on the National Hurricane Center best track data (USGS, 2016). The SFINCS model covered the Texas southeast region based on topography details extracted from the USGS NED dataset (USGS, 2015), the grid spacing uses was of 200m (~3.2 million points) and the model took 15 minutes to run 5 cumulative days in a regular desktop laptop. The model was used to observe the effect of rain and wind forcing on the extent of flooding in the region affected by Harvey. In this case SFINCS was used as a large scale flooding modeling tool, and some of the results of the simulation can be observed throughout Figure 145 to Figure 148.

From this model some conclusions were drawn for the area, which stated that for the Harvey Study case, flooding around Galveston Bay was mostly a result of storm surge. Nonetheless, for the region of Houston the flooding was dominated by rainfall in the region, having in mind that wind and storm surge also played a key role on the inundation event since the surge at the Bay reduced the run-off of flooded areas in the city, while wind increased the areas that experienced flooding since water was being further pushed on land. The speed of the model itself proves that SFINCS could be a meaningful tool to quickly asses flood hazards and the effect of different processes as it was shown in the previous figures.

Due to the fact that the model was based on coarse data (Low resolution) to be able to quickly asses flood hazard in a large area, the results could be always improved if the resolution is increased and the input of the rainfall data is better characterized (at the time of assessment only 5 days have passed since Harvey made landfall, not giving enough time to obtain high quality rainfall data). This of course will increase the computational time but this will be compensated by the increased accuracy of the model.

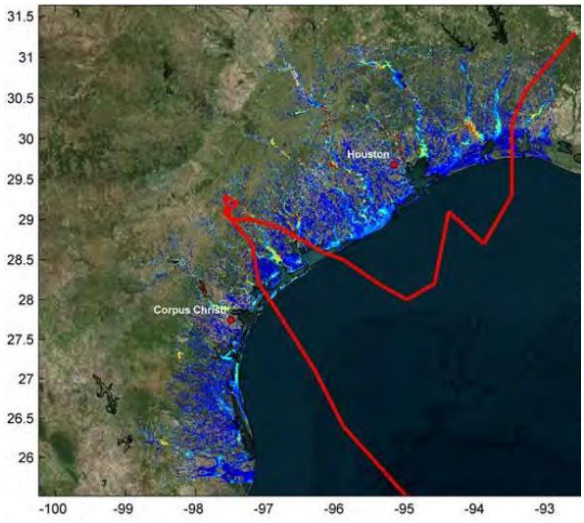

Figure 145. Maximum wave height due to inland and coastal flooding- Large scale flooding. Source: (Van Ormondt, 2017)

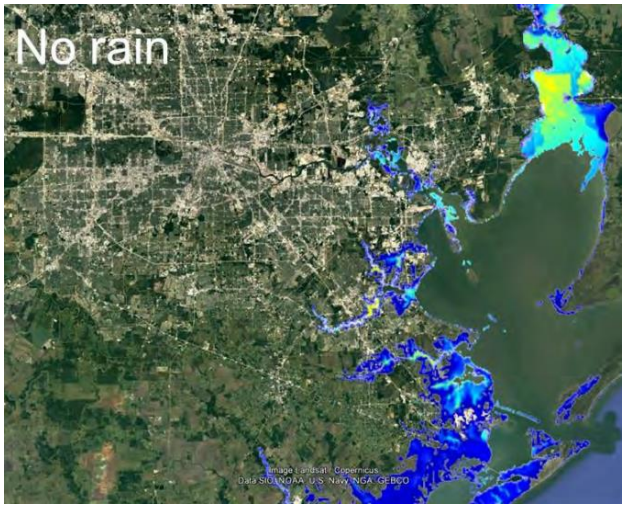

Figure 146. Flood extent due to hurricane Harvey without rainfall in the model (only surge). Source: (Van Ormondt, 2017)

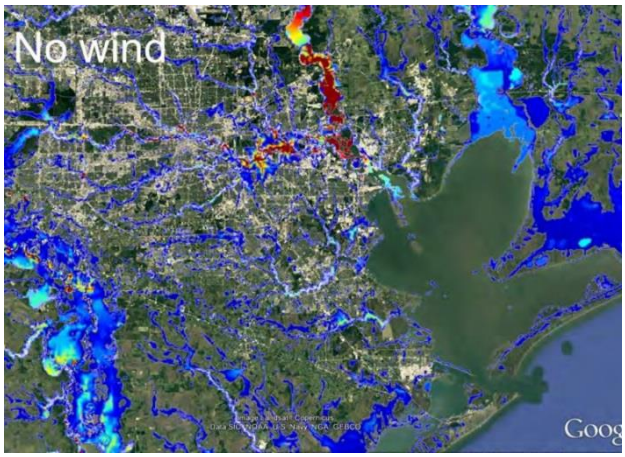

Figure 147. Flood extent due to hurricane Harvey without wind input in the model (rain and surge). Source: (Van Ormondt, 2017)

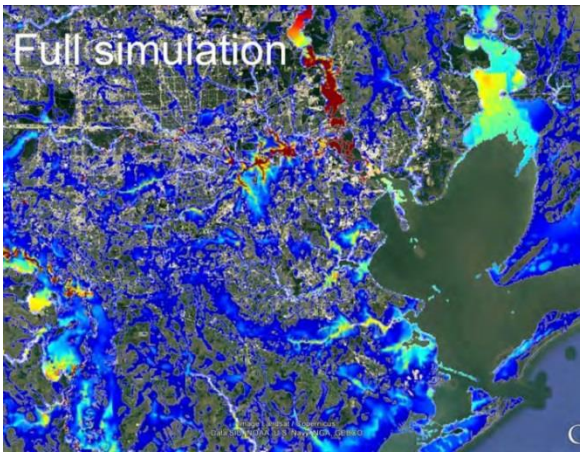

Figure 148. Flood extent due to hurricane Harvey when rain and wind are considered in the model Source: (Van Ormondt, 2017)

9.1.6.2 Hurricane Irma at Jacksonville, Florida.

Hurricane Irma made landfall in South Florida in September 2017. 400 miles north from Irma's first landfall, the city of Jacksonville suffered a huge flooding event due to a combination of surge, heavy precipitation and wind-induced setup. This study case was analyzed by Leijnse (2018) and it used SFINCS as the inundation modeling tool to analyze the compound flooding in the area (refer to chapter 5 Leijnse (2018)).

The main objective of this study case was to assess if a semi-advanced model is able to reproduce the compound flooding at Jacksonville as well as an advances model. In this case the advance model was Delft3D-Flow. The final results are presented in Figure 149 and it was shown that SFINCS was able to reproduce all main hydrodynamic processes relevant for the case study but 2 orders of magnitude faster than the Delft3D-Flow model, the RMSD between models regarding maximum water levels was of only 0.06m. Moreover, it was seen that excluding advection, atmospheric pressure, Coriolis and viscosity terms was an appropriate choice since the model results didn't vary significantly. Finally, during this study case each flooding process was analyzed separately (see chapter 5 Leijnse (2018)) and it was concluded that only when all processes were combined (offshore water levels, rainfall and wind-driven setup) a good approximation of the flooding predictions was obtained, meaning that hurricane Irma indeed triggered compound flooding in the area

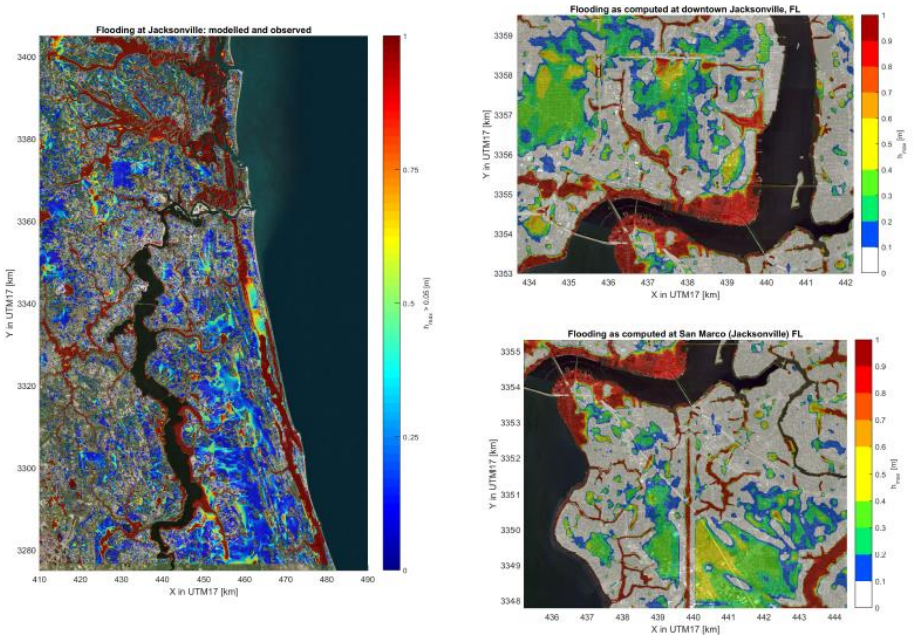

Figure 149. Maximum water depths at Jacksonville modeled with SFINCS. Source: (Leijnse, 2018)

9.1.6.3 Additional cases

In most of the other study cases, SFINCS has been used only to model coastal wave driven inundation, focusing mainly on dissipative coastal environments. This is the case for Flooding on the Philippines due to Typhoon Haiyan. This event caused tsunami-like waves generated by a surf beat over a coral reef (Leijnse, 2018) which impacted regions of the Philippines causing huge devastation and causalities in the area. SFINCS was also uses to simulated storm-driven coastal inundation at La Jolla shores along the coast of Southern California (Van Engelen, 2016). The results when compared to a calibrated Xbeach model gave satisfactory results for predicting the maximum flooding extent and overall flow depth, but showed some overestimation of the water levels and flow velocities for some storm scenarios. More details on both studies can be found on chapter 5 Leijnse (2018) and in chapter 8 of Van Engelen (2016).

A comparison between common models used in the industry was performed by Leijnse (2018) to summarize the functionalities of each model and compare their advantages and disadvantages depending on the relevant flooding processes included in each model. This information is summarized in Table 15 which compares static, semi-advanced (SFINCS) and advances models

Table 15. Model comparison for general offshore ,wave, flow and compound flooding related processes. Source: (Leijnse, 2018).

Model	General Characteristics		Offshore Processes			Wave processes					
	Dimensions	Grid Type	Parallelisation	Tropical Cyclones	Wave Generation	Storm Surge	Tides	Wave resolving	Shoaling Zone	Surf Zone	Swash Zone	Morphology
STATIC												
Bathtub	2D	no	no	no	no	no	no	no	no	no	no	no
SEMI-ADVANCED												
LFP	2DH	rectangular	OpenMP/no	no	no	no	no	no	no	no	no	no
SFINCS-LIE	2DH	rectilinear	OpenMP	no	no	input	input	only IG Waves (under research)	simple	simple	yes	no
SFINCS-SSWE	2DH	rectilinear	OpenMP	no	no	input	input	all (under research)	simple	simple	yes	no
3Di	1D/2D	Rectangular using quadtree and subgrids	Unknown, Cloud-based	no	no	no	no	no	no	no	no	no
ADVANCED												
ADCIRC	2DH/3D	unstructured	MPI/no	yes	yes (via SWAN)	yes	yes	yes	yes	yes	yes	no
Delft3D	2DH/3D	rectilinear/curvilinear/ unstructured	MPI/no	yes	yes (via SWAN)	yes	yes	no	yes	yes	no	sedtrans
FINEL2D	2DH	unstructured	yes, Type Unknown	no	yes (via SWAN)	yes	input	no	yes	yes	no	sedtrans
FINEL3D	3D	unstructured	yes, Type Unknown	yes	yes (via SWAN)	yes	input	no	yes	yes	no	no
Funwave	2DH	rectilinear	MPI/no	yes	yes	yes	input	all	yes	yes	yes	no
MIKE 21/3	2DH/3D	rectilinear/unstructured	GPU/MPI/OpenMP/ no	yes	yes	yes	yes	no/all	yes	yes	yes	sedtrans
SWASH	2DH/3D	rectilinear/curvilinear	MPI/no	yes	no	yes	input	all	yes	yes	yes	no
XBSB	2DH	rectilinear/curvilinear	MPI/no	no	no	input	input	only IG Waves	yes	yes	yes	sedtrans + avalanching
XBNH	2DH	rectilinear/curvilinear	MPI/no	no	no	input	input	all	yes	yes	yes	sedtrans
XBNH+	2 Layer 3D	rectilinear/curvilinear	MPI/no	no	no	input	input	all	yes	yes	yes	sedtrans

Model	Flow Processes					Other Processes			Wind-induced set-up
	Equations	Viscosity	Advection	Coriolis	Infiltration	Precipitation	River Discharge		
STATIC									
Bathtub	no	no	no	no	no	no	no		no
SEMI-ADVANCED									
LFP	LIE	no	no	no	no	no	yes		no
SFINCS-LIE	LIE	no	no	no	simple	yes	simple		yes
SFINCS-SSWE	SSWE	no	yes	no	simple	yes	simple		yes
3Di	SSWE	no	yes	no	yes	yes	yes		no
ADVANCED									
ADCIRC	SWE	yes	yes	yes	no	yes	yes		yes
Delft3D	SWE	yes	yes	yes	no	yes	yes		yes
FINEL2D	NHSWE	yes	yes	no	no	no	no		yes
FINEL3D	NS	yes	yes	yes	no	no	no		yes
Funwave	Boussinesq	yes	yes	yes	no	no	no		yes
MIKE 21/3	SWE/Boussinesq	yes	yes	yes	yes/simple	yes/simple	yes		yes
SWASH	NHSWE	yes	yes	yes	no	no	no		yes
XBSB	SWE	yes	yes	yes	no	no	yes		simple
XBNH	NHSWE	yes	yes	yes	yes	no	yes		simple
XBNH+	NHSWE	yes	yes	yes	yes	no	yes		simple

9 Appendix B

9.2. Probabilistic Analysis – Compound flooding conditions

In this section the details of the probabilistic analysis carried out for chapter 4 are presented. The probabilistic analysis of the synthetic data includes a fitting of the marginal distributions (Storm surge and precipitation) and a selection of the best copula describing the correlation between the variables of interest.

9.2.1 Fitting of Marginal distributions

As explained in chapter 4 only the distributions included on the Statistics and Machine Learning Toolbox of Matlab© (Version R2016b) were used to select the best fit to the data. The following sub-sections present the final results of the probabilistic analysis performed for the synthetic data set.

9.2.1.1 Storm Surge

The theoretical distributions tested for the storm surge data are the ones listed below.

- Exponential
- Generalized Extreme Value (GEV)
- Gamma
- Stable
- Extreme value
- Rayleigh
- t-location
- Normal
- Half-normal
- Kernel
- Logistic

The previous distributions were fitted to the data by means of the "**fitdist**" function included in the Statistics and Machine Learning Toolbox of Matlab© (Version R2016b) which fits each one of the theoretical probability distributions to the storm surge data coming from the synthetic data set. The results of the theoretical fitted distributions were tested against the empirical pdf of the storm surge data and the results can be observed in Figure 150 and Figure 151.

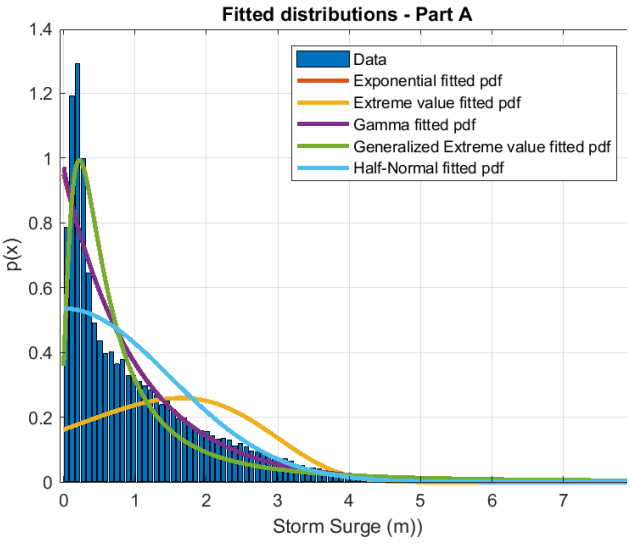

Figure 150. Fitted PDF distributions to storm surge – Part A

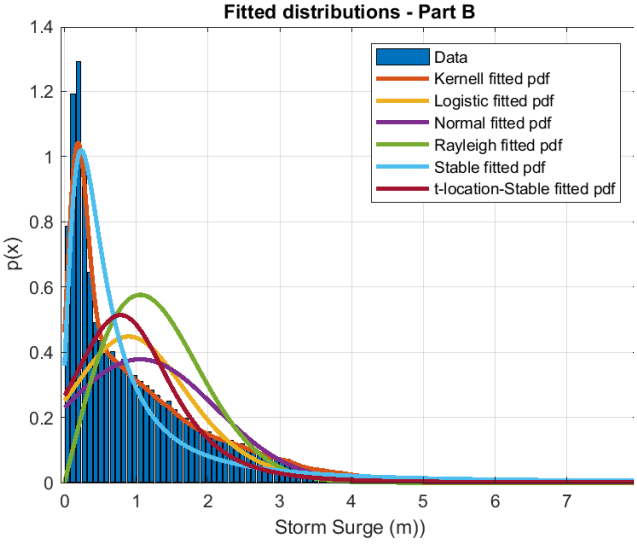

Figure 151. Fitted PDF distributions to storm surge – Part B

From Figure 150 and Figure 151 it can be seen that none of the tested distributions could represent the peak of data included in the region from 0 to 0.5m of storm surge. It can be observed from Figure 150 that the best distributions are the GEV and the Gamma when compared to the other fittings, while Figure 151 shows that the Stable distribution and the Kernel fit better the data.

If the CDF is looked instead of the PDF, the results from Figure 152 and Figure 153 can be observed in which the empirical cumulative distribution of the data has been plotted against the tested distributions. It is clear from Figure 152 that the Gamma distribution presents a better fit to the data when compared to the GEV distribution which only shows a fit in the lower part if the distribution. From Figure 153 it can be seen that the best fit is the Kernel distribution which fits the data exactly and can be only observed in the upper part of the graph since it is masked by the data itself. The same conclusion can be made if the probability of exceedance is plotted as it can be seen in Figure 154 and Figure 155 in which again the Kernel and Gamma distributions seems as the appropriate choice.

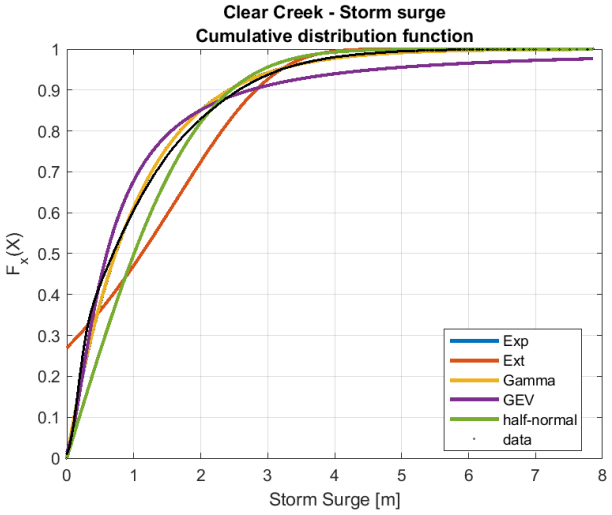

Figure 152. Fitted CDF distributions to storm surge – Part A

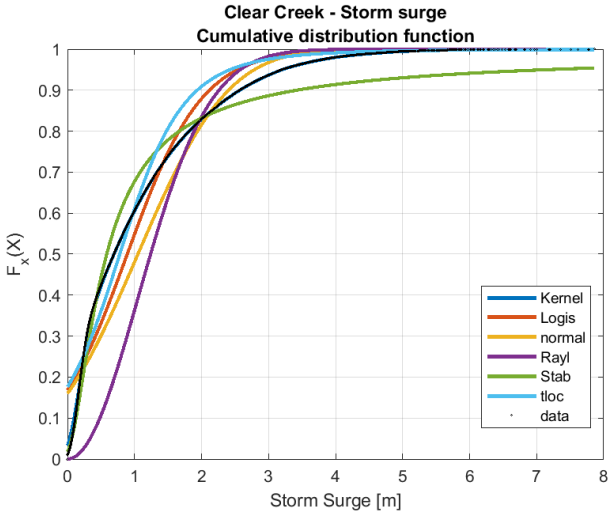

Figure 153. Fitted CDF distributions to storm surge – Part B

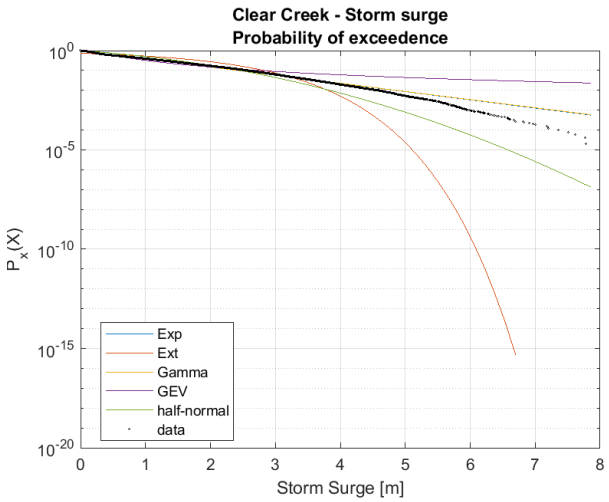

Figure 154. Probability of exceedance comparison for storm surge – Part A

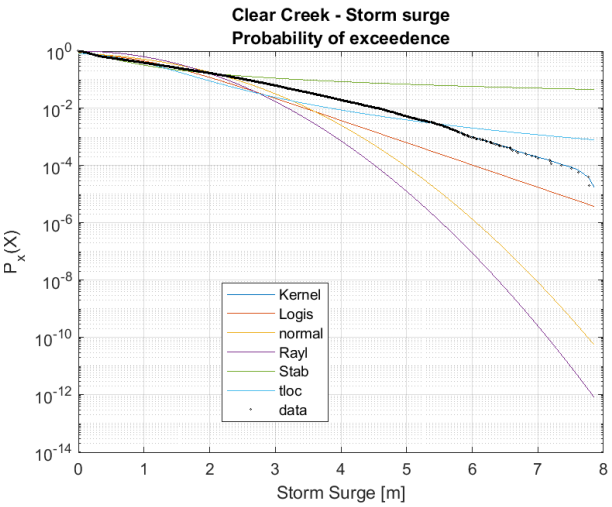

Figure 155. Probability of exceedance comparison for storm surge – Part B

Further analysis for selecting the final distribution for the data included a Q-Q plot (Quantile-Quantile) in which the quantiles of the fitted distribution are plotted in the x axis while the storm surge quantiles are plotted on the y-axis. a good distribution to the data will plot along or close to the $y = x$ line. The results of this analysis for all tested distributions can be seen in Figure 156, which clearly show that the Gamma distributions deviates on the upper quantiles and therefore it is not a good distribution for the storm surge

data. It is clear by this analysis that the best fit will be a Kernel distribution, which can be observed on Figure 84 as the final selection of the marginal distribution of storm surge. Goodness-of-fit tests implemented in Matlab© (Version R2016b) were also carried out to confirm the decision such as the normalized mean squared error (NMSE) and the normalized root mean square error (NRMSE). For both tests a value closer to 1 indicates a better fit to the data. The results from these tests can be observed in Figure 157 and Figure 158.

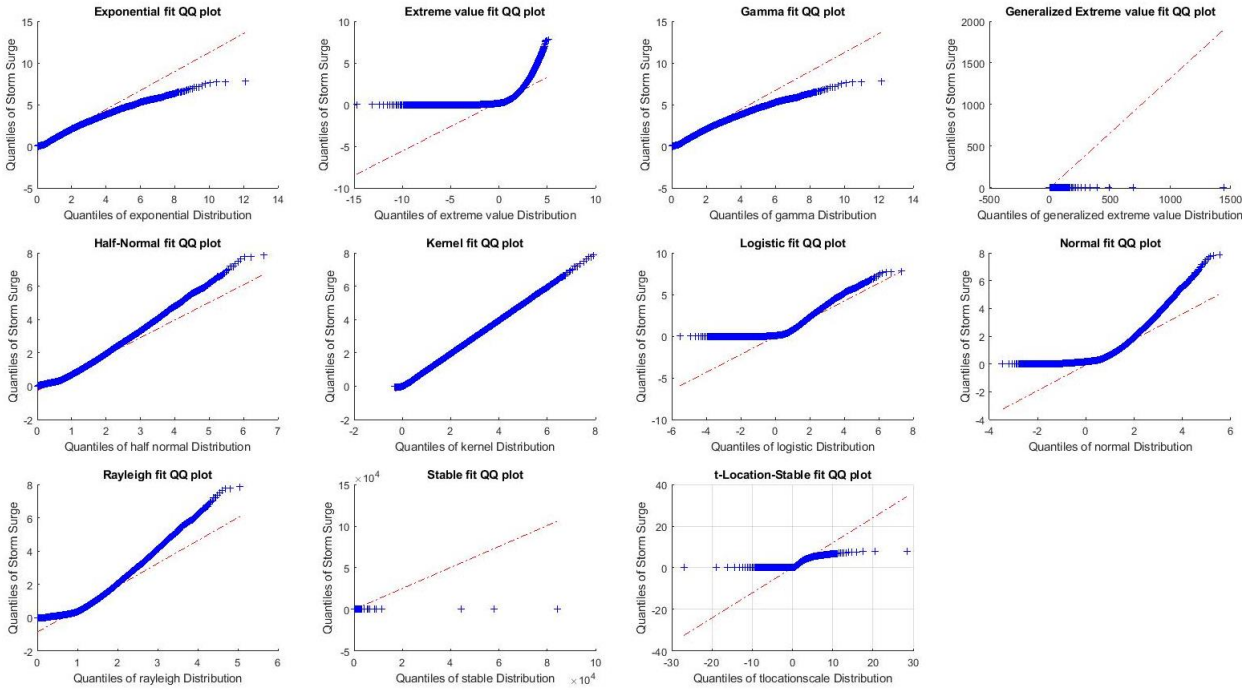

Figure 156. Clear Creek Storm Surge Q-Q plots

NMSE	Distributions_cdf
0.9895	'Exponential fitted cdf'
0.68636	'Extreme value fitted cdf'
0.98999	'Gamma fitted cdf'
0.98061	'Generalized Extreme value fitted
0.90071	'Half-Normal fitted cdf'
0.99894	'Kernell fitted cdf'
0.94144	'Logistic fitted cdf'
0.89283	'Normal fitted cdf'
0.68956	'Rayleigh fitted cdf'
0.97875	'Stable fitted cdf'
0.94624	't-location-Stable fitted cdf'

Figure 157. NMSE Goodness-of-Fit Test – Storm surge Clear Creek

NRMSE	Distributions_cdf
0.89755	'Exponential fitted cdf'
0.43996	'Extreme value fitted cdf'
0.89995	'Gamma fitted cdf'
0.86076	'Generalized Extreme value fitted
0.6849	'Half-Normal fitted cdf'
0.96738	'Kernell fitted cdf'
0.758	'Logistic fitted cdf'
0.67263	'Normal fitted cdf'
0.44283	'Rayleigh fitted cdf'
0.85423	'Stable fitted cdf'
0.76813	't-location-Stable fitted cdf'

Figure 158. NRMSE Goodness-of-Fit Test – Storm surge Clear Creek

9.2.1.2 Precipitation

The theoretical distributions tested for the precipitation data are the ones listed below.

- Exponential
- (GEV)
- Gamma
- EV
- Rayleigh
- Log-Logistic
- Log-Normal
- Nakagami
- Rician
- Weibull
- Birnbaum-Saunders
- Burr Type XII
- Generalized Pareto
- t-location
- Inverse Gaussian
- Half-normal
- Kernel
- Logistic
- Normal
- Stable

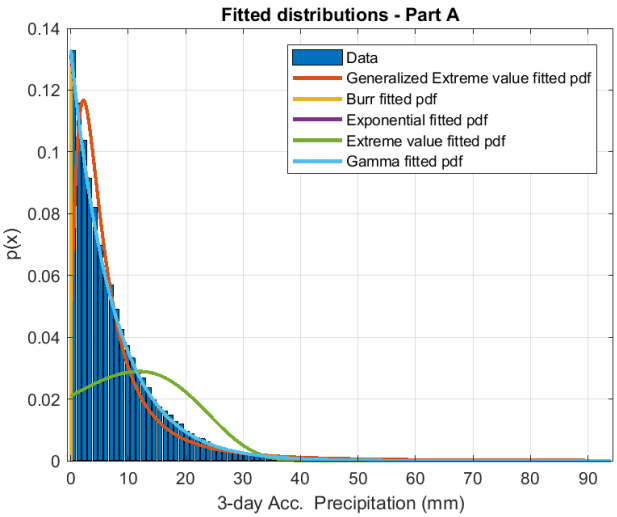

Figure 159. Fitted PDF distributions to precipitation–A

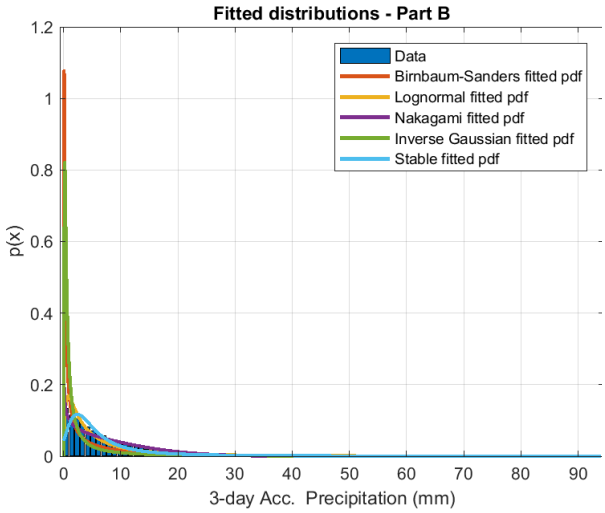

Figure 160. Fitted PDF distributions to precipitation–B

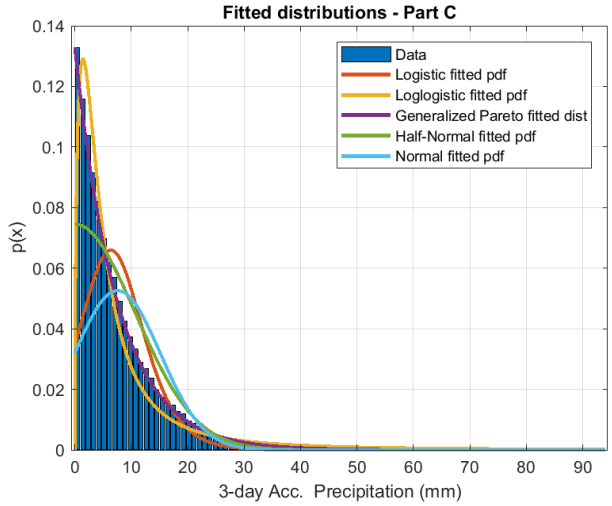

Figure 161. Fitted PDF distributions to precipitation–C

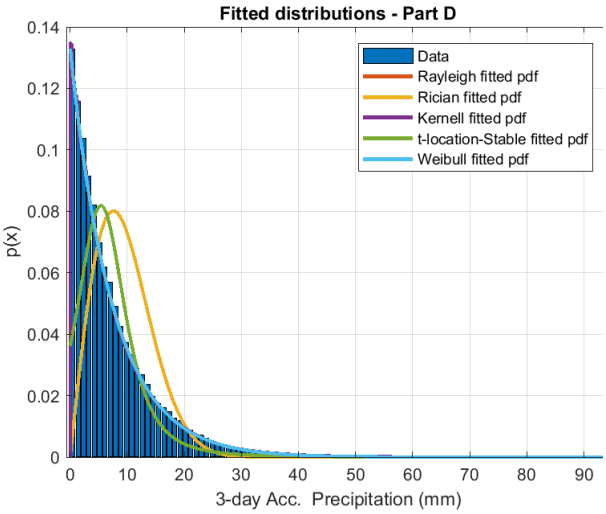

Figure 162. Fitted PDF distributions to precipitation–D

From Figure 159 to Figure 162 it can be seen that the worst fitting distributions are in Figure 160 and that neither the Birnbaum-Saunders, the Inverse Gaussian, the Stable, the Lognormal or the Nakagami distributions are a good fit to the precipitation data. From Figure 159 only the Extreme value distribution can be neglected due to its poor fit to the data, while from Figure 161 and Figure 162 the Normal, Half-Normal, Logistic, t-location and Rician distributions can be taken out from the analysis.

If the CDF is looked instead of the PDF, the results from Figure 163 to Figure 166 show that the best distributions are the Burr Type XII, Exponential, Gamma, Kernel, Generalized Pareto, Reyleigh and Weibull distributions. A similar and additional conclusion can be made if the probability of exceedance is plotted as it can be seen in Figure 167 to Figure 170 in which it's seen that the Gamma and the Exponential distribution present exactly the same behaviour making that choosing either of this is the same. In addition, if Figure 164 is observed, is clear that the Generalized Pareto distributions shows a better fit than the Kendal distribution since it fits better the upper tail of the data. In Figure 170 it can be observed that the Weibull distribution shows a better fit that the Rayleigh distribution.

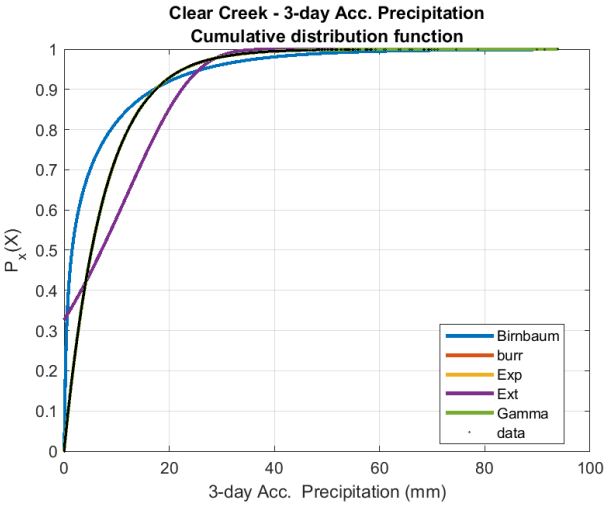

Figure 163. Fitted CDF distributions to precipitation–A

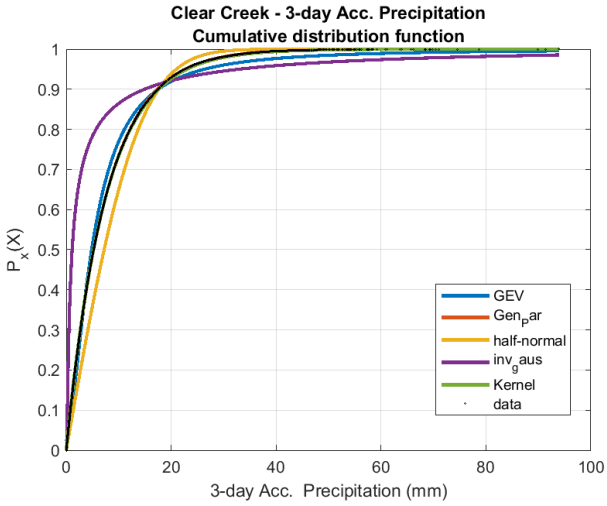

Figure 164. Fitted CDF distributions to precipitation–B

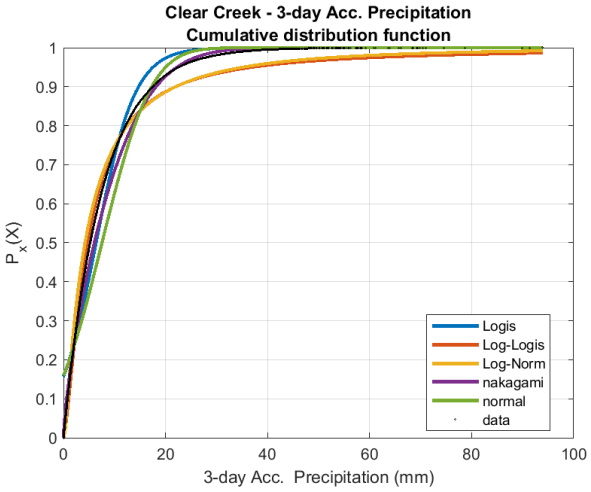

Figure 165. Fitted CDF distributions to precipitation– C

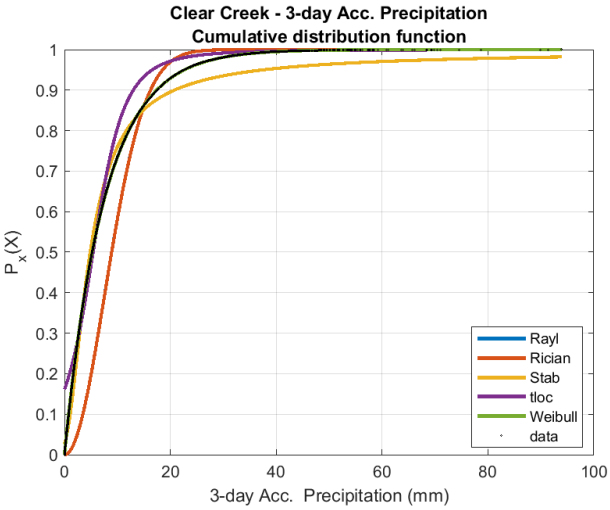

Figure 166. Fitted CDF distributions to precipitation– D

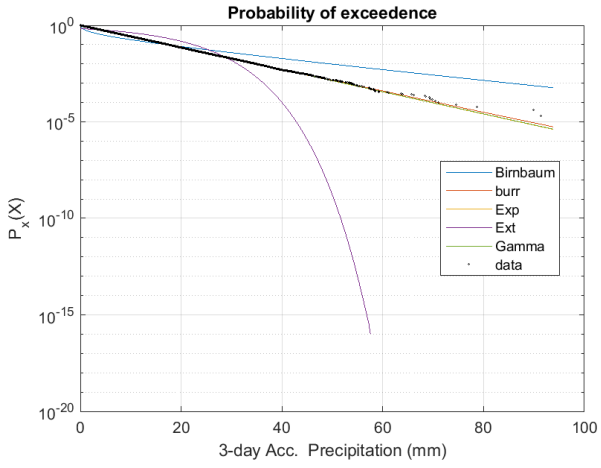

Figure 167. Probability of exceedance comparison for precipitation –A

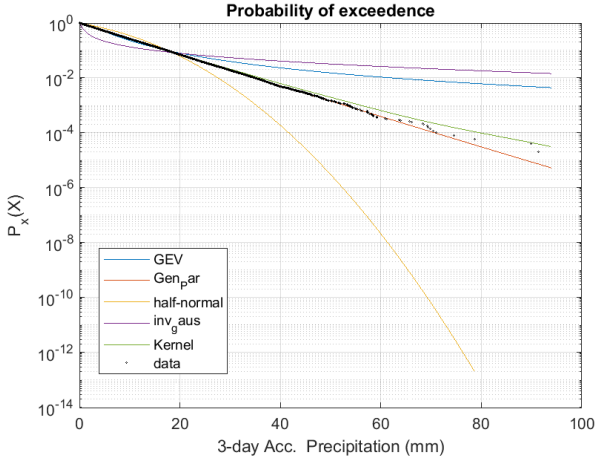

Figure 168. Probability of exceedance comparison for precipitation –B

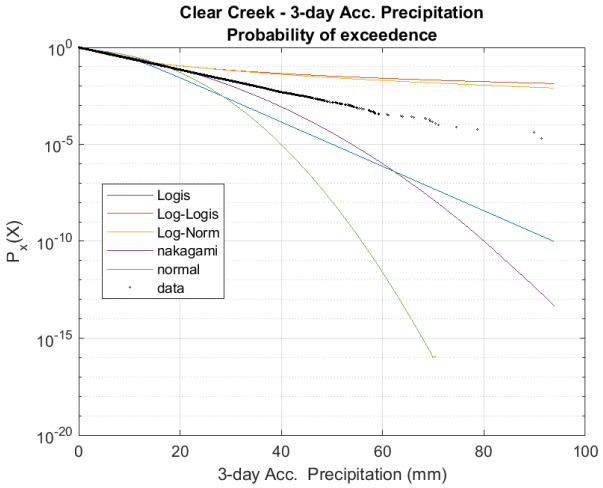

Figure 169. Probability of exceedance comparison for precipitation – C

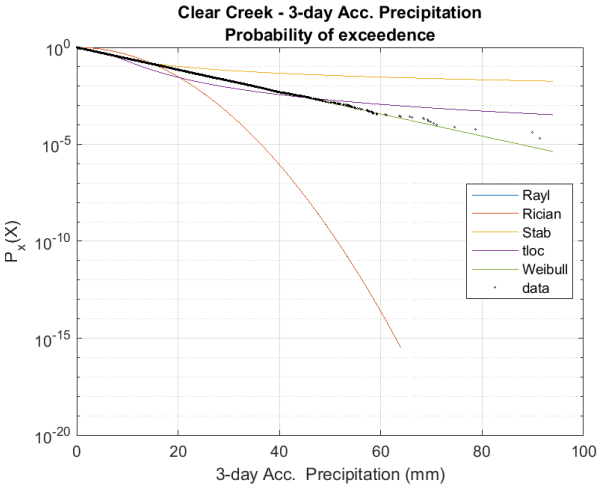

Figure 170. Probability of exceedance comparison for precipitation – D

Further analysis for selecting the final distribution for the data included a Q-Q plot (Quantile-Quantile) in which the quantiles of the fitted distribution are plotted in the x axis while the storm surge quantiles are plotted on the y-axis. a good distribution to the data will plot along or close to the $y = x$ line. The results of this analysis for all tested distributions can be seen in Figure 171 which shows very similar results for all the preselected distributions. The solely conclusion that can be determined from this analysis is that the Kernel distribution is discarded since it underestimates the precipitation for the upper tail which in this case is not a conservative choice.

Due to the similar results, some Goodness-of-fit tests implemented in Matlab© (Version R2016b) were carried out to confirm the final selection. These tests were the NMSE and the NRMSE. For both tests a value closer to 1 indicates a better fit to the data. The results from these tests can be observed in Figure 172 and Figure 173 from which it can be concluded according to the NMSE and NRSE, that the best choice is either Burr Type XIII distribution or a Generalized Pareto distribution. As the GPD distribution has been used before to be fit hydrological data, this is the final distribution selected for the precipitation in the Clear Creek watershed.

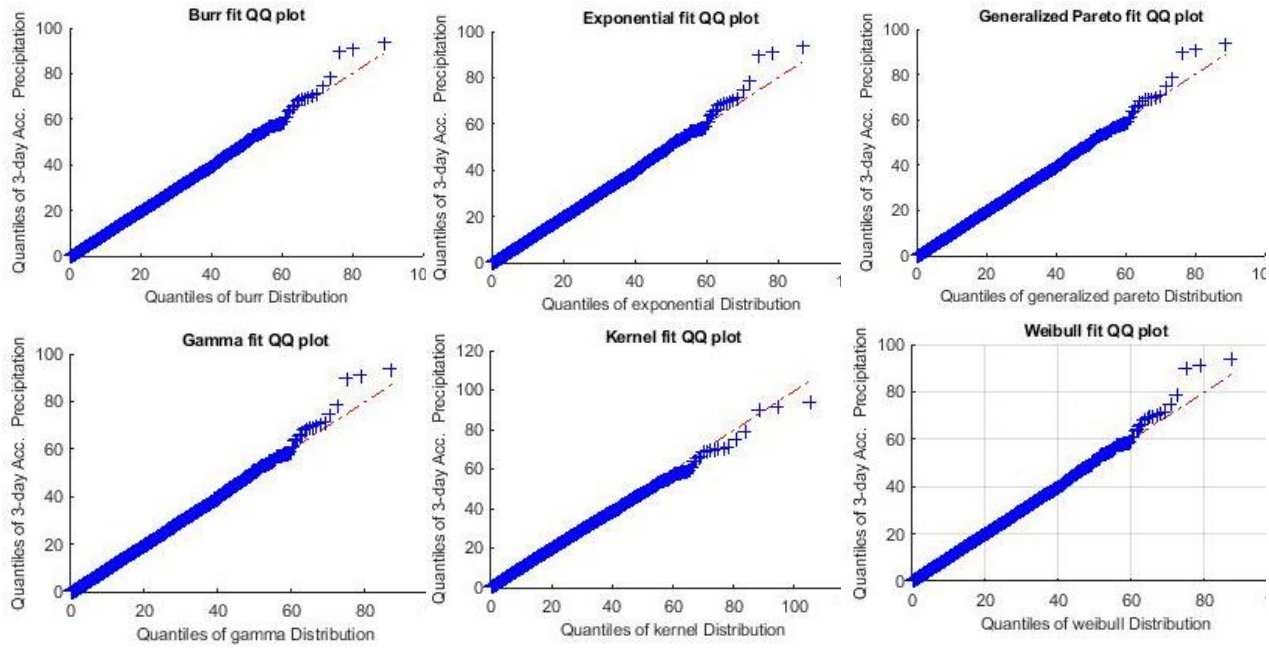

Figure 171. Clear Creek precipitation Q-Q plots

NMSE	Distributions_cdf
-0.012469	'Birnbaum_Saunders fitted cdf'
1	'Burr fitted cdf'
0.99999	'Exponential fitted cdf'
0.29696	'Extreme value fitted cdf'
0.99999	'Gamma fitted cdf'
0.99227	'Generalized Extreme value fitted
1	'Generalized Extreme Pareto fitted
0.91788	'Half-Normal fitted cdf'
-0.49281	'Inverse gaussian fitted cdf'
0.99997	'Kernell fitted cdf'
0.95253	'Logistic fitted cdf'
0.99206	'Loglogistic fitted cdf'
0.97406	'Lognormal fitted cdf'
0.98477	'Nakagami fitted cdf'
0.88095	'Normal fitted cdf'
0.68248	'Rayleigh fitted cdf'
0.68239	'Rician fitted cdf'
0.99111	'Stable fitted cdf'
0.95681	't-location-Stable fitted cdf'
0.99999	'Weibul; fitted cdf'

Figure 172. NMSE Goodness-of-Fit Test – Precipitation Clear Creek

NRMSE	Distributions_cdf
-0.0062154	'Birnbaum_Saunders fitted cdf'
0.99784	'Burr fitted cdf'
0.99704	'Exponential fitted cdf'
0.16153	'Extreme value fitted cdf'
0.99761	'Gamma fitted cdf'
0.91207	'Generalized Extreme value fitted
0.99782	'Generalized Extreme Pareto fitted
0.71344	'Half-Normal fitted cdf'
-0.22181	'Inverse gaussian fitted cdf'
0.99469	'Kernell fitted cdf'
0.78213	'Logistic fitted cdf'
0.9109	'Loglogistic fitted cdf'
0.83894	'Lognormal fitted cdf'
0.87659	'Nakagami fitted cdf'
0.65496	'Normal fitted cdf'
0.43651	'Rayleigh fitted cdf'
0.43643	'Rician fitted cdf'
0.90569	'Stable fitted cdf'
0.79219	't-location-Stable fitted cdf'
0.99771	'Weibul; fitted cdf'

Figure 173. NRMSE Goodness-of-Fit Test – Precipitation Clear Creek

9.2.2 Copula Fitting

As described in chapter 4 (Section 4.1.1.2.1), in order to find the best copula that fits the data, the three main Archimedean copula families were tested (first three copulas listed below) in addition to two popular Copulas families (see blue families below)

- Gumbel
- Frank
- Clayton
- Gaussian
- t-Student

An Archimedean Copula is a specific type of copula which presents the following format:

$$C(u,v) = \phi^{[-1]}(\phi(u) + \phi(v)) \qquad \textbf{(9.2.1)}$$

Where, $\phi : [0,1] \rightarrow [0,\infty), \phi(1) = 0$ is known as the copula generator and $\phi^{[-1]}$ is a pseudo inverse which is equal to $\phi^{-1}(t)$ if $0 \leq t \leq \phi(0)$ and zero (0) otherwise.

The mains characteristics of Archimedean copulas is that they are continuous, strictly decreasing, convex, commutative ($C(u,v) = C(v,u)$) and associative $C(u, C(v,w)) = C(C(u,v), w)$. In this type of copulas, dependence is modelled with only one parameter.

In order to fit a copula to the synthetic pairwise data, the original dataset must be transformed via the ranked data to the copula space $[0,1]$. This process was described in chapter 4 (Section 4.1.1.2.1) and shown in Figure 89 and Figure 90.

Once the data is transformed according to equation (4.1.5), the Empirical copula CDF is constructed using equation 9.2.2. This is done in order to compare it with the fitted CDF copula families tested in this analysis. The empirical copula for the Clear Creek watershed can be seen in Figure 174.

$$C_n(u,v) = \frac{1}{n}\sum_{i=1}^{n}\left(\frac{R_i}{n+1} \leq u, \frac{S_i}{n+1} \leq v\right) \qquad \textbf{(9.2.2)}$$

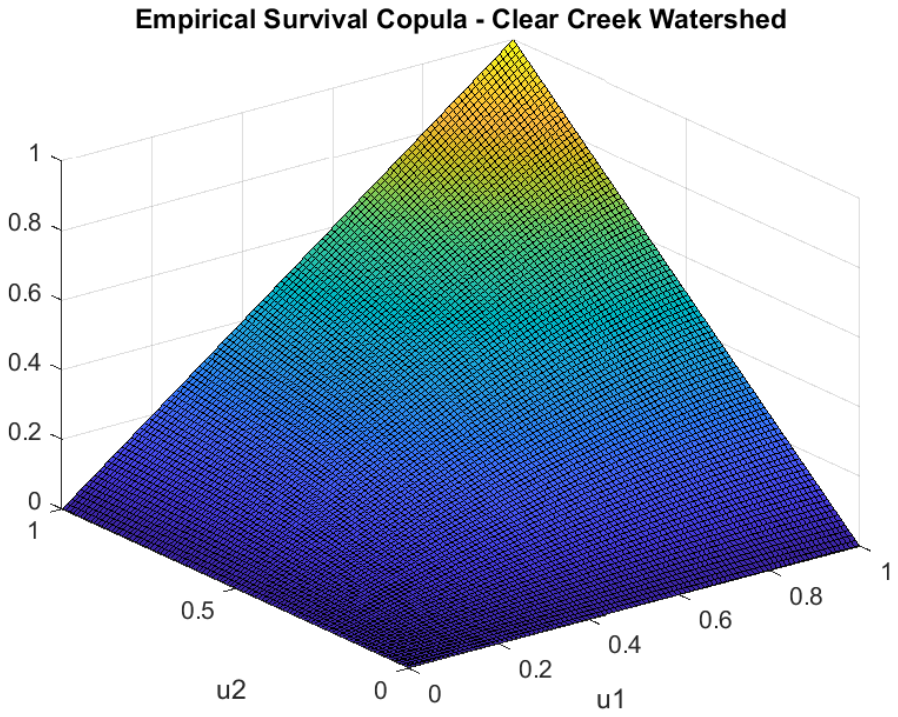

Figure 174. Empirical CDF copula for the Clear Creek watershed

Using the Statistics and Machine Learning Toolbox of Matlab© (Version R2016b).the theoretical copula CDF's for different families can be constructed (see Figure 175 to Figure 179) and tested against the empirical Copula using the Cramer von Mises Test which is given by the following expression (equation 9.2.3), which basically states that the Goodness-of-Fit of the copula family to the joint data is given by the squared difference between the empirical and the theoretical CDF's copulas. The Cramer von Mises tests stays that the lower the squared difference, the better the fit. The results from the subtracted CDF copulas are shown in Figure 180 to Figure 184 and the final summary result is reported in Table 16 in which is indicated that the best copula describing the data is a Frank Copula with Tetha parameter 1.7604.

$$CM_m = n\sum_{i=1}^{n}\left\{C_n\left(\frac{R_i}{n+1},\frac{S_i}{n+1}\right) - C_{\theta n}\left(\frac{R_i}{n+1},\frac{S_i}{n+1}\right)\right\}^2 \qquad \textbf{(9.2.3)}$$

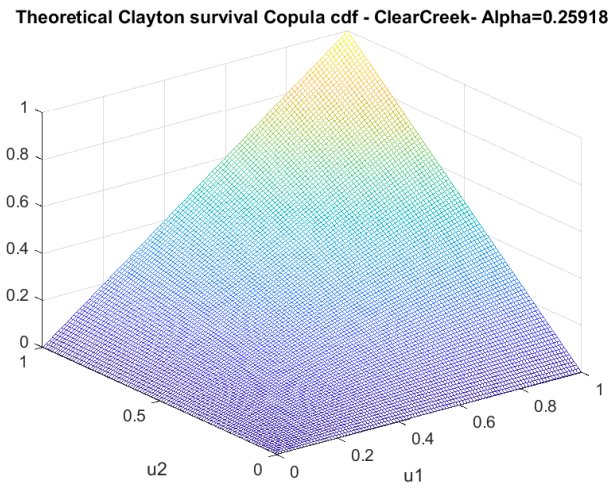

Figure 175. Theoretical CDF - fitted Clayton Copula and Parameter

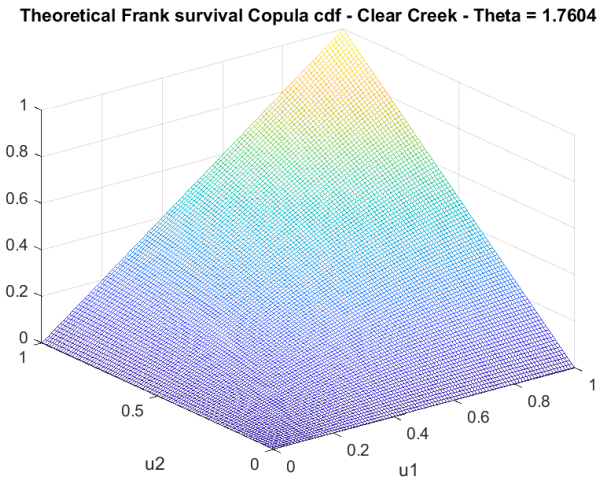

Figure 176. Theoretical CDF - fitted Frank Copula and Parameter

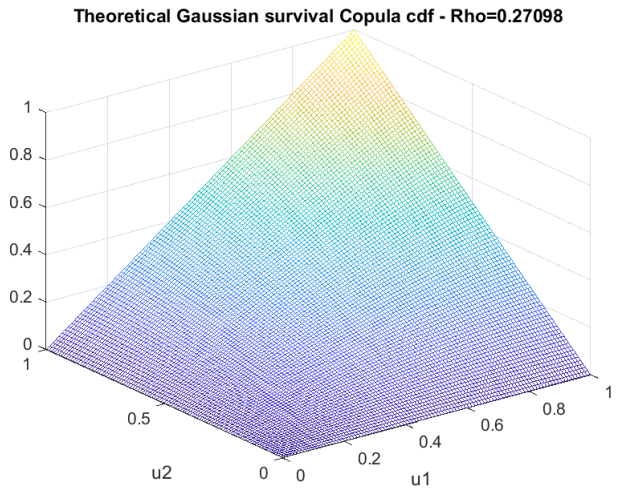

Figure 177. Theoretical fitted Gaussian Copula and Parameter

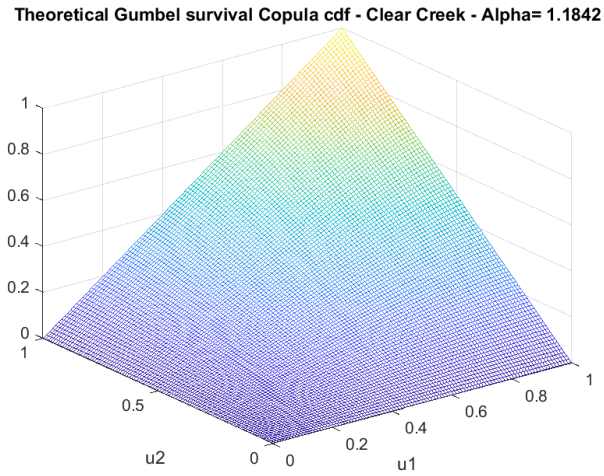

Figure 178. Theoretical fitted Gumbel Copula and Parameter

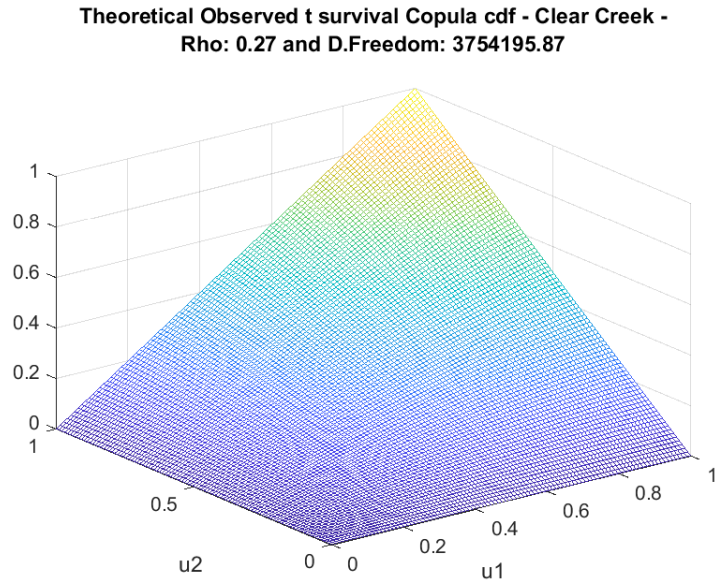

Figure 179. Theoretical fitted t-student Copula and Parameters

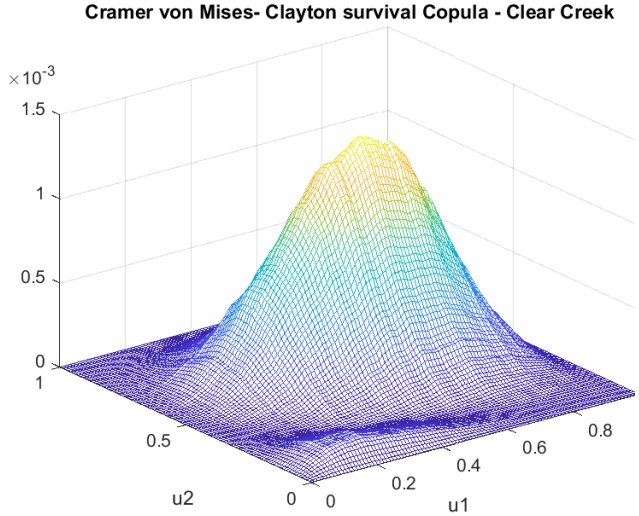

Figure 180. Cramer-von-Mises test for Clayton Copula

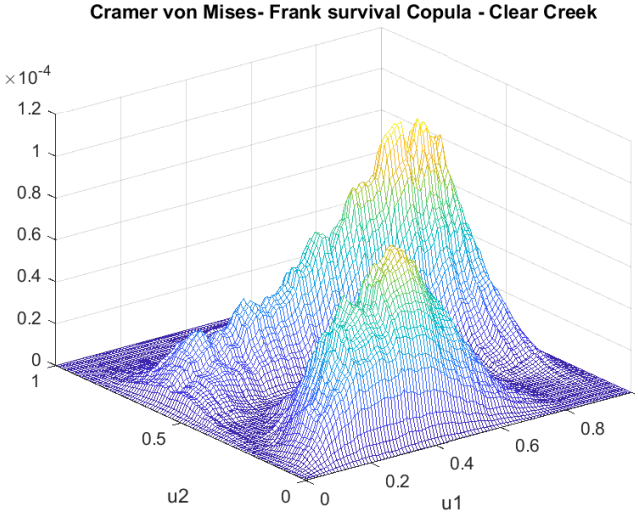

Figure 181. Cramer-von-Mises test for Frank Copula

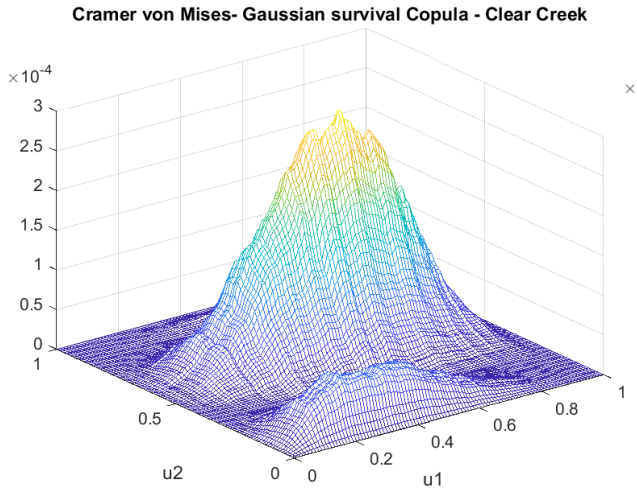

Figure 182. Cramer-von-Mises test for Gaussian Copula

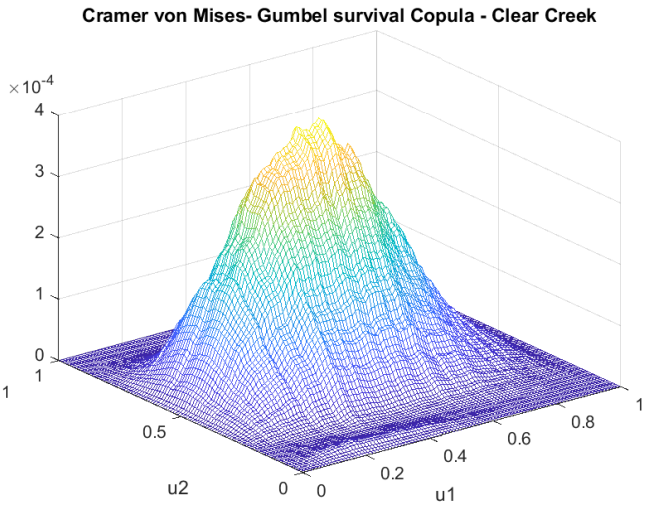

Figure 183. Cramer-von-Mises test for Gumbel Copula

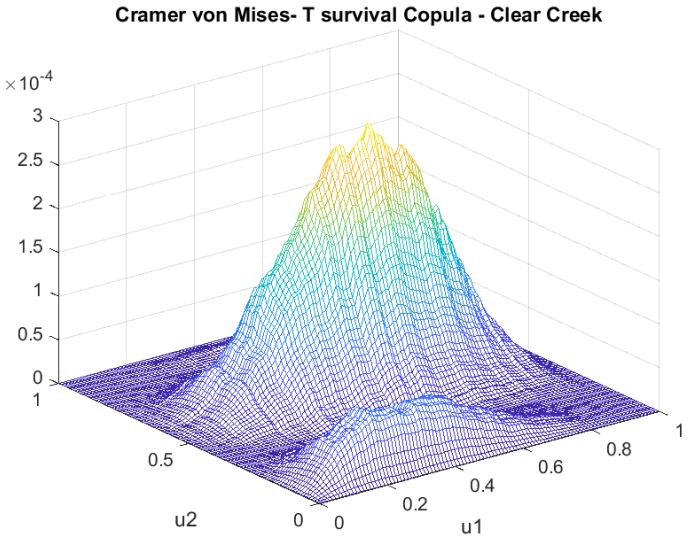

Figure 184. Cramer-von-Mises test for t-student Copula

Table 16. Total Sum of squared differences for each survival copulas in the Clear Creek watershed

Sum_Cramer_s	Copulas_s
0.35774	'Gaussian'
2.1627	'Clayton'
0.64679	'Gumbel'
0.16323	'Frank'
0.35301	't'

In addition to the Cramer von Mises test, a study per quadrants of the copula can be done if the original data is transformed to the standard normal space (See Figure 185). Then using the Statistics and Machine Learning Toolbox of Matlab© (Version R2016b) random data is generated for each copula family with the fitted respective parameter (see Figure 175 to Figure 179) and the data is transformed to the standard normal space as well. With this transformation the Pearson correlation Rho (ρ) is computed for each quadrant of each copula family, taking into account that the coordinate (0,0) the central point (see blue lines in Figure 185). The results in each quadrant are then compared to the Pearson correlation coefficient computed in each of the quadrants of Figure 185. A good fit should resemble the original Pearson's correlation. The summary of the results for the previously described method is shown in Table 17.

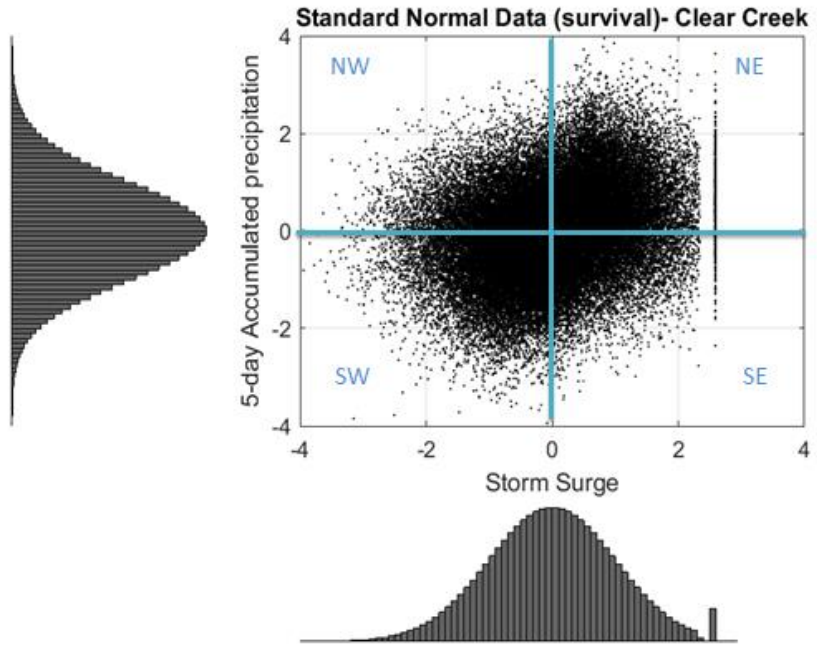

Figure 185. Synthetic data transformed to the standard normal space for standard copula

Table 17. Pearson Correlation Coefficient comparison between data and survival Copula families. Analysis for North West, North East, South West and South East quadrants

NW_CC_s	NE_CC_s	SW_CC_s	SE_CC_s	Copula_ClearCreek_s
0.047037	0.078081	0.012493	0.10028	'Standard Normal'
0.070196	0.11901	0.11546	0.073225	'Gaussian'
0.025714	0.020269	0.21079	0.031768	'Clayton'
0.0051088	0.27875	0.055723	0.030364	'Gumbel'
0.048114	0.07943	0.097377	0.060277	'Frank'
0.074855	0.13127	0.10946	0.084404	't'

From Table 17 it can be observed that the Frank copula shows good behavior in all quadrants except in the North-West, were the Gaussian or t family present a better fit to the data. This points to the final decision that is to adopt a Frank copula with theta parameter 1.7604 and not the Gaussian copula which ranks in second according to the Cramer von Mises test (the t-family is physically not a good representation of the phenomena therefore is neglected from the analysis).

9.2.3 Numerical grid probabilities for computing risk due to compound flooding

As described in chapter 5, a numerical grid was used (see Figure 116) in order to select the scenarios that were going to be used for the compound flood analysis of the Clear Creek watershed. The numerical grid as explained in chapter 5, gave 400 scenarios that had to be related with a specific probability of occurrence. Therefore, the procedure on computation of the probability of each cell along the numerical grid is presented below.

If the numerical grid is zoomed in to illustrate the calculation for one specific cell, Figure 186 is obtained, in which is observed that the probability of interest is the one enclosed by corners I, II, III and IV or the one expressed by the following equation:

$$P(cell_{I,II,III,IV}) = p(0_m < Surge < 0.4_m \cap 0_m < precipitation < 50_{mm}) \quad \textbf{(9.3.1)}$$

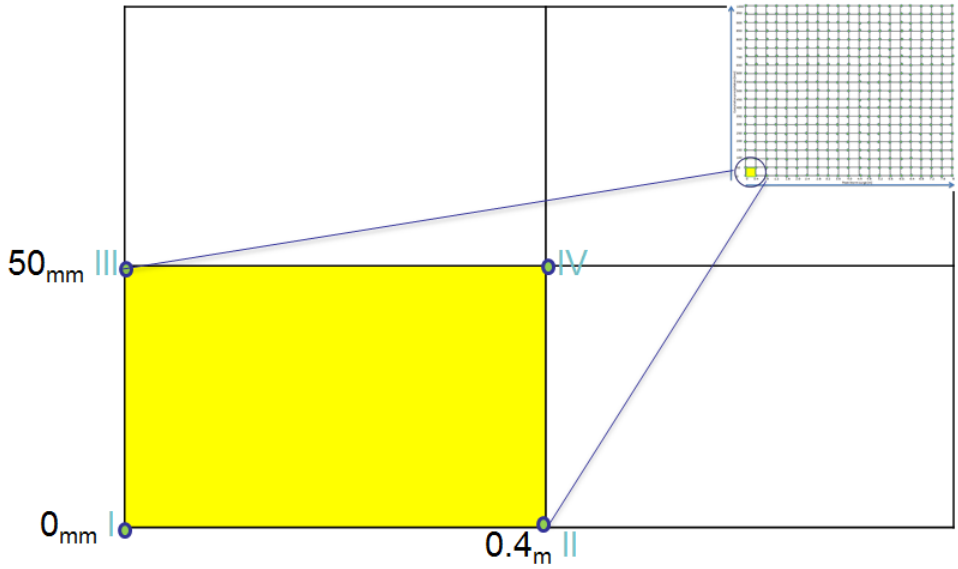

Figure 186. Zoom in of numerical grid for compound scenarios.

As the numerical grid was determined from the synthetic data set created by Sebastian et al., (2017a), and as described in Section 9.2.2, a Frank survival copula was fitted to the synthetic data, this copula definition was used to determine the probabilities of interest by means of equations 4.1.3, 4.1.6 (see chapter 4) and Figure 88, which are presented again below to illustrate better the concept.

$$p_{\widehat{u,v}} = P\{U > u \wedge V > v\} = 1 - u - v + C(u,v) = C(1-u, 1-v) \quad \textbf{(4.1.3)}$$

$$C(1-u,1-v) = -\frac{1}{\theta}\ln[1+\frac{(e^{-\theta(1-u)}-1)(e^{-\theta(1-v)}-1)}{e^{-\theta}-1}] \quad \textbf{(4.1.6)}$$

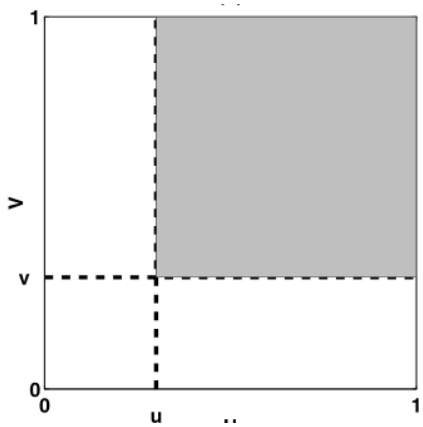

Figure 187. AND case (Survival Copula $C(1-u, 1-v)$)

It can be seen that the probability for an event $(surge\,(x)\,,\ precipitation(y))$ transformed to the copula space [0,1] (u,v), is given by the shaded grey are in Figure 187. This means that if the probability of the pair-wise data corresponding to each of the corners of the cell (I,II, III and IV) is determined using the fitted Frank copula, the areas shown from Figure 188 to Figure 191 can be observed.

Moreover, if the areas seen from Figure 188 to Figure 191 are analyzed, it can be easily seen that in order to obtain the probability enclosed by corners I, II, II and IV (see Figure 186) the following expression has to be used:

$$for\ cell\ = i : 400$$
$$P_I + P_{IV} - P_{III} - P_{II} = P_{grid} \quad \textbf{(9.3.2)}$$

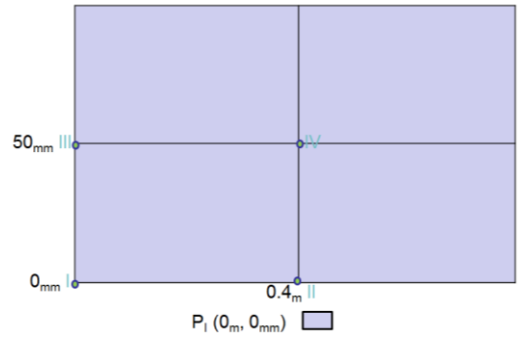

Figure 188. Probability given by Copula for corner I

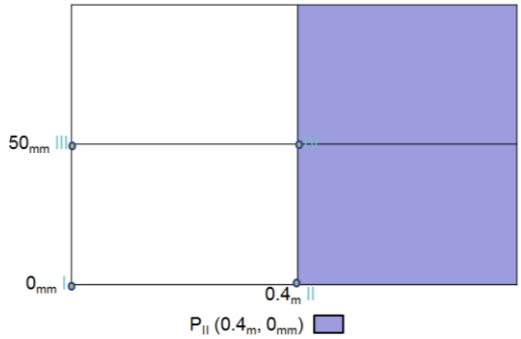

Figure 189. Probability given by Copula for corner II

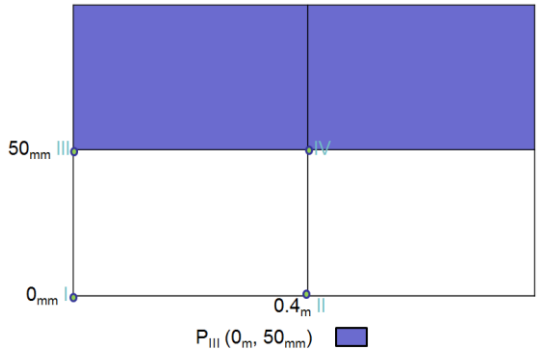

Figure 190. Probability given by Copula for corner III

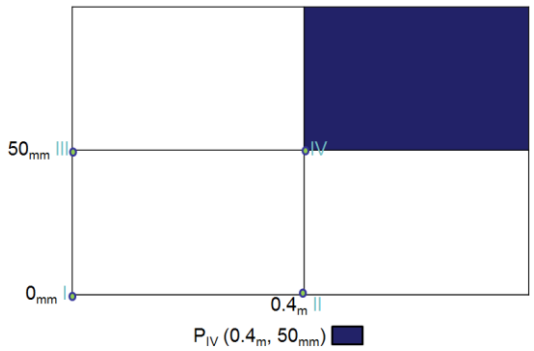

Figure 191. Probability given by Copula for corner IV

The process explained above was done for every grid in Figure 116. Afterwards, each scenario run in chapter 5 (Section 5.1.2), was associated to its respective numerical cell probability.

9 Appendix C

9.3. Delft-FIAT Model

The Delft - Flood Impact Assessment Tool (FIAT) is a flexible Open Source toolset developed by Deltares used to build and run flood impact models based on the unit-loss method (Deltares, 2018a) which relates the flood parameters to damage at the unit level. The model requires that the exposure data is given as Tiff file, but the impact functions and maximum damages can be all managed through a simple excel worksheet.

The basic damage formula than Delft-FIAT uses is described by equation 9.3.1, where s is the potential/maximum damage [€/object], d is the water depth [m], $f(d)$ represents the damage function, giving a damage fraction [-], n is the number of objects, i is the category count and j is the location count.

$$Damage = \sum_{i=1}^{m} s_i \sum_{j=1}^{n} f_{ij}(d_j) n_{ij} \qquad \textbf{(9.3.1)}$$

In the following sections, detailed information about the configuration of the model is going to be presented.

9.3.1 Delft-FIAT Components

The basic components of the Delft-FIAT model include a model configuration file (Excel) which makes reference to separate folders that include the exposure data (object maps), the damage or impact functions and the maximum damage per impact category. All of these data sets were described on chapter 5 and they are illustrated in Figure 192. The calculation core then uses the configuration file with all the information of the area and it can be run using Python, through a website or even as part of an operational flood early warning system (FEWS).

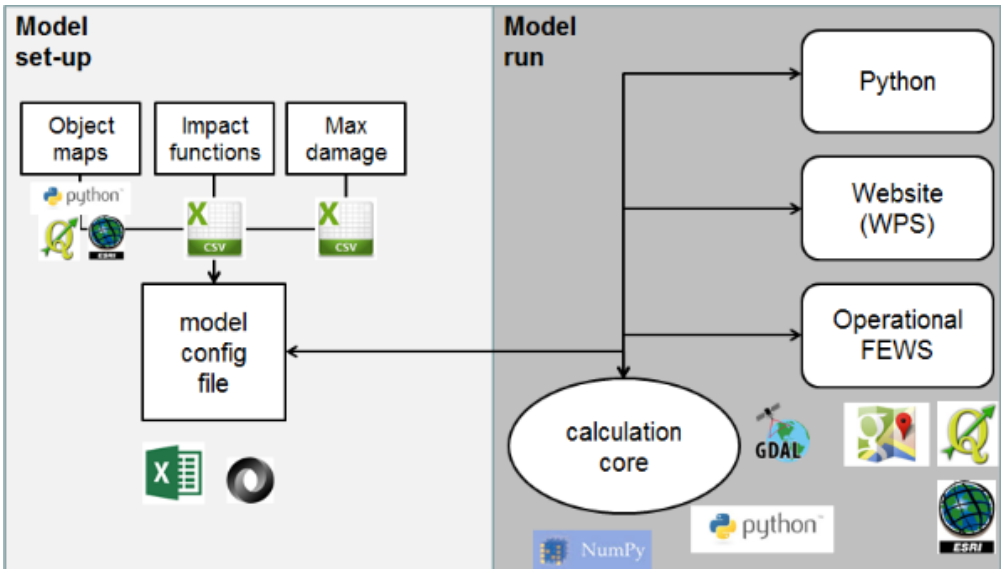

Figure 192. Delft-FIAT model set-up and model run. Source:(Deltares, 2018a)

9.3.2 Set up of flood impact model

In order to set up the flood impact model, some configurations to the datasets have to be performed. The object maps or exposure rasters need to have an identical coordinate reference system as the one used to calculate the flood hazard maps, these rasters also need to have an identical extent, identical cell size, origin and a clear unit value. In addition, a different raster per each damage class has to be created. In the case of this research, four rasters, each one for each type of land use reported in chapter 5 needs to be created.In the case of the Impact or damage functions, Table 13 needs to be modified and used as a comma separated value files for each one of the depth-damage classes found for the area of study. The function includes two columns, one with the water depth and the other one describing the damage factor (between 0 and 1)(Deltares, 2018a).

For the maximum damage values, this information is updated directly on the main configuration file using the correct units and rescaling when necessary given the cell size of the hazard and exposure maps (e.g. cell sixe 50x50m, unit of damage €/m2).

Finally, the last input for the FIAT model are the hazard maps, which include the flood characteristics as water depth, velocity, time of arrival, etc. The model is able to run output from different models but the only requirement is that the extent of the hazard map is entirely overlapping the object or exposure map extents and that as mentioned before, both the coordinate system and cell size between maps agree completely.

Delft-FIAT also includes advanced settings that allow the user to configure the model to perform risk calculations. This can be done by describing in the configuration file which is the lower and upper bound for the integration of risk and also by describing the location of the water depth files being considered (SFINCS compound flooding scenarios) and their respective probabilities of occurrence.

9.3.3 Running flood impact model

As mentioned before, Delft-FIAT can be run in several ways. Once the model is properly constructed, FIAT can be run using a Macro button incorporated in the configuration file or it can be run using the python command window. For multiple runs as the ones needed for this particular research, python is the best alternative since it allows running multiple scenarios using a batch file.

The standard output of the model for each scenario is a total damage grid and an impact report with summary indicators either as a text file or a spreadsheet. If the advanced settings are used, the output can also include individual damage grids, shapefile with zonal summary statistics per region and most importantly risk information that includes a summary report and a risk grid that could be used to generate flood risk maps. For further details, consult Deltares (2018a).


TUDelft
Deltares
Enabling Delta Life